Nonperturbative studies in QCD

A Dissertation presented

by

Yizhuang Liu

to

The Graduate School

in Partial Fulfillment of the

Requirements

for the Degree of

Doctor of Philosophy

in

Physics

Stony Brook University

August 2018

Stony Brook University

The Graduate School

Yizhuang Liu

We, the dissertation committe for the above candidate for the

Doctor of Philosophy degree, hereby recommend

acceptance of this dissertation

Ismail Zahed
Professor of Physics

Edward Shuryak
Professor of Physics

Martin Rocek
Professor of Physics

Dominik Schneble
Professor of Physics

Dennis Sullivan
Professor of Mathematics

This dissertation is accepted by the Graduate School

Richard Gerrig
Dean of the Graduate School

Abstract of the Dissertation

Nonperturbative Studies in QCD

by

Yizhuang Liu

Doctor of Philosophy

in

Physics

Stony Brook University

2018

QCD in the non-perturbative regime is theoretically still very challenging. This thesis consists of four different studies using newly developed non-perturbative techniques. In the first study, we develop a many-body analysis of the QCD vacuum as a semi-classical ensemble of instanton- and anti-instanton-dyons with light quarks. We show that at low temperature, the ensemble confines and breaks spontaneously chiral symmetry. The rate at which both symmetries are restored at high temperature depend on the nature of the quark representation and boundary conditions. In the second study, we analyze the dual effect of a rotation and a magnetic field on light quarks both in the free and interacting regimes in various space-dimensions. We show that for QCD in the spontaneously broken phase, the dual effect can induce pion condensation that can take place at current collider energies and potentially in neutron stars. In the third study, we detail a new holographic construction for addressing both heavy and light quarks in AdS/QCD with manifest chiral and heavy quark symmetry. We use to study heavy-light mesons and baryons and predicts a number of new hadronic exotics, some of which have currently been detected by the LHCb collaboration. In the fourth study, we combine the universal aspects of Random matrix theory

with hydrodynamics to investigate aspects of the QCD Polyakov-line at finite temperature in and out-of-equilibrium as a way to estimate typical relaxation times, and at finite chemical potential to derive universal spectral edge laws. Some of our observations can be explored using current lattice QCD simulations.

Dedication Page

To my father

Contents

List of publications

Below is the list of my publications during my PhD research.

1. Published articles

1.Pion Condensation by Rotation in a Magnetic field
Yizhuang Liu, Ismail Zahed (SUNY, Stony Brook). Nov 20, 2017. 5 pp.
Phys.Rev.Lett. 120 (2018) no.3, 032001

2.Heavy and Strange Holographic Baryons
Yizhuang Liu, Ismail Zahed (SUNY, Stony Brook)May 3, 2017. 12 pp
Phys.Rev. D96 (2017) no.5, 056027

3.Heavy Baryons and their Exotics from Instantons in Holographic QCD
Yizhuang Liu, Ismail Zahed (SUNY, Stony Brook). Apr 11, 2017. 11 pp.
Phys.Rev. D95 (2017) no.11, 116012

4.Disorder in the Sachdev-Yee-Kitaev Model
Yizhuang Liu (SUNY, Stony Brook), Maciej A. Nowak (Jagiellonian U.)
Ismail Zahed (SUNY, Stony Brook). Dec 15, 2016. 7 pp. Phys.Lett. B773
(2017) 647-653

5. Heavylight mesons in chiral AdS/QCD
Yizhuang Liu, Ismail Zahed (SUNY, Stony Brook). Nov 14, 2016. 8 pp.
Phys.Lett. B769 (2017) 314-321

6. Holographic Heavy-Light Chiral Effective Action
Yizhuang Liu, Ismail Zahed (SUNY, Stony Brook). Nov 11, 2016. 14 pp.

Phys.Rev. D95 (2017) no.5, 056022

7. Heavy Exotic Molecules
Yizhuang Liu, Ismail Zahed (SUNY, Stony Brook). Oct 20, 2016. 9 pp.
Int.J.Mod.Phys. E26 (2017) no.01n02, 1740017

8.Heavy Exotic Molecules with Charm and Bottom
Yizhuang Liu, Ismail Zahed (SUNY, Stony Brook). Aug 23, 2016. 9 pp.
Phys.Lett. B762 (2016) 362-370

9. The Instanton-Dyon Liquid Model III: Finite Chemical Potential
Yizhuang Liu, Edward Shuryak, Ismail Zahed (SUNY, Stony Brook). Jun 22, 2016. 11 pp. Phys.Rev. D94 (2016)

10. The Instanton-Dyon Liquid Model V: Twisted Light Quarks
Yizhuang Liu, Edward Shuryak, Ismail Zahed (SUNY, Stony Brook). Jun 9, 2016. 13 pp. Phys.Rev. D94 (2016) no.10, 105013

11. Light Adjoint Quarks in the Instanton-Dyon Liquid Model IV
Yizhuang Liu, Edward Shuryak, Ismail Zahed (SUNY, Stony Brook). May 24, 2016. 23 pp. Phys.Rev. D94 (2016) no.10, 105012

12. Chiral Random Matrix Model at Finite Chemical Potential: Characteristic Determinant and Edge Universality
Yizhuang Liu (Stony Brook U.), Maciej A. Nowak (Jagiellonian U. (main)), Ismail Zahed (SUNY, Stony Brook). Feb 2, 2016. 29 pp. Nucl.Phys.B909 (2016) 14-42

13. Hydrodynamics of the Dirac spectrum
Yizhuang Liu (Stony Brook U.), Piotr Warcho (Jagiellonian U.), Ismail Zahed (SUNY, Stony Brook). Jun 29, 2015. 5 pp. Phys.Lett. B753 (2016) 303-307

14.Hydrodynamical Description of the QCD Dirac Spectrum at Finite Chemical Potential
Yizhuang Liu (Stony Brook U.), Piotr Warcho (Jagiellonian U.), Ismail Zahed (SUNY, Stony Brook). Jul 20, 2015. 8 pp. Phys.Rev. D92 (2015) no.11,

114020

15. Hydrodynamics of the Polyakov line in SU(Nc) Yangills
Yizhuang Liu (Stony Brook U.), Piotr Warcho(Jagiellonian U.), Ismail Zahed (SUNY, Stony Brook). May 8, 2015. 4 pp. Phys.Lett. B753 (2016) 65-68

16. Light quarks in the screened dyon-antidyon Coulomb liquid model. II.
Yizhuang Liu, Edward Shuryak, Ismail Zahed (SUNY, Stony Brook). Mar 31, 2015. 17 pp. Phys.Rev. D92 (2015) no.8,

17. Confining dyon-antidyon Coulomb liquid model. I.
Yizhuang Liu (Stony Brook U.), Edward Shuryak, Ismail Zahed (SUNY, Stony Brook). Mar 10, 2015. 19 pp. Phys.Rev. D92 (2015) no.8, 085006

18. Probing Wilson Loops in the QCD Instanton Vacuum
Yizhuang Liu (Stony Brook U.), Ismail Zahed (SUNY, Stony Brook). Aug 14, 2014. 8 pp. Phys.Rev. D91 (2015) no.3, 034023, Erratum: Phys.Rev. D92 (2015) no.11, 119901

19. Probing Wilson Loops in AdS/QCD
Yizhuang Liu (Stony Brook U.), Ismail Zahed (SUNY, Stony Brook). Jul 1, 2014. 7 pp. Phys.Rev. D91 (2015) no.5, 055001, Erratum: Phys.Rev. D92 (2015) no.11, 119902

20. Heavy exotic molecules Yizhuang Liu, Ismail Zahed (SUNY, Stony Brook). 2017. 9 pp. In Quarks, Nuclei and Stars, Memorial Volume Dedicated to Gerald E Brown

21.Hydrodynamical corrections to electromagnetic emissivities in QCD
Yizhuang Liu, Ismail Zahed (SUNY, Stony Brook). Jul 26, 2017. 20 pp. Phys. Rev. D96 (2017) no.11, 116021

2. Submitted articles

1.QCD Dirac Spectrum at Finite Chemical Potential: Anomalous Effective Action, Berry Phase and Composite Fermions

Yizhuang Liu, Ismail Zahed (SUNY, Stony Brook). Sep 2, 2015. 6 pp. arXiv:1509.00812

2.Rotating Dirac fermions in a magnetic field in 1+2,3 dimensions
Yizhuang Liu, Ismail Zahed (SUNY, Stony Brook).Oct 8, 2017. 16 pp. arXiv:1710.02895, submitted to Phys. Rev. D

3.Dense Instanton-Dyon Liquid Model: Diagrammatics
Yizhuang Liu, Edward Shuryak, Ismail Zahed (SUNY, Stony Brook). Feb 1, 2018. 12 pp. arXiv:1802.00540, submitted to Phys. Rev. D

4.Entanglement in Reggeized Scattering using AdS/CFT
Yizhuang Liu, Ismail Zahed (SUNY, Stony Brook). March. 24, 2018. 5pp arXiv:1803.09157, submitted to Phys. Rev. Lett.

List of Figures

Figure 14. (a) Typical diagrammatic contribution to the pair correlation function $h(r)$ where each hanging ring is $-\beta\mathcal{V}+\chi$; (b) Typical contribution to χ_a; (c) Typical contribution to χ_b.

Figure 15. Crystal energy for the bcc arrangement E_L/M versus Ma as given in (153) with $\alpha_s = 1$.

Figure 16. 3-dimensional bcc crystal composed of the instanton- and antinstanton-dyons with the lowest winding, for 2 colors.

Figure 17. Pressure (156) versus $\tilde{a}$ for $m = 20$ and $\nu = \frac{1}{2}$ upper-solid-curve. The separate contributions from the crystal (first term in (156)) is shown as the lower-solid-curve, and the entropy of the re-summed trees (second term in (156)) is shown as the dashed-curve.

Figure 18 . The particle $(+M)$ and anti-particle $(-M)$ LLL for $\Omega = 0$ are shown in (a) each with degeneracy N. For $\Omega \neq 0$ the degeneracy is lifted. In (b) we illustrate how the centrifugation lifts the degeneracy on the states with angular momentum N by shifting them down by $\pm M - \Omega(N + \frac{1}{2})$. The rotating vacuum now includes the particle LLL which needs to be filled.

Figure 19. Effective potential $\mathcal{V}$ as a function of σ in units of $\sqrt{eB}$ at $T = 0$: $\Omega = 0.0001\sqrt{eB}$ (top); $\Omega = 0.00049\sqrt{eB}$ (middle); $\Omega = 0.0005\sqrt{eB}$ (bottom).

Figure 20. Effective mass as a function of $\sqrt{eB}$ and Ω in units of Λ. The mass gap disappears for $\Omega \geq \Omega_c$ as given by (194) through a first order transition.

Figure 21. Finite temperature effective potential $\mathcal{V}$ as a function of σ in units of $\sqrt{eB}$: $\beta = 100/\sqrt{eB}$ and $\Omega = 0.0003\sqrt{eB}$ (top); $\beta = 43/\sqrt{eB}$ and $\Omega = 0.0001\sqrt{eB}$ (bottom).

Figure 22. Effective mass as a function of β and Ω in units of $\sqrt{eB}$ at $T \neq 0$.

Figure 23. The current density in the weak coupling regime with $g_r = 1$, as a function of x=$\frac{eBr^2}{2}$ in unit of $\frac{eB}{2\pi}$ at $T = 0$ and $\Omega = 0.0005$ (in unit of $\sqrt{eB}$) (first); $\beta = 100$, $\Omega = 0.0001$ (second); $\beta = 100$, $\Omega = 0.0005$ (third); $\beta = 40$, $\Omega = 0.0001$ (fourth)

Figure 24. Finite temperature effective potential $\mathcal{V}(\sigma)$ at $\beta = 80/\sqrt{eB}$ and $\mu = 0.007/\sqrt{eB}$ as a function of σ in units of $\sqrt{eB}$: $\Omega = 0$ (top) and $\Omega = 0.0003\sqrt{eB}$ (bottom)

Figure 25. Mass gap σ/Λ in the strong coupling regime with $g_r = -4$, as a function of $\Omega/(10^{-4}\Lambda)$ for $\Lambda/\sqrt{eB} = 5$ (top) and $\Lambda/\sqrt{eB} = 3$ (bottom).

Figure 26. The charge distribution (214) in the LLL in a closed volume V

with overall charge neutrality, for $N = 1000$ as a function of r and in units of eB.

Figure 27. Under the action of an external magnetic field B the $\pi^{\pm}$ undergo opposite rotations in the Lowest Landau Level (LLL) which is degenerate. The action of a parallel rotation ($\vec{\Omega} \cdot \vec{B} > 0$) lifts the degeneracy in the LLL. The energy of the π^+ shifts down and splits away from the energy of the π^- that shifts up. The action of an anti-parallel rotation ($\vec{\Omega} \cdot \vec{B} < 0$) exchanges the role of π^+ and π^-.

Figure 28. The mean number of condensed pions $\mathbb{N}_{\pi^+} = \mathbb{N}_{\pi^-}$ in the range $0.04\, m_\pi \leq \Omega \leq 0.06\, m_\pi$, for $\mu_f = 0.86\, m_\pi$ and $0.5\, m_\pi \leq T \leq 1.5\, m_\pi$.

Figure 29. $N_f - 1 = 2$ antipodal 8_L light branes, and one 8_H heavy brane shown in the τU plane, with a bulk $SU(2)$ instanton embedded in 8_L and a massive HL-string connecting them.

Figure 30. $T_c/\sqrt{\sigma_1}$ versus N_c in (368) (upper curve) compared to the numerical fit to the lattice results (lower curve) from [100].

Figure 31. $T_c/\sqrt{\sigma_1}$ versus N_c in (386). The dots are the lattice results from [101].

Figure 32. Eigenvalue distribution for the chiral Dirac matrices $\mathbf{D}$ for $\mu/\mu_c = 0.9$ and $\tau = 1$.

Figure 33. Eigenvalue distribution for the deformed Wishart $\mathbf{W}$ matrices for $\mu/\mu_c = 0.9$ and $\tau = 1$.

Figure 34. Saddle point surface $r_0(x_0, y_0)$ viewed along $0 < x_0 < 2$ for $\mu^2 = \frac{1}{4}$ and $\tau = 1$. The lateral axis is y_0, the height is r_0 and the depth is x_0.

Figure 35. Saddle point surface $r_0(x_0, y_0)$ viewed along $-2 < x_0 < 0$ for $\mu^2 = \frac{1}{4}$ and $\tau = 1$. The lateral axis is y_0, the height is r_0 and the depth is x_0. The pinch at $r_0(x_0, y_0) \equiv 0(-1, 0)$ is the chiral point in the deformed Wishart spectrum.

Acknowledgements

No words could express my gratitude to Prof Ismail Zahed for his constant support and guidance during the last four years. At no time I will forget all those discussions we have had from sunrise to moon-rise, all the night we spent together in the physics building ,all invaluable knowledge and principles inculcated to me, and all his encouragements and inspirations that will always sustain me at hard times.

I would like to thank Prof Edward Shuryak for our discussion on instanton dyon model and other physics topics, and to Prof Maciej A. Nowak for our discussion on random matrix theories. I would like to thank nuclear theory group for providing me financial support. I will also thanks Professor Martin Roceck for his honest help in Spring 2014.

Thanks professor Peter van Nieuwenhuizen for his helpful class on advanced quantum field theory. Thanks all those with whom we have had discussions, arguments or even disputes. Thanks all those with whom we share classrooms ,office spaces and living apartments.

Finally, best wishes to my family for their priceless understanding and care.

1 Introduction and Organization

This thesis consists of several studies in non-perturbative QCD, most of which have appeared in several published works summarized earlier. The common theme of these studies evolve around the complexity of addressing QCD in the infrared using various non-perturbative theoretical tools that can be viewed as complementary to the numerical studies using primarily the lattice. The thesis will consists mainly of four studies, each of which will be detailed in separate chapters below. This introduction will help streamline the chapters by giving a brief overall perspective of their content and the key achievements.

Part I: Instanton-dyon liquid model

Instantons are self-dual or anti self-dual solutions to the Yang-Mills equations in R^4. At zero temperature, they are classified by their topological charge and can be systematically analyzed using the ADHM-construction. Physically, they are tunneling solutions between local-minima with different Chern-number, and when coupled to fermions, they distinguish chirality by the index theorem.

At finite temprature on $S^1 \times R^3$ with periodic boundary condition along S^1, we have more self-dual and anti self-dual solutions. The simplest set of such solutions are instanton-dyons. The basic building block is essentially the $SU(2)$ BPS monopole whereA^4 plays they role of the Higgs field. For an $SU(N_c)$ theory at finite temperature $\beta = \frac{1}{T}$ with a Polyakov line

$$P = Pe^{i\int_0^\beta A_4 dx_4}|_{\vec{x}\to\infty} = diag(e^{i\mu_1}, ...e^{i\mu_N})$$

there are N_c independent instanton-dyons, of which $N_c - 1$ are time independent, and one that is time dependent. For $SU(2)$, the time independent one is referred to as an M dyon, and the time dependent one as an L dyon. Their charges (q, e, m) are given by $(\nu, 1, 1)$, $(1-\nu, -1, -1)$ for the M,L dyons, and $(-\nu, 1, -1)$ and $(\nu - 1, -1, 1)$ for their anti-dyon partners $\bar{M}, \bar{L}$. Here $P = \cos \pi\nu$. When $\nu = \frac{1}{2}$ we have $P = 0$ with restored center-symmetry, which is an important feature of the confining vacuum.

While mathematically the instanton-dyons and their topological counterparts are relatively simple to construct, their many-body contribution

to thermal Yang-Mills theory is involved and is the main subject of our study. At asymptotically high temperature T, QCD-like theories are in a weakly coupled state known as the Quark-Gluon Plasma (QGP). In it solitons – instantons and their constituents, monopoles etc – have large action $S = O(1/\alpha_s) \gg 1$. Their semi-classical treatment is parametrically reliable, but their density is exponentially suppressed by e^{-S}. As a result their effects are small.

However, as the temperature decreases the semi-classical action S decreases. Since the soliton density grows as a power of $1/T$ their contribution to the QCD partition increases. At a critical density fixed by T_c, confinement sets in, and the near-zero expectation value of the Polyakov line $\langle P \rangle \approx 0$ switches off the quark component of the QGP, as well as the (non-diagonal) gluons. Below the critical temperature T_c, the solitons dominate the field ensemble.

The major questions at the transition point are: (i) are these objects still made of strong enough fields, allowing for a semi-classical analysis; (ii) are their interactions weak enough to preserve their individual identity; (iii) are the semi-classical interactions in the thermal ensemble amenable to known methods of many-body theory. As we will argue below, the two first questions will be answered in the affirmative, and the third one also, provided that the ensemble is dense enough.

The instanton liquid model developed in the 1980′s is an example of such a semi-classical treatment. In vacuum at $T = 0$, the action per typical SU(3) instanton was found to be large with $S \sim 12$, and the inter-instanton and anti-instanton interactions tractable. The non-perturbative vacuum topological fluctuations are related to the explicit violation of the axial U(1), and the formation of fermionic zero modes. The collectivization of the fermionic zero modes leads to the spontaneous breaking of flavor chiral symmetry [1] (and references therein). More recently, instanton-induced effects were found to be important for hadronic spin physics [2].

However, around the critical temperature $T \sim T_c$, instantons should know about the non-vanishing of the Polyakov line expectation value, also referred to as a non-trivial holonomy. Instantons with non-trivial holonomies were found in [3]. The key discovery was that large holonomies split instantons into N_c constituents, the self-dual instanton-dyons. Since these objects have nonzero Euclidean electric and magnetic charges and source Abelian (diagonal) massless gluons, the corresponding ensemble is an "instanton dyon plasma"

We note that the electric dyon field is real in Euclidean space-time but imaginary in Minkowski space. The instanton-dyons are also referred to as instanton-monopoles or instanton-quarks. However, the notion of a non-zero holonomy and all the instanton-related contructions do not exist outside of the Euclidean finite-T formulation. On the lattice, both the electric and magnetic charges of the instanton-dyons are observable by standard Gaussian surface integrals.

Diakonov and Petrov [83] emphasized that, unlike the (topologically protected) instantons, the dyons interact directly with the holonomy field. They further suggested that since such dyon (anti-dyon) fields become significant at low temperature, they may be at the origin of a vanishing of the mean Polyakov line, or confinement. This mechanism is similar to the Berezinsky-Kosterlitz-Thouless-like transition of instantons into fractional "instanton quarks" suggested earlier by Zhitnitsky and others [6], inspired by the fractionalization of the topological charge in 2-dimensional CPN models [7], although it is substantially different in details. It is also different from the random dyon-anti-dyon ensemble suggested earlier by Simonov and others [8]. It is not yet clear how this Euclidean mechanism relates to the the quantum condensation of magnetic monopoles suggested initially by t$'$ Hooft [9] and Mandelstam [10], and subsequently supported in the supersymmetric model discussed by Seiberg and Witten [11]. In many ways, it is similar to the 3-dimensional monopole plasma discussed by Polyakov [12].

Unsal and Yaffe [13] , using a double-trace deformation of Yang-Mills at large N on $S^1 \times R^3$, argued that it prevents the spontaneous breaking of center symmetry. A similar trace deformation was used in the context of two-dimensional (confining) QED with unequal charges on $S^1 \times R$ [14] to analyze the nature of center symmetry and its spontaneous breaking. This construction was extended to QCD with adjoint fermions by Unsal [15], and by Unsal and others [44] to a class of deformed supersymmetric theories with soft supersymmetry breaking. While the setting includes a compactification on a small circle, with weak coupling and an exponentially *small* density of dyons, the minimum at the confining holonomy value is induced by the repulsive interaction in the dyon-anti-dyon pairs (called *bions* by the authors). The supersymmetry is needed to calculate the contribution of the dyon-anti-dyon pairs , and, even more importantly, for the cancellation of the perturbative Gross-Pisarski-Yaffe-Weiss (GPYW) holonomy potential [16].

Before we get into the details of the various approximations to our analysis, let us try to provide some qualitative answers to the three generic ques-

tions formulated above: (i) At $T \sim T_c$, we will consider the action per dyon (anti-dyon) to be still large or $S \sim 4$ whatever N_c; (ii) The dyon interactions will be of the order of $\Delta S_{\rm int} \sim 1 \ll S$. The quantum (one-loop) interactions are several times smaller and naively can be considered small. However they are quite non-trivial and the repulsion they provide would be our key finding. (iii) In general, the dyon plasma is strongly coupled and it is hard to treat it analytically. However we will argue below that in some window of temperatures (below T_c) one can still use the Debye-Huckel plasma theory, and more generally the hypernetted chain re-summation developed for dense Coulomb liquids.

A major contribution to the understanding of the one-loop dyon interaction has been made by Diakonov and others [83, 5]. They have found that at $T > T_c$ their interaction with the surrounding QGP leads to a linear (confining) potential between the dyons, proportional to the perturbative Debye mass. Since in this work we will only consider the opposite case $T < T_c$, this will not be included in what follows. Key to the one-loop effect is the explicit quantum weight of the KvBLL instantons in terms of the collective coordinates of the constitutive dyons at all separations. The self-dual sector is characterized by a moduli space with a hyper-Kahler metric. Its volume element is given by the determinant of Coulomb-like matrix. We will refer to it as Diakonov determinant.

In his first attempts to treat the dyonic plasma, Diakonov kept only the one loop determinant, the volume of the moduli space, ignoring the QGP screening effects and – as we will discuss in detail – the even larger classical dyon-anti-dyon interaction. Furthermore, he assumed that the attractive and repulsive terms induced by the determinant cancel out on average. We disagree on this conclusion as we detail below. Indeed, Bruckmann and others in [20] tried to generate configurations of randomly placed dyons using the determinantal measure, and observed that for the physically relevant dyonic densities, the determinantal measure develops negative eigenvalues. This makes no sense if the measure is to account for the volume of the dyonic moduli space. We will show that this issue may become resolved in a strongly correlated ensemble.

It is well known that the separate treatment of self dual and anti-selfdual sectors is only justified in the context of supersymmetry where self-duality is dual to holomorphy. In QCD-like theories, the interaction between self dual and anti-selfdual sectors is strong and not factorizable. It is described semi-classically by a "streamline" with a classical inter-particle potential of

order $1/\alpha_s$, which is larger than the 1-loop quantum induced potential of order α_s^0. Furthermore, configurations with too strongly overlapping objects with small action, are not subject to the semiclassical treatment. To account for that one usually relies on the use of a "repulsive core" as in the instanton liquid model for instance.

As we will discuss in detail, the classical dyon-antidyon interaction [21] is about an order of magnitude stronger than the one-loop Coulomb effects. It generically leads to the dyon plasma in the strongly coupled regime, with $e^{-V_{D\bar{D}}} \gg 1$. We will however focus on the very dense regime of such plasma, in which screening is strong enough that statistical mechanics of the ensemble can be treated by a variant of the Debye-Huckel mean field plasma theory. In such case the screening length is short enough to fence the system from strong coupling correlations and molecular-type instabilities induced by the streamline. The more dilute systems such as those appearing at $T > T_c$, will not be discussed in this work, as they need more powerful many-body methods, such as e.g. strongly coupled Coulomb plasmas many-body physics re-summations [22, 23] (and references therein). As we will show, in this case the free energy has a minimum at the "confining" holonomy value $v = \pi T$

The organizagion of part I is as follows:

In this first section, we will be (i) introducing the strong correlations between dyons and anti-dyons as described by the streamline [21]; (ii) showing that the determinantal interactions induced by the moduli space for dyons or anti-dyons are mostly repulsive causing the moduli volume to vanish for randomly distributed dyons; (iii) showing that suitably organized dyons to account for screening correlations yield finite moduli volumes; (iv) deriving an explicit 3 dimensional effective action that account exactly for the screening of dyons and anti-dyons on the moduli space with strong inter-dyon-anti-dyon streamline interactions; We then stay in the confining vaccum, leave the question about the potential determination of ν to the next section in more detail , and (v) deriving the Debye-Huckel corrections induced by the dyons and anti-dyons to the leading Pressure for the dyonic plasma and using it to asses the critical temperature for the SU(2) plasma; (vi) providing the explicit results for the gluon topological susceptibility and compressibility near the critical temperature in the center symmetric phase; (vii) deriving the scalar and charged structure factors of the dyonic plasma showing explicit screening of both electric and magnetic charges at large distances with

explicit predictions for the electric and magnetic masses; (viii) showing that the strongly coupled dyonic plasma supports both electric and magnetic confinement.

In the second section, we continue our investigation of the instanton-dyon model in the dense regime . Using the same lineraized expansion for the constraint equation which is valid in the dense regime, we obtain an effective description for the ensemble in terms of uncontraint instanton-dyons interact via the new effective interaction which is atractive in the magnetic channel. For this ensmble, we show that by summing over all tree diagrams it generates an effetic potential for the holonomy ν which prefer the center-symetric vacuum as one increase the one-dyon fugacity. And all one-loop results in the frist section remains unchanged. We also show how multi-chain and rings can be further re-summed beyond the leading clusters and explicit them with some applications. We extend our arguments to a finite vacuum angle θ. We also discuss a larger class of resummation pertinent for dense systems referred to as a hypernetted chain re-summation (HCN). We further suggest that a melted crystal of instanton-dyons and anti-instanton dyons may provide a semi-classical description of a Yang-Mills ensemble at very low temperature.

Part II: Chiral vortical and magnetic effects in QCD-like theories

The combined effects of rotations and magnetic fields on Dirac fermions are realized in a wide range of physical settings ranging from macroscopic spinning neutron stars and black holes [75], all the way to microscopic anomalous transport in Weyl metals [76]. In any dimensions, strong magnetic fields reorganize the fermionic spectra into Landau levels, each with a huge planar degeneracy that is lifted when a paralell rotation is applied. The past decade has seen a large interest in the chiral and vortical effects and their relationship with anomalies [77] (and references therein).

Perhaps, a less well known effect stems from the dual combination of a rotation and magnetic field on free or interacting Dirac fermions. Recently, it was noted that this dual combination could lead to novel effects for composite fermions at half filling in 1+2 dimensions under the assumption that they are Dirac fermions [111], and more explicitly for free and interacting Dirac fermions in 1+3 dimensions [54, 55, 56]. Indeed, when a rotation is applied

along a magnetic field, the charge density was observed to increase *in the absence* of a chemical potential. A possible relationship of this phenomenon to the Chern-Simons term in odd dimensions, and the chiral anomaly in even dimensions was suggested.

Current heavy ion collisions at collider energies in non-central collisions involve large angular momenta in the range $10^3 - 10^5\,\hbar$ [68, 69]. Recently, STAR reported a large vorticity with $\Omega \sim (9 \pm 1)\,10^{21}\,s^{-1} \sim 0.05\,m_\pi$, by measuring the global polarization of Λ and $\bar{\Lambda}$ in off central AuAu collisions in the Beam Energy Scan program [70]. During the prompt part of the collision, large magnetic fields $B \sim m_\pi^2$ are expected [73].We will show that the combined effects of magnetism plus a rotation can induce a pion superfluid phase in off-central heavy ion collision. This superfluid phase maybe at the origin of the large multi-pion correlations reported by ALICE [**?**], as also suggested by a recent non-equilibrium study [74].

The organization of part II is as follows:

In the first section we analyze fermionic systems in the presence of B and Ω in a more explicit way in both 1+2 and 1+3 dimensions. The case of 1+2 dimensions is of interest to planar materials in the context of solid state physics, while the case of 1+3 dimensions is of more general interest with relation to QCD. Recently, there have been few studies along these lines using effective models of the NJL type in 1+3 dimensions, where the phenomenon of charge density enhancement was also confirmed with new observations [55, 56]. Also, recent analyses using pion effective descriptions have suggested the possibility of Bose condensation in strong magnetic fields [57] and dense matter with magnetism or rotations [58]. In the secound section we show how the combination of a magnetic field and rotation will yields a charged scalar condensation. We make an estimate of the amount of pion condensation in current heavy ion collisions at collider energies.

Part III: Heavy-Light hadrons using Holography

In QCD the light quark sector (u, d, s) is dominated by the spontaneous breaking of chiral symmetry. The heavy quark sector (c, b, t) is characterized by heavy-quark symmetry [175]. The combination of both symmetries is at

the origin of the chiral doubling in heavy-light mesons [176, 177] as measured by both the BaBar collaboration [178] and the CLEOII collaboration [179].

Recently the Belle collaboration [132] and the BESIII collaboration [133] have reported many multiquark exotics uncommensurate with quarkonia, e.g. the neutral $X(3872)$ and the charged $Z_c(3900)^{\pm}$ and $Z_b(10610)^{\pm}$. These exotics have been also confirmed by the DO collaboration at Fermilab [134], and the LHCb collaboration at CERN [135]. LHCb has reported new pentaquark states $P_c^+(4380)$ and $P_c^+(4450)$ through the decays $\Lambda_b^0 \to J\Psi p K^-, J\Psi p \pi^-$ [136]. More recently, five narrow and neutral excited Ω_c^0 baryon states that decay primarily to $\Theta_c^+ K^-$ were also reported by the same collaboration [137]. These flurry of experimental results support new phenomena involving heavy-light multiquark states, a priori outside the canonical classification of the quark model.

Some of the tetra-states exotics maybe understood as molecular bound states mediated by one-pion exchange much like deuterons or deusons [138, 139, 140, 141, 142, 143, 144, 145]. Non-molecular heavy exotics were also discussed using constituent quark models [147], heavy solitonic baryons [148, 149], instantons [150] and QCD sum rules [151]. The penta-states exotics reported in [136] have been foreseen in [152] and since addressed by many using both molecular and diquark constructions [153], as well as a bound anti-charm to a Skyrmion [154]. String based pictures using string junctions [155] have also been suggested for the description of exotics, including a recent proposal in the context of the holographic inspired string hadron model [156].

The holographic construction offers a framework for addressing both chiral symmetry and confinement in the double limit of large N_c and large t'Hooft coupling $\lambda = g^2 N_c$. A concrete model was proposed by Sakai and Sugimoto [157] using a $D4$-$D8$ brane construction. The induced gravity on the probe N_f $D8$ branes due to the large stack of N_c $D4$ branes, causes the probe branes to fuse in the holographic direction, providing a geometrical mechanism for the spontaneous breaking of chiral symmetry. The DBI action on the probe branes yields a low-energy effective action for the light pseudoscalars with full global chiral symmetry, where the vectors and axial-vector light mesons are dynamical gauge particles of a hidden chiral symmetry [158]. In the model, light baryons are identified with small size instantons by wrapping $D4$ around S^4, and are dual to Skyrmions on the boundary [162, 163]. Remarkably, this identification provides a geometrical description of the baryonic core that is so elusive in most Skyrme models [164]. A first principle description of the baryonic core is paramount to the understanding of heavy

hadrons and their exotics since the heavy quarks bind over their small Compton wavelength. In this construction, the heavy baryons will be sought in the form of a bulk instanton in the worldvolume of $D8$ bound to heavy-light vector mesons, primarily the heavy-light $(0^-, 1^-)$ multiplet. This approach will extend the bound state approach developed in the context of the Skyrme model [154, 166] to holography. We note that alternative holographic models for the description of heavy hadrons have been developed in [159, 160] without the dual strictures of chiral and heavy quark symmetrty.

The organization of part III is as follows:

In the first part we propose a holographic description of heavy baryons and their exotics that involve light and heavy degrees of freedom through a variant of the $D4$-$D8$ model that includes a heavy flavor [165] with both chiral and heavy-quark symmetry. The model uses 2 light and 1 heavy branes where the heavy-light mesons are identified with the string low energy modes, and approximated by bi-fundamental and local vector fields in the vicinity of the light probe branes. Their masses follow from the vev of the moduli span by the dilaton fields in the DBI action. The model allows for the description of the radial spectra of the $(0^\pm, 1^\pm)$ heavy-light multiplets, their pertinent vector and axial correlations, and leads reasonable estimates for the one-pion axial couplings and radiative decays in the heavy-light sector. In the first section of this chapter, we setup our model and study the heavy-light baryons and exotic in $N_f = 2$ theory. We then move to $N_f = 3$ in the second section, with the prediction of many hadronic exotices to be explored at the current electron machines BELLE and BESIII, and the proton collider LHCb.

Part IV: Random matrix models for QCD

Random matrix models provide simple and universal description for many physical systems. Chiral random matrix models have been successfully applied to the study of Dirac spectra in the microscopic (ergodic) limit and some aspects of the chiral phase transition in the macroscopic (diffusive) regime. Our studies will be on these successes by extending these equilibrium type analyses of spectra to non-equilibrium set ups by formulating a hydrodynamical description for both the eigenvalues of the Polyakov line and

the Dirac operator.

In the first study of this chapter, we develop a hydrodynamical description of the gauge invariant eigenvalues of the Polyakov line for an SU(N_c) Yang-Mills theory at large but finite N_c. Lattice simulations of Yang-Mills theory in even and odd dimensions show that the confined phase is center symmetric [20, 81]. At high temperature Yang-Mills theory is in a deconfined phase with broken center symmetry. The transition from a center symmetric to a center broken phase is non-perturbative and is the topic of intense numerical and effective model calculations [82] (and references therein). Of particular interest are the semi-classical descriptions and matrix models.

In the semi-classical approximations, the confinement-deconfinement transition is understood as the breaking of instantons into a dense plasma of dyons in the confined phase and their re-assembly into instanton molecules in the deconfined phase [83, 111]. A mechanism similar to the Berezinsky-Kosterlitz-Thouless transition in lower dimensions [85], and to the transition from insulators to superconductors in topological materials [86]. In matrix models, the Yang-Mills theory is simplified to the eigenvalues of the Polyakov line and an effective potential is used with parameters fitted to the bulk pressure to study such a transition [87, 88], in the spirit of the strong coupling transition in the Gross-Witten model [89].

Matrix models for the Polyakov line share much in common with unitary matrix models in the general context of random matrix theory [120]. The canonical example is Dyson circular unitary ensemble and its analysis in terms of orthogonal polynomials or a one-component Coulomb plasma. The Dyson circular unitary ensemble relates to the Calogero-Sutherland model which is an effective model for quantum Luttinger liquids. A useful analysis of this model uses the collective quantization method developed in [91] with its hydrodynamical interpretation [92, 93].

Then ,in the second section of this part, we move to the Chiral random matrix theory for QCD at finite chemical potential. As we know, QCD breaks spontaneously chiral symmetry with a wealth of evidence in hadronic processes at low energies [103]. First principle lattice simulations strongly support that [20]. The spontaneous breaking is characterized by a large accumulation of eigenvalues of the Dirac operator near zero-virtuality [105]. The zero virtuality regime is ergodic, and its neighborhood is diffusive [106].

The ergodic regime of the QCD Dirac spectrum is amenable to a chiral random matrix model [107]. In short, the model simplifies the Dirac spectrum to its zero-mode-zone (ZMZ). The Dirac matrix is composed of

hopping between N-zero modes and N-anti-zero modes because of chirality, which are Gaussian sampled by the maximum entropy principle. The model was initially suggested as a null dynamical limit of the random instanton model [108].

QCD at finite chemical potential μ is subtle on the lattice due to the sign problem [109]. A number of effective models have been proposed to describe the effects of matter in QCD with light quarks [103]. Chiral random matrix models offer a simple construct that retains some essentials of chiral symmetry both in vacuum and matter. For instance, in the chiral 1-matrix model finite μ is captured by a constant deformation of Gaussian matrix ensembles [110, 111]. In the chiral 2-matrix model the deformation with μ is also random [112, 113]. Chiral matrix models in matter were discussed by many [114, 115]. Recently both a universal shock analysis [116] and a hydrodynamical description of the Dirac spectra were suggested [117] both at zero and finite chemical potential.

The matrix models were shown to exhibit the same microscopic universality for small eigenvalues in the ergodic regime with vanishingly small μ^2 in the large volume limit [115]. The chief observation is that in the weakly non-hermitean limit, the matrix models can be deformed in a way that preserves the global aspects of the coset manifold under the general strictures of spontaneously broken chiral symmetry and power counting in the so-called epsilon-regime [118].

At finite μ the distribution of Dirac eigenvalues in the complex plane maps onto a 2-dimensional Coulomb gas whose effective action is mostly controlled by Coulomb's law, the conformal and gravitational anomalies in 2-dimensions [117]. These constraints on the Dirac spectrum are beyond the range of chiral symmetry. The eigenvalues form Coulomb droplets that stretch and break at finite μ. The accumulation of the complex eigenvalues at the edge of the droplet may signal a new form of universality unknown to chiral symmetry. The purpose of our study is to explore this possibility using the concept of characteristic determinants for a unitary random matrix model at finite μ.

With this in mind, we start by developing a stochastic evolution for a Wishart characteristic determinant associated to the standard chiral random matrix model for QCD Dirac spectra at finite chemical potential μ, much along the lines suggested in [116] for the Ginibre ensemble. At finite μ the eigenvalues of the Dirac operator spread in the complex plane. Their accumulation in droplets break spontaneously holomorphic symmetry [110, 111].

The characteristic determinant acts as an order parameter for this breaking being zero within the droplet and finite outside. The evolution involves the eigenvalues as complex masses and their conjugates and is diffusion-like asymptotically. The universal behavior of the characteristic determinant at the edge of the Ginibre droplet observed in [116] will be exploited here to derive a universal edge behavior for the Dirac spectra at finite chemical potential.

Finally, we note that the study of deformed and non-hermitean Wishart matrices is interesting on its own as it is of interest to many other areas such as telecommunications and finances, where issues of signal to noise in the presence of attenuation or losses are relevant in designing more efficient routers or financial instruments [119].

The organization of part IV is as follows:

In the first part using the effective matrix-model based hydrodynamical description developed as mentioned before, we derive the following new results: 1/ a hydrostatic solution for the eigenvalue density that interpolates between a confining (uniform) and de-confining (localized) phase; 2/ explicit critical temperatures for the Yang-Mills transitions in $1+2$ and $1+3$ dimensions; 3/ a hydrodynamical instanton for the density distribution that captures the stochastic relaxation of the eigenvalues of the Polyakov line; 4/ an estimate of the fugacity or probability to form a $\mathrm{Z}(\mathrm{N}_c)$ bubble using a piece-wise sound-wave.

In the second part, we work out: 1/ The derivation of a closed evolution equation for the characteristic determinant for a non-hermitean deformation of Wishart matrices in relation to a 1-matrix model for the phase quenched QCD with $N_f = 4$ flavors at finite μ; 2/ An explicit derivation of the envelope of the complex eigenvalues for the deformed Wishart matrices; 3/ An explicit microscopic scaling law for the distribution of the deformed Wishart eigenvalues at the edge as traced by the envelope; 4/ An explicit scaling law on the real edge of the complex eigenvalue distribution that scales with the chiral condensate at finite μ, allowing its extraction from current and quenched Dirac spectra; 5/ An explicit microscopic scaling law for the characteristic determinant at the chiral point that scales with infinitesimal μ.

Part I: Confining instanton-dyon ensembles

2 The Confining instanton-dyon model

This section is an edited version of my publication :
Confifning dyon-antidyon Coulomb liquid model. I.
Yizhuang Liu (Stony Brook U.), Edward Shuryak, Ismail Zahed (SUNY, Stony Brook). Mar 10, 2015. 19 pp. Phys.Rev. D92 (2015) no.8, 085006

2.1 Introduction

This section is organized as follows: In section 2 we review the key elements of the dyon and anti-dyon measure derived in [83, 5] using the KvBLL instanton. The dyon-anti-dyon measure is then composed of the product of two measures with streamline interactions between the dyons and anti-dyons. We briefly detail the exact re-writing of the 3-dimensional grand-partition function in terms of a 3-dimensional effective theory in the SU(2) case. We also show that the ground state of this effective theory is center symmetric. In sections 3-6 we show that in the linearized screening approximation the dyon-anti-dyon liquid still screens both electric and magnetic charges, generates a linearly rising potential between heavy charges and confines the large spatial Wilson loops. The t′ Hooft loop in the dyon-anti-dyon ensemble is shown to be 1 modulo $\mathcal{O}(\alpha_s)$ self-energy corrections which are perimeter-like in section 7. Our conclusions are in section 8.

2.2 Interacting Dyon-Anti-Dyon Ensemble

2.2.1 The setting

The first step is the introduction of the nonzero expectation value of the 4-th component of the gauge field, which is gauge invariant since at finite temperature it enters the holonomy integral over the time period, known also as the Polyakov line. Working in a gauge in which $\langle A_4 \rangle$ belongs to the diagonal and traceless sub-algebra of $N_c - 1$ elements, one observes the standard Higgsing via the adjoint field. All gluons except the diagonal ones

become massive. We will work with the simplest case of two color gauge theory $N_c = 2$, in which there is only one diagonal matrix and the VEV of the gauge field (holonomy) is normalized as follows

$$\left\langle A_4^3 \right\rangle = v\frac{\tau^3}{2} = 2\pi T\nu\frac{\tau^3}{2} \tag{1}$$

where $\tau^3/2$ is the only diagonal color generator of SU(2). At high T it is trivial with $\nu \to 0$, and at low $T < T_c$ it takes the confining value $\nu = 1/2$. With this definition, the only dimensional quantity in the classical approximation is the temperature T, while the quantum effects add to the running coupling and its Λ parameter. Since we are working near and below T_c, we will follow the lattice practice and we use the latter as our main unit.

In the semi-classical approximation, the Yang-Mills partition function is assumed to be dominated by an interacting ensemble of dyons (anti-dyons) [83, 5]. For large separations or a very dilute ensemble, the semi-classical interactions are mostly Coulombic, and are encoded in the collective or moduli space of the ensemble. For multi-dyons a plausible moduli space was argued starting from the KvBLL caloron [3] that has a number of pertinent symmetries, among which permutation symmetry, overall charge neutrality, and clustering to KvBLL at high temperature. Since the underlying calorons are self-dual, the induced metric on the moduli space was shown to be hyper-Kahler.

The SU(2) KvBLL instanton (anti-instanton) is composed of a pair of dyons labeled by L, M (anti-dyons by $\overline{L}, \overline{M}$) in the notations of [83]. Specifically M carries $(+,+)$ and L carries $(-,-)$ for (electric-magnetic) charges, with fractional topological charges $v_m = \nu$ and $v_l = 1-\nu$ respectively. Their corresponding actions are $S_L = 2\pi v_m/\alpha_s$ and $S_M = 2\pi v_l/\alpha_s$.

The statistical measure for a correlated ensemble of dyons and anti-dyons is

$$\begin{aligned} d\mu_{D\overline{D}}[K] \equiv \quad & e^{-V_{D\overline{D}}(x-y)} \\ & \times \prod_{m=1}^{N}\prod_{i=1}^{K_m} \frac{f\, d^3x_{mi}}{K_m!}\det(G_{mi}[x]) \\ & \times \prod_{n=1}^{N}\prod_{j=1}^{\overline{K}_n} \frac{f\, d^3y_{nj}}{\overline{K}_n!}\det(G_{nj}[y]) \end{aligned} \tag{2}$$

The streamline interactions induced by the potential $V_{D\bar{D}}$ correlate the two otherwise statistically independent dyon and anti-dyon sectors. (Note that by the potential we mean the extra action and not the energy, thus no extra $1/T$). Asymptotically,

$$V_{D\overline{D}}(x-y) \to \sum_{mn,ij} \frac{C_D/2}{\alpha_s T} \frac{Q_{mi}\overline{Q}_{nj}}{|x_{mi}-y_{nj}|} \tag{3}$$

is a Coulomb-like classical interaction between dyons and anti-dyons. Here x_{mi} and y_{nj} are the 3-dimensional coordinate of the i-dyon of m-kind and j-anti-dyon of n-kind. At shorter separations the streamline stops at certain distance $a_{D\bar{D}}$, we will refer to it as a "core size". While the interaction is more complex than just electric Coulomb, it is proportional to the electric charges $Q, \overline{Q}$. In general those are the (Cartan) roots of $SU(N_c)$ supplemented by the affine root. They satisfy

$$Q_{mi}\overline{Q}_{nj} \equiv -\left(2\delta_{mn} - \delta_{m,n+1} - \delta_{m,n-1}\right) \tag{4}$$

The dimensionality of $G[x]$ is $(K_1 + ... + K_N)^2$ and similarly for $G[y]$. Their explicit form can be found in [83, 5]. In the SU(2) case there is only one electric charge.

The semiclassical 3-density of all dyon species $n_D \equiv n_L + n_M + n_{\bar{L}} + n_{\bar{M}}$ is

$$n_D = \frac{dN}{d^3x} = \frac{CT^3\, e^{-\frac{\pi}{\alpha_s}}}{\alpha_s^2} \tag{5}$$

where C is a constant to be determined below (see (55)). (5) can be re-written using the asymptotic freedom formula for SU(2) pure gauge theory with $2\pi/\alpha_s(T) = (22/3)\ln(T/\Lambda)$ in terms of the scale parameter Λ. The dimensionless density

$$\frac{n_D}{T^3} \sim \left(\frac{\Lambda}{T}\right)^{11/3} \tag{6}$$

is small at high T but increases as T decreases. With the exception of section 2.3.7, where we will estimate the critical deconfinement temperature

by including perturbative $\mathcal{O}(\alpha_s^0)$) effects in the dimensionless pressure, we will always assume the temperature to be small enough, so that the dyons effect are the dominant ones. The dyon fugacity f is

$$f \approx \frac{n_D}{8\pi} \tag{7}$$

to order $\mathcal{O}(n_D^{3/2})$ in the dyon density (see below). The absolute value of the parameter Λ appearing in the semiclassical formulae can be related to standard parameters like $\Lambda_{\overline{MS}}$, but this has no practical value since the accuracy with which they are known is too low to give an accurate value of the dyonic density. In practice it is obtained from the fit to the lattice instanton data performed in [107] in the range $0.5 < T/T_c < 3$. The caloron action – the sum of S_L and S_M – is then writen as

$$S_{L+M}(T) \equiv \frac{2\pi}{\alpha_s(T)} \equiv \frac{22}{3}\ln\left(\frac{T}{0.36\,T_c}\right) \tag{8}$$

We will use this fit as a basis for our running coupling. In particular, the action of the SU(2) caloron at T_c $S_{\rm L+M}(T_c) \approx 7.47$ translates to the value of the coupling $\alpha_s(T_c) = 0.84$. Since in this section we only work in the confining regime of the holonomy with all dyon actions identical, the action per dyon is about 3.75.

The repulsive linear interaction between unlike dyons (anti-dyons) found in [5] acts as a linearly confining force in the center asymmetric phase, favoring the molecular or KvBLL configuration at $T > T_c$. This interaction stems from QGP thermal quanta scattering on the dyons. However, we will be interested in this section in the center symmetric phase at $T > T_c$, in which there is no QGP, we do not include this interaction.

Since the classical $V_{D\bar{D}} \sim 1/\alpha_s$ it dominates the quantum determinants, which include Coulomb interaction of order α_s^0. On this point we differ from the argument presented in [83] regarding the re-organization of (3) in an extended quantum determinant. At large relative separations between all particles the measure (3) is exact. It is also exact when each bunch of dyons or anti-dyons coalesce into a KvBLL instanton or anti-instanton at all separations.

The above notwithstanding, the grand-partition function associated with the measure (3)

$$\mathcal{Z}_{D\overline{D}}[T] \equiv \sum_{[K]} \int d\mu_{D\overline{D}}[K] \tag{9}$$

describes a highly correlated ensemble of dyon-anti-dyons which is no longer integrable in the presence of the streamline. The case $V_{D\overline{D}} = 0$ amounts to $\mathcal{Z}_{D\overline{D}} \to \mathcal{Z}_D \mathcal{Z}_{\overline{D}}$ where each factor can be exactly re-written in terms of a 3-dimensional effective theory. We now analyze (9) for the SU(2) case following and correcting the arguments in [83].

$$\begin{aligned}\mathcal{Z}_{D\overline{D}}[T] \quad &\equiv \sum_{[K]} \prod_{i_L=1}^{K_L} \prod_{i_M=1}^{K_M} \prod_{i_{\bar{L}}=1}^{K_{\bar{L}}} \prod_{i_{\bar{M}}=1}^{K_{\bar{M}}} \\ &\times \int \frac{f d^3 x_{L i_L}}{K_L!} \frac{f d^3 x_{M i_M}}{K_M!} \frac{f d^3 y_{\bar{L} i_{\bar{L}}}}{K_{\bar{L}}!} \frac{f d^3 y_{\bar{M} i_{\bar{M}}}}{K_{\bar{M}}!} \\ &\times \det(G[x]) \det(G[y])\ e^{-V_{D\overline{D}}(x-y)}\end{aligned} \tag{10}$$

with $G[x]$ a $(K_L + K_M)^2$ matrix and $G[y]$ a $(K_{\bar{L}} + K_{\bar{M}})^2$ matrix whose explicit form are given in [83, 5].

2.2.2 Classical dyon-antidyon interactions

The explicit form of the Coulomb asymptotic in (103) for the SU(2) case is

$$\begin{aligned}&V_{D\overline{D}}(x-y) \to -\frac{C_D}{\alpha_s T} \\ &\times \left(\frac{1}{|x_M - y_{\overline{M}}|} + \frac{1}{|x_L - y_{\overline{L}}|} - \frac{1}{|x_M - y_{\overline{L}}|} - \frac{1}{|x_L - y_{\overline{M}}|} \right)\end{aligned} \tag{11}$$

The strength of the Coulomb interaction in (11) is C_D/α_s and is of order $1/\alpha_s$. It follows from the asymptotics of the streamline configuration. In Fig. 1 we show the attractive potential for the SU(2) streamline configuration in the $M\bar{M}$ channel [21]. The solid curve is a numerical fit to the data given by

$$V_{D\bar{D}}(r) \equiv s_{D\bar{D}}\, V(r) = s_{D\bar{D}}\, \frac{Av}{g^2} \frac{(r \cdot v - B)^2}{(r \cdot v)^3 + C} \tag{12}$$

with $s_{M\bar{M}} = -1$ in units of the critical temperature T_c and g set to 1 and $A = 30.9, B = 0.9072, C = 15.795$. The dashed line corresponds to the Coulomb asymptotics

$$V_{M\bar{M}}(r) \approx -\frac{C_D}{\alpha_s r} \tag{13}$$

with $C_D = A/4\pi = 2.46$. We recall that in the uncombed $D\bar{D}$ potential, the asymptotic Coulomb interaction corresponds to $C_D = 2$. The attraction in the streamline is stronger asymptotically owing to the relative combing between the dyons. Fig. 1 shows that the $D\bar{D}$ core is about $a_{D\bar{D}} \approx 1/T$. The second observation is that one should not use the Coulomb asymptotic (the lower dashed curve) but the actual potential which correctly takes care of the dyons, as extended charged objects rather than point charges.

Below the core value of $a_{D\bar{D}}$, the streamline configuration annihilates into perturbative gluons making the parametrization (12) arbitrary. Throughout, we will parametrize the core by a constant, replacing (12) by

$$V_{D\bar{D}}(r) \equiv s_{D\bar{D}} \left(V(r)\theta(r - a_{D\bar{D}}) + V(a_{D\bar{D}})\theta(a_{D\bar{D}} - r)\right) \tag{14}$$

with $s_{M\bar{M}} = s_{L\bar{L}} = -1$ (attractive) and $s_{L\bar{M}} = s_{L\bar{M}} = +1$ (repulsive).

The ensemble (103) can be viewed as a 4-component dense and strongly coupled liquid. The quantity in the exponent, known as the classical plasma parameter

$$\Gamma_{D\bar{D}} = V(a_{D\bar{D}}) \approx \frac{C_D/\alpha_s a_{D\bar{D}}}{3T_c} \approx 1 \tag{15}$$

is not small. Its exponent $e^{\Gamma_{D\bar{D}}}$ can be even large. This implies that the "dyonic plasma" we want to study belongs to a class of *strongly coupled* plasmas, with non-negligible correlations between the particles. So a priori, this problem should be studied by methods more powerful than the usual mean field approximations, such as the Debye-Huckel theory. However, we will show below that when the dyonic densities are sufficiently large (and that implies the overall T of the ensemble to be sufficiently low), the screening mass gets large enough to put the effective – screened – interaction inside the domain in which the analytic Debye-Huckel theory becomes justified.

Furthermore, as we will detail below, the treatment of the repulsive core is in fact a rather sensitive issue. We chose the "most smooth" version of the potential, shown by the solid curve in Fig. 1. Its Fourier transform provides a smooth form factor in momentum space. We note that the actual streamline was only found for distances $r > a_{D\bar{D}} \approx 1.2$ (about $4/v$ in the dyon units). The upper (blue) dashed curve is an example of an arbitrary parameterization discussed in [21], extending it to smaller values of r. If one uses it, or even cut off the small $r < a_{D\bar{D}}$ region completely – the approach known as hard core or excluded volume – the Fourier transform of the potential develops large oscillations. In this case the instability of the Debye-Huckel theory becomes stronger and its applicability domain shrinks.

The use of (12) in the repulsive channels $M\bar{L}$ and $L\bar{M}$ approximates a smaller repulsion than Coulomb at shorter distances. A numerical investigation of these channels would be welcome. Note that both the measure in (103) and the asymptotic (11) do not include the quantum corrections around the streamline configuration. Both of which should add more repulsion to the interaction between D and $\bar{D}$. A leading quantum correction to the asymptotic (11) follows by analogy from the Coulomb corrections emerging from the DD and $\bar{D}\bar{D}$ determinantal interactions. In our case they are repulsive and amount to the shift

$$C_D \to C_D - \frac{2\alpha_s}{\pi} + \mathcal{O}(\alpha_s^2) \tag{16}$$

in the Coulomb constant. The relevance of this correction will be briefly discussed below.

2.2.3 Qualitative effect of the one-loop moduli space

The volume element of the moduli space of self-dual SU(2) dyons is given by $\sqrt{g_{HK}} \equiv \det G$ with g_{HK} its associated Hyper-Kahler metric [83]. As we already mentioned in the introduction, the one-loop determinant in the measure (3) must be positive definite for all configurations. Furthermore, the positivity of all eigenvalues is required, since they have the meaning of the volume element in the corresponding subspace. As noted in [20], this is not the case for ensembles with randomly placed dyons. These ensembles get denser and the positivity condition is only fulfilled for a very small fraction of the configurations.

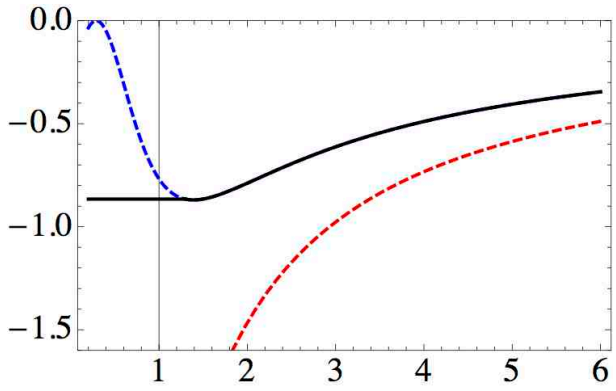

Figure 1: (Color online) Black solid line is the SU(2) $D\bar{D}$ (dimensionless) potential versus the distance r (in units of $1/T$). Upper (blue) dashed line is the parameterization proposed in Ref.[21], the lower (red) (dashed) line is the Coulomb asymptotics.

In fact one of the main issues of the dyonic ensembles is the non-trivial character of the one-loop interaction induced by the Diakonov determinant. Before we show how this carries to our case through various fermionization and bosonization and diagrammatic re-summations, it is instructive to provide a qualitative understanding of the issues using simple explicit examples.

Although it is well known, for completeness let us start with the simplest case of two dyons in the SU(2) theory with symmetric holonomy $\nu = \bar{\nu} = 1/2$. Omitting the overall factors, Diakonov 2×2 matrix G reads

$$G_{2\times 2}[x] \sim \begin{pmatrix} 1 \pm \frac{1}{vx_{12}} & \mp \frac{1}{vx_{12}} \\ \mp \frac{1}{vx_{12}} & 1 \pm \frac{1}{vx_{12}} \end{pmatrix} \tag{17}$$

with $x_{12} \equiv |\vec{x}_{(1)} - \vec{x}_{(2)}|$ the distance between the dyons in units of $1/v = 1/\pi T$. The upper signs are for different (ML) dyons, and the lower for similar (MM, LL) pairs. The metric-induced potential is thus $V(x_{12}) \equiv -\ln\det G = -\ln\left(1 \pm 2/(vx_{12})\right) \approx \mp 2/(vx_{12})$ is Coulomb-like at large distances. (At short distances the induced potential is proportional to $\ln(1/r)$ and not $1/r$. There is no divergence in the partition function.)

Let us now consider an ensemble of several ($N = 8$) dyons with $N_M = N_L = 4$ and set them randomly in a cube of size a. We then evaluate all

inter-dyon distances and calculate $\det G[x]$ (which is now an 8×8 matrix) as a function of the Coulomb parameter $\epsilon = 1/(\pi a T)$. For each sampling, the determinant is a polynomial of ϵ of degree N. The results of 10 random samplings are displayed in Fig.2 by the dashed lines. For small ϵ the determinant deviates from 1 in a non-uniform way. Some configurations are Coulomb attractive with $\det G > 1$, while some others are repulsive with $\det G < 1$ for small ϵ. To first order, they average to zero for a large number of charges as there are equal number of positive and negative ones. At next order, the attraction is to win thanks to the general theorem of second order perturbation theory. However, we observe that already for $\epsilon = 1/(\pi a T) \sim 0.2$ the repulsive trend is dominant and $\det G < 0$ for some samplings. This means that the moduli space of these configurations vanishes at the corresponding density. This sets an upper limit on the density of random ensembles of dyons

$$n < n_{\rm max} = 8\,(0.2\,\pi T)^3 \sim 1.98\,T^3 \tag{18}$$

The lesson: Diakonov determinantal interaction for randomly placed dyons is strongly repulsive, reducing dramatically the moduli space all the way to zero size for small ϵ. It amounts to a strong effective core of order α_s^0.

However this is not the end of the story. Let us look at the opposite case of a well ordered arrangement of dyons in the unit box. For that we pre-arrange the 8 dyons of the previous ensemble in a salt-like or fcc configuration on the unit cube, and assess the corresponding $\det G$. The result is shown in Fig. 2 by the solid line. While the qualitative trend is the same – attraction at some interval of densities, changing to repulsion and then reaching zero at some density – the value of the maximal density to be reached is changed by a large factor of about $5^3 = 125$. Here is lesson number 2: the moduli space can be made much larger for the same inter-particle Coulomb strength ϵ, if the correlations between charges are correctly taken into account.

The overall lesson we get from those examples is the following: Diakonov's original suggestion that attraction and repulsion would always cancel out is incorrect. Our analysis shows that ultimately the repulsion always wins and at some density the volume of the moduli space always goes to zero. However, correctly implemented correlations between charges to maximize screening locally, can increase this critical density by about two orders of magnitude.

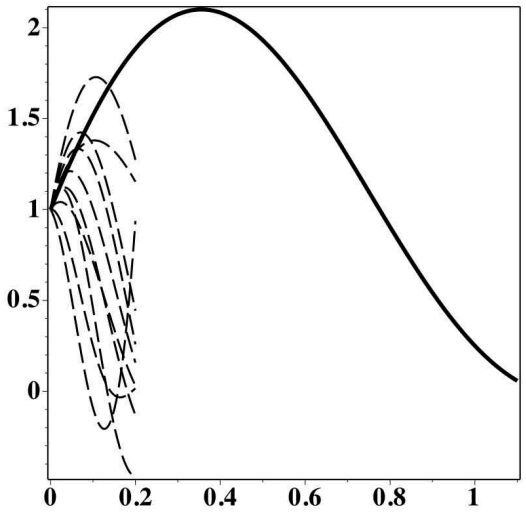

Figure 2: (Color online) $\det G$ as a function of $\epsilon = 1/(\pi a T)$. The dashed lines are for 8 dyons randomly placed in a cube of size $a \equiv 1$. The solid line is for correlated dyons in a salt-like or fcc configuration also in a unit cube.

2.2.4 Fermionization and Bosonization

Following [83] each determinant in (103) can be fermionized using 4 pairs of ghost fields $\chi^\dagger_{L,M}, \chi_{L,M}$ for the dyons and 4 pairs of ghost fields $\chi^\dagger_{\bar{L},\bar{M}}, \chi_{\bar{L},\bar{M}}$ for the anti-dyons. The ensuing Coulomb factors from the determinants are then bosonized using 4 boson fields $v_{L,M}, w_{L,M}$ for the dyons and similarly for the anti-dyons. The result is a doubling of the 3-dimensional free actions obtained in [83]

$$\begin{aligned} S_{1F}[\chi, v, w] &= -\frac{T}{4\pi}\int d^3x \\ &\big(|\nabla\chi_L|^2 + |\nabla\chi_M|^2 + \nabla v_L\cdot\nabla w_L + \nabla v_M\cdot\nabla w_M\big) + \\ &\big(|\nabla\chi_{\bar{L}}|^2 + |\nabla\chi_{\bar{M}}|^2 + \nabla v_{\bar{L}}\cdot\nabla w_{\bar{L}} + \nabla v_{\bar{M}}\cdot\nabla w_{\bar{M}}\big) \end{aligned} \tag{19}$$

For the interaction part $V_{D\bar{D}}$, we note that the pair Coulomb interaction in (11) between the dyons and anti-dyons can also be bosonized using the standard trick [12] in terms of σ and b fields. Here σ and b are the un-Higgsed long range U(1) parts of the original magnetic field F_{ij} and electric potential

A_4 (modulo the holonomy) respectively. As a result each dyon species acquire additional fugacity factors such that

$$M : e^{-b-i\sigma} \quad L : e^{b+i\sigma} \quad \bar{M} : e^{-b+i\sigma} \quad \bar{L} : e^{b-i\sigma} \tag{20}$$

These assignments are consistent with those suggested in [44, 45] using different arguments. As a result there is an additional contribution to the free part (19)

$$\begin{aligned} S_{2F}[\sigma, b] &= T \int d^3x\, d^3y \\ &\times \big(b(x)V^{-1}(x-y)b(y) + \sigma(x)V^{-1}(x-y)\sigma(y)\big) \end{aligned} \tag{21}$$

with $V(r)$ defined in (12). The interaction part is now

$$\begin{aligned} S_I[v, w, b, \sigma, \chi] &= -\int d^3x \\ & e^{-b+i\sigma} f\left(4\pi v_m + |\chi_M - \chi_L|^2 + v_M - v_L\right) e^{w_M - w_L} + \\ & e^{+b-i\sigma} f\left(4\pi v_l + |\chi_L - \chi_M|^2 + v_L - v_M\right) e^{w_L - w_M} + \\ & e^{-b-i\sigma} f\left(4\pi v_{\bar{m}} + |\chi_{\bar{M}} - \chi_{\bar{L}}|^2 + v_{\bar{M}} - v_{\bar{L}}\right) e^{w_{\bar{M}} - w_{\bar{L}}} + \\ & e^{+b+i\sigma} f\left(4\pi v_{\bar{l}} + |\chi_{\bar{L}} - \chi_{\bar{M}}|^2 + v_{\bar{L}} - v_{\bar{M}}\right) e^{w_{\bar{L}} - w_{\bar{M}}} \end{aligned} \tag{22}$$

In terms of (19-22) the dyon-anti-dyon partition function (9) can be exactly re-written as an interacting effective field theory in 3-dimensions,

$$\mathcal{Z}_{D\overline{D}}[T] \equiv \int D[\chi]\, D[v]\, D[w]\, D[\sigma]\, D[b]\, e^{-S_{1F}-S_{2F}-S_I} \tag{23}$$

In the absence of the screening fields σ, b (23) reduces to the 3-dimensional effective field theory discussed in [83] which was found to be integrable. In the presence of σ, b the integrability is lost as the dyon-anti-dyon screening upsets the hyper-Kahler nature of the moduli space. We will investigate them by linearizing the screening effects in the symmetric state.

Since the effective action in (23) is linear in the $v_{M,L,\bar{M},\bar{L}}$, the latters are auxiliary fields that integrate into delta-function constraints. However and for convenience, it is best to shift away the b, σ fields from (22) through

$$
\begin{aligned}
w_M - b + i\sigma &\to w_M \\
w_{\bar{M}} - b - i\sigma &\to w_{\bar{M}}
\end{aligned} \tag{24}
$$

which carries unit Jacobian and no anomalies, and recover them in the pertinent arguments of the delta function constraints as

$$
\begin{aligned}
-\frac{T}{4\pi}\nabla^2 w_M + f e^{w_M - w_L} - f e^{w_L - w_M} &= \frac{T}{4\pi}\nabla^2 (b - i\sigma) \\
-\frac{T}{4\pi}\nabla^2 w_L + f e^{w_L - w_M} - f e^{w_M - w_L} &= 0
\end{aligned} \tag{25}
$$

and similarly for the anti-dyons. In [83] it was observed that the classical solutions to (25) can be used to integrate the w's in (23) to one loop. The resulting bosonic determinant was shown to cancel against the fermionic determinant after also integrating over the χ's in (23). This holds for our case as well. However, the presence of σ, b makes the additional parts of (23) still very involved in 3 dimensions.

After inserting the constraints in the 3-dimensional effective action in (23), the ground state corresponds to constant fields because of translational invariance. Thus, the potential per unit 3-volume V_3 following from(22) after the shifts (24) is

$$
\begin{aligned}
-\mathcal{V}/V_3 \quad &= 4\pi f \left(v_m e^{w_M - w_L} + v_l e^{w_L - w_M} \right) \\
&+4\pi f \left(v_{\bar{m}} e^{w_{\bar{M}} - w_{\bar{L}}} + v_{\bar{l}} e^{w_{\bar{L}} - w_{\bar{M}}} \right)
\end{aligned} \tag{26}
$$

To determine the ground state, we solve the constraint equation (25) with constant w's. It is easy to see that $e^{w_L - w_M} = e^{\bar{w}_L - \bar{w}_M} = 0$. Put them back into the potential, we see denpendence on ν get cancled!This lead to the conclusion that a potential for the holonomy can not be generated without going to details of the interaction. In the next section of this part, we will provide a carefull analyse of this issue and show that a potential $V(\nu)$ for ν can be generated by going beyond constant solution for the constraint equation .This potential will favor the center-symmetric ground state for large dyon fugacity f. In the remaining part of this section, we will stay in the canter-symmetric phase and probe its properties.

2.3 Linearized Screening Approximation in Center Symmetric State

For the center symmetric ground state of the 3-dimensional effective theory, we may assess the correction to the potential $\mathcal{V}$ to one-loop in the b, σ fields. This is achieved by linearizing the constraints (25) around the ground state solutions. Specifically

$$\begin{aligned}\left(-\frac{T}{4\pi}\nabla^2 + 2f\right) w_M - 2f w_L &\approx \frac{T}{4\pi}\nabla^2(b - i\sigma) \\ \left(-\frac{T}{4\pi}\nabla^2 + 2f\right) w_L - 2f w_M &\approx 0\end{aligned} \tag{27}$$

and similarly for the anti-dyons. The one-loop correction to $\mathcal{V}$ follows by inserting (27) in (23). The ensuing quadratic contributions before integrations are

$$S_{1L} = \mathcal{V} - 4\pi f \int \frac{d^3p}{(2\pi)^3} \frac{(\frac{T}{4\pi}p^2)^2}{(\frac{T}{4\pi}p^2 + 4f)^2} \left(b(p)^2 - \sigma(p)^2\right) \tag{28}$$

The coefficient of the b field appears tachyonic but is momentum dependent and vanishes at zero momentum.

2.3.1 Pressure

Carrying the Gaussian integration in b, σ in (28) yields to one-loop

$$\ln Z_{1\mathrm{L}}/V_3 = -\mathcal{V} - \frac{1}{2}\int \frac{d^3p}{(2\pi)^3} \ln\left|1 - \frac{V^2(p)}{16}\frac{p^8 M^4}{(p^2 + M^2)^4}\right| \tag{29}$$

with $V(p)$ the Fourier transform of (12)

$$V(p) = \frac{4\pi}{p^2}\int_0^\infty dr \sin r\, V_{D\bar{D}}(r/p) \tag{30}$$

and the screening mass $M = \sqrt{2n_D/T}$ with $|Q^2| = 2$ for SU(2). In Fig. 3 we show the form factor (30) in dots line in units of T_c. A simple parametrization is shown in solid line of the form

$$V(p) \approx 4\alpha \, \frac{e^{-p\, a_{D\bar{D}}}}{p^2} \, \cos(p\, a_{D\bar{D}}) \tag{31}$$

with $\alpha = \pi C_D/\alpha_s$ and a core $a_{D\bar{D}} \approx 1/T_c$. Inserting (31) into (29) and setting $\tilde{p} = p/M$ yield

$$\ln Z_{1\mathrm{L}}/V_3 = -\mathcal{V} - \frac{M^3}{2} \int \frac{d^3\tilde{p}}{(2\pi)^3} \ln \left| 1 - \tilde{\alpha}^2(\tilde{p}) \frac{\tilde{p}^4}{(\tilde{p}^2+1)^4} \right| \tag{32}$$

with

$$\tilde{\alpha}(\tilde{p}) \equiv \alpha \, e^{-M a_{D\bar{D}} \tilde{p}} \cos\left(M a_{D\bar{D}} \tilde{p}\right) \tag{33}$$

The dominant contribution to the integral in (29) comes from the region $\tilde{p} \approx 1$ for which (33) can be approximated by $\tilde{\alpha}(1) \equiv \tilde{\alpha}$. As a result (29) can be done approximately by fixing $\tilde{\alpha}$ and we have the classical contribution to the pressure

$$\frac{\mathcal{P}_{\mathrm{cl}}}{T} \equiv \ln Z_{1\mathrm{L}}/V_3 \approx n_D + \kappa(\tilde{\alpha}) \frac{M^3}{12\pi} \tag{34}$$

with

$$\kappa(\tilde{\alpha}) = \frac{2 + \frac{5}{2}\tilde{\alpha} + \frac{1}{2}\tilde{\alpha}^2}{\sqrt{1 + \frac{\tilde{\alpha}}{4}}} + \frac{2 - \frac{5}{2}\tilde{\alpha} + \frac{1}{2}\tilde{\alpha}^2}{\sqrt{1 - \frac{\tilde{\alpha}}{4}}} - 4 \tag{35}$$

(35) is seen to vanish for $\tilde{\alpha} = 0$ or in the absence of $D\bar{D}$ interactions. Near T_c the screening mass is $M \approx \sigma_E/T_c$ (see below), thus

$$\tilde{\alpha} \equiv (\pi C_D/\alpha_s) \, e^{-M a_{D\bar{D}}} \cos\left(M a_{D\bar{D}}\right) \approx -0.52 \tag{36}$$

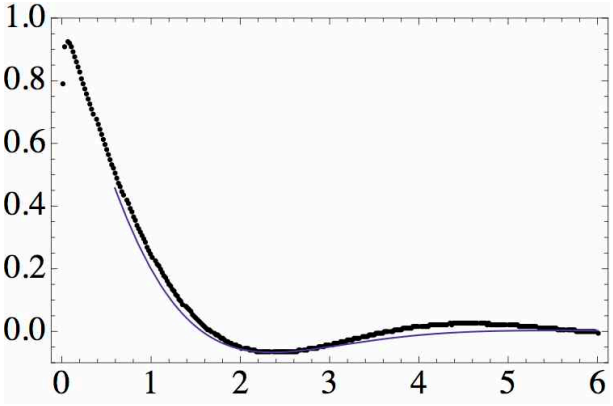

Figure 3: (Color online) The dots show the form factor, the ratio $V(p) \cdot (p^2/4\pi)$ of the Fourier transform of (12) to that of a pure Coulomb law versus p/T. The thin line is its parameterization. See text.

For $|\tilde{\alpha}| < 4$ the 1-loop contribution to the pressure from the charged $D\bar{D}$ dyons is real with no dimer or molecular instability. The large core produced by the form factor (33) is considerably screened by the large dyon density as captured by the large dielectric constant $1/\kappa(-0.52) \approx 5.26$ in (34).

The correction in (34) to the free contribution is a Debye-Huckel correction [22] (and references therein). A simple but physical way to understand it is to note that a screened Coulomb charge carries a lower constant energy

$$\frac{e^{-M|x|}}{4\pi|x|} \approx \frac{1}{4\pi|x|} - \frac{M}{4\pi} + ... \tag{37}$$

The Debye-Huckel as a mean-field estimate for the pressure follows

$$\frac{\mathcal{P}_{DH}}{T} \approx \frac{n_D M}{4\pi T} = \frac{M^3}{8\pi} \to \frac{M^3}{12\pi} \tag{38}$$

where $n_D = M^2T/2$ is the density of charged particles (see below). The standard Debye-Huckel limiting result for a multi-component ionic plasma in 3 spatial dimensions is shown on the right-most side of (38).

The correction in (34) is considerably reduced by the large screening through the effective dielectric constant played by $1/\kappa(\tilde{\alpha}) \approx 32/(15\tilde{\alpha}^2)$ for

$\tilde{\alpha} \ll 1$. In particular $1/\kappa(-0.52) \approx 5.26 \gg 1$ as noted earlier. It can be recast in the form

$$\frac{\mathcal{P}_{\rm cl}}{T^4} = \tilde{n}_D + \frac{\kappa(\tilde{\alpha})}{3\pi\sqrt{2}}\,\tilde{n}_D^{\frac{3}{2}} \tag{39}$$

with $\tilde{n}_D = n_D/T^3$. Using $Ma_{D\bar{D}} \approx \sigma_E/T_c^2 \approx 1/(0.71)^2$ for SU(2) we have $\tilde{n}_D \approx 1$, so that $\mathcal{P}_{\rm cl}/T^4 \approx (1 + 0.01))$. The screening corrections are small of the order of 1% thanks to the large dyonic densities.

The limitations of the Debye-Huckel approximation are readily seen from (29). In Fig. 4a we plot the argument of the logarithm in the last term of (29). The different curves from top to bottom follow from $Ma_{D\bar{D}} = 1.5, 1, 0.7, 0.56$ respectively. The smaller the Debye mass M the stronger the dip. For $Ma_{D\bar{D}} < 0.56$, the argument of the logarithm becomes negative resulting into an $i\pi$ contribution to the pressure and thus an instability. This is a clear indication of a well known phenomenon: the Debye-Huckel approximation is in general inapplicable for strongly coupled plasmas, and the interaction mediated by the streamline is strong. Only a large enough density of dyons, producing sufficiently strong screening, allows for the use of the Debye-Huckel theory. In Fig. 4b we show how the total integrated contribution to the free energy changes as a function of the dimensionless Debye mass $Ma_{D\bar{D}}$

$$(Ma_{D\bar{D}})^3 \int_0^\infty dp\, p^2 \ln\left|1 - \frac{V^2(pM)}{16}\frac{p^8}{(p^2+1)^4}\right| \tag{40}$$

The main lesson is that beyond the critical value of the screening, this contribution becomes rapidly very small. This is consistent with the analytical estimate above. This justifies the use of the Debye-Huckel mean-field analysis in general, and the use of the semi-classical expansion in particular.

2.3.2 Beyond the Debye-Huckel theory

The unravelling of the Debye-Huckel approximation may be due to corrections to an interacting Coulomb system, such as 1/ core corrections; 2/ dimer, tetramer and so on many-body interactions. The large core corrections were already identified and discussed above and yield a substantial reduction in the Debye-Huckel contribution near the critical value of $Ma_{D\bar{D}} \sim 0.56$.

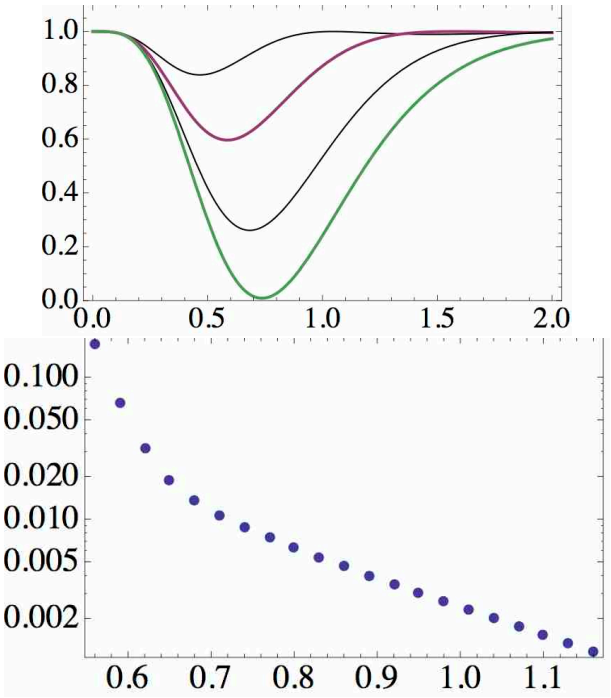

Figure 4: (Color online) (a) The argument of the logarithm in the last term of (29) versus the dimensionless momentum p, for different values of the dimensionless Debye mass $Ma_{D\bar{D}} = 1.5, 1, 0.7, 0.56$, top to bottom. As the screening mass decreases to its critical value, the lower (green) curve touches zero. The smaller values of M leads to a negative argument of the logarithm, thus an instability. (b) A semi-logarithmic plot of the integral entering in (29) as defined in (40) as a function of $Ma_{D\bar{D}}$. The decrease is steady from its maximum at the critical value of the screening mass or $Ma_{D\bar{D}} = 0.56$.

Bound state corrections in the form of electrically charged $L\bar{L}$ or $M\bar{M}$ dimers, or electrically neutral $L\bar{L}\,M\bar{M}$ tetramers commonly referred to as instanton-anti-instanton molecules, can bind through the streamline interaction (11-12). The combinations $L\bar{M}$ and $M\bar{L}$ are repulsive. The binding energy in a dimer is $\epsilon_{D\bar{D}} \approx (C_D/3)/(\alpha_s a_{D\bar{D}}) = T$. The dimer enhancement is expected to be of order $e^{\epsilon_{D\bar{D}}/T} \approx e^{(C_D/3)/\alpha_s} \approx 2.72$ for $T \approx T_c$ using the reduced effective Coulomb coupling. As we noted earlier, this enhancement becomes substantially larger at high temperature as α_s decreases with the onset of dimerization set at about $\alpha_{s,\rm crit} = \pi(C_D/3)/4 \approx 0.67$. At this coupling which occurs above T_c, the Coulomb dimer enhancement factor is $e^{C_D/3\alpha_{s,\rm crit}} \approx 3.57$.

In sum, the dyons and anti-dyons form a Coulomb liquid with strong short range correlations induced by both the finite cores and bindings. The liquid supports center symmetry and confines. The deconfinement transition is characterized by clustering into charged dimers and possibly uncharged and topologically neutral tetramers, forming mixtures with the restoration of center symmetry. Coulomb mixtures present rich phase diagrams [25].

2.3.3 Dyonic densities

(29) can be readily used to assess the dyon densities K_M and K_L (and similarly for $K_{\bar{M}}$ and $K_{\bar{L}}$) in the center symmetric vacuum with screening dyons-anti-dyons. For that we need to change $f \to \sqrt{f_M f_L}$ and take derivatives of (29) with respect to $\ln f_{M,L}$ separately and then setting them equal by bulk charge neutrality. The result per species is

$$K = \frac{1}{4} n_D + \kappa(\tilde{\alpha}) \frac{M^3}{32\pi} \tag{41}$$

for all dyon and anti-dyon species.

Each dyon (anti-dyon) is characterized by an SU(2) core of size $\rho \approx 1/(2\pi T\,\nu) \approx 0.33$ fm in the center symmetric phase with $\nu = 1/2$ at $T = 1/\text{fm}$. The Debye length $\lambda_D = 1/M \approx \sqrt{T/2n_D} \approx 0.70\,\text{fm}$ is about twice the core size. The classical Coulomb ratio for the $DD, \bar{D}\bar{D}$ pairs with a core of 2ρ is about

$$\Gamma_{DD,\bar{D}\bar{D}} \equiv \frac{1}{2\pi(2\rho)T} \approx \frac{\nu}{2} = \frac{1}{4} \tag{42}$$

is small. Recall from (15) that $\Gamma_{D\bar{D}} \approx 1$. The Coulomb $DD, \bar{D}\bar{D}$ interactions are quantum and of order α_s^0 with strength $1/\pi$ as can be seen by expanding the exponential form of the determinantal interaction in (17). The dyon-anti-dyon ensemble is close to a strongly coupled 4-component Coulomb liquid. Since the measure for the unlike dyons is exact, it is valid even in the dense configuration. It is only asymptotically exact for like dyons. For the dyons and anti-dyons the streamline is numerically exact at all separations outside its core. However its corresponding quantum determinant was not calculated. Only a qualitative correction was argued in (24).

2.3.4 Gluon condensates and susceptibilities

The topological charge fluctuates locally in this dyon-anti-dyon model. The topological susceptibility at 1-loop follows from (29) through the substitution $f \to f\cos(\theta/2)$ both in $\mathcal{V}$ and also $M \to M\sqrt{\cos(\theta/2)}$. At finite vacuum angle θ and in leading order we have

$$\begin{aligned} &\left\langle F\tilde{F} \right\rangle_\theta \equiv -\frac{T}{V_3}\frac{\partial \ln Z_{1L}}{\partial \theta} = \\ &\sin(\theta/2)\left(\frac{1}{2}n_D T + \kappa(\tilde{\alpha})\frac{M^3 T}{16\pi}\sqrt{\cos(\theta/2)}\right) \end{aligned} \tag{43}$$

Thus the topologicl susceptibility

$$\chi_T \equiv \frac{V_3}{T}\left\langle (F\tilde{F})^2 \right\rangle_0 \approx \left(\frac{1}{2}\right)^2 (n_D T) \tag{44}$$

in leading order. Since the dyons carry half the topological charge (44) shows that the topological fluctuations are Poissonian to order $\mathcal{O}(n_D^{3/2})$. The behavior of χ_T/T^4 versus T/T_c is shown in Fig. 5 with n_D defined in (55) below.

The gluon condensate to 1-loop in the screening approximation follows from

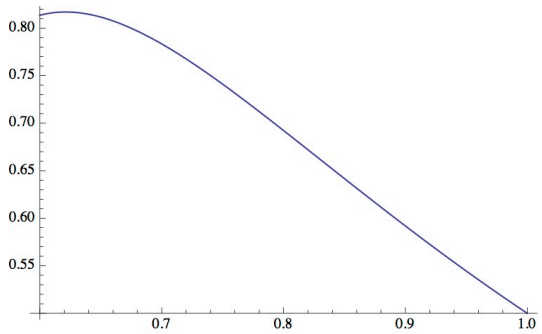

Figure 5: Topological susceptibility in units of T versus T/T_c

$$\begin{aligned}\frac{1}{16\pi^2}\left\langle F^2\right\rangle_0 &\equiv -\frac{T}{4\pi V_3}\frac{\partial \ln Z_{1L}}{\partial\, 1/\alpha_s}\\ &\approx -\frac{T}{4\pi}\left(\frac{2}{\alpha_s}-\pi\right)\left(n_D+\frac{\kappa(\tilde{\alpha})M^3}{8\pi}\right)\end{aligned} \tag{45}$$

which is non-Poissonian because of the scale anomaly. The compressibility of the ground state is

$$\begin{aligned}\sigma_\chi &\equiv \frac{V_3}{T}\left\langle\left(\frac{F^2}{16\pi^2}\right)^2\right\rangle_c \\ &\approx \frac{T}{16\pi^2}\left(2\left(n_D+\frac{\kappa M^3}{8\pi}\right)+\left(\frac{2}{\alpha_s}-\pi\right)^2\left(n_D+\frac{3\kappa M^3}{16\pi}\right)\right)\end{aligned} \tag{46}$$

for the connected correlator.

We can use (34) and (45) to extract the electric $\langle E^2\rangle_0$ and magnetic $\langle B^2\rangle_0$ condensates in the dyonic ensemble. For that we note that the energy per volume in Euclidean space follows from (34) through

$$\frac{1}{8\pi}\left\langle B^2-E^2\right\rangle_0 = T^2\frac{\partial}{\partial T}\frac{P_{\rm cl}}{T} \tag{47}$$

The results are

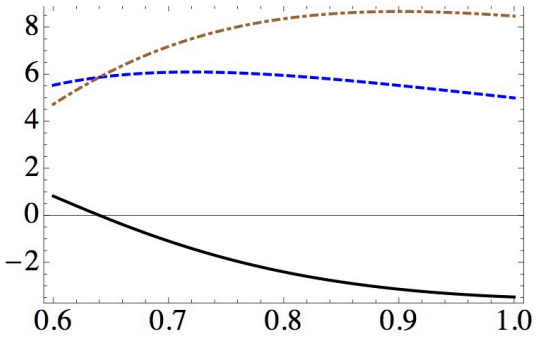

Figure 6: The electric $\langle E^2\rangle$ (solid-black), magnetic $\langle B^2\rangle$ (dashed-blue) and (Euclidean) energy density $\langle B^2-E^2\rangle$ (dot-dashed-brown) in units of T versus T/T_c. See text.

$$\begin{aligned}\frac{\langle B^2\rangle_0}{4\pi T} &= \left(+3-(1+\frac{2\alpha_s'}{\alpha_s^2})\left(\frac{1}{\alpha_s}-\frac{\pi}{2}\right)\right)\left(n_D+\frac{\kappa M^3}{8\pi}\right)\\ \frac{\langle E^2\rangle_0}{4\pi T} &= \left(-3-(1-\frac{2\alpha_s'}{\alpha_s^2})\left(\frac{1}{\alpha_s}-\frac{\pi}{2}\right)\right)\left(n_D+\frac{\kappa M^3}{8\pi}\right)\end{aligned} \tag{48}$$

with $\alpha_s'=\partial\alpha_s/\partial\ln T$. In Fig. 6 we show the behavior of the chromo-electric condensate $\langle E^2\rangle$ (solid-black), the chromo-magnetic condensate $\langle B^2\rangle$ (dashed-blue) and the (Euclidean) energy density $\langle B^2-E^2\rangle$ (dot-dashed-brown) in units of T versus T/T_c in the center symmetric phase. We used the dyon density fixed in (55) below. The chromo-magnetic condensate is about constant in the range of $0.6<T/T_c<1$ while the chromo-electric condensate decreases monotoneously. The condensates are about equal and opposite near T_c a point supported by the lattice extracted condensates in [24].

2.3.5 Electric and magnetic screening masses

The center symmetric phase of the dyon-anti-dyon liquid screens the long-range U(1) gauge fields left un-Higgsed by the holonomy $A_4(\infty)/2\pi T=\nu T^3/2$. The electric and magnetic correlations in these Abelian U(1) charges can be obtained by introducing the U(1) Abelian sources $\eta_{m,e}$ for the magnetic and electric charge densities

$$\rho_{m,e}(x) = \sum_i Q_{m,e,i}\, \delta^3(x - x_i) \tag{49}$$

with $|Q_{m,e}| = 1$, and shifting the U(1) fields $\sigma \to \sigma + \eta_m$ and $b \to b + \eta_e$ in the 3-dimensionsl effective action. To 1-loop the generating functional for the charge density correlators is

$$Z_{1L}[\eta_m, \eta_e] = \int D[\sigma] D[b]\, e^{-S_{2F}[\sigma,b] - S_{1L}[\sigma+\eta_m, b+\eta_e]} \tag{50}$$

which is Gaussian in the sources and therefore readily integrated out. Thus

$$\ln Z_{1L}[\eta_m, \eta_e] = -\int \frac{d^3p}{(2\pi)^3} \sum_{i=e,m} \eta_i(p) \mathbf{G}_i(p) \eta_i(-p) \tag{51}$$

with the electric and magnetic density correlators following by variation,

$$\mathbf{G}_{m,e}(p) \equiv \frac{1}{V_3} \left\langle |\rho_{m,e}(p)|^2 \right\rangle \approx \frac{1}{4} \frac{TM^2p^4}{(p^2 + M^2)^2 \pm \tilde{\alpha}\, M^2p^2} \tag{52}$$

The upper sign is for magnetic and the lower sign for electric. In x-space, (52) can be inverted by Fourier transforms. The result for the electric correlator in spatial coordinates is

$$\begin{aligned} & -\frac{TM^4}{16\pi|x|}\, e^{-\sqrt{1-\frac{\tilde{\alpha}}{4}}\, M|x|} \\ & [\cos\left(\frac{\sqrt{\tilde{\alpha}}}{2}\, M|x|\right)\, (\tilde{\alpha} - 2) \\ & +\sin\left(\frac{\sqrt{\tilde{\alpha}}}{2}\, M|x|\right)\, \frac{1 - 2\tilde{\alpha} + \frac{\tilde{\alpha}^2}{2}}{\sqrt{\tilde{\alpha}\,(1 - \frac{\tilde{\alpha}}{4})}}] \end{aligned} \tag{53}$$

The magnetic correlator follows by analytical continuation through the substitution $\tilde{\alpha} \to -\tilde{\alpha}$ in (53). The electric screening masses $M_{M,E}$ follow from

the large distance asymptotics. Using our estimate of $\tilde{\alpha} \approx -0.52 < 0$ from the Debye-Huckel analysis above, we have

$$\frac{M_E}{M} \approx \left(\sqrt{1 + \frac{|\tilde{\alpha}|}{4}} - \frac{\sqrt{|\tilde{\alpha}|}}{2} \right) \approx 0.70$$
$$\frac{M_M}{M} \approx \left(\sqrt{1 - \frac{|\tilde{\alpha}|}{4}} \right) \approx 0.93 \tag{54}$$

with $M^2 = 2n_D/T$. Also the arguments below show that $M = \sigma_E/T$. Combining these two results allow us to fix C in (5) above. Indeed, at T_c the SU(2) lattice results give $T_c/\sqrt{\sigma_E} \approx 0.71$. So (5) now reads

$$\frac{n_D}{T^3} \approx 2\,\frac{\alpha_s^2(T_c)}{\alpha_s^2(T)}\, e^{\frac{\pi}{\alpha_s(T_c)} - \frac{\pi}{\alpha_s(T)}} \tag{55}$$

which gives $M_E \approx 1.4\,T_c$ and $M_M \approx 1.8\,T_c$, both of which are remarkably close to the reported SU(2) lattice results in the vicinity of the critical temperature [26]. In Fig. 7 we display the results (54) for $M_{E,M}/T$ in the range $(0.5-1)\,T_c$ versus T/T_c. The points at $T > T_c$ are shown for comparison. We note that the electric mass drops down at T_c. In the region we study $M_M > M_E$, while above T_c, in a more familiar QGP region, $M_M < M_E$. This switching of the magnitude of the two screening masses is better documented in lattice works with the $SU(3)$ gauge group. It has a simple explanation in our case. Since at $T > T_c$ the dyon density drops it follows that M decreases as well. As a result, the form factor in Fig. 3 is probed at smaller momentum $p \approx M$ (larger distances) making $\tilde{\alpha}(p \approx M)$ in (33) switch from negative ($T < T_C$) to positive ($T > T_C$). From (52) it follows that the expressions for $M_{E,M}$ in (54) are now switched with M_M lighter than M_E. A simple estimate of the critical temperature at the crossing follows from the vanishing of (36) or $Ma_{D\bar{D}} = \pi/2$. This translates to a critical dyon density $n_D^C \approx \pi^2 T_c^3/8$ which is consistent with our estimate of T_c below (see (70)).

Finally, we note that the value of $\alpha_s(T_c) \approx 0.84$ extracted from the cooled caloron data in [107] is also consistent with the reported value from bulk thermodynamics in [27]. In the dyon-anti-dyon Coulomb liquid the correlators are modified at intermediate distances as we now detail in terms of the static structure factors.

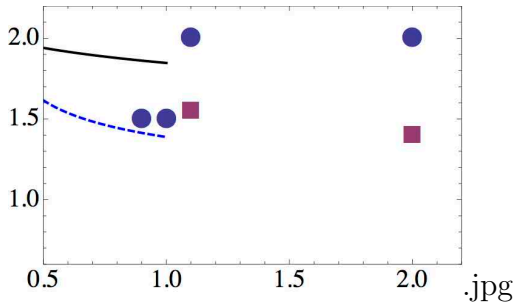

Figure 7: (Color online) The electric M_E/T (dashed line) and magnetic M_M/T (solid line) screening masses in (54) versus T/T_c. The points are SU(2) lattice data from [26] shown for comparison, (blue) circles are M_E/T, (red) squares are M_M/T.

2.3.6 Static structure factors

The charged structure factor between pair of magnetic or electric charges is (52) which can be re-written as

$$\mathbf{G}_{M,E}(p) \equiv \left\langle \frac{1}{N_{m,e}} \left| \sum_{j=1}^{N_{m,e}} Q_{m,e,j} e^{ik\cdot x_j} \right|^2 \right\rangle \tag{56}$$

Thus

$$\mathbf{G}_{M,E}(p) = \frac{\mathbf{G}_{m,e}(p)}{n_D/2} \equiv \frac{\tilde{p}^4}{(\tilde{p}^2+1)^2 \pm \tilde{\alpha}\tilde{p}^2} \tag{57}$$

with $\tilde{p} = p/M$. We note that the pre-factor in (57) involves two static electric or magnetic exchanges with an identical screening mass M. The charged structure factors vanish as $\mathbf{G}_{M,E}(p) \approx \tilde{p}^4$. For large momenta or $\tilde{p} \gg 1$ both structure factors asymptote one from below as shown in Fig. 8. The magnetic hole is slightly smaller than the electric one around the same pairs. The absence of oscillations in the structure factor, is a consequence of our linearized approximation.

To characterize further the 4-component plasma of dyons and anti-dyons we define the scalar static pair correlation function

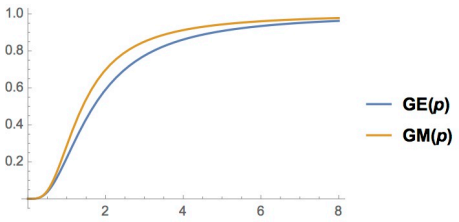

Figure 8: (Color online) The electric and magnetic structure factors (52) as a function of p/M.

$$\mathbf{G}_S(x) = \left\langle \frac{1}{N} \sum_{i \neq j}^{N} \delta^3(x + x_i - x_j) \right\rangle \tag{58}$$

normalized to the total number of particles N. (58) defines the probability to find two particles a distance $|x|$ apart. Its Fourier transform

$$\mathbf{G}_S(p) = \left\langle \frac{1}{N} \left| \sum_{j=1}^{N} e^{ip \cdot x_j} \right|^2 \right\rangle \tag{59}$$

is the scalar structure factor.

(59) can be evaluated by switching $f \to f + \delta f(x_i)$ in (103) and then linearizing the resulting effective action around the mean-density. Specifically, we can re-write the linearized constraint (27) formally as

$$(w_M - w_L) = \frac{1}{\Delta_0 + 4\delta f} \left(\frac{T\nabla^2}{4\pi} \right) (b - i\sigma) \tag{60}$$

with $\Delta_0 = -T\nabla^2/4\pi + 4f$ and use perturbation theory to expand the denominator in (60) to order $\mathcal{O}(\delta f^3)$. The result can be formally written as

$$(w_M - w_L)(p) = \int \frac{d^3k}{(2\pi)^3} G(p,k)(b - i\sigma)(k) \tag{61}$$

Inserting (61) into the potential (26) yields a quadratic action in b and σ. Integrating over the latters yields the 1-loop determinant or the effective action for $\delta \equiv \delta f/f$. Specifically

$$\det(1+\mathbf{S}[\delta]) = e^{\mathrm{Trln}(1+\mathbf{S}[\delta])} \approx e^{\mathrm{Tr}\,\mathbf{S}[\delta]} \tag{62}$$

with the quadratic effective action for the scalar fluctuations as

$$\mathrm{Tr}\,\mathbf{S}[\delta] = -\int \frac{d^3p}{(2\pi)^3}\,\delta(p)\mathbf{G}^{-1}(p)\delta(-p) \tag{63}$$

with to order $\mathcal{O}(\tilde{\alpha}^3)$

$$\begin{aligned}\mathbf{G}^{-1}(p) \quad &\approx n_D + 4\,\tilde{\alpha}^2 M^8 \int \frac{d^3k}{(2\pi)^3} \\ &\Big[\,\frac{k^4}{(k^2+M^2)^4}\frac{1}{((k+p)^2+M^2)^2} \\ &+\frac{2k^2}{(k^2+M^2)^3}\frac{1}{((k+p)^2+M^2)^2}\,\Big]\end{aligned} \tag{64}$$

The n_D contribution in (64) follows from the expansion of the leading contribution $\mathcal{V}$ using arguments similar to those used for the derivation of the dyonic densities above.

The scalar structure factor follows from (64) through the normalization

$$\mathbf{G}_S(p) \equiv \frac{n_D}{V_3}\left\langle|\delta(p)|^2\right\rangle = n_D\,\mathbf{G}(p) \tag{65}$$

We note that the small momentum fluctuations in δf couple to the sound-like modes. Specifically,

$$\mathbf{G}_S(p) \approx \frac{p^2}{c_s^2 p^2} \tag{66}$$

is dominated by a massless pole at zero momentum with

$$c_s^2 \approx 1 + 8\,\tilde{\alpha}^2\left(\frac{M}{T}\right)\int\frac{d^3k}{(2\pi)^3}\left[\frac{k^4}{(k^2+1)^6}+\frac{2k^2}{(k^2+1)^5}\right] \tag{67}$$

Alternatively from the pressure (34) we expect

$$c_s^2 \equiv \frac{\partial \mathcal{P}_{\rm cl}}{T \partial n_D} \approx 1 + \frac{\kappa(\tilde{\alpha})}{4\pi} \left(\frac{M}{T} \right) \tag{68}$$

with $\kappa(\tilde{\alpha}) \approx 15\, \tilde{\alpha}^2/32$ in leading order and in total agreement with (67). Also, at large momentum (65) asymptotes $\mathbf{G}_S(\infty) = 1$. The slight super-luminal character of (67) reflects on the fact that dyons are in essence Euclidean configurations with no physical particle realization.

2.3.7 Estimate of the critical T_c

The total thermodynamical pressure of the dyon-anti-dyon liquid consists of the classical and non-perturbative contribution (39) plus the perturbative holonomy potential known as Gross-Pisarski-Yaffe-Weiss (GPYW) potential [16], plus the purely perturbative black-body contribution (ignoring the higher order $\mathcal{O}(\alpha_s)$ quantum corrections). Specifically ($N_c = 2$)

$$\begin{aligned} \frac{\mathcal{P}_{\rm tot}}{T^4} \quad & \approx \tilde{n}_D + \frac{\kappa(\tilde{\alpha})}{3\pi\sqrt{2}}\, \tilde{n}_D^{\frac{3}{2}} \\ & -\frac{\pi^2}{45} \left(N_c^2 - \frac{1}{N_c^2} \right) + \frac{\pi^2}{45} \left(N_c^2 - 1 \right) \end{aligned} \tag{69}$$

The Debye-Huckel contribution is of order N_c^3, while the leading classical contribution is of order N_c^2. So screening and large N_c are not commutative. For the SU(2) case of interest, the transition temperature T_c from the disordered phase ($\nu = 1/2$) to the ordered phase ($\nu = 0$) occurs when the first three contributions in (69) cancel out. Thus

$$\tilde{n}_D + \frac{\kappa(\tilde{\alpha})}{3\pi\sqrt{2}}\, \tilde{n}_D^{\frac{3}{2}} \approx \frac{\pi^2}{12} \tag{70}$$

For $\kappa(-0.52) \approx 0.19$, the critical density is $n_D^C \approx \pi^2 T_c^3/12 \approx 0.88$. Since the SU(2) electric string tension is $\sigma_E = TM = \sqrt{2 n_D T}$ (see below), it follows that $T_c/\sqrt{\sigma} = 6^{\frac{1}{4}}/\sqrt{\pi} \approx 0.88$ which is somehow larger than the SU(2) lattice result $T_c/\sqrt{\sigma_E} = 0.71$ [101].

2.4 Polyakov lines

To probe the confining nature of the dyon-anti-dyon liquid in the 3-dimensional effective theory we will compute explicitly the expectation of a heavy quark through the traced Polyakov line and the corelator of a heavy quark-anti-quark pair through the correlator of the traced Polyakov line and its conjugate at fixed spatial separation. The insertion of these charges in the dyon-anti-dyon liquid modifies the ground state through solitonic solutions around these sources.

In this section we present a new derivation of the pertinent solitonic equations for the SU(2) case that makes explicit use of the presence of the long range U(1) b and σ fields. In the linearized screening approximation, we show that the solitonic equations for the heavy source probes are in agreement with those established in [83] using different arguments.

2.4.1 $\langle L \rangle$

In the SU(2) case the Polyakov line consists of inserting a heavy quark whose free energy consists of its Coulomb interactions with all the Coulomb charged dyons and anti-dyons. Specifically, the traced Polyakov line before averaging is

$$L(x_1) = \tag{71}$$
$$e^{2\pi i\mu_M + \frac{i}{2T}\sum_i \left(\frac{1}{|x_1 - x_{Mi}|} + \frac{1}{|x_1 - x_{\bar{M}i}|} - \frac{1}{|x_1 - x_{Li}|} - \frac{1}{|x_1 - x_{\bar{L}i}|}\right)} +$$
$$e^{2\pi i\mu_L + \frac{i}{2T}\sum_i \left(\frac{1}{|x_1 - x_{Li}|} + \frac{1}{|x_1 - x_{\bar{L}i}|} - \frac{1}{|x_1 - x_{Mi}|} - \frac{1}{|x_1 - x_{\bar{M}i}|}\right)}$$

with $\mu_L - \mu_M = v_m$. When averaging using the ensemble (3) it is clear that each of the contributors to the string of factors in (71) will match its analogue from the measure and re-exponentiate. For instance the first contribution in (71) re-exponentiates through the substitution

$$e^{-b \pm i\sigma} \rightarrow \qquad e^{-b \pm i\sigma} e^{\frac{i}{2T|x_1 - x|}} \tag{72}$$

The extra Coulomb factors can be re-defined away by shifting

$$b \rightarrow b + \frac{i}{2T|x_1 - x|} \tag{73}$$

thereby changing the constraint equation (25) to

$$
\begin{aligned}
&-\frac{T}{4\pi}\nabla^2 w_M + f(e^{w_M-w_L} - e^{w_L-w_M}) \\
&= \frac{T}{4\pi}\nabla^2(b-i\sigma) + \frac{i}{2}\delta^3(x-x_1) \\
&-\frac{T}{4\pi}\nabla^2 w_L + f(e^{w_L-w_M} - e^{w_M-w_L}) = 0
\end{aligned}
\tag{74}
$$

and similarly for the second contribution in (71) with $L \leftrightarrow M$. The effect of the first contribution in the Polyakov line (71) is to add a source term to the constraint equation for w_M. It is in agreement with [83] after setting $b = \sigma = 0$. (74) is a Poisson-Boltzmann type equation. It is also referred to as an elliptic and periodic Toda lattice [83, 29]. The solution is a local Debye-like cloud around the inserted heavy quark

$$
(w_M - w_L)(x) \approx \frac{2\pi i}{T}\int \frac{d^3p}{(2\pi)^3}\frac{e^{ip\cdot(x-x_1)}}{p^2+M^2} \tag{75}
$$

This causes almost no change in the vacuum holonomies $v_{m,l}$. Thus, after the shift

$$
\langle L(x_1)\rangle \approx e^{i2\pi\mu_M} + e^{i2\pi\mu_L} = 0 \tag{76}
$$

2.4.2 $\langle LL^\dagger\rangle$

The preceding analysis can also be applied to the correlator of two heavy quarks through $LL^\dagger$ which consists now of 4 contributions before averaging

$$
L(x_1)L^\dagger(x_2) = \sum_{m,n=M,L} e^{2\pi i(\mu_m-\mu_n)} e^{\frac{i}{2T}(F_m(x_1)-F_n(x_2))} \tag{77}
$$

with the pertinent Coulomb free energies $F_m(x_{1,2})$ following from (71). When averaged over the measure (3), each of the factors in (77) can be matched with its analogue in the measure. The preceding observations show that the Coulomb factors in the probing correlator can be paired with

$$e^{-b\pm i\sigma} \to e^{-b\pm i\sigma} e^{\frac{i}{2T|x-x_1|}-\frac{i}{2T|x-x_2|}} \tag{78}$$

A rerun of the preceding arguments shows that the constraint equations acquire now two source contributions, one for each of the heavy quark inserted

$$\begin{aligned} &-\frac{T}{4\pi}\nabla^2 w_M + f(e^{w_M-w_L} - e^{w_L-w_M}) \\ &= \frac{T}{4\pi}\nabla^2(b-i\sigma) + \frac{i}{2}[\delta^3(x-x_1) - \delta^3(x-x_2)] \\ &-\frac{T}{4\pi}\nabla^2 w_L + f(e^{w_L-w_M} - e^{w_M-w_L}) = 0 \end{aligned} \tag{79}$$

Since $\nabla^2 1/|x-x_2| = -4\pi\delta^3(x-x_2)$, we can symmetrize (79) by shifting $\delta^3(x-x_2)$ from the first to the second equation through

$$w_{M,L} \to w_{M,L} + \frac{i/T}{2|x-x_2|} \tag{80}$$

with unit Jacobian. The symmetrized (79-80) equations are in agreement with those established in [83] for the SU(2) case after setting $b = \sigma = 0$. In this case the solution is peaked around the heavy quark sources

$$(w_M - w_L)(x) \approx \frac{2\pi i}{T}\int \frac{d^3p}{(2\pi)^3}\frac{e^{ip\cdot(x-x_1)} - e^{ip\cdot(x-x_2)}}{p^2+M^2} \tag{81}$$

Inserting this back in the expectation value of the correlator (77) yields asymptotically

$$\left\langle L(x_1)L^\dagger(x_2)\right\rangle \approx e^{-M|x_1-x_2|} \tag{82}$$

in the 3-dimensional effective theory in agreement with the result in [83]. In 4-dimensions (82) translates to confinement of the electric charges with the electric string tension $\sigma_E = MT$. The additional Coulomb screening in (3) does not affect the asymptotics of the linearly rising heavy quark potential to leading order. The dyon-anti-dyon Coulomb liquid still electrically confines in the center symmetric phase.

2.5 Single-Winding Wilson loop

To study the large spatial Wilson loops we use the same observations made above in the presence of the U(1) fields σ and b. As an observable the traced spatial Wilson loop of area S supported by the spatial contour $\partial S = C$ reads

$$\mathrm{Tr}\, W(C) = e^{i\int_S B_+\cdot dS} + e^{i\int_S B_-\cdot dS} \tag{83}$$

and sources the static magnetic field

$$B_{\pm\,\mu} = \pm \sum_i Q_i \frac{(x-x_i)_\mu}{|x-x_i|^3} \tag{84}$$

When averaged using (3), the spatial Wilson loop (83) modifies the additional U(1) fugacity factors in the dyon sector. Their contribution follows again by shifting $b \mp i\sigma \to b \mp i(\sigma - \eta_\pm)$ in the constraint equations with

$$\eta_\pm(x) = \pm \int_S dS_y \cdot \frac{x-y}{2|x-y|} \tag{85}$$

As a result, (25) in the presence of (83) are now modified to read

$$\begin{aligned} -\frac{T}{4\pi}\nabla^2 w_M + f(e^{w_M - w_L} - e^{w_L - w_M}) &= \frac{iT}{4\pi}\nabla^2\eta_+(x) \\ -\frac{T}{4\pi}\nabla^2 w_L + f(e^{w_L - w_M} - e^{w_M - w_M}) &= 0 \end{aligned} \tag{86}$$

for the first contribution and similarly for the second contribution in (83) with $\eta_+ \to \eta_-$. After choosing the spatial Wilson loop to lay in the x-y plane through $\nabla^2\eta_\pm = \pm 4\pi\delta'(z)$, the results (86) are in agreement with those derived in [83] for the SU(2) case but without the long range U(1) σ and b fields in the leading order approximation. Thus $\langle \mathrm{Tr}\, W(C)\rangle \approx e^{-\sigma_M S}$ is saturated by the pinned soliton, with the magnetic string tension $\sigma_M = \sigma_E = MT$. This result is expected from the equality of the electric and magnetic masses in (54).

A simple understanding of this result is as follows: while a heavy quark sources an electric field, a large spatial Wilson loop sources a magnetic field

by Ampere′s law which is classically composed of all the magnetic poles fluxing S as is explicit in (84). The typical contribution to (83) for a planar surface in the xy-plane is then

$$\left\langle e^{i\int_S B\cdot dS}\right\rangle \approx e^{-\frac{S}{2}\int_S \langle B_z(x,y)B_z(0,0)\rangle dS} \tag{87}$$

by keeping only the first cumulant in the average and using translational invariance for large S. In this limit, S acts as a uniformly charged magnetic sheet made of magnetic dyons classically, so that

$$\langle B_z(x,y)B_z(0,0)\rangle \approx \left\langle \left(\frac{Q_M}{S}\right)^2\right\rangle \approx \frac{\langle Q_M\rangle}{S^2} \tag{88}$$

where the variance in the magnetic charge is assumed Poissonian. The magnetic charge density per unit 4-volume is $(TM)^2/2$. The typical magnetic charge per unit area is then about its square root or $\langle Q_M\rangle/S \approx TM$. Thus

$$\left\langle e^{i\int_S B\cdot dS}\right\rangle \approx e^{-\frac{1}{2}MT\,S} \tag{89}$$

which is the expected behavior up to a factor of order one in the string tension.

2.6 Double-Winding Wilson Loop

Recently it was pointed out in [31] that a co-planar and double winding Wilson loop in the SU(2) pure gauge theory version of the model discussed by Diakonov and Petrov [83] shows an exponentl fall-off with the sum of the areas. In contrast lattice SU(2) simulations appear to show an exponential fall off with the difference of the areas. The main observation in [31] is that the solitonic configuration contributing to the single-winding spatial Wilson loop as for instance from our linearized version with $b = \sigma = 0$ in (86), factors out in the the double-winding and co-planar Wilson loop.

For two identical loops with $C_1 = C_2 = C$, we have the formal SU(2) identities [32] (and references therein)

$$\begin{aligned}\left(\mathrm{Tr}\,W(C)\right)^2 = &\quad \mathrm{Tr}_S\left(W(C)\right) + \mathrm{Tr}_A\left(W(C)\right)\\ \mathrm{Tr}\left(W(C)^2\right) = &\quad \mathrm{Tr}_S\left(W(C)\right) - \mathrm{Tr}_A\left(W(C)\right)\end{aligned} \tag{90}$$

The simple trace Tr is carried over the fundamental representation of N-ality $k = 1$ as in (83), and $\mathrm{Tr}_{S,A}$ are carried over the symmetric and anti-symmetric of N-ality $k = 2$ (modulo 2) representations of SU(2) respectively. The identities (91) are commensurate with the Young-Tableau decomposition. In the dyonic plasma considered here, the k-string tensions σ_k in the linearized plasma approximation are identical to those derived in [83] with $\sigma_k/\sigma_1 = \sin k\pi/2$ for SU(2) with $\sigma_1 = \sigma_E$. For $k = 2$ we have $\sigma_2 = 0$ and the second identity in (91) implies for large loops

$$\left\langle \mathrm{Tr}\left(W(C)^2\right)\right\rangle = \left\langle \mathrm{Tr}_S\left(W(C)\right)\right\rangle - 1 \tag{91}$$

We have set all self-energies to zero for simplicity as they depend on the subtraction procedure. (91) is consistent with the doubly traced Wilson loop as dominated by the $k = 2$ modulo 2 colorless di-quark-like (qq) or baryon-like configuration in SU(2). In the dyonic plasma, the double Wilson loop with $C_1 = C_2$ is a bound colorless state with zero-size that is strongly correlated within the dyons cores and therefore is consistent with the arguments presented in [31].

For largely separated loops $C_{1,2}$ of arbitrary sizes but still lying in the spatial directions, clearly

$$\langle \mathrm{Tr}(W(C_1)W(C_2))\rangle \approx e^{-\sigma_E(A_1+A_2)} \tag{92}$$

for $(A_1 + A_2) < A_{12}$ where $A_{1,2}$ are the planar areas supported by $C_{1,2}$ separately, and A_{12} is the minimal area with boundaries C_1 and C_2. The main issue is what happens for the same doubly wound SU(2) spatial Wilson loops when $A_{12} < (A_1 + A_2)$? Here we note that $L\bar{L}$ and $M\bar{M}$ dimers carrying $(-2, 0)$ and $(+2, 0)$ (electric, magnetic) charge assignments could cluster around the probe qq (baryon) and $\bar{q}\bar{q}$ (anti-baryon) configurations respectively, to form neutral molecular bound states with masses that scale with A_{12} instead of $(A_1 + A_2)$. They are commensurate with the massive off-diagonal and charged gluons Higgsed by the holonomy and dropped in the dyon liquid analysis. These configurations were not retained in [83].

2.7 t′ Hooft Loops

In an important study of the nature of confinement in gauge theories, t′ Hooft [33] has introduced the concept of a disorder operator or t′ Hooft loop

to quantify confinement in the Hilbert space of gauge configurations. The t′ Hooft loop is a canonical operator much like the Wilson loop. In a Lorentz invariant confining vacuum, t′ Hooft has argued that the temporal Wilson loop and the t′ Hooft loop cannot exhibit an area law simultaneously. The temporal Wilson loop obeys an area law, while the t′ Hooft loop obeys a perimeter law.

Physically, the Wilson loop corresponds to a color charge in the fundamental representation running around a closed loop and measuring the the chromo-magnetic flux across the loop. The t′ Hooft loop corresponds to a dual charge in the center of the gauge group running around a closed loop and measuring the chromo-electric flux across the loop. The t′ Hooft loop is the dual of the Wilson loop.

In the temperature range $0.5\,T_c < T < T_c$ confinement is still at work and we expect the temporal Wilson and t′ Hooft loops to exhibit behaviors similar to those in the vacuum state. In section 2.5 we have explicitly checked that the closed spatial Wilson loop obeys an area law. The temporal Wilson loop is not amenable to our dimensionally reduced and Euclideanized effective field theory.

The t′ Hooft loop $V(C)$ enforces a gauge transformation Ω_C which is singular on a closed curve C. If a curve C' winds $n_{CC'}$ times around C then

$$V^\dagger(C)W(C')V(C) = e^{i\frac{2\pi}{N_c}n_{CC'}}W(C') \tag{93}$$

$V(C)$ amounts to a multi-valued gauge transformation on the loop C,

$$\Omega_C(\theta = 2\pi) = e^{i\frac{2\pi}{N_c}n_{CC'}}\Omega_C(\theta = 0) \tag{94}$$

with θ an affine parameter along C. A simple choice is

$$\Omega_C(x) = e^{i\frac{2\pi}{N_c}Q\varphi_C(x)} \tag{95}$$

where $\varphi_C(x)$ is a multi-valued scalar potential for the magnetic field $\vec{B}_C$ generated by a loop of current $\vec{j}_C$ running along C, and $Q = (1, 1, ..., -N_c + 1)$ a Cartan generator of SU(N_c). An alternative construction using a discontinuous solid angle was discussed in [37, 38]. The effects of (95) on an Abelianized Wilson loop is

$$\Omega_C^\dagger \left(e^{i\int_{C'} ds\cdot A} \right) \Omega_C = e^{i\int_{C'} ds\cdot (A - \frac{2\pi}{N_c} Q B_C)} \tag{96}$$

with $\vec{B}_C = -\vec{\nabla}\varphi_C$. Note that since φ_C is multivalued we have $\vec{\nabla} \times \vec{B}_C = 4\pi \vec{j}_C$. If we normalize the loop current $\vec{j}_C$ such that

$$\int_{C'} ds \cdot B_C = 4\pi \int_{A(C')} dS \cdot j_C = -n_{CC'} \tag{97}$$

then (96) reduces to

$$\Omega_C^\dagger \left(e^{i\int_{C'} ds\cdot A} \right) \Omega_C = e^{i\frac{2\pi}{N_c} n_{CC'}} e^{i\int_{C'} ds\cdot A} \tag{98}$$

In the space of gauge configurations, the gauge transformation Ω_C is inforced through

$$V(C) = e^{i\frac{2\pi}{gN_c}\int d^3x \mathrm{Tr}(E_i D_i(Q\varphi_C))} \tag{99}$$

For SU(2) we have

$$V(C) = e^{i\frac{2\pi}{g}\int d^3x \vec{E^3}\cdot\vec{B}_C} \to e^{-\frac{2\pi}{g}\int d^3x \vec{E^3}\cdot\vec{B}_C} \tag{100}$$

where the latter substitution $E \to iE$ follows in Euclidean space. With this in mind, the expectation value of the t′ Hooft loop in the dyonic ensemble involves a string of sources to be inserted in (103). In leading order

$$\begin{aligned} V(C) \to & \quad \prod_{i=1}^{N+\bar{N}} e^{\frac{2\pi}{g}\int d^3x\, B_C\cdot\nabla \frac{Q_{Ei}}{|x-x_i|}} \\ = & \quad \prod_{i=1}^{N+\bar{N}} e^{-\frac{2\pi}{g}\int d^3x\, \nabla\cdot B_C \frac{Q_{Ei}}{|x-x_i|}} = 1 \end{aligned} \tag{101}$$

Thus $\langle V(C)\rangle = 1$ modulo $\mathcal{O}(\alpha_s)$ Coulomb-like self-energy corrections which are perimeter-like in general.

Finally, the Polyakov line as a Wilson loop around the periodic temporal direction has a dual Polyakov loop with a dual magnetic charge in the center. In the confined phase, the temporal component of the gauge field A_4 asymptotes fixed electric-type holonomies, while its dual $\tilde{A}_4$ asymptotes zero dual magnetic-type holomies thanks to parity. A rerun of the arguments in 2.4.1 shows that while $\langle L(\mathbf{x})\rangle = 0$ in (76) as expected in an Euclidean and confining thermal state, its dual does not vanish, i.e.

$$\left\langle \tilde{L}(\mathbf{x}) \equiv \mathrm{Tr}\left(e^{i\frac{4\pi}{gN_c}\int_0^\beta Q\tilde{A}_4^Q(x)d\tau}\right)\right\rangle = 1 \tag{102}$$

again modulo $\mathcal{O}(\alpha_s)$ Coulomb corrections. This behavior is consistent with the one reported on the lattice for $N_c = 2, 3$ [34].

2.8 Conclusions

The central theme in this section is non-perturbative gauge theory for temperatures in the range $(0.5-1)\,T_c$ modeled by a dense plasma of instanton-dyons. The new element in our discussion is the introduction of the leading classical $\mathcal{O}(1/\alpha_s)$ interactions between the dyons and anti-dyons as recently obtained in [21] using the classical "streamline" set of configurations for $M\bar{M}, L\bar{L}$ pairs. We have assumed that the $M\bar{L}, L\bar{M}$ channels are repulsive and opposite in sign to the streamline interaction. While carrying this work, this assumption has now been confirmed numerically [35]. Another important element of our analysis is the one-loop measure of the dyon and anti-dyon moduli space, in the form proposed by Diakonov and Petrov [83]. It leads to a small moduli space volume and thus repulsive interaction at higher density, which however can be made much less repulsive by introducing correlaltions between the charges.

On general grounds, an ensemble of instanton-dyons is a strongly coupled plasma, with significant correlations between the particles. Therefore, the statistical mechanics of a generic instanton-dyon ensemble is very nontrivial and remains unsolved. However – and this is the main argument of the section – when the plasma is dense enough for temperatures below T_c, it generates a large screening mass M which screens the interaction. A standard weak coupling plasma theory, in a form similar to the Debye-Huckel theory is then applicable . The dimensionless 3-density of each dyon species $n_D/4$ in the regime considered is in the range of $n_D/4 \approx T^3/4$, in agreement with the qualitative arguments in [107].

Using it, we get a number of results concerning the details of the non-perturbative gauge fields, in the temperature range $(0.5-1)\,T_c$. First , in the presence of strong screening the minimum of the free energy is still at the confining (center symmetric) value of $\nu = 1/2$, with a vanishing Polyakov line $\langle L\rangle \approx \cos(2\pi\nu) = 0$. Second, a re-summation of the the linearized screening effects yields Debye-Huckel type corrections to the pressure and dyonic densities. We have also analyzed the topological susceptibility, the gluonic compressibility, and the electric and magnetic gluonic condensates in this linearized approximation.

We have calculated also the electric and magnetic screening masses, generated by the dyon ensemble. We have found that the latter are larger than the former in the confined phase. This is qualitatively consistent with the existing lattice data, which however are much better measured for the SU(3) gauge theory rather than the SU(2) one we have studied here. Finally, we have calculated the structure factors in the electric and magnetic sector in the linearized screening approximation as well. For an estimate of the transition temperature from $\nu = 1/2$ (confinement) to $\nu = 0$ (deconfinement) we have switched the perturbative (GPYW) holonomy potential [16] in section 2.3.7. For SU(2) the transition is observed to take place at $T_c/\sqrt{\sigma_E} \approx 0.88$.

In the dyonic plasma the large spatial Wilson loops exhibit area law, while the spatial t$'$ Hooft loops are found to be 1 modulo $\mathcal{O}(\alpha_s)$ Coulomb-like self-energy corrections. These dual behaviors were argued in [33] for confining gauge theories at zero temperature. We found them to hold in the confining dyon-ensemble in the regime $0.5 < T < T_c$.

Needless to say, that all these predictions can and should be confronted with the lattice data in the corresponding temperature range.

Finally, let us speculate about the dyon ensemble beyond the validity domain of the Debye-Huckel approximation. First of all, strongly coupled Coulomb plasmas are tractable by certain analytic and/or numerical (molecular dynamics) methods, see Refs [22, 23] for similar development. Another option is to use brut force numerical simulations of the dyon ensemble [36]. Qualitatively, sufficiently strongly coupled plasmas develop either (i) correlations between particles, resembling either a liquid with crystal-like correlations ("molten salt"), or (ii) particular neutral clusters, the simplest of which can be the LM instantons themselves or $LM\bar{L}\bar{M}$ "instanton molecules". Recent (unquenched) lattice simulations indicate that the instantons and anti-instantons recombine into topologically neutral molecules across the transition temperature [39, 40]. At much higher temperature, the perturbative

gluons dwarf all classical gauge configurations forcing the holonomy to zero.

One obvious extension of this work should be into the large number of colors N_c. Strong correlations can appear, since $\Gamma_{D\bar{D}} \approx 1/\alpha_s \approx N_c \gg 1$. Similar mechanism, leading to crystallization appears to take place in dense holographic matter where the baryons as instantons in the holographic direction split into a pair of dyons and re-arrange in salt crystals [41].

3 The dense regime

This section is an edited version of my publication :
Dense Instanton-Dyon Liquid Model: Diagrammatics Yizhuang Liu, Edward Shuryak, Ismail Zahed (SUNY, Stony Brook). Feb 1, 2018. 12 pp. arXiv:1802.00540, submitted to Phys. Rev. D.

3.1 Introduction

In this section, we continue our study of the instanton-dyon liquid model without quarks, at low temperature in the center symmetric phase, through various many-body re-summations of the Coulomb interactions in the dense limit. We will show that the re-summations provide a specific interpolation between bion-like correlations in the dilute phase and mostly screened interactions in the dense phase.

In section II we briefly review the salient aspects of the instanton-dyon liquid model. We perform a non-linear Debye-Huckel re-summation of the coulomb interactions stemming from the moduli space, and combine them with a cluster expansion of the coulomb interactions originating from the streamlines. We show that the expansion is rapidly converging and the phase center symmetric already in the second cluster approximation. In section III we also show how multi-chain and rings can be further re-summed beyond the leading clusters and explicit them with some applications. In section IV, we extend our arguments to a finite vacuum angle θ. In section V, we discuss a larger class of resummation pertinent for dense systems referred to as a hypernetted chain re-summation (HCN). In section VI, we suggest that a melted crystal of instanton-dyons and anti-instanton dyons may provide a semi-classical description of a Yang-Mills ensemble at very low temperature. Our conclusions are in section VII. In the Appendix we outline the elements for a future molecular dynamics simulation.

3.2 Thermal Yang-Mills

Here we fowllow the rules of previous section. A semi-classical ensemble of instanton-antiinstanton-dyons can be regarded as a statistical ensemble of semi-classical charges interacting mostly through their moduli space for like instanton- or aniti-instanton-dyons, and through streamlines for unlike instanton-anti-instanton-dyons. The grand partition function for such an ensemble is of the form (zero vacuum angle)

$$\begin{aligned}\mathcal{Z}[T,f] \quad &\equiv \sum_{[K]} \prod_{i_L=1}^{K_L} \prod_{i_M=1}^{K_M} \prod_{i_{\bar{L}}=1}^{K_{\bar{L}}} \prod_{i_{\bar{M}}=1}^{K_{\bar{M}}} \\ &\times \int \frac{f d^3x_{Li_L}}{K_L!} \frac{f d^3x_{Mi_M}}{K_M!} \frac{f d^3y_{\bar{L}i_{\bar{L}}}}{K_{\bar{L}}!} \frac{f d^3y_{\bar{M}i_{\bar{M}}}}{K_{\bar{M}}!} \\ &\times e^{-V(x-y)+\ln\det(G[x]G[y])}\end{aligned} \tag{103}$$

The stream-line interactions V are large and of order $1/\alpha_s$. They are attractive between like $D\overline{D}$ and repulsive between unlike $D\overline{D}$ [46]. Their relevant form for our considerations will be detailed below. In contrast, the moduli induced interactions captured in the $(K_L + K_M)^2$ matrix $G[x]$, and in the $(K_{\bar{L}} + K_{\bar{M}})^2$ matrix $G[y]$ are of order α_s^0. While the explicit form of these matrices can be found in [83, 5], it is sufficient to note here that these induced interactions are attractive between unlike instanton-dyons, and repulsive between like instanton-dyons. The bare fugacity f will be regarded as an external parameter in what follows. Note that in the absence of V, $\mathcal{Z} \to \mathcal{Z}_D \mathcal{Z}_{\overline{D}}$ where each factor can be exactly re-written in terms of a 3-dimensional effective theory.

3.2.1 Effective action

The streamline interaction part V can be bosonized using the complex fields $b \pm i\sigma$ through standard tricks. Here b, σ refers to the Abelian magnetic and electric potentials stemming from the instanton-dyon charges. Also, each moduli determinant in (103) can be fermionized using ghost fields, and the ensuing Coulomb factors bosonized using complex $w, \overline{w}$ fields also through standard tricks as detailed in [83, 5]. The net result of these repeated fermionization-bosonization procedures is an exact 3-dimensional effective action (p-space)

$$
\begin{aligned}
-S_B[b,\sigma,w,\bar{w}] \quad &= \int d^3p \Big[\frac{1}{4}(b-i\sigma)V^{-1}(p)(b+i\sigma) \\
&\quad + 4\pi \left(\nu f e^{w} + \overline{\nu} f e^{-w} \right) \\
&\quad + 4\pi \left(\nu f e^{\bar{w}} + \overline{\nu} f e^{-\bar{w}} \right) \Big]
\end{aligned}
\tag{104}
$$

subject to the constraint from the moduli (x-space)

$$
\begin{aligned}
-\frac{T}{4\pi}\nabla^2(w) + 4\pi f \sinh(w) &= \frac{T}{4\pi}\nabla^2(b-i\sigma) \\
-\frac{T}{4\pi}\nabla^2(\bar{w}) + 4\pi f \sinh(\bar{w}) &= \frac{T}{4\pi}\nabla^2(b+i\sigma)
\end{aligned}
\tag{105}
$$

(353-286) allow to re-write exactly the partition function (103) in terms of a 3-dimensional effective theory. In [43] we have analyzed this partition function using the Debye-Huckel (one-loop) approximation. Here we will seek a more systematic organization of the dense phase described by (353-286), that is more appropriate for the description of the confined phase at low temperature.

3.2.2 Cluster expansion

Our starting point is the linearization of (286) around $w = 0$ which amounts to the solution

$$
w(p) = \frac{p^2}{p^2 + M^2}(b - i\sigma)(p) \tag{106}
$$

with the squared screening mass $M^2 = \frac{16\pi f}{T}$. Inserting (162) into (353), we can carry the cluster expansion for the $4\pi f$ terms by integrating over the b, σ fields as the measure is Gaussian in the partition function defined now in terms of the 3-dimensional effective action (353). The result at second order is

$$\frac{\ln Z}{V_3} = 8\pi f + (4\pi f)^2(\nu^2+\overline{\nu}^2)\int d^3r\,(e^{-V_1(r)}-1) + (4\pi f)^2(2\nu\overline{\nu})\int d^3r\,(e^{-V_2(r)}-1) \quad (107)$$

with

$$V_1(p) = -V_2(p) = -\frac{p^4\,V(p)}{(p^2+M^2)^2} \quad (108)$$

While the instanton-antiinstanton-dyon interaction is accessible numerically, for simplicity we will use here only its Coulomb asymptotic form $V(p) \approx \frac{4\pi C_D}{\alpha_s p^2}$ with $C_D = 2$, so that

$$V_1(r) = -V_2(r) \approx \frac{MC_D}{2\alpha_s}\left(-\frac{2}{Mr}+1\right)e^{-Mr} \quad (109)$$

The large r-interaction between the pairs with magnetic charge 0 ($\bar{M}M$ and $\bar{L}L$) turns repulsive at large r, while that between the pairs with magnetic charge 2 ($\bar{M}L$ and $\bar{L}M$) turns attractive. Remarkably, the sign of the induced interaction between the pairs in (232) is flipped in comparison to the unscreened or bare interaction between the pairs, a sign of *over-screening*.

The chief effect of the moduli constraint (286-162) is to induce a non-linear Debye-Huckel screening effects between the charged instanton- and anti-instanton-dyons through the Mayer functions $e^{-V_{1,2}}-1$. This is a re-arrangement of the many-body dynamics that does not assume diluteness. In contrast, the cluster expansion in (354) is limited to the second cumulant and subsume diluteness in the ensemble of $D, \bar{D}$ but with non-linear Debye-Huckel effective interactions. This shortcoming will be addressed later.

For small r, we need to set a core for the attractive pair with magnetic charge 2. We choose the core to be $a = \frac{1}{T}$. As a result (354) plus the perturbative contribution reads

$$
\begin{aligned}
z_b(m,\nu) = & \quad \frac{\ln Z}{V_3 T^3} - \frac{4\pi^2}{3}\nu^2\overline{\nu}^2 \\
= & \quad \frac{m^2}{2} + F(m,\nu) - \frac{4\pi^2}{3}\nu^2\overline{\nu}^2
\end{aligned} \tag{110}
$$

with $m = \frac{M}{T}$ and $V(x) = (-2/x+1)e^{-x}$ and

$$
\begin{aligned}
F(m,\nu) \quad & = \frac{\pi m}{4}(\nu^2+\overline{\nu}^2)\int_1 x^2(e^{-\frac{mC_D}{2\alpha_s}V(x)}-1) \\
& + \frac{\pi m}{2}\nu\overline{\nu}\int_{c1} x^2(e^{\frac{mC_D}{2\alpha_s}V(x)}-1)
\end{aligned} \tag{111}
$$

For $C_D \approx 2$ and $\alpha_s = 1$, the transition from a center symmetric (confining) to a center asymmetric (deconfining) phase occurs for $m_c \approx 2.1$, 2.3 for the two choices of the cutoff parameter $c1 = 1, 0$. The choice $c1 = 0$ corresponds to the formal argument presented in [44]. In terms of the density of charged particles $n = 8\pi f$, the transition occurs for $n \approx 2T^3$. For large density, the screening length scales like $\sqrt{T}/\sqrt{n}$, while the average separation scales like $1/n^{\frac{1}{3}}$. Our expansion is therefore justified. In Fig. 9 we show the behavior of the Polyakov line versus m for the cutoff choice $c1 = 1$.

3.3 Open and closed chains

To go beyond the second cumulant approximation in (286) with bare fugacities, we will discuss in this section a systematic way for re-summing all tree diagrams between the charged particles, and also all ring diagrams with an arbitrary number of trees at the charged verticies. One of the chief effect of the resummation of all the trees is a re-definition of the fugacities of the charged particles as we will show below.

3.3.1 Diagrammatics

A systematic book-keeping procedure for the re-summation of all the trees and the rings with re-defined fugacities follows from a semi-classical treatment of the Coulomb-like field theory

$$
\mathcal{L} = -\frac{1}{2}\phi^T\mathcal{V}^{-1}\phi + f_1(e^{i\phi_1}+e^{i\phi_3}) + f_2(e^{i\phi_2}+e^{i\phi_4}) \tag{112}
$$

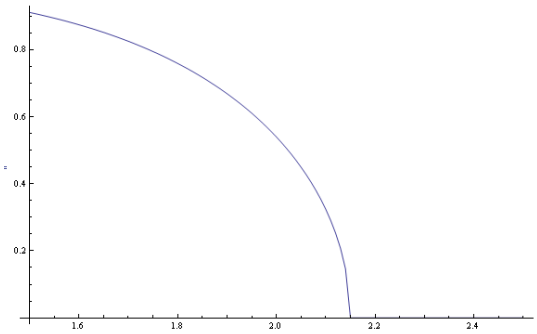

Figure 9: Polyakov line P=$|\cos(\pi\nu)|$ versus m.

with $f_1 = 4\pi f\nu, f_2 = 4\pi f\bar{\nu}$, and the effective fields in 3-dimensions $\phi = (\phi_1, \phi_2, \phi_3, \phi_4)^T$,

$$\mathcal{V} = \begin{pmatrix} 0 & \mathbf{V} \\ \mathbf{V} & 0 \end{pmatrix} \qquad \mathbf{V} = \begin{pmatrix} F_1 & F_2 \\ F_2 & F_1 \end{pmatrix} \tag{113}$$

and the Mayer functions $-F_{1,2} = e^{-\beta V_{1,2}} - 1$. The 4×4 block-structure follows from the fact that the statistcal ensemble consists of 4-species of charged particles $D = L, M$ ($\bullet$) and $\bar{D} = \bar{L}, \bar{M}$ ($\circ$). The block off-diagonal character of $\mathcal{V}$ follows from the fact that the Mayer functions $-F_{1,2}$ resum the non-linear Debye-screening induced by the moduli between like-instanton-dyons, and are left acting only between unlike $D\bar{D}$ instanton-antiinstanton-dyons. It can be checked that (168) reproduces all Coulomb diagrams with the correct symmetry and weight factors as Feynman graphs when the vertices are linked by *single lines only* as illustrated in Figs. 10,11.

A re-summation of all trees and rings with arbitrary trees at the vertices amounts to a one-loop expansion around the saddle point approximation to (168) which is given by

$$\phi_c^T = i\mathcal{V}(p=0)(f_1 e^{i\phi_{1c}}, f_2 e^{i\phi_{2c}}, f_1 e^{i\phi_{3c}}, e^{i\phi_{4c}}) \tag{114}$$

Because of symmetry, the solution satisfies $\phi_1 = \phi_3$, $\phi_2 = \phi_4$. If we define $\alpha_1 = i\phi_{1c}, \alpha_2 = i\phi_{2c}$ and use the symmetry, then (171) reads

$$\begin{aligned} \alpha_1 &= c_1 f_1 e^{\alpha_1} + c_2 f_2 e^{\alpha_2} \\ \alpha_2 &= c_1 f_2 e^{\alpha_2} + c_2 f_1 e^{\alpha_1} \end{aligned} \tag{115}$$

Here

$$c_{1,2} = \int d^3x (e^{-\beta V_{1,2}} - 1) \tag{116}$$

are the integrated Mayer functions. The saddle point contribution which resums all connected trees yield the pressure

$$\Omega_{\rm tree} = \frac{\ln Z_{\rm tree}}{V_3} = f_1 e^{\alpha_1}(2 - \alpha_1) + f_2 e^{\alpha_2}(2 - \alpha_2) \tag{117}$$

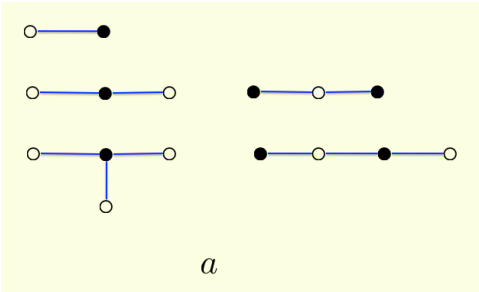

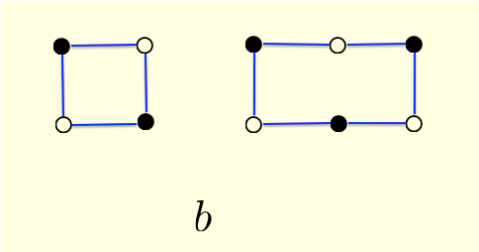

Figure 10: Typical open chain contributions to $\Omega_{\rm tree}$ (a), and closed chain or ring contributions to Ω_{ring} (b). $\bullet$ refers to $D = L, M$ and $\circ$ refers to $\bar{D} = \bar{L}, \bar{M}$.

with $\alpha_{1,2}$ solutions to the non-linear classical equations (361). The resummed rings with arbitrary trees, follow by expanding (171) around the classical solution (361) to one-loop. The result is

$$\Omega_{\rm ring} = -\frac{1}{2}\int \frac{d^3p}{(2\pi)^3}(\ln(1+\mathbb{A})-\mathbb{A}) \tag{118}$$

with in p-space

$$\mathbb{A} = -(\tilde{f}_1^2+\tilde{f}_2^2)F_1^2 + 2\tilde{f}_1\tilde{f}_2F_2^2 + \tilde{f}_1^2\tilde{f}_2^2(F_1^2-F_2^2)^2 \tag{119}$$

In the special case with $F \equiv F_1 \approx -F_2$, the one-loop result simplifies

$$\mathbb{A} = -(\tilde{f}_1+\tilde{f}_2)^2F^2 \tag{120}$$

where $\tilde{f}_{1,2} = f_{1,2}e^{\alpha_{1,2}}$ are the tree-modified fugacites.

3.3.2 Approximations

The preceding expansion around the small fugacities follows by seeking the classical solution to (361) in powers $f_{1,2}$ or $\alpha_1 \approx c_1f_1+c_2f_2$, $\alpha_2 \approx c_1f_2+c_2f_1$. The tree contributions to the pressure in (174) to quadratic order are

$$\Omega_{\rm tree} \approx 2(f_1+f_2) + c_1(f_1^2+f_2^2) + 2c_2f_1f_2 \tag{121}$$

in agreement with (354). For large fugacities $f_{1,2}$ and for $c_1 = -c_2 = -c < 0$, the solution to (175) satisfies $\alpha_1 = -\alpha_2 = \alpha$ with $\nu e^{\alpha} = \bar{\nu}e^{-\alpha} = \sqrt{\bar{\nu}\nu}$. As a result, the leading contribution in (354) is now changed to

$$8\pi f \to 8\pi\tilde{f} \equiv 8\pi f\sqrt{4\bar{\nu}\nu} \tag{122}$$

The resummation of all the trees for large bare fugacities amount to *dressing* the bare fugacities through $f \to \tilde{f}$ in a cluster expansion for the rings with no trees attached as illustrated in Fig. 10b. Some of the diagrams not included in the dressed fugacity expansion with ring-diagrams are illustrated in Fig. 11 which are of the 2-loop types. The first appear in the 5th cumulant, and the

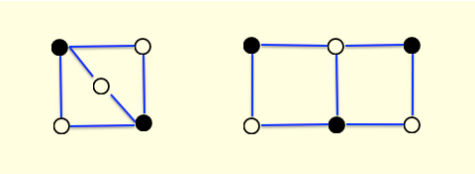

Figure 11: Examples of 2-loop contributions not included in the fugacity redefined 1-loop or ring re-summation.

second in the 6th cumulant. So this re-organization resums a large class of diagrams, yet exact up to the 5th cumulant. Remarkably, in the center symmetric phase with $\nu = \bar{\nu} = \frac{1}{2}$, (122) amounts to the fugacity of *non-interacting* instanton- and anti-instanton-dyons, as all Coulomb interactions from the (linearized) moduli and the streamlines average out.

In general, the solution to (361) for intermediate fugacities is not emanable analytically. One way to go beyond the second cumulant approximation (179) at low density is to insert the leading solutions $\alpha_1 \approx c_1 f_1 + c_2 f_2$, $\alpha_2 \approx c_1 f_2 + c_2 f_1$ in (174) without expanding the exponent,

$$\Omega_{\rm tree} \approx 4\pi f \left(\frac{1}{2}+b\right)(2Kb+2)e^{-2Kb} + (b \to -b) \tag{123}$$

where we have set $\nu = \frac{1}{2} + b$, $K = 4\pi f c$, and noted that $c_1 = -c_2 = -c < 0$. (381) resums all tree contributions with charge vertices that include an arbitrary number of 2-body links. (179) follows by expanding the exponents to first order in f. We note that (381) has always a maximum at $b = 0$ or $\nu = \frac{1}{2}$ for positive c which is center symmetric (confining). This conclusion remains unchanged when the ring contributions are added. Indeed, we note that the ring contribution (175) is an increasing function of the combination $\tilde{f}_1 + \tilde{f}_2$ or more specifically

$$\tilde{f}_1 + \tilde{f}_2 \approx 8\pi f \left(\frac{1}{2}+b\right) e^{-2Kb} + 8\pi f \left(\frac{1}{2}-b\right) e^{-2Kb} \tag{124}$$

with

$$2K = 8\pi f c = \frac{2\pi}{m} \int dx x^2 (e^{\frac{mC_D}{2\alpha_s} V(x)} - 1) \tag{125}$$

using the previous notations. For $2K > 4$ or $cf > \frac{1}{2\pi}$, this combination has a maximum away from 0 and competes against the classical contribution towards the center-symmetric solution. For $m < 10$ we have $2K < 4$. The ring contribution preserves center symmetry.

The center symmetric phase can be probed more acuratly by setting $\nu = \frac{1}{2} - b$. The semiclassical equation (181) reads

$$\alpha = -K \left(\frac{1}{2}+b\right) e^{\alpha} + K \left(\frac{1}{2}-b\right) e^{-\alpha} \tag{126}$$

At $b = 0$ we have $\alpha = 0$. We now can solve (183) by expanding exactly around $b = 0$. Since α is an odd function of b, we seek a solution to (183) using $\alpha = x_1 b + x_2 b^3 + ...$, with x_1 satisfying

$$x_1 = \quad -2K - Kx_1 \tag{127}$$

Since the leading contribution to the pressure is given by

$$\frac{\ln Z}{V_3} \approx 4\pi f \nu e^{\alpha}\left(1-\frac{\alpha}{2}\right) + 4\pi f \bar{\nu} e^{-\alpha}\left(1+\frac{\alpha}{2}\right) + c.c \tag{128}$$

its expanded form to order $\mathcal{O}(b^4)$ reads

$$\begin{aligned} \frac{\ln Z}{V_3} \approx & \quad 8\pi f - 8\pi f \frac{2K}{K+1} b^2 + \mathcal{O}(b^4) \\ \rightarrow & \quad 8\pi f \left(\frac{1+K\sqrt{4\nu\bar{\nu}}}{1+K}\right) \end{aligned} \tag{129}$$

where the last relation follows after restoring the full ν dependence. (129) shows that only the open chains with no tree-like-star insertions contribute to the leading b^2 and therefore $\sqrt{\nu\bar{\nu}}$ in the pressure. Note that (129) is independent of the integrated Mayer function c in $K = 4\pi f c$ in the center symmetric phase and/or large fugacities, in agreement with (122).

3.4 Finite vacuum angle θ

At finite vacuum angle θ, the bare fugacities for $\phi_{1,2}$ are now complex and given by $f_1 = 4\pi f \nu e^{\frac{i\theta}{2}}$ and $f_2 = 4\pi f \bar{\nu} e^{\frac{i\theta}{2}}$, while the bare fugacities for $\phi_{3,4}$ are their conjugate $f^{\dagger}_{1,2}$. For $c_1 = c_2 = -c < 0$, we first note that the solution to the analogue of the classical equations (361) at finite θ satisfies $\alpha_{3,4} = \alpha^{\dagger}_{1,2}$, and $\alpha_1 = -\alpha_2 = \alpha$, with α complex and satisfying

$$\alpha = -Ke^{-i\frac{\theta}{2}}\overline{\nu}e^{\alpha^{\dagger}} + Ke^{-i\frac{\theta}{2}}\nu e^{-\alpha^{\dagger}} \tag{130}$$

The solution for small or large fugacities can be obtained analytically. We now discuss them sequentially.

3.4.1 Large K

For large fugacities or large K, the solution to (130) in leading order gives $e^{\alpha} = \sqrt{\nu/\overline{\nu}}$ independently of K. In this limit, the summation of all the tree diagrams amount to a dressed fugacity with a leading (dimensionless) pressure

$$\frac{\ln Z}{V_3 T^3} \to \frac{m^2}{2}\sqrt{4\nu\bar{\nu}}\cos(\theta/2) - \frac{4\pi^2}{3}\nu^2\overline{\nu}^2 \tag{131}$$

with $m^2 = \frac{2n}{T^3}$ and including the perturbative contribution. (131) resums all the tree cumulant contributions at finite θ and is to be compared to (358-167) with only the second cumulant retained. (131) implies a transition from the center symmetric (confined) phase to the center asymmetric (deconfined) phase at a critical temperature

$$\frac{T_c(\theta)}{T_c(0)} = \left(\cos\left(\frac{\theta + 2k\pi}{N_c}\right)\right)^{\frac{1}{3}} \tag{132}$$

with $T_c^3(0) = \frac{12n}{\pi^2}$ for $N_c = 2$. Although our derivation was for $N_c = 2$, our arguments for the re-summation of the trees extend to any N_c. Also, (131-132) were derived for $|\theta| < \pi$ in a 2π-branch with $k = 0$. The general result is multi-branch and 2π-periodic following the substitution $\theta \to \theta + 2k\pi$. Numerical lattice simulations have established that the transition temperature $T_c(\theta)$ decreases with θ as ($k = 0$ branch)

$$\frac{T_c(\theta)}{T_c(0)} = 1 - R_\theta\theta^2 + \mathcal{O}(\theta^2) \tag{133}$$

with $R_\theta = 0.0175(7)$ for $N_c = 3$ [48], in good agreement with $R_\theta = 1/6N_c^2 = 0.0185$ from (132). Our result (132) is predictive of the N_c dependence of R_θ and of the higher θ coefficients, with a cusp at $T_c(\pi)/T_c(0) = 1/2^3$ at the CP symmetric point. This point is actually a tri-critical point where the CP breaking first order transition line at $\theta = \pi$ meets the first order transtion cusp from (132). Although (132) suggests that the CP transition line reduces to a point for $N_c = 2$, this conclusion requires further amendments as it occurs at 0 temperature where the liquid is very dense requiring additional re-summations, some of which will be detailed below.

3.4.2 Intermediate K

The onset of the center symmetric phase depends on the details of the arrangement of the parameters K, θ, as (131) was only established for large K or high density. The center symmetric phase can be probed more accurately for different densities or K by again setting $\nu = \frac{1}{2} - b$ in (130), and solving exactly around $b = 0$. The result for the pressure to order $\mathcal{O}(b^4)$ is

$$\frac{\ln Z}{V_3} = 8\pi f \cos\frac{\theta}{2} - 8\pi f\, 2K \frac{K\cos\frac{\theta}{2} - 1}{K^2 - 1} b^2 + \mathcal{O}(b^4) \tag{134}$$

which is seen to reduce to (129) at $\theta = 0$. At finite vacuum angle θ, the expanded result (385) develops a singularity at $K = 4\pi f c = 1$, the origin of which requires a more careful analysis.

In general, we have $\alpha_1 = -\alpha_2$ and $\alpha_3 = -\alpha_4$. At finite θ, all $\alpha_{1,2,3,4}$ are complex and satisfy the coupled equations

$$\begin{aligned} \alpha_1 = &\quad -Ke^{-i\frac{\theta}{2}}\nu e^{\alpha_3} + Ke^{-i\frac{\theta}{2}}\overline{\nu}e^{-\alpha_3} \\ \alpha_3 = &\quad -Ke^{+i\frac{\theta}{2}}\nu e^{\alpha_1} + Ke^{+i\frac{\theta}{2}}\overline{\nu}e^{-\alpha_1} \end{aligned} \tag{135}$$

At small θ, these equations can be analyzed numerically by analytically continuing $\theta \to -i\theta$, so that

$$\begin{aligned} \alpha_1 = &\quad -Ke^{-\frac{\theta}{2}}\left(\frac{1}{2} + b\right)e^{\alpha_3} + Ke^{-\frac{\theta}{2}}\left(\frac{1}{2} - b\right)e^{-\alpha_3} \\ \alpha_3 = &\quad -Ke^{+\frac{\theta}{2}}\left(\frac{1}{2} + b\right)e^{\alpha_1} + Ke^{+\frac{\theta}{2}}\left(\frac{1}{2} - b\right)e^{-\alpha_1} \end{aligned} \tag{136}$$

with $\alpha_{1,2,3,4}$ now all real. If we define

$$f(b, K, \theta, x) = -Ke^{-\frac{\theta}{2}}\left(\frac{1}{2} + b\right)e^{x} + Ke^{-\frac{\theta}{2}}\left(\frac{1}{2} - b\right)e^{-x} \tag{137}$$

Figure 12: $x(b)$ as a function of b for $K = 1$, $\theta = 0.1$ (upper) and $K = 1.01$, $\theta = 0.1$ (lower).

Then $\alpha_3 = x$ satisfies the transcendental equation

$$f(b, K, -\theta, f(b, K, \theta, x)) - x = 0 \tag{138}$$

A numerical analysis of (138) reveals a solution with a 3-branch structure in the parameter space. In the region $b \ll 1$ around the center symmetric state, it turns out that for K sufficiently close to 1 but less than 1 there exists a critical $b_c(K, \theta)$. For $b < b_c(K, \theta)$, the expansion leading to (385) is valid. However for $b > b_c(K, \theta)$, the branch which leads to (385) no longer exists, and the solution to (138) jumps to a third branch! For $K \geq 1$ and small b only the third branch exists and will lead to the expansion (385) for $K > 1$. For $K = 1$, the solution is more tricky. In Fig. 12 we show the solution $x(b)$ at $\theta = 0.1$ and $K = 1$. In terms of the pressure, it is interesting to see if a "window" appears for $K = 1$. For imaginary θ, we can see a "window" for $(1/\cosh(\theta/2)) < K < 1$ numerically. Indeed, for $\theta = 0.01$ and $K = 0.99999$ we show in Fig. 13 the pressure $\frac{\ln Z}{V_3}$ versus b, with no maximum at $b = 0$. In contrast, for K outside the window, we always have $b = 0$ as the maximum,

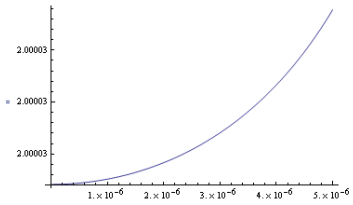

Figure 13: Pressure $\frac{\ln Z}{V_3}$ versus b for $\theta = 0.01$ and $K = 0.99999$.

which corresponds to the center symmetric phase. The window disappears for $\theta = 0$. Its occurence at finite θ signals the incompleteness of the tree re-summation for K in the range $(1/\cos(\theta/2)) < K < 1$ after analytical continuation.

3.5 Hypernetted chains (HNC)

The static properties of a strongly coupled fluid are usually expressed in terms few-body reduced distribution functions of which the two-body distribution $g(\vec{r}_1, \vec{r}_2)$ or radial distribution $g(r_{12})$ is the standard example. The radial distribution function describes how the fluid density varies as a function of distance from a reference particle, providing a link between the microscopic content of the fluid and its macroscopic structure. $g(r_{12})$ can be obtained either from simulations using molecular dynamics (see below) or by solving the Ornstein-Zernicke (OZ) equation [47] subject to an additional closure relation. In this section we discuss such a closure in the form of the well-known hypernetted chain re-summation adapted to our dense dyon liquid. For that, we will provide a diagrammatic derivation based on our effective field theory (168).

3.5.1 Diagrammatic derivation

In the dense instanton-dyon liquid, the radial distribution following from the many-body analysis of (168) is a 4×4 matrix with instanton-dyon entries $g^{ij}(r_{12})$. It is related to the irreducible density 2-point correlation function through

$$h^{ij}(r) = g^{ij}(r) - 1 \equiv e^{-\beta \mathcal{V}^{ij}(r) + \chi^{ij}(r)} - 1 \tag{139}$$

where the use of the barometric form in (139) defines $\chi^{ij}(r)$, and the 4×4 matrix $\mathcal{V}$ is given in (360). χ^{ij} obeys a set of formal matrix equations

$$\begin{aligned} \chi^{ij} &= \chi_a^{ij} + \chi_b^{ij} \\ \chi_a^{ij} &= c^{il}\,\rho^l\,c^{lj} + c^{il}\,\rho^l\,c^{lm}\,\rho^m\,c^{mj} + ... \\ c^{ij} &= h^{ij} - \chi_a^{ij} \end{aligned} \tag{140}$$

where $\rho^{ij} = \rho^i \delta^{ij}$ is a diagonal matrix with species density ρ^i. We now provide a diagrammatic derivation of (140) using the effective formulation (168).

The total pair correlation function h^{ij} follows from summing all irreducible graphs with two external vertices fixed between $\vec{0}$ and $\vec{r}$. Between these two vertices we can hang an arbitrary number of independent 2-point functions as illustrated in Fig. 14a. The minimal insertion that cannot be decomposed into such a hanging structure is denoted by $-\beta\mathcal{V}+\chi$ with $\beta=\frac{1}{T}$. The diagrams contributing to χ can be separated in type-a and type-b. Type-a have at least one cutting point, i.e. a vertex that one can cut to split the diagram into two disconnected pieces as illustrated in Fig. 14b, while type-b have none as illustrated in Fig. 14c. For type-a, we can further count by enumerating the number of cutting points and define a summation over all possible 2-point diagrams that can be put between two nearest cutting points as $c(r)$, which defines the direct correlation function. It is readily seen that $c=h-\chi_a$. With these definitions in mind, simple diagrammatic arguments yield (140). The hypernetted chain approximation (HNC) amounts to setting $\chi_b=0$. In this case, (140) can be cast in the more standard form

$$\begin{aligned} h^{ij} &= \quad c^{ij}+c^{ik}\rho^k\star h^{kj} \\ c^{ij} &= \quad -\beta\mathcal{V}^{ij}+h^{ij}-\ln(1+h^{ij}) \end{aligned} \tag{141}$$

where $\star$ means convolution in x-space. The first of these equations is known as the Ornstein-Zernicke (OZ) equation, while the second equation as the HNC closure condition. The interaction energy per 3-volume and therefore the pressure can be re-constructed using the pair correlation function, for instance

$$\frac{\mathcal{E}}{V_3}=\left(\frac{2N}{V_3}\right)\frac{1}{2}\sum_{i,j}\int d^3r\,\beta\mathcal{V}^{ij}(r)h^{ij}(r) \tag{142}$$

3.5.2 Linear and non-linear DH approximations

The linear Debye-Huckel (DH) approximation follows by performing one iteration in the OZ equation with the initial condition $h=0$ or $c\approx-\beta\mathcal{V}$, to obtain formally in p-space

$$h_{DH}=\frac{-\beta\mathcal{V}}{1+\beta\rho\mathcal{V}} \tag{143}$$

For the instanton-dyon ensemble we have $\rho = \rho_1 = \rho_2 = M^2T/8$ and $V_1 = -V_2 = -V(p) = -\frac{8\pi p^2}{(p^2+M^2)^2}$ in $\mathcal{V}$, so that

$$h_{DH} \quad = \frac{\beta V}{1-(2\beta\rho V)^2} \begin{pmatrix} 2\beta\rho V & 1 \\ 1 & 2\beta\rho V \end{pmatrix} \otimes (1-\sigma_1) \tag{144}$$

Here σ_1 is a Pauli matrix. (144) defines two independent pair correlation functions in p-space

$$\begin{aligned} h_{MM} = h_{LL} = -h_{ML} &= \frac{2\rho\,(8\pi\beta)^2 p^4}{(p^2+M^2)^4 - (16\pi\beta\rho)^2 p^4} \\ h_{M\bar{M}} = h_{L\bar{L}} = -h_{M\bar{L}} &= \frac{(8\pi\beta)\,p^2(p^2+M^2)^2}{(p^2+M^2)^4 - (16\pi\beta\rho)^2 p^4} \end{aligned} \tag{145}$$

For $\rho = M^2T/8$ the denominator

$$(p^2+M^2)^4 - 4\pi^2 p^4 M^4 \tag{146}$$

is negative for $p > \frac{M}{\sqrt{2\pi-1}} \approx \frac{M}{2}$. The spatial cutoff $a = \frac{1}{T}$ used earlier, translates to a p-cutoff of T. Since $M \approx 2T$, the negative range is physically not relevant. These observations are similar to the ones encountered in the DH analysis of the electric and magnetic correlation functions in [43] (first reference).

The HNC equations (141) allow to go beyond the DH approximation in the dense ensemble, but requires a numerical calculation. Here, we only mention that a simple non-linear correction to the DH result follows from (141) by retaining the leading correction to the direct correlation function, namely $c^{ij} \approx -\beta\mathcal{V}^{ij} + \frac{1}{2}(h^{ij})^2$, and use it to iterate the OZ equation after the substitution $h \to h_{DH}$. The net effect is a non-linear correction to the DH result (143) in p-space

$$h_{DH2} = \frac{-\beta\mathcal{V} + \frac{1}{2}h_{DH}^2}{1+\rho(\beta\mathcal{V} - \frac{1}{2}h_{DH}^2)} \tag{147}$$

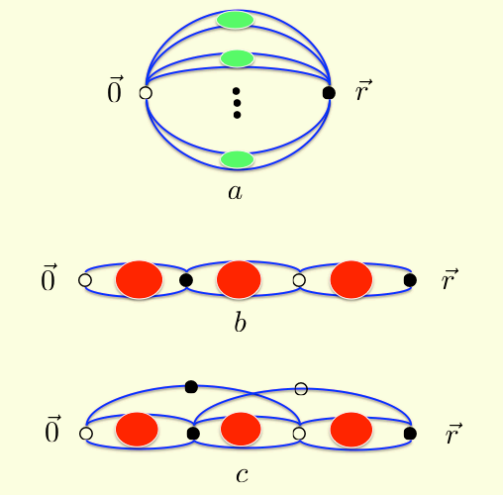

Figure 14: (a) Typical diagrammatic contribution to the pair correlation function $h(r)$ where each hanging ring is $-\beta\mathcal{V}+\chi$; (b) Typical contribution to χ_a; (c) Typical contribution to χ_b.

3.5.3 Instanton-dyon crystal

At even higher fugacity or density, the instanton- and anti-instanton dyons are expected to crystalize. A typical bcc cubic crystal arrangement with low energy is illustrated in Fig. 16. Recall that the re-summed $M\bar{M}$ interactions and $L\bar{L}$ interactions are repulsive, while the LM and $\bar{L}M$ interactions are attractive. In the bcc crystal structure, we note that the nearest neighbor LM vertices are close to an instanton configuration, while their alternate nearest neighbors $\bar{L}M$ vertices are close to a magnetically charge 2 bion. We will refer to this as crystal duality. We note that holographic dyonic-crystals composed only of L, M in salt-like or popcorn-like crystal configurations were suggested in [49] for a holographic description of dense matter.

The instanton- and anti-instanton-dyons considered throughout are the lightest of a Kaluza-Klein tower with higher winding numbers which carry larger actions (more massive). We expect them to crystallize following a similar pattern, albeit with higher windings. We expect this tower of 3-dimensional crystal arrangements along the extra winding direction to be dual to a 4-dimensional crystal arrangement of monopoles and anti-monopoles (or instantons and anti-instantons by crystal duality), using the Poisson duality suggested in [44]. Remarkably, the resulting 4-dimensional and semiclassical description at very low temperature, can be either described as instanton-like (topologically charged) or monopole-like (magnetically charged) as the two descriptions are tied by crystal duality.

The crystal is an idealized description of the strongly coupled and dense phase as both the low temperature and the quantum fluctuations cause it to melt. The melted form of Fig. 16 resembles an ionic liquid with 4 species of ions with strong local order. This semi-classical description of the Yang-Mills state at very low temperature appears to reconcile the instanton liquid model without confinement, with the t′Hooft-Mandelstam proposal with confinement. In the former, the low temperature thermal state is composed of a liquid of instanton and anti-instantons, while in the latter it is a superfluid of monopoles and anti-monopoles with bions as precursors [44]. The dual descriptions allow for a center symmetric thermal state with both strong and local topological and magnetic correlations.

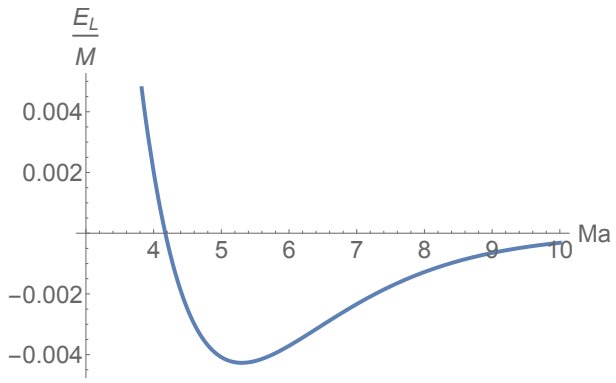

Figure 15: Crystal energy for the bcc arrangement E_L/M versus Ma as given in (153) with $\alpha_s = 1$.

3.5.4 Crystal energy

To assess the crystal contribution to the pressure at high density, we first evaluate the interaction energy for the crystal structure in Fig. 16. Consider the L instanton-dyon sitting in the center of the M cell. The interaction summation within the L-lattice reads

$$2E_L = \sum_{n_1,n_2,n_3\neq 0} (1-(-1)^{n_1+n_2+n_3}) V(\vec{r}_{n_1,n_2,n_3}) \tag{148}$$

The mutual interaction between the L- and M-lattice is

$$\begin{aligned} -2E_{ML} = & \sum_{n_1,n_2,n_3} (1-(-1)^{n_1+n_2+n_3}) \\ & \times V\left(\frac{1}{2}\vec{r}_{111} + \vec{r}_{n_1,n_2,n_3}\right) \end{aligned} \tag{149}$$

In momentum space, these sums can be cast using the dual lattice $\vec{b}_n = \frac{2\pi}{a}\vec{n}$, using the identity

$$\sum_{a_n} e^{ip\cdot a_n} = \sum_n \delta(p-b_n) \tag{150}$$

The results are

$$\begin{aligned} 2E_L = &\quad \sum_n \left(V(b_n) - V\left(b_n + \frac{\pi}{a}(1,1,1) \right) \right) \\ -2E_{ML} = &\quad \sum_n (-1)^n \left(V(b_n) - V\left(b_n + \frac{\pi}{a}(1,1,1) \right) \right) \end{aligned} \tag{151}$$

where we made use of

$$e^{ib_n \cdot \frac{r_{111}}{2}} = (-1)^{n_1+n_2+n_3} = (-1)^n \tag{152}$$

Both the x-space sums (148-149) and the p-space sums (151) can only be carried numerically. However, we note that the x-sum is converging exponentially and can be approximated by the leading contribution involving only the nearest neighbors,

$$E_L \equiv M E_L(\tilde{a}) \approx M \left(6V(\tilde{a}) - 4V\left(\frac{\sqrt{3}\tilde{a}}{2} \right) \right) \tag{153}$$

with $V(x) = \frac{1}{\alpha_s}(-\frac{2}{x} + 1)e^{-x}$ from (232) with $C_D = 2$. Here we have set $\tilde{a} = Ma$, with $M^2 = \frac{2n}{T}$ and $n = 8\pi f$. Note that the total energy of the crystal is extensive

$$E(N, M) \approx 2NME_L \left(\tilde{a} \equiv Ma = \left(\frac{M^3 V_3}{2N} \right)^{\frac{1}{3}} \right) \tag{154}$$

In Fig. 15 we show the behavior of (153) for $\alpha_s = 1$. The bcc configuration is bound for $\tilde{a} = Ma \approx 5$, but the binding energy is very small $E_L/M \approx -0.004$.

3.5.5 Disordered crystal pressure

The pressure for a disordered crystal follows from the corresponding partition function

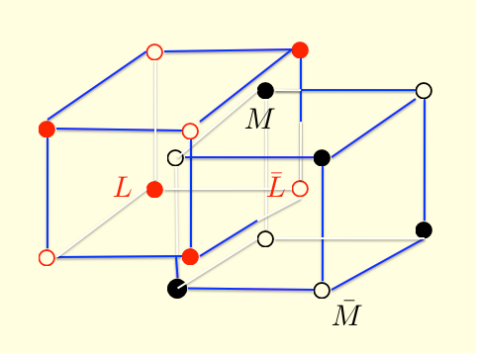

Figure 16: 3-dimensional bcc crystal composed of the instanton- and antinstanton-dyons with the lowest winding, for 2 colors.

$$\Omega_{\rm bcc}(\tilde{a}) = \sum_N \frac{(V_3 2\pi\tilde{f})^{4N}}{(N!)^4} e^{-\frac{2NM}{T}E_L(\tilde{a})} \tag{155}$$

where we used the quantum and dressed fugacity $2\pi\tilde{f} = 2\pi f\sqrt{4\nu\bar{\nu}}$ from (122). In the large N-limit, the pressure $\mathcal{P} = \ln\Omega_{\rm bcc}/V_3$ can be cast in the form

$$\frac{\mathcal{P}(\tilde{a})}{T^3} \approx -\frac{m^4}{\tilde{a}^3}E_L(\tilde{a}) + \frac{2m^3}{\tilde{a}^3}\left(1 + \ln\left(\frac{\tilde{a}^3\sqrt{\nu\bar{\nu}}}{2m}\right)\right) \tag{156}$$

with $m = M/T$ (the ratio of the screening mass to the temperature). The first contribution in (156) is the crystal energy, and the second contribution is the entropy of the competing trees at large density as discussed in IVA. For large m (very low temperature) the pressure is dominated by the crystal contribution, while for small m (intermediate temperature) the pressure is dominated by the entropy of the trees. In Fig. 17 we show the behavior of the pressure $\mathcal{P}(\tilde{a})$ versus $\tilde{a}$ for $m = 20$ for the center symmetric case with $\nu = \frac{1}{2}$ upper-solid-curve, while the crystal contribution is shown as the lower-solid-curve, and the tree contribution as the dashed-curve. The pressure is maximum at

$$\begin{aligned}\frac{\mathcal{P}_{\rm max}}{T^3} = \quad & \frac{m^2}{2}\sqrt{4\nu\bar{\nu}}e^{-\frac{m}{2}(E_L(\tilde{a}_\star)-\tilde{a}_\star^3 E_L'(\tilde{a}_\star))} \\ & \times\left(1 - \frac{m\tilde{a}_\star^3}{2}E_L'(\tilde{a}_\star\right)\end{aligned} \tag{157}$$

with $\tilde{a}_\star$ solution to the transcendental equation

$$\frac{\tilde{a}_\star^3\sqrt{\nu\bar{\nu}}}{2m} = e^{\frac{m}{2}(E_L(\tilde{a}_\star)-\tilde{a}_\star^3 E_L'(\tilde{a}_\star))} \tag{158}$$

If we were to assume E_L fixed at the crystal minimum and constant as in Fig. 15, i.e $E_{L\rm min} \approx -0.004$, then (157) simplifies

$$\frac{\mathcal{P}_{\rm max}}{T^3} \to \frac{m^2}{2}\sqrt{4\nu\bar{\nu}}\, e^{-\frac{m}{2}E_{L\rm min}} \tag{159}$$

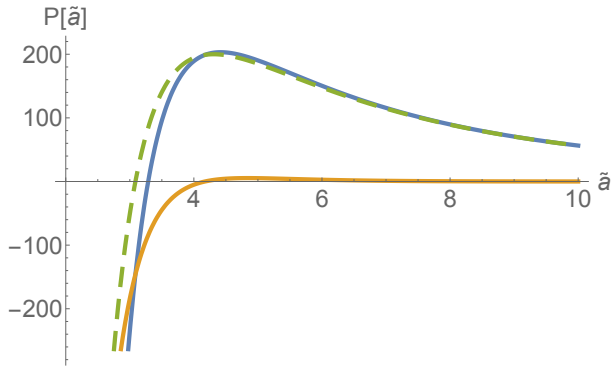

Figure 17: Pressure (156) versus $\tilde{a}$ for $m = 20$ and $\nu = \frac{1}{2}$ upper-solid-curve. The separate contributions from the crystal (first term in (156)) is shown as the lower-solid-curve, and the entropy of the re-summed trees (second term in (156)) is shown as the dashed-curve.

which is seen to interpolate between the re-summed tree contribution (131) at small m (intermediate temperature) and the crystal at large m (very low temperature). Due to the small binding energy of the crystal shown in Fig 15, the crystal contribution takes over only when $\frac{m}{2}$ is large or very high density (very low temperature). This is confirmed numerically. Note that in both (156) and (159) the ratio $\frac{m}{2}$ plays the role of the Coulomb factor. It is rather large with $\frac{m}{2} = 500$ for the onset of the crystal.

3.6 Conclusions

We have provided a many-body analysis of the instanton-dyon liquid model in the center symmetric phase. The starting point of the analysis was a linearization of the moduli interactions beween like instanton-dyons DD and anti-instanton-dyons ($\bar{D}\bar{D}$), followed by a cluster expansion. This re-organization of the many-body physics was shown to be captured exactly by a 3-dimensional effective theory between charged particles. A semi-classical treatment of this effective theory amounts to re-summing the tree contributions in the form of effective fugacities, while the 1-loop correction amounts to re-summing all ring or chain diagrams with effective fugacities. The tree or chain contributions are found to yield a center symmetric phase even at finite vacuum angle. They are dominant in the range $1 \leq \frac{m}{2} \leq 10$.

At very low temperature or large fugacities, an even larger class of diagrams need to be re-summed. In this vein we have carried the HNC resummation as is commonly used for dense and charged liquids, and used it to estimate the pair correlation function around the DH approximation in the dense instanton-dyon liquid. The very low temperature phase is argued to be a melted bcc crystal with strong local topological and magnetic correlations. A simple description of the thermodynamics of an ensemble composed of trees and bcc crystals show that the tree-like contributions are dominant for most temperatures, with the exception of the very low temperature regime where the crystal arrangement is more favorable owing to its very small binding. To better understand the range of validity of the present diagrammatic results, it will be important to carry a full molecular dynamics calculation for comparison. This point will be addressed in the future.

Part II: Chiral vortical and magnetic effects in QCD-like theories.

4 Rotating Fermionic system in 1+2 dimension

This section is an edited version of my publication :
Rotating Dirac fermions in a magnetic field in 1+2,3 dimensions
Yizhuang Liu, Ismail Zahed (SUNY, Stony Brook).Oct 8, 2017. 16 pp. arXiv:1710.02895, submitted to Phys. Rev. D.

4.1 Introduction

This section consists of a number of new results: 1/ a full analysis of the combined effects of a rotation and magnetic field on free and interacting Dirac fermions in 1+2 dimensions, both at weak and strong coupling; 2/ a correspondence with anomalies in arbitrary dimensions; 3/ a deformation of the current densities by centrifugation in the presence of a magnetic field; 4/ a depletion of the QCD chiral condensate in leading order in the pion interaction; 5/ a charge pion condensation induced by centrifugation in a magnetic field.

The outline of this section is as follows: In subsection II we detail the Landau level problem for free Dirac fermions in 1+2 dimensions in the presence of an arbitrary rotation described using a local metric. In subsection III we explore the effects of the interaction on the free results through a 4-Fermi interaction both in the weak and strong coupling regime. In subsection IV and V we extend our chief observations to 1+3 dimensions to the free and interacting fermionic cases with particular interest to the shift in the chiral condensate in QCD. In subsection VI, we discuss the possibility for the formation of a pion BEC phase in off-central heavy ion collisions. Our conclusions are in subsection VII. We record in the Appendices useful details regarding some of the calculations.

4.2 Dirac fermions in 1+2

In this subsection we will outline how to implement a global rotation through a pertinent metric. We will then use it to derive explicit results for massless Dirac fermions with a global $U(2)$ symmetry in the presence of a parallel magnetic field in 1+2 dimensions. The basic mechanism of the shift caused by the rotation on the LLL will be clearly elucidated, and both the scalar and vector densities evaluated.

4.2.1 Metric for a rotating frame

To address the effects of a finite rotation Ω in $1+2$ dimensions we define the rotating metric

$$ds^2 = (1 - \Omega^2\rho^2)dt^2 + 2y\Omega dxdt - 2x\Omega dydt \tag{160}$$

The frame fields or veilbeins are defined as $g^{\mu\nu} = e^\mu_a e^\nu_a \eta_{ab}$ with signature $\sqrt{-g} = 1$, in terms of which the co-moving frame is $\theta^a = e^a_\mu dx^\mu$ and $e_a = e^\mu_a \partial_\mu$ are explicitly given by

$$\begin{aligned}(\theta^0, \theta^1, \theta^2) &= (dt, dx - y\Omega dt, dy + x\Omega dt)\\ (e_0, e_1, e_2) &= (\partial_t + y\Omega\partial_x - x\Omega\partial_y, \partial_1, \partial_2)\end{aligned} \tag{161}$$

with the spin connections

$$\begin{aligned}\omega^1_0 = \omega^0_1 &= +\Omega(dy - \Omega x dt)\\ \omega^2_0 = \omega^0_2 &= -\Omega(dx + \Omega y dt)\end{aligned} \tag{162}$$

In a fixed area of size $S = \pi R^2$, the time-like nature of the metric (353) and therefore causality are maintained for $\Omega R \leq 1$. The importance of a finite size for rotating fermions was emphasized in [56]. This will be understood throughout.

4.2.2 Rotation plus magnetic field

The Lagrangian that describes free rotating Dirac fermions in a fixed magnetic field in $1 + 2$ dimensions, reads

$$\begin{aligned}\mathcal{L} &= \bar{\psi}(i\gamma^\mu(D_\mu+\Gamma_\mu)-M)\psi \\ &= \bar{\psi}(i\gamma^0(\partial_t-\Omega(x\partial_y-y\partial_x+iS^z))+i\gamma^i D_i-M)\psi\end{aligned} \tag{163}$$

with the long derivative $D=\partial-ieA$, and the following choice of gamma matrices, γ^a as $\gamma^0=\text{diag}(\sigma_3,-\sigma_3)$,$\gamma^1=\text{diag}(i\sigma_1,-i\sigma_1)$,$\gamma^2=\text{diag}(i\sigma_2,-i\sigma_2)$, to accomodate for both particles and anti-particles.

A thorough analysis of (354) for an external vector potential in a rotationally non-symmetric gauge was given in [62]. Here we insist on preserving rotational symmetry by choosing $A_\mu=(0,By/2,-Bx/2,0)$. As a result, the LL spectrum is characterized explicitly by both energy and angular momentum conservation which are described in terms of the anti-commutative harmonic oscillator a,b operators

$$\begin{aligned}a &= \frac{i}{\sqrt{2eB}}(D_x+iD_y)=-\frac{i}{\sqrt{2eB}}\left(2\bar{\partial}+\frac{eBz}{2}\right) \\ b &= \frac{1}{\sqrt{2eB}}\left(2\partial+\frac{eB\bar{z}}{2}\right)\end{aligned} \tag{164}$$

Throughout, we will assume $eB>0$ unless specified otherwise. The rotating Landau levels are labelled by m,n as

$$E^\pm+\Omega(m-n+\frac{1}{2})=\pm\sqrt{M^2+2eBn}=\pm\tilde{E} \tag{165}$$

for particles and anti-particles. The corresponding normalized scalar wave functions for the n-th Landau level with good angular momentum $l_z=xp_y-yp_z=b^\dagger b-a^\dagger a$ with eigenvalue $m-n$, are

$$f_{nm}=\frac{(a^\dagger)^n(b^\dagger)^m}{\sqrt{n!m!}}f_{00} \tag{166}$$

with the lowest Landau level (LLL) $f_{00}\propto e^{-\frac{1}{4}eB(x^2+y^2)}$. Note that for n=0, we have only one positive energy state with spin up, and one negative energy state with spin down, each with degeneracy $N=eBS/2\pi$. For $\Omega=0$ and

$n > 0$ all Landau level (LL) have degeneracy $2N = eBS/\pi$. The degeneracy is lifted by centrifugation for $\Omega \neq 0$.

In terms of (358) the quantized Dirac fields follow in the form

$$\psi(t,\vec{x}) = \sum_{nmi} (u^i_{nm}(\vec{x}) e^{-iE^+ t}\, a^i_{nm} + v^i_{nm}(\vec{x}) e^{-iE^- t}\, b^{i\dagger}_{nm}) \tag{167}$$

where a^i_{nm} annihilates a particle with positive energy E^+ and spin $i = \pm\frac{1}{2}$, and $b^{i\dagger}_{nm}$ creates a hole with negative energy E^- and spin $i = \mp\frac{1}{2}$. Their corresponding wavefunctions are

$$\begin{aligned}
u_{0m} &= (f_{0m}, 0, 0, 0) \\
v_{0m} &= (0, 0, f_{0m}, 0) \\
u^+_{nm} &= \sqrt{\frac{\tilde{E}+M}{2\tilde{E}}} \left(f_{nm}, \frac{i\sqrt{2eB}}{\tilde{E}+M} f_{n-1,m}, 0, 0 \right) \\
u^-_{nm} &= \sqrt{\frac{\tilde{E}-M}{2\tilde{E}}} \left(0, 0, f_{nm}, -\frac{i\sqrt{2eB}}{\tilde{E}-M} f_{n-1,m} \right) \\
v^+_{nm} &= \sqrt{\frac{\tilde{E}-M}{2\tilde{E}}} \left(f_{nm}, -\frac{i\sqrt{2eB}}{\tilde{E}-M} f_{n-1,m}, 0, 0 \right) \\
v^-_{nm} &= \sqrt{\frac{\tilde{E}+M}{2\tilde{E}}} \left(0, 0, f_{nm}, \frac{i\sqrt{2eB}}{\tilde{E}+M} f_{n-1,m} \right)
\end{aligned} \tag{168}$$

4.2.3 Scalar density

For $M = 0$, (354) exhibits a $U(2)$ symmetry as the set $(\mathbf{1}, \gamma^5, -i\gamma^3, \gamma^{1+2} = -i\gamma^0\gamma^1\gamma^2)$ leaves (354) unchanged. This symmetry rotates particles to anti-particles. The mass upsets this symmetry, and is only $U(1)\times U(1)$ symmetric under the action of $(\mathbf{1}, \gamma^{1+2})$. In [62] it was noted, that for $\Omega = 0$, (354) breaks spontaneously $U(2) \to U(1) \times U(1)$ with a finite condensate $\langle \bar{\psi}\psi \rangle = -N/S$ without fermionic interactions. This is readily understood from the illustration in Fig. 18a, where only the LLL for particle states with spin up and mass $+M$, and antiparticle states with spin down and mass $-M$ are

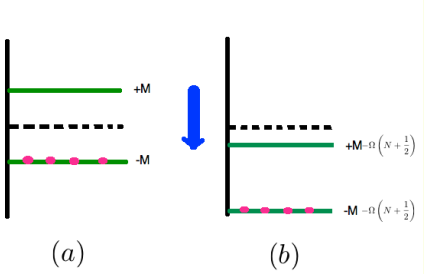

Figure 18: The particle $(+M)$ and anti-particle $(-M)$ LLL for $\Omega = 0$ are shown in (a) each with degeneracy N. For $\Omega \neq 0$ the degeneracy is lifted. In (b) we illustrate how the centrifugation lifts the degeneracy on the states with angular momentum N by shifting them down by $\pm M - \Omega(N + \frac{1}{2})$. The rotating vacuum now includes the particle LLL which needs to be filled.

shown. Each level is N degenerate. The vacuum state consists of filling the anti-particle states only. Clearly, for finite M the $U(2)$ symmetry is explicitly broken. However, as $M \to 0$ the explicit breaking is removed, but the anti-particle states remain still occupied eventhough they have the same zero energy as the particle states. The state breaks spontaneously the balance between particles and anti-particles or $U(2) \to U(1) \times U(1)$. We now show that this *free* scalar condensate disappears for any finite rotation Ω.

For a heuristic arguments for the role of a finite rotation Ω along the magnetic field, we show in Fig. 18b its effect on the LLL with maximum orbital angular momentum N. Both the particle and anti-particle states are shifted down and below the zero energy mark even for $M = 0$. This means that in the rotating vacuum, the particle LLL needs to be filled. Since typically the unordered scalar condensate operator is $\bar{\psi}\psi \sim (a^\dagger a + b^\dagger b - 1)\bar{u}u$, it follows for Fig. 18b that $\bar{\psi}\psi \sim (1 + 0 - 1)\bar{u}u = 0$.

Formally, the scalar condensate carried by the rotating LLL can be explicitly constructed using the fermionic field operator (167). At finite temperature $1/\beta$ and Ω, it is readily found in the form

$$\left\langle \bar{\psi}\psi \right\rangle (r) = \frac{eB}{2\pi} \sum \frac{e^{-\frac{eBr^2}{2}}}{m!} \left(\frac{eBr^2}{2}\right)^m$$
$$\times (n_F(-\beta\Omega(m+1/2)) + n_F(\beta\Omega(m+1/2)) - 1) = 0 \tag{169}$$

which is identically zero even for zero temperature $\beta = \infty$. So any finite rotation, however infinitesimal will cause the scalar density to vanish for free rotating fermions at finite B in $1+2$ dimensions.

4.2.4 Vector density

The local density of Dirac fermions in the rotating frame in $1+2$ dimensions is readily found using (167) in the current density

$$\left\langle j^0(x) \right\rangle = \left\langle : \bar{\psi}\gamma^0\psi : \right\rangle = \sum_{n=0} j^0_n(x) \tag{170}$$

The normal ordering is carried with respect to the true vacuum at finite Ω. Each LL in (360) including the LLL contribute through a tower of rotational states $-n < m < N-n$ for both particles and anti-particles. This finite range in the angular momentum is further detailed in Appendix I. Specifically, and for finite temperature $1/\beta$, the contributions of the LL and the LLL are respectively

$$\begin{aligned} j^0_{n>0}(x) = \quad & \sum_m |f_{nm}|^2 + |f_{n-1,m}|^2 \\ & \times (n_F(E^+_{nm}) - n_F(E^-_{nm})) \\ j^0_{n=0}(x) = \quad & \frac{eB}{2\pi} \sum_m \frac{e^{-\frac{eBr^2}{2}}}{m!} \left(\frac{eBr^2}{2}\right)^m \\ & \times \frac{\sinh(\beta\Omega(m+\frac{1}{2})/2)}{\cosh(\beta\Omega(m+\frac{1}{2})/2)} \end{aligned} \tag{171}$$

with the definition

$$
\begin{aligned}
E^{\pm}_{nm} &= E_n \mp \left(m - n + \frac{1}{2}\right)\Omega \\
&= \sqrt{eBn} \mp \left(m - n + \frac{1}{2}\right)\Omega
\end{aligned}
\tag{172}
$$

We first note that the particle density is inhomogeneous in the plane and peaks at the edge of the disc $S = \pi R^2$ under the effects of centrifugation. For small $\beta\Omega \ll 1$, i.e. small rotations or high temperature, the inhomogeneous particle density carried by the LLL is

$$
\begin{aligned}
j^0_0|_\Omega(r) = &\quad \beta\Omega\frac{eB}{4\pi}\sum_m \frac{e^{-\frac{eBr^2}{2}}}{m!}\left(\frac{eBr^2}{2}\right)^m\left(m+\frac{1}{2}\right) \\
= &\quad \frac{\beta\Omega eB}{4\pi}\frac{1+eBr^2}{2}
\end{aligned}
\tag{173}
$$

Under the combined effect of the rotation and the magnetic field the particle density undergoes a *centrifuge effect* with a maximum at the edge of the rotational plane. This effect will persist even in the presence of interactions as we will discuss below (see Fig. 23).

The total number of particles follow from (360-361) by integration over $S = \pi R^2$. The results for the LL and LLL are respectively

$$
\begin{aligned}
n_n = &\quad 2\sum_m (n_F(E^+_{nm}) - n_F(E^-_{nm})) \\
n_0 = &\quad \sum_m \frac{\sinh(\beta\Omega(m+\frac{1}{2})/2)}{\cosh(\beta\Omega(m+\frac{1}{2})/2)}
\end{aligned}
\tag{174}
$$

For small $\beta\Omega$, which is similar to small Ω or large temperature, the results in (174) simplify

$$
\begin{aligned}
n_n|_\Omega = &\quad 4\beta\Omega\sum_m\left(m-n+\frac{1}{2}\right)\frac{e^{\beta E_n}}{(1+e^{\beta E_n})^2} \\
= &\quad 4\beta\Omega\left(\frac{N^2+2N}{2}-n\right)\frac{e^{\beta E_n}}{(1+e^{\beta E_n})^2} \\
n_0|_\Omega = &\quad \frac{1}{2}\beta\Omega\sum_m\left(m+\frac{1}{2}\right) = \frac{\beta\Omega(N^2+2N)}{4}
\end{aligned}
\tag{175}
$$

We note that in 1+2 dimensions, the LLL generates a net density at $\beta\Omega \ll 1$. For strictly zero temperature (174) gives the exact result

$$n_0|_{\beta=\infty} = \mathrm{sgn}(\Omega)N \tag{176}$$

which can be understood from Fig. 18b for $M \to 0$. Since the *normal ordered* density operator $:\psi^\dagger\psi: \sim (a^\dagger a - b^\dagger b)u^\dagger u \sim (1-0)u^\dagger u$ which precisely gives N. Note that for a rotation opposite to the magnetic field, the LLL shift up and above the zero energy mark. Therefore, we have instead $:\psi^\dagger\psi: \sim (a^\dagger a - b^\dagger b)u^\dagger u \sim (0-1)u^\dagger u$ which precisely gives $-N$, as expected from (176).

These observations are not restricted to only finite temperature. Indeed, at zero temperature but finite chemical potential, the rotation induces changes in the population of the LLL. This can seen through the substitution [56, 59]

$$\beta\Omega\left(m+\frac{1}{2}\right) \to \beta\left(\mu + \Omega\left(m+\frac{1}{2}\right)\right) \tag{177}$$

in (174), with the result

$$\begin{aligned} &n_0(\mu) = N, && \mu \geq -\frac{\Omega}{2} \\ &n_0(\mu) \approx N + 1 + \frac{2\mu}{\Omega}, && -\left(N+\frac{1}{2}\right)\Omega \leq \mu \leq -\frac{\Omega}{2} \\ &n_0(\mu) = -N, && \mu \leq -\left(N+\frac{1}{2}\right) \end{aligned} \tag{178}$$

4.3 Interacting fermions in $1+2$

Consider now fermions in $1+2$ dimensions interacting via 4-Fermi interactions, as a way to model QCD_{1+2} in strong and rotating magnetic fields. The advantage of this reduction is that it will allow for closed form results with physical lessons for QCD_{1+3} dimensions, which even when modeled with 4-Fermi interactions is only tractable numerically. Following [63, 62], we now consider N_c copies of the preceding Dirac fermions, interacting via local 4-Fermi $U(2)$ symmetric interactions

$$\mathcal{L}_{\rm int} = \frac{G}{2}(|\bar{\psi}\psi|^2 + |\bar{\psi}i\gamma^5\psi|^2 + |\bar{\psi}\gamma^3\psi|^2) \tag{179}$$

Standard bosonization gives

$$\mathcal{L}_{\rm int} \to -\bar{\psi}(\sigma + \gamma^3\tau + i\gamma^5\pi)\psi - \frac{1}{2G}(\sigma^2 + \pi^2 + \tau^2) \tag{180}$$

with the scalar fields

$$-\frac{1}{G}\,(\sigma, \tau, \pi) = \left(\bar{\psi}\psi, \bar{\psi}\gamma^3\psi, i\bar{\psi}\gamma^5\psi\right) \tag{181}$$

For large N_c, (381) can be analyzed in the leading $1/N_c$ approximation using the loop expansion for the effective action. Explicit $U(2)$ symmetry makes the effective ation only a function of $\sigma^2 + \tau^2 + \pi^2$, so it is sufficient to search for saddle points with $\tau = \pi = 0$, as others follow by symmetry.

The effective potential stemming from (381) can be organized in three parts

$$\mathcal{V} = \mathcal{V}_0 + \mathcal{V}_T = \frac{\sigma^2}{2G} + \mathcal{V}_\Lambda + \mathcal{V}_T \tag{182}$$

The zero temperature (vacuum) contribution from the fermion loop is

$$\mathcal{V}_\Lambda = -\frac{N_c}{4\pi^{\frac{3}{2}}} \int_{\frac{1}{\Lambda^2}}^{\infty} \frac{ds}{s^{\frac{3}{2}}} e^{-s\sigma^2} eB \coth(eBs) \tag{183}$$

which is cut off in the UV by $1/\Lambda^2$, while the thermal contribution is

$$\mathcal{V}_T = -\frac{N_c T}{S} \sum_{j=1,-1} \sum_{n=0}^{N} \sum_{l=-n}^{N-n} \ln(1 + e^{-\beta(E_n - j\Omega(l+\frac{1}{2}))}) \tag{184}$$

with $E_n = \sqrt{\sigma^2 + 2eBn}$ and $N/S = eB/2\pi$. A complementary but numerically useful approximation to (184) is given in Appendix II using the proper time formalism.

4.3.1 Weak coupling regime

At zero temperature and in the absence of B, Ω, the effective potential (383) for the interacting Dirac fermions in $1+2$ dimensions simplifies

$$\mathcal{V} \to \frac{\sigma^2}{2G} - \frac{N_c}{4\pi^{\frac{3}{2}}} \int_{\frac{1}{\Lambda^2}}^{\infty} \frac{ds}{s^{\frac{5}{2}}} e^{-s\sigma^2} \tag{185}$$

If we set $g = \frac{G\Lambda}{\pi}$, then (185) exhibits a minimum at $\sigma = \Lambda/g_r$ with $1/g_r = 1/g - 1/g_c$, only for sufficiently strong coupling $g > g_c = \sqrt{\pi}$. The minimum breaks spontaneously $U(2) \to U(1) \times U(1)$ with a finite $\langle \bar{\psi}\psi \rangle = -N_c\sigma/G$. The putative chargeless Goldstone mode signals a BKT phase at any finite N_c.

At zero temperature and zero rotation $\Omega = 0$ but with $B \neq 0$, the effective potential (383) can be made more explicit by rescaling and expanding in $1/\Lambda$. For small σ and large Λ the dominant contributions are

$$\begin{aligned} \mathcal{V}_\Lambda = \quad & + \frac{N_c \Lambda^3}{4\pi^{\frac{3}{2}}} \int_1^{\infty} \frac{dx}{s^{\frac{3}{2}}} \frac{eBx}{\Lambda} \coth\left(\frac{eBx}{\Lambda}\right) \\ & - \frac{N_c \Lambda \sigma^2}{2\pi^{\frac{3}{2}}} + \frac{N_c \sigma^3}{3\pi} \\ & + \frac{N_c}{4\pi^{\frac{3}{2}}} \int \frac{ds}{s^{\frac{5}{2}}} (e^{-s\sigma^2} - 1)(eBs \coth(eBs) - 1) \\ & + \mathcal{O}\left(\frac{1}{\Lambda}\right) \end{aligned} \tag{186}$$

The first contribution is independent of σ, so we will ignore it. Therefore, the vacuum contribution to the effective potential combines the first term in (383) and the second and third contributions in (186)

$$\frac{\mathcal{V}_0}{N_c} \approx \frac{\Lambda \sigma^2}{2\pi g_r} - \frac{eB}{2\pi}\sigma + \frac{\sigma^3}{3\pi} \tag{187}$$

In the weak coupling regime

$$0 \leq \left(\frac{1}{g_r} \equiv \frac{1}{g} - \frac{1}{g_c}\right)^{-1} \leq \frac{\Lambda}{eB} \tag{188}$$

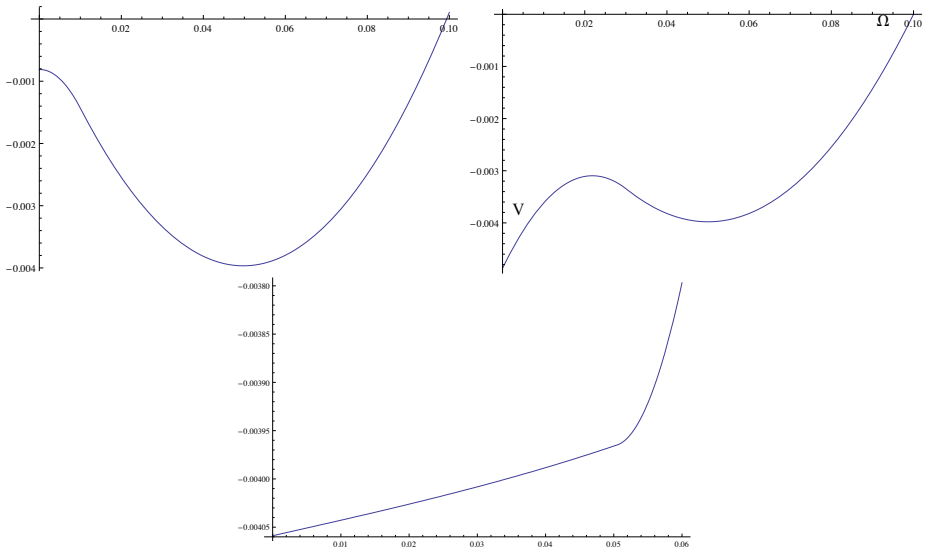

Figure 19: Effective potential $\mathcal{V}$ as a function of σ in units of $\sqrt{eB}$ at $T = 0$: $\Omega = 0.0001\sqrt{eB}$ (top); $\Omega = 0.00049\sqrt{eB}$ (middle); $\Omega = 0.0005\sqrt{eB}$ (bottom).

we can ignore the cubic contribution in (187). A minimum of (187) always exists for arbitrarily weak coupling, with a mass gap $\sigma = \pi g_r N/S\Lambda$ and a finite chiral condensate $\langle\bar{\psi}\psi\rangle = -N_c N/S(1-g/g_c) \approx -N_c N/S$. The latter is in agreement with the result for free Dirac fermions. This is the phenomenon of magnetic catalysis [62].

4.3.2 Vacuum with $\Omega \neq 0$

At zero temperature, the effective potential for rotating Dirac particles in a strong magnetic field is given by the first two contributions in (383) plus the contribution from the rotating anti-particles in the LL,

$$\begin{aligned}\frac{\mathcal{V}}{N_c} = \quad & +\frac{\Lambda\sigma^2}{2\pi g_r} - \frac{eB}{2\pi}\sigma \\ & -\frac{eB}{2\pi N}\sum_{l=0}^{N}\left(\left(l+\frac{1}{2}\right)\Omega-\sigma\right)\theta\left(\left(l+\frac{1}{2}\right)\Omega-\sigma\right)\end{aligned} \tag{189}$$

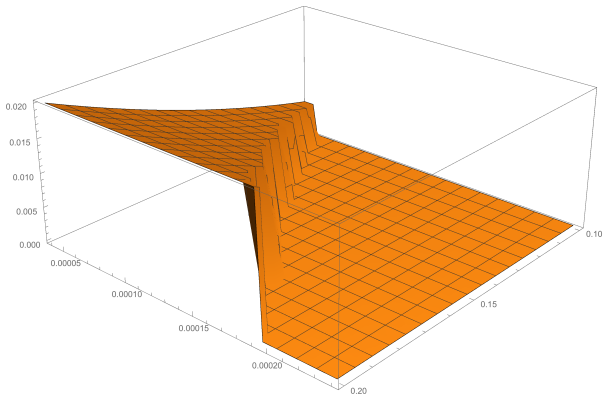

Figure 20: Effective mass as a function of $\sqrt{eB}$ and Ω in units of Λ. The mass gap disappears for $\Omega \geq \Omega_c$ as given by (194) through a first order transition.

For small rotation the summation can be approximated by a continuous integration with the result

$$\frac{\mathcal{V}}{N_c} \approx \frac{\Lambda\sigma^2}{2\pi g_r} - \frac{eB}{2\pi}\sigma - \frac{1}{2\Omega S}\theta(E_\Omega - \sigma)(E_\Omega - \sigma)^2 \tag{190}$$

with $E_\Omega = (N + \frac{1}{2})\Omega$. For $\sigma > E_\Omega$, the effective potential is independent of Ω, and develops a minimum for

$$\begin{aligned} \sigma_2 &= +\frac{\pi g_r}{\Lambda}\frac{eB}{2\pi} \\ \frac{\mathcal{V}_2}{N_c} &= -\frac{\pi g_r}{2\Lambda}\left(\frac{eB}{2\pi}\right)^2 \end{aligned} \tag{191}$$

In contrast, for $\sigma < E_\Omega$, (190) depends on Ω through

$$\frac{\mathcal{V}}{N_c} \approx \left(\frac{\Lambda}{2\pi g_r} - \frac{eB}{4\pi N\Omega}\right)\sigma^2 + \frac{eB}{4\pi N}\sigma - \frac{eB\Omega}{4\pi}\left(N + \frac{1}{2}\right) \tag{192}$$

and prefers always

$$\begin{aligned} \sigma_1 &= \quad 0 \\ \frac{\mathcal{V}_1}{N_c} &= \quad -\frac{E_\Omega}{2}\frac{eB}{2\pi} \end{aligned} \tag{193}$$

For $E_\Omega < \frac{\pi g_r}{\Lambda}\frac{eB}{2\pi}$ the 2-minimum (193) is dominant. The rotating vacuum develops a scalar condensate $\langle\bar{\psi}\psi\rangle \neq 0$ with finite σ_2 but zero fermion density $\langle\bar{\psi}\gamma^0\psi\rangle = 0$. In the opposite, with $E_\Omega > \frac{\pi g_r}{\Lambda}\frac{eB}{2\pi}$, the 1-minimum (193) takes over. The rotating vacuum prefers a gapless solution with $\sigma_1 = 0$ and zero scalar condensate $\langle\bar{\psi}\psi\rangle = 0$, but a finite fermion density $\langle\bar{\psi}\gamma^0\psi\rangle \neq 0$. In large N, the critical value for which this occurs is

$$\Omega_c = \frac{g_r}{2N+1}\frac{eB}{\Lambda} \tag{194}$$

This is the phenomenon of rotational inhibition of the magnetic catalysis noted in $1+3$ dimensions in [56]. At finite but large N and without the use of the continuum approximation and keeping the σ^3 term, the results remain quantitatively almost the same, with one exception that the local minimum $\sigma_1 = 0$ can overtake the finite local minimum σ_2 slightlly before the Ω_c. For $\Lambda = 10\sqrt{eB}$ and $N = 100$, (194) yields Ω_c=0.000497$\sqrt{eB}$. We note that in the free case with $\Lambda \to \infty$, (194) yields $\Omega_c \to 0$ in agreement with the observation in (380). Any finite rotation destroys the free scalar condensate.

In Fig. 19 we show the behavior of the effective potential for finite but small Ω with the two local minima (191) and (193). We have used $\Lambda/\sqrt{eB} = 10$, $N = 100$ and $g_r = 1$. A transition sets in numerically $\Omega_c = 0.000488\sqrt{eB}$ in agreement with (194). In Fig. 20 we display the effective mass as as function of $\sqrt{eB}$ and Ω in units of Λ, for $g_r = 1$ (weak coupling regime) and $T = 0$. While the mass gap is seen to increase slightly faster than linearly with $\sqrt{eB}$ at $\Omega = 0$, the effects of the rotation is to cause it to disappear at the critical value (194) through a first order transition at weak coupling.

4.3.3 Thermal state with $\Omega \neq 0$

First we note that the existence of a mass gap for any finite temperature does not contradict the Mermin-Wagner-Coleman (MWC) theorem, since the thermal state is in a BKT phase rather than a spontaneously broken or Goldstone phase. Having said that, at finite temperature and weak coupling,

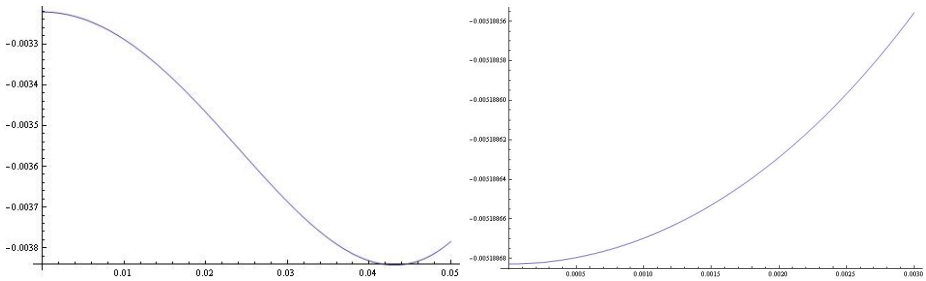

Figure 21: Finite temperature effective potential $\mathcal{V}$ as a function of σ in units of $\sqrt{eB}$: $\beta = 100/\sqrt{eB}$ and $\Omega = 0.0003\sqrt{eB}$ (top); $\beta = 43/\sqrt{eB}$ and $\Omega = 0.0001\sqrt{eB}$ (bottom).

we note that since $\sigma_2 \ll \sqrt{eB}$, the temperatures of interest for the vanishing of the mass gap, are in the low range with $T \ll \sqrt{eB}$. Therefore, only the $j = \pm 1$ LLL contribute in (184). For $T \approx T_c \approx \sigma_2$, the potential flattens out and the centrifugation near $\sigma = 0$ becomes visible leading to a small value for the critical Ω_c.

In Fig. 21 we show the behaviour of the effective potential for $\Lambda/\sqrt{eB} = 10$, $N = 100$ and $g_r = 1$ (weak coupling) for $\beta = 80/\sqrt{eB}$ and $\beta = 43/\sqrt{eB}$. For $\beta \geq 80/\sqrt{eB}$ the transition occurs at $\Omega_c \approx 0.0005\sqrt{eB}$, and for $\beta = 43/\sqrt{eB}$, the transition is around $\Omega_c = 0.0001\sqrt{eB}$. The critical temperature is numerically in the range $\beta_c \approx (40-43)/\sqrt{eB}$. The behavior of the effective mass is shown in in Fig. 22 for the same value of $g_r =$ (weak coupling) and $\Lambda = 10\sqrt{eB}$, as a function of β and Ω for the ranges $50 < \beta < 80$ and $0.0003 \leq \Omega \leq 0.0006$ in units of $\sqrt{eB}$.

In Fig. 23 we show the analogue of the profile density (173) in units of $\sqrt{eB}$, in the weak coupling regime with $g_r = 1$ and for $1/\beta \ll \Omega$ as a function of $x = eBr^2/2$. The first figure from the top is for $\Omega = 0.00005\sqrt{eB}$ for $1/\beta = 0$. It is roughly constant and drops sharply at the edge of the causality disc fixed by $\Omega R = 1$. However, for $\Omega \ll 1/\beta \ll \sqrt{eB}$ a linear behavior sets in the middle of the disc, to drop only sharply at the edge. The second and third figures from the top are for $\beta = 100/\sqrt{eB}$ and $\Omega = 0.0001\sqrt{eB}$ and $\Omega = 0.0005\sqrt{eB}$ respectively. The fourth figure is for $\beta = 40/\sqrt{eB}$ at $\Omega = 0.0001\sqrt{eB}$. As we indicated in section IID for the free case, this *centrifugation effect* holds for the interacting case as well and carries to higher dimensions as we show below. We will suggest a possible physical application

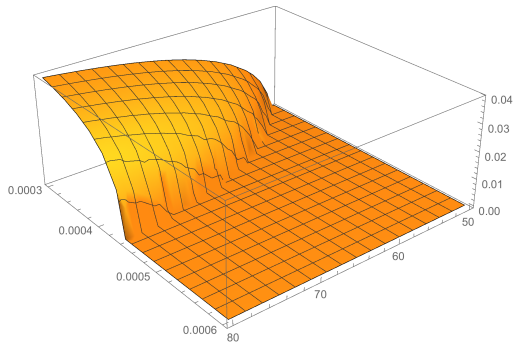

Figure 22: Effective mass as a function of β and Ω in units of $\sqrt{eB}$ at $T \neq 0$.

in 1+3 dimensions. Finally, the occurence of surface or edge modes was noted recently in [60]. We show in Appendix IX that they do not alter our current discussion for large N.

4.3.4 Dense state with $\Omega \neq 0$

For completeness, we now explore the effects of a finite chemical potential μ on the mass gap for $\bar{\psi}\psi$ pairing. Just as a caution, we note that a more complete treatment would require the inclusion of the competing $\psi\psi$ channel as well. However, we note that in leading order in $1/N_c$ the $\psi\psi$ channel is $1/N_c$ suppressed in comparison to the $\bar{\psi}\psi$ channel and can be ignored. With this in mind, the effect of a finite chemical potential follows from (385) through the substitution $\Omega(l + \frac{1}{2}) \to \mu + \Omega(l + \frac{1}{2})$, which we now briefly address.

In Fig. 24 we show the behavior of the effective potential $\mathcal{V}$ for $\beta = 80/\sqrt{eB}$ and $\mu = 0.007/\sqrt{eB}$ as a function of σ in units of $\sqrt{eB}$. The top figure is for $\Omega = 0$ and the bottom figure is for $\Omega = 0.0003\sqrt{eB}$. The increase in the rotation causes the loss of the gapped solution. In particular, for $g_r = 1$ (weak coupling), $\beta = 80/\sqrt{eB}$ and $\Omega = 0$, the critical value is $\mu_c = 0.02\sqrt{eB}$, while for $\Omega = 0.0003\sqrt{eB}$, the critical value is $\mu_c = 0.007\sqrt{eB}$.

Finally and for completeness, we discuss in Appendix III the dense state with *negative* μ. Since the model under consideration can be viewed as an effective description of planar condensed matter systems [63], a negative chemical potential is experimentally accessible.

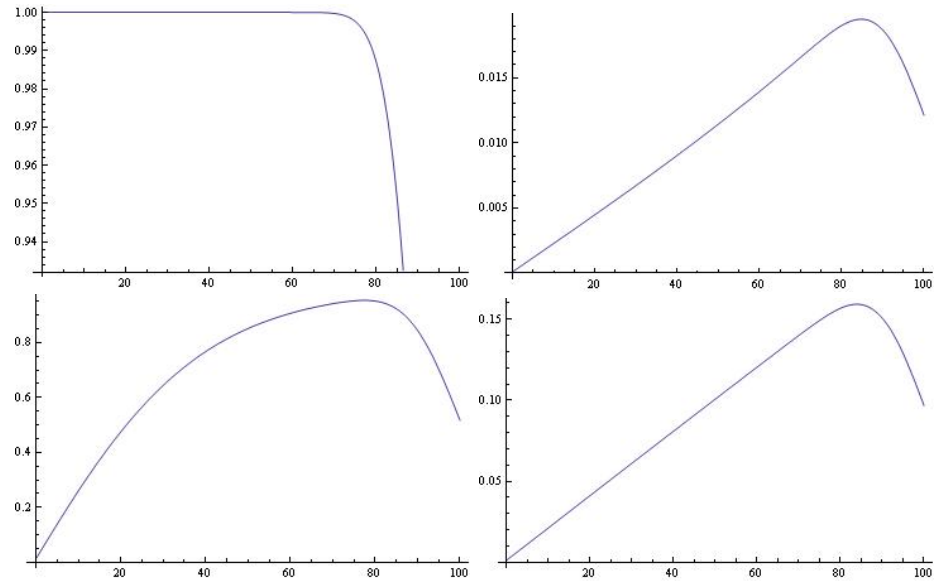

Figure 23: The current density in the weak coupling regime with $g_r = 1$, as a function of x=$\frac{eBr^2}{2}$ in unit of $\frac{eB}{2\pi}$ at $T = 0$ and $\Omega = 0.0005$ (in unit of $\sqrt{eB}$) (first); $\beta = 100$, $\Omega = 0.0001$ (second); $\beta = 100$, $\Omega = 0.0005$ (third); $\beta = 40$, $\Omega = 0.0001$ (fourth)

4.3.5 Strong coupling regime

In the opposite regime of strong coupling with $g > g_c$, a mass gap also forms. In the regime where the ratio $\frac{\Lambda}{\sqrt{eB}}$ is large and $g > g_c$ or $g_r < 0$, the minimum of the effective potential is now controlled by the first and third contributions in (187) namely

$$\frac{\mathcal{V}_0}{N_c} \approx -\frac{\Lambda\sigma^2}{2\pi|g_r|} + \frac{\sigma^3}{3\pi} \tag{195}$$

with a mass gap $\bar{\sigma} = \Lambda/|g_r|$. For $\sqrt{eB}/\Lambda < 1$, the leading contribution shifts the mass and the scalar condensate quadratically,

$$\frac{\langle\bar{\psi}\psi\rangle_B}{\langle\bar{\psi}\psi\rangle_0} - 1 \approx \frac{(eB)^2}{12(\Lambda/g_r)^4} \tag{196}$$

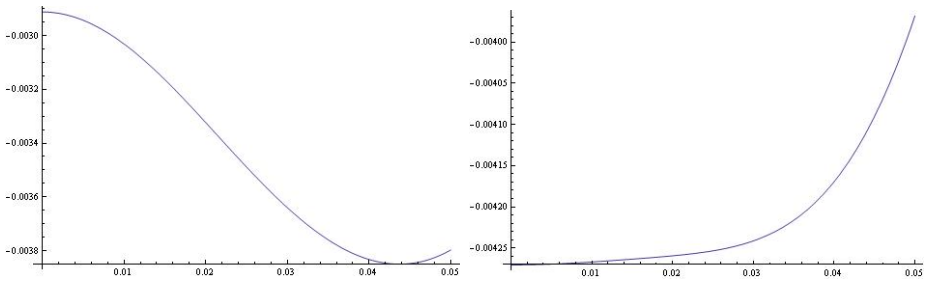

Figure 24: Finite temperature effective potential $\mathcal{V}(\sigma)$ at $\beta = 80/\sqrt{eB}$ and $\mu = 0.007/\sqrt{eB}$ as a function of σ in units of $\sqrt{eB}$: $\Omega = 0$ (top) and $\Omega = 0.0003\sqrt{eB}$ (bottom)

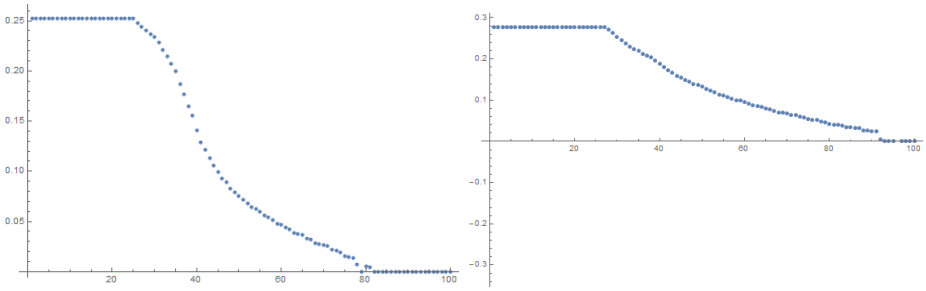

Figure 25: Mass gap σ/Λ in the strong coupling regime with $g_r = -4$, as a function of $\Omega/(10^{-4}\Lambda)$ for $\Lambda/\sqrt{eB} = 5$ (top) and $\Lambda/\sqrt{eB} = 3$ (bottom).

We note that the ratio of the mass gap to the LL gap $\bar{\sigma}/\sqrt{eB}$ can be very large. Therefore, the critical Ω_c for which the mass gap can be depleted is much larger in strong coupling than in weak coupling. For fixed Ω , the mass $\bar{\sigma}$ decreases as the ratio $\Lambda/\sqrt{eB}$ decreases. For instance, for $g_r = -4$ and $\Lambda/\sqrt{eB} = 5$, $\Omega_c \approx 0.008\Lambda$, but for $\Lambda/(\sqrt{eB}|g_r|) = 3$, $\Omega_c \approx 0.009\Lambda$. In Fig. 28 we show the behavior of the mass gap for strong coupling with $g_r = -4$ versus σ in units of Λ as a function of Ω expressed in units of $\Lambda/10^4$. The top figure is for $\Lambda/\sqrt{eB} = 5$ and the bottom figure is for $\Lambda/\sqrt{eB} = 3$.

4.4 Free Dirac fermions in 1+3

The extension of the previous analysis to 1+3 dimensions for free Dirac fermions is straightforward. In Appendix IV we detail the rotating wavefunctions in the presence of a magnetic field, for the free case. The interacting case is more challenging for say the case of QCD which is strongly coupled and gapped in the vacuum. Below, we will focus on the combined effects of a rotation and magnetic field on the QCD chiral condensate in the spontaneously broken phase using mesoscopic arguments, and leading order chiral perturbation.

4.4.1 Free left currents

We now extend the analysis for the left or L-currents to show the generic nature of the observations made in $1+2$ dimensions above. From Appendix IV, the L-wavefunctions in $1+3$ dimensions take the simplifying form

$$\begin{aligned} u_L(n=0) = \quad & v_l(n=0) = \sqrt{\frac{\tilde{E}-p}{2\tilde{E}}}(f_{0,m},0) \\ u_L(n,m) = \quad & \frac{1}{\sqrt{2\tilde{E}(\tilde{E}+p)}}(\sqrt{2eBn}f_{nm},(\tilde{E}+p)f_{n-1,m}) \\ v_L(n,m) = \quad & \frac{1}{\sqrt{2\tilde{E}(\tilde{E}+p)}}(\sqrt{2eBn}f_{nm},-(\tilde{E}+p)f_{n-1,m}) \end{aligned} \tag{197}$$

The left particle density at the origin is

$$
\begin{aligned}
&\frac{2\pi}{eB} n_L(0) = \\
&+ \int_{-\infty}^{0} \frac{dp}{2\pi} (n_F(-p-\mu_{00}) - n_F(-p+\mu_{00})) \\
&+ \sum_{n=1} \int_{-\infty}^{\infty} \frac{dp}{4\pi} (n_F(E_n-\mu_{00}) + n_F(E_n-\mu_{10})) \\
&- \sum_{n=1} \int_{-\infty}^{\infty} \frac{dp}{4\pi} (n_F(E_n+\mu_{00}) + n_F(E_n+\mu_{10}))
\end{aligned}
\tag{198}
$$

while the current density at the origin is

$$
j_L^3(0) = \frac{eB}{2\pi} \left(J_{L,0}^3 + \sum_{n=1} J_{L,n}^3 \right) \tag{199}
$$

with

$$
\begin{aligned}
J_{L,0}^3 = \quad & - \int_{-\infty}^{0} \frac{dp}{2\pi} (n_F(-p-\mu_{00}) - n_F(-p+\mu_{00})) \\
= \quad & -\frac{\Omega}{4\pi} - \frac{\mu_L}{2\pi} \\
J_{L,n}^3 = \quad & - \sum_{n=1} \int_{-\infty}^{\infty} \frac{dp}{4\pi} (n_F(E_n-\mu_{00}) - n_F(E_n-\mu_{10})) \\
& + \sum_{n=1} \int_{-\infty}^{\infty} \frac{dp}{4\pi} (n_F(E_n+\mu_{00}) - n_F(E_n+\mu_{10}))
\end{aligned}
\tag{200}
$$

with $\mu_{00} = \frac{\Omega}{2} + \mu_L$ and $\mu_{10} = -\frac{\Omega}{2} + \mu_L$. For small B and zero μ_L, the summation in (199) gives

$$
\sum \frac{eB}{2\pi} f(\sqrt{p^2 + 2gBn}) \to \int \frac{kdk}{2\pi} f(\sqrt{p^2+k^2}) \tag{201}
$$

This reproduces the known result at $B = 0$ [75]

$$-\frac{T\Omega}{12\pi^2}-\frac{(\Omega+2\mu_L)^3+(\Omega-2\mu_L)^3}{96\pi^2} \tag{202}$$

While the current density at the origin reproduces the expected result, the distribution of the current density in the radial direction is not homogeneous. Indeed, the centrifugation causes it to peak at the edge as in 1+2 dimensions. This is readily seen from the contribution of the LLL which can be worked out explicitly with the result

$$J^3_{Ln=0}=-\frac{eB}{4\pi^2}\sum_{m=0}e^{-\frac{eBr^2}{2}}\left(\frac{eBr^2}{2}\right)^m\frac{(m+1/2)\Omega+\mu_L}{m!} \tag{203}$$

The sum can be performed exactly with the result

$$J^3_{Ln=0}(r)=\frac{eB}{4\pi^2}\left(\mu_L+\Omega\left(\frac{1}{2}+\pi Nr^2\right)\right) \tag{204}$$

The *centrifugal effect* causes the current density to peak at the edge of the rotational plane in $1+3$ dimensions.

A possible application of this phenomenon maybe in current heavy ion collisions at collider energies such as RHIC and LHC. Indeed, for semi-central collisions both the rotational (orbital) and electric magnetic fields are sizable with $\Omega\sim eB\sim m_\pi$ which may induce partonic densities of the type (204) that are largely deformed in the transverse plane. While the rotation and magnetic fields tend to separate the partonic charges in concert along the rotational axis, the centrifugation causes this separation to peak in the orthogonal direction where the observed particle flow is more important. If true, this effect should be seen as an enhancement of v_4 in the charged particle flow.

4.4.2 Number of free left particles

As we noted in $1+2$ dimensions, the number of free left particles increases in $1+3$ dimensions due to the sinking of the particle LLL in the Dirac sea. More explicitly, we have

$$
\begin{aligned}
n_L &= \int dxdy \left\langle : \bar{\psi}_L \gamma^0 \psi_L : \right\rangle \\
&= \sum_m \int_{-\infty}^{0} \frac{dp}{2\pi} (n_F(-p-\mu_m) - n_F(-p+\mu_m)) \\
&+ \sum_{n=1,m} \int_{-\infty}^{\infty} \frac{dp}{2\pi} (n_F(E_n-\mu_{nm}) - n_F(E_n+\mu_{nm}))
\end{aligned}
\tag{205}
$$

Here $\mu_{nm} = (m - n + \frac{1}{2})\Omega + \mu_L$ and $E_n = \sqrt{p^2 + 2eBn}$. The flowing left current along the rotational-magnetic axis is

$$
\begin{aligned}
j_L^3 = & \int dxdy \left\langle \bar{\psi}_L \gamma^3 \psi_L \right\rangle \\
= & -\sum_m \int_{-\infty}^{0} \frac{dp}{2\pi} (n_F(-p-\mu_m) - n_F(-p+\mu_m)) \\
= & -\frac{1}{2\pi} \sum_{m=0}^{N} \left(m + \frac{1}{2} \right) \Omega + \mu_L \\
= & -\frac{\Omega}{2\pi} \left(N + \frac{N^2}{2} \right) - \frac{\mu_L N}{2\pi}
\end{aligned}
\tag{206}
$$

The first contribution in (206) was noted in [54, 56]. (205-206) generalize to arbitrary $1 + d$ dimensions. In particular, for $\mu_L = 0$

$$
n_{L0} = \frac{2^{\frac{d-3}{2}} V_{d-2}}{(2\pi)^{d-2}} \mathrm{sgn}(\Omega) |\Omega|^{d-2} \sum_{m=1}^{N} \left(m + \frac{1}{2} \right)^{d-2} \tag{207}
$$

with the volume $V_{d-2} = \pi^{\frac{d}{2}-1} / \Gamma(\frac{d}{2})$.

4.4.3 Relation to anomalies

These observations can be used to generalize (208) to arbitrary $1 + d = 2n$ dimensions. Consider the case with non-vanishing and non-parallel magnetic

fields $B_{2k,2k+1} \neq 0$ with $1 \leq k \leq n-3$. The general anomaly induced chiral magnetic effect for the left current is [61]

$$J^{2n-1}_{L\mu_L} = -\frac{\mu_L}{2\pi}\left(\frac{e}{2\pi}\right)^{n-1} B_{12}B_{34}....B_{2n-4,2n-3} \tag{208}$$

We now observe from (204) that the role of the rotation is to tag to μ_L in $2n = 4$ dimensions as

$$\frac{eB}{2\pi}\left(\mu_L + \Omega\left(\frac{1}{2} + \pi N r^2\right)\right) \equiv \mu_L \frac{eB}{2\pi} + \Omega\, J(r) \tag{209}$$

The anomalous result (208) relates to the rotationally induced current by a similar subsitution in $2n$ dimensions, namely

$$J^{2n-1}_{L\Omega}(r) = -\frac{1}{2\pi}\left(\frac{e}{2\pi}\right)^{n-2} B_{12}B_{34}....B_{2n-6,2n-5}(\Omega, J(r)) \tag{210}$$

where $J(r)$ refers to the current spin density in the radial direction within the $2n-4, 2n-3$ plane

$$J_{2n-4,2n-3}(r) = \frac{eB_{2n-4,2n-3}}{2\pi}\left(\frac{1}{2} + B_{2n-4,2n-3}\frac{r^2}{2}\right) \tag{211}$$

The rotational contribution to the current density (210) in 2n dimensions is related to the chiral magnetic effect (208) in $2n-2$ dimensions.

4.4.4 Charge neutral volume

Most of the analyses for the fermions presented above hold for the *absolute* ground state with overall charge conservation not enforced (open volume V). If we require total charge neutrality of the system (closed volume V) then we expect an induced charge chemical potential $\mu_{\rm in}$ such that $(\vec{\Omega}\cdot\vec{B} > 0)$

$$\sum_{n,m=0}^{N}\int\frac{dp}{2\pi}n_F\left(E_n-\mu_{\rm in}-\Omega\left(\frac{1}{2}+m-n\right)\right)=$$
$$\sum_{n,m=0}^{N}\int\frac{dp}{2\pi}n_F\left(E_n+\mu_{\rm in}+\Omega\left(\frac{1}{2}+m-n\right)\right) \tag{212}$$

where the number of π^+ (first contribution) balances the number of π^- (second contribution). For large eB or small temperature T, only the $n=0$ term survives as before. In this case, the solution for $\mu_{\rm in}$ follows by inspection

$$\mu_{\rm in}=-\frac{\Omega}{2}-\frac{N\Omega}{2} \tag{213}$$

The ground state consists of negative charge filling the LLL with $m=0$ to $m=\frac{N}{2}$, and positive charge filling the LLL with $m=\frac{N}{2}$ to N. The corresponding charge density for masless fermions is

$$\begin{aligned}&\left\langle J^0_{L,n=0}(x)\right\rangle=\\&\frac{eB}{4\pi^2}\sum_{m=0}^{[\frac{N}{2}]}e^{-\frac{eBr^2}{2}}\left(\frac{eBr^2}{2}\right)^m\frac{(m-\frac{N}{2})\Omega}{m!}\\&+\frac{eB}{4\pi^2}\sum_{m=[\frac{N}{2}]+1}^{N}e^{-\frac{eBr^2}{2}}\left(\frac{eBr^2}{2}\right)^m\frac{(m-\frac{N}{2})\Omega}{m!}\end{aligned} \tag{214}$$

The first line is the contribution from all negative charge contributions, and the second line from all positive charge contributions. After integration, the total negative charge density is

$$\left\langle\int d^2x J^0_{L,n=0}(x)\right\rangle_{\rm negative}=\frac{1}{2\pi}\sum_{m=0}^{[\frac{N}{2}]}\left(m-\frac{N}{2}\right)\Omega \tag{215}$$

and similarly for the positive charge density. In Fig. 26 we display the charge density in the LLL in a closed volume $V=SL$ with total charge neutrality

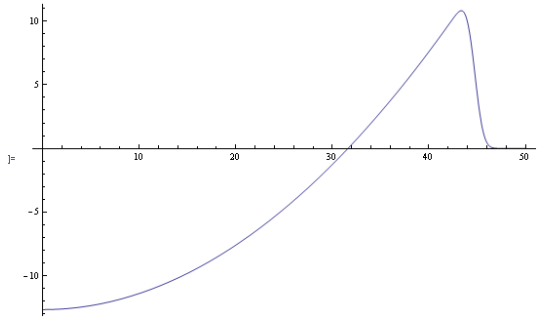

Figure 26: The charge distribution (214) in the LLL in a closed volume V with overall charge neutrality, for $N = 1000$ as a function of r and in units of eB.

as given by (214). We expect the same distribution of charge around a fluid vortex when overall charge neutrality is enforced, which is to be contrasted with a vortex with only positive (negative) charge accumulation when the charge neutrality constrain is not enforced [54].

4.5 Conclusions

We analyzed the combined effects of a rotation and a magnetic field on free and interacting Dirac fermions in 1+2 dimensions. Our results show that the rotation causes massless positive states in the LLL to sink into the Dirac sea, followed by an increase in the density of particles. The scalar density of particles does not change in the free case, but is modified in the interacting case. These results strenghten our earlier observation that an increase in the density of composite fermions in the quantum Hall effect at half filling under rotation would signal their Dirac nature [111]. They may also be of relevance to planar condense matter systems when subject to a parallel rotation plus a magnetic field.

We showed that the mechanism behind the sinking of the LLL for free Dirac fermions, holds in any dimension, leading to a finite increase in the density of particles that is related to anomalies. For QCD in the spontaneously broken phase with Dirac fermions, this mechanism manifests itself in a novel way through the condensation of charged pions. We used this observation to derive the shift in the chiral condensate in leading order in

the pion interaction.

On a more speculative way in QCD, the charged separation caused by the dual combination of a rotation parallel to a magnetic field, may impact on the flow of charged particles in semi-central collisions of heavy ions at present collider energies, provided that the magnetic field is still strong in the freeze-out region. While both the rotation and the magnetic field separate charges along the rotational axis as known through the standard chiral vortical and magnetic effect, the combined effect causes them to centrifuge. The resulting charge separation is quadrupolar as opposed to polar with some consequences for the charged particle flow. Also, the possibility of an induced and coherent charge accumulation by rotation in a magnetic field, whether in the form of partons or pions, may affect the fluctuations in the charge and pion number, the transport coefficients such as the viscous coefficients, and potentially the electromagnetic emissivities in the prompt and intermediate part of the collision, especially their distribution and flow in the low mass region. These issues are worth further investigations.

5 Pion condensation induced by Ω and B

This section in an edited version of my publication :
Pion Condensation by Rotation in a Magnetic field
Yizhuang Liu, Ismail Zahed (SUNY, Stony Brook). Nov 20, 2017. 5 pp.
Phys.Rev.Lett. 120 (2018) no.3, 032001

5.1 Introduction

In this section, we continue our study of the combined effect of B and Ω in the previous section by moving to bosonic system. We will show that new ground state will formed under the combined effect of a strong magnetic field and rotation . In section II we show how this combination yields a charged pion condensation. In section III, we make an estimate of the amount of pion condensation in current heavy ion collisions at collider energies. Our conclusions are in section V.

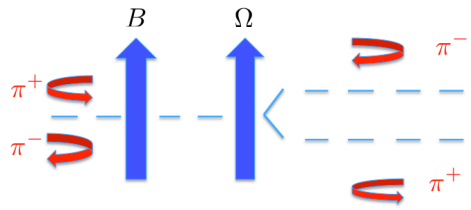

Figure 27: Under the action of an external magnetic field B the $\pi^{\pm}$ undergo opposite rotations in the Lowest Landau Level (LLL) which is degenerate. The action of a parallel rotation ($\vec{\Omega}\cdot\vec{B}>0$) lifts the degeneracy in the LLL. The energy of the π^+ shifts down and splits away from the energy of the π^- that shifts up. The action of an anti-parallel rotation ($\vec{\Omega}\cdot\vec{B}<0$) exchanges the role of π^+ and π^-.

5.2 Pion condensation

In the presence of a fixed magnetic field in the +z direction $\mathbf{B}=B\hat{z}$, the charged $\pi^{\pm}$ pion spectrum is characterized by highly degenerate Landau Levels (LL)

$$E_{np}=\left(|eB|(2n+1)+p^2+m_\pi^2\right)^{\frac{1}{2}} \tag{216}$$

with p the pion momentum along the 3-direction, each with a degeneracy $N=|eB|S/2\pi$ with $S=\pi R^2$ the area of the plane transverse to B. We will assume that the magnetic length $l_M=1/\sqrt{|eB|}\ll R$ for the LL to fit within S. In the circular gauge the degeneracies of the LL are identified with the eigenstates of the z-component of the angular momentum in position space. They are labeled by l which enters the azimuthal wave-function as $e^{il\varphi}$ with the restriction $-n\leq l\leq N-n$ where n labels the LL. For the Lowest Landau Level (LLL) with $n=0$, l has a fixed sign since $0\leq l\leq N$. After quantization, the angular momentum for positive charged particles is l and for negative charged particles is $-l$. This means that in the LLL, the π^+

spins along the magnetic field, while the π^- spins opposite to the magnetic field as illustrated in Fig. 27.

When a rotation Ω along the magnetic field is applied, it causes the spectrum to shift linearly. Throughout we will consider the parallel case with $\vec{\Omega} \cdot \vec{B} > 0$ unless specified otherwise. With this in mind, and in the rotating frame

$$E_{np} \to E_{np} - \Omega L_z \equiv E_{np} - j\Omega l \tag{217}$$

with $j = +1$ for positively charged pions (particles) and $j = -1$ for negatively charged pions (anti-particles). As a result, the degeneracy of each LL is lifted. In particular, the π^+ in the LLL splits down and the π^- in the LLL splits up as also illustrated in Fig. 27. Since the chargeless pions π^0 are unaffected by the magnetic field, their rotational shift averages out. Also we note that causality requires $v = \Omega R \leq 1$ [56] which together with the magnetic length constraint (see above) translates to $l_M \ll R < 1/\Omega$.

The mechanism of $\pi^\pm$ splitting by a rotation parallel to a magnetic field in the LLL can cause π^+ pion condensation. Indeed, in the shifted spectrum (217), the combination $\mu_l = \Omega l$ plays the role of a chemical potential for π^+ and $-\mu_l = -\Omega l$ for π^-, in much the same way as noted for fermionic particles and anti-particles in the LLL [75, 56, 59, 30]. Therefore, when $\mu_N = N\Omega$ apparently exceeds the π^+ effective mass in the LLL, $m_0 = \sqrt{eB + m_\pi^2}$, but is still below the π^+ effective mass in the first LL with $n = 1$, the LLL π^+ may Bose condense, provided that charge conservation is enforced.

For a fixed and isolated volume $V = SL$ with no charge allowed to flow in or out, strict charge conservation in the co-moving frame is achieved by introducing a charge chemical potential μ, in addition to the induced chemical potential $j\Omega l$ by rotation. (For an open volume discussion see [30] and references therein). For the LLL, charge conservation requires that the number of $\pi^\pm$ in V are equal at any temperature

$$\begin{aligned} &\sum_{l=0}^{N} \int \frac{dp}{2\pi} \frac{1}{e^{\frac{1}{T}(E_{0p} - l\Omega - \mu)} - 1} = \\ &\sum_{l=0}^{N} \int \frac{dp}{2\pi} \frac{1}{e^{\frac{1}{T}(E_{0p} + l\Omega + \mu)} - 1} \end{aligned} \tag{218}$$

This equation is solved by inspection with $\mu = -\frac{N\Omega}{2}$. Therefore, the orbital assignments $l = N - m$ and $l = m$ for π^+ and π^- in the LLL will have the same ocupation number

$$\begin{aligned} & n_{\pi^+}(l = N - m) = n_{\pi^-}(l = m) \\ & = \int \frac{dp}{2\pi} \frac{1}{e^{\frac{1}{T}(E_{0p} - N\Omega/2 + l\Omega)} - 1} \end{aligned} \tag{219}$$

with $0 \leq m \leq N$. For $N\Omega > 2m_0$ simultaneous condensation occurs for $m = 0$, i.e. π^+ with $l = N$ and π^- with $l = 0$. For $(N-2)\Omega > 2m_0$ the condensation involves both $m = 0, 1$. As we increase Ω such that $\Omega = 2m_0$, all $m \leq \frac{N}{2}$ will condense, i.e. π^+ with $\frac{N}{2} \leq l \leq N$ and π^- with $0 \leq l \leq \frac{N}{2}$, and so on.

Now consider the rotating ground state with $T = 0$ and $N\Omega > 2m_0$ but $(N-2)\Omega < 2m_0$, so that only the $l = N$ state for π^+ and $l = 0$ state for π^- condense. The energy per unit length in the Bose-Einstein condensate (BEC) state is

$$\mathcal{E}_{\pi\Omega} = -\mathbf{n}\,(N\Omega - 2m_0) + d_N \mathbf{n}^2 \tag{220}$$

with the Coulomb factor

$$d_N \approx \frac{e^2}{2} \int_{l_M}^{R} 2\pi r dr \left(\frac{1}{2\pi r}\right)^2 = \frac{e^2}{4\pi} \ln \frac{R}{a} \approx \frac{e^2}{8\pi} \ln N \tag{221}$$

d_N characterizes the electric field energy stored between two charged rings with radius $l_M \sim 1/\sqrt{eB}$ and charge $-e$ (π^-), and radius $R \gg l_M$ and charge $+e$ (π^+). The Coulomb self-energy is subleading and omitted. In the ground state, the BEC density $\mathbf{n}$ is fixed by minimizing the energy density $\mathcal{E}_{\pi\Omega}$ in (220), with the result

$$\mathbf{n} = \theta(N\Omega - 2m_0) \frac{N\Omega - 2m_0}{2d_N} \tag{222}$$

The rotating π^+ condensate induces a uniform magnetic field $\mathbf{b}_z$ that enhances the applied initial field B, and back-reacts on the formation of the

charged condensates to order $\alpha = e^2/4\pi$. Indeed, the rotating BEC of π^+ at $r = R$ generates an azimutal current

$$J^\theta[\mathbf{n}] = \frac{e\mathbf{n}N}{m_0 r}|f_{0N}|^2 \approx \frac{e^2 B\mathbf{n}}{4\pi m_0}\delta(r-R) \tag{223}$$

where f_{0N} is the LLL with angular momentum $l = N$. The corresponding induced magnetic field

$$\mathbf{b}_z[\mathbf{n}] = \frac{e^2 B\mathbf{n}}{4\pi m_0} \tag{224}$$

modifies the applied magnetic field to order $\alpha = e^2/4\pi$ through $B \to B + \mathbf{b}_z[n]$. The back-reacted LL problem amounts to the following substitutions for m_0 and N

$$\begin{aligned} m_0^2[\mathbf{n}] &= m_\pi^2 + eB\left(1 + \frac{e^2\mathbf{n}}{4\pi m_0}\right) \\ N[\mathbf{n}] &= N\left(1 + \frac{e^2\mathbf{n}}{4\pi m_0}\right) \end{aligned} \tag{225}$$

The back-reacted density for the $\pi^\pm$ condensates follows by minimizing the energy per unit length

$$\begin{aligned} &\mathcal{E}[\Omega, \mathbf{n}] = \\ &-\mathbf{n}(N[\mathbf{n}]\Omega - 2m_0[\mathbf{n}]) + \mathbf{n}^2 e^2\left(\frac{eBN}{16\pi m_0^2[\mathbf{n}]} + \frac{\ln N[\mathbf{n}]}{8\pi}\right) \end{aligned} \tag{226}$$

This is the analogue of (220) with $d_N = \frac{e^2 \ln N(\mathbf{n})}{8\pi}$, including the additional magnetic energy from the back reaction

$$\pi R^2\,\frac{\mathbf{b}_z^2}{2} = \frac{\mathbf{n}^2 e^4 B^2 R^2}{32\pi m_0^2[\mathbf{n}]} = \frac{e^3 BN\mathbf{n}^2}{16\pi m_0^2[\mathbf{n}]} \tag{227}$$

The true ground state follows by minimizing (226) with respect to $\mathbf{n}$. Both $m_0[\mathbf{n}]$ and $N[\mathbf{n}]$ are observed to be weakly dependent on the $\mathbf{n}$-contributions from the back-reaction. We now explore the physical implication of (226) in heavy ion collisions.

5.3 Pion BEC in heavy-ion collisions

Current heavy ion collisions at collider energies are characterized by large angular momenta $l \sim 10^3 - 10^5\,\hbar$ [70] and large magnetic fields $B \sim m_\pi^2$ [73] in off central collisions. Assuming that at chemical freeze-out, $R \sim 10$ fm with still $eB \sim m_\pi^2$, this would translates to a LL degeneracy $N = eBR^2/2 \sim (m_\pi \times 10\,\text{fm})^2 \sim 100/4$ and a rotational chemical potential $\mu_N = N\Omega \sim 1.25\,m_\pi$. From the hadro-chemistry analysis, the pion chemical potentials at freeze-out are typically $\mu_f \sim 0.5\,m_\pi$ at RHIC, and $\mu_f \sim 0.86\,m_\pi$ at the LHC [74]. With the rotation at finite B, they would translate to $\mu_\pi = \mu_N + 2\mu_f \sim 1.96\,m_\pi$ and $2.98\,m_\pi$ respectively. Since the threshold of the LLL for the combined $\pi^\pm$ pion energy is $2\sqrt{2}\,m_\pi$, charge pion condensation is possible. Using (226) at finite T, μ_f, the number of $\pi^\pm$ pions in the BEC are

$$\mathbb{N}_{\pi^\pm} = \frac{\sum_{n=0}^{\infty} n\, e^{-\frac{1}{T}(L\mathcal{E}[\Omega,\frac{n}{L}]-2n\mu_f)}}{\sum_{n=0}^{\infty} e^{-\frac{1}{T}(L\mathcal{E}[\Omega,\frac{n}{L}]-2n\mu_f)}} \tag{228}$$

For $L \sim 10$ fm, $eB \sim m_\pi^2$ and $N \approx 25$, we show in Fig. 28 the average number of condensed $\pi^\pm$ for temperatures in the range $0.5\,m_\pi \leq T \leq 1.5\,m_\pi$ and rotations in the range $0.04\,m_\pi \leq \Omega \leq 0.06\,m_\pi$ for the most favorable case with $\mu_f = 0.86\,m_\pi$ at the LHC. It is interesting to note that the ALICE collaboration has recently reported a large coherent emission from multi-pion correlation studies in Pb-Pb collisions [78].

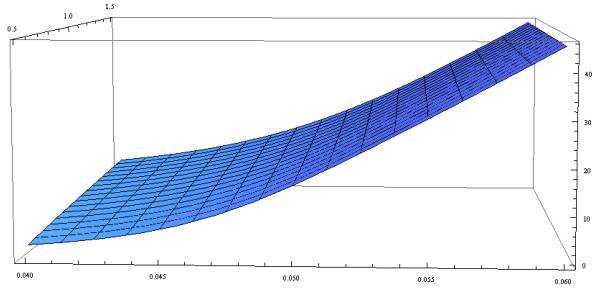

Figure 28: The mean number of condensed pions $\mathbb{N}_{\pi^+} = \mathbb{N}_{\pi^-}$ in the range $0.04\,m_\pi \leq \Omega \leq 0.06\,m_\pi$, for $\mu_f = 0.86\,m_\pi$ and $0.5\,m_\pi \leq T \leq 1.5\,m_\pi$.

5.4 Conclusions

The combined effects of a rotation parallell to a magnetic field yields to pion condensation both in the vacuum and at finite temperature. The π^+ condense at the edge, wile the π^- at the center in equal amount when charge conservation is strictly enforced in a closed volume. Since parallell rotations and magnetic fields can be generated in current heavy ion collisions at collider energies, charged pion condensation could be generated if the combined effects survive with considerable strength in the freeze-out phase. Such effects are likely to affect both the flow of charge particles and their number fluctuations. This separation of charged bosons by centrifugation in a magnetic field may also be probed in atomic physics (trapped and cooled atoms), in condensed matter physics (quantum Hall effect) and possibly compact stars (magnestars).

Finally, we note that this pion superfluid phase maybe substantial in neutron stars. Indeed, for a star of size $R \approx 10\,\mathrm{km}$ with a moderate magnetic field $B \approx 10^{-6} m_\pi^2$, and a typical period $T = 1\,\mathrm{ms}$, the degeneracy $N = eBR^2/2 \approx 10^{31}$ is very large. For a rotational velocity $\Omega = 2\pi/T \approx 10^{-22}\, m_\pi$, the induced pion chemical potential in a neutron star is large with $\mu_N = N\Omega \approx 10^7 m_\pi$ in comparison to the LL gap of $2m_0 \approx 2m_\pi$. So such a phase is likely to form in a neutron star, and clearly in a magnestar where the magnetic field is even larger, e.g. $B \approx 10^{-3} m_\pi^2$.

.

Part III: Heavy-light hadrons using holography

6 Heavy-light Baryons from AdS/QCD

This section is an edited version of my previous publication :
Heavy Baryons and their Exotics from Instantons in Holographic QCD
Yizhuang Liu, Ismail Zahed (SUNY, Stony Brook). Apr 11, 2017. 11 pp.
Phys.Rev. D95 (2017) no.11, 116012

6.1 Introduction

The organization of this section is as follows: In subsection 2 we briefly outline the geometrical set up for the derivation of the heavy-light effective action through the pertinent bulk DBI and CS actions. In subsection 3, we detail the heavy-meson interactions to the flavor instanton in bulk. In subsection 4, we show how a vector meson with spin 1 binding to the bulk instanton transmutes to a spin $\frac{1}{2}$. In subsection 5, we identify the moduli of the bound zero-mode and quantize it by collectivizing some of the soft modes. The mass spectra for baryons with single- and double-heavy quarks are explicitly derived. Some of our exotics are comparable to those recently reported by several collaborations, while others are new. Our conclusions are in subsection 6. In the Appendix we briefly review the quantization of the light meson moduli without the heavy mesons.

6.2 Holographic effective action

6.2.1 D-brane set up

The $D4$-$D8$ construction proposed by Sakai and Sugimoto [157] for the description of the light hadrons is standard and will not be repeated here. Instead, we follow [165] and consider the variant with N_f-1 light $D8$-$\bar{D}8$ (L) and one heavy (H) probe branes in the cigar-shaped geometry that spontaneously breaks chiral symmetry. For simplicity, the light probe branes are always assumed in the anti-podal configuration. A schematic description of the set up for $N_f=3$ is shown in Fig. 29. We assume that the L-brane world volume consists of $R^4\times S^1\times S^4$ with $[0-9]$-dimensions. The light 8-branes are embedded in the $[0-3+5-9]$-dimensions and set at the antipodes of

S^1 which lies in the 4-dimension. The warped $[5-9]$-space is characterized by a finite size R and a horizon at U_{KK}.

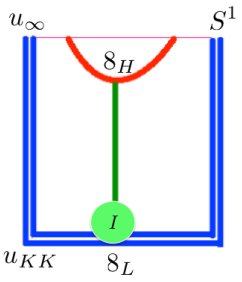

Figure 29: $N_f - 1 = 2$ antipodal 8_L light branes, and one 8_H heavy brane shown in the τU plane, with a bulk $SU(2)$ instanton embedded in 8_L and a massive HL-string connecting them.

6.2.2 DBI and CS actions

The lowest open string modes streched between the H- and L-branes are attached to a wrapped S^4 in $D4$ shown as an instanton in Fig. 29. Near the L brane world volume, these string modes consist of tranverse modes Φ_M and longitudinal modes Ψ, both fundamental with respect to the flavor group $SU(N_f - 1)$. At non-zero brane separation, these fields acquire a vev that makes the vector field massive [161]. Strictly speaking these fields are bi-local, but near the L-branes we will approximate them by local vector fields that are described by the standard DBI action in the background of a warped instanton field. In this respect, our construction is distinct from the approaches developed in [159].

With this in mind and to leading order in the $1/\lambda$ expansion, the effective

action on the probe L-branes consists of the non-Abelian DBI (D-brane Born-Infeld) and CS (Chern-Simons) action. After integrating over the S^4, the leading contribution to the DBI action is

$$S_{\rm DBI} \approx -\kappa \int d^4x dz \, {\rm Tr}\, (\mathbf{f}(z)\mathbf{F}_{\mu\nu}\mathbf{F}^{\mu\nu} + \mathbf{g}(z)\mathbf{F}_{\mu z}\mathbf{F}^{\nu z}) \tag{229}$$

Our conventions are $(-1,1,1,1)$ with $A_M^\dagger = -A_M$. The warping factors are

$$\mathbf{f}(z) = \frac{R^3}{4U_z}\,, \qquad \mathbf{g}(z) = \frac{9}{8}\frac{U_z^3}{U_{KK}} \tag{230}$$

with $U_z^3 = U_{KK}^3 + U_{KK}z^2$, $\kappa = \tilde{T}(2\pi\alpha') = a\lambda N_c$ and $a = 1/(216\pi^3)$ [157]. All dimensions are understood in units where the Kaluza-Klein mass $M_{KK} \equiv 1$ unless specified otherwise. The effective fields in the field strengths are (M, N run over (μ, z))

$$\mathbf{F}_{MN} = \begin{pmatrix} F_{MN} - \Phi_{[M}\Phi^\dagger_{N]} & \partial_{[M}\Phi_{N]} + A_{[M}\Phi_{N]} \\ -\partial_{[M}\Phi^\dagger_{N]} - \Phi^\dagger_{[M}A_{N]} & -\Phi^\dagger_{[M}\Phi_{N]} \end{pmatrix} \tag{231}$$

The CS contribution to the effective action is (form notation used)

$$S_{\rm CS} = \frac{N_c}{24\pi^2}\int_{R^{4+1}} {\rm Tr}\left(\mathbf{A}\mathbf{F}^2 - \frac{1}{2}\mathbf{A}^3\mathbf{F} + \frac{1}{10}\mathbf{A}^5\right) \tag{232}$$

where the normalization to N_c is fixed by integrating the F_4 RR flux over the S^4. The matrix valued 1-form gauge field is

$$\mathbf{A} = \begin{pmatrix} A & \Phi \\ -\Phi^\dagger & 0 \end{pmatrix} \tag{233}$$

For N_f coincidental branes, the Φ multiplet is massless. However, their brane world-volume supports an adjoint and traceless scalar Ψ in addition to the adjoint gauge field A_M both of which are hermitean and $N_f \times N_f$ valued, which we have omitted from the DBI action in so far for simplicity. They are

characterized by a quartic potential with finite extrema and a vev v for the diagonal of Ψ [161]. As a result the Φ multiplet acquires a Higgs-like mass of the type

$$\frac{1}{2}m_H^2 \mathrm{Tr}\left(\Phi_M^\dagger \Phi_M\right) \sim \frac{1}{2}v^2 \mathrm{Tr}\left(\Phi_M^\dagger \Phi_M\right) \tag{234}$$

The vev is related to the separation between the light and heavy branes [161], which we take it to be the mass following from the length of the streched HL string, and which we identify as the mass of the heavy-light $(0^-, 1^-)$ multiplet for either charm (D, D^*) or bottom (B, B^*). In the heavy quark limit, the radial spectra, axial and vector correlations, and the one-pion radiative decays of the $(0^-, 1^-)$ multiplet are fairly reproduced by this model [165].

6.3 Heavy-Light-Instanton interactions

In the original two-flavor $D4$-$D8$ set up by Sakai and Sugimoto [157] light baryons are first identified with a flavor instanton in bulk [162] and its moduli quantized to yield the nucleon and Delta [163]. This construction holds in our case in the light sector of (353) verbatum and we refer the interested reader to [162, 163] for the details of the analysis. The key observations is that the instanton size is small at strong coupling $\rho \sim 1/\sqrt{\lambda}$, as a result of balancing the large and leading attraction due to gravity in bulk (large warpings) and the subleading U(1) Coulomb-like repulsion induced by the Chern-Simons term.

In the geometrical set up described in Fig. 29, the small size instanton translates to a flat space 4-dimensional instanton [162]

$$\begin{aligned} A_M^{cl} = & \quad -\bar{\sigma}_{MN}\frac{x_N}{x^2+\rho^2}, \\ A_0^{cl} = & \quad \frac{-i}{8\pi^2 a x^2}\left(1-\frac{\rho^4}{(x^2+\rho^2)^2}\right) \end{aligned} \tag{235}$$

after using the rescalings

$$\begin{aligned} & x_0 \to x_0, x_M \to x_M/\sqrt{\lambda}, \sqrt{\lambda}\rho \to \rho \\ & (A_0, \Phi_0) \to (A_0, \Phi_0), \\ & (A_M, \Phi_M) \to \sqrt{\lambda}(A_M, \Phi_M) \end{aligned} \tag{236}$$

in (353). From here and throughout the rest of the section, M, N run only over $1, 2, 3, z$. To order λ^0 the rescaled contributions describing the interactions between the light gauge fields A_M and the heavy fields Φ_M to quadratic order split in the form

$$S = aN_c\lambda S_0 + aN_c S_1 + S_{CS} \tag{237}$$

with each contribution given by

$$\begin{aligned}
S_0 = \quad & -(D_M\Phi_N^\dagger - D_N\Phi_M^\dagger)(D_M\Phi_N - D_N\Phi_M) \\
& +2\Phi_M^\dagger F_{MN}\Phi_N \\
S_1 = \quad & +2(D_0\Phi_M^\dagger - D_M\Phi_0^\dagger)(D_0\Phi_M - D_M\Phi_0) \\
& -2\Phi_0^\dagger F^{0M}\Phi_M - 2\Phi_M^\dagger F^{M0}\Phi_0 \\
& -2m_H^2\Phi_M^\dagger\Phi_M + \tilde{S}_1 \\
S_{CS} = \quad & -\frac{iN_c}{24\pi^2}(d\Phi^\dagger A d\Phi + d\Phi^\dagger dA\Phi + \Phi^\dagger dAd\Phi) \\
& -\frac{iN_c}{16\pi^2}(d\Phi^\dagger A^2\Phi + \Phi^\dagger A^2 d\Phi + \Phi^\dagger(AdA + dAA)\Phi) \\
& -\frac{5iN_c}{48\pi^2}\Phi^\dagger A^3\Phi + S_C(\Phi^4, A)
\end{aligned} \tag{238}$$

and

$$\begin{aligned}
\tilde{S}_1 = \quad & +\frac{1}{3}z^2(D_i\Phi_j - D_j\Phi_i)^\dagger(D_i\Phi_j - D_j\Phi_i) \\
& -2z^2(D_i\Phi_z - D_z\Phi_i)^\dagger(D_i\Phi_z - D_z\Phi_i) \\
& -\frac{2}{3}z^2\Phi_i^\dagger F_{ij}\Phi_j + 2z^2(\Phi_z^\dagger F_{zi}\Phi_i + \text{c.c.})
\end{aligned} \tag{239}$$

6.4 Bound State as a Zero-Mode

We now show that in the double limit of large λ followed by large m_Q, a heavy meson in bulk always binds to the flavor instanton in the form of a 4-dimensional $(123z)$ flavor zero-mode that effectively is a spinor. This holographic zero-mode translates equally to either a bound heavy flavor or anti-heavy flavor in our space-time (0123). This is remarkable to holography, as the heavy bound states in the Skyrme-type involve particles but

with difficulties anti-particles [166, 167]. Indeed, in the Skyrme model, the Wess-Zumino-Witten term which is time-odd, carries opposite signs for heavy particles and anti-particles that are magnified by N_c in comparison to the heavy-mesonic action. As a result the particle state is attractive, while the anti-particle state is repulsive.

6.4.1 Field equations

We now consider the bound state solution of the heavy meson field Φ_M in the (rescaled) instanton background 294). We note that the field equation for Φ_M is independent of Φ_0 and reads

$$D_M D_M \Phi_N + 2F_{NM}\Phi_M - D_N D_M \Phi_M = 0 \tag{240}$$

while the contraint field equation (Gauss law) for Φ_0 depends on Φ_M through the Chern-Simons term

$$\begin{aligned} & D_M(D_0\Phi_M - D_M\Phi_0) \\ & -F^{0M}\Phi_M - \frac{\epsilon_{MNPQ}}{64\pi^2 a}K_{MNPQ} = 0 \end{aligned} \tag{241}$$

with K_{MNPQ} defined as

$$\begin{aligned} K_{MNPQ} = \quad & +\partial_M A_N \partial_P \Phi_Q + A_M A_N \partial_P \Phi_Q \\ & +\partial_M A_N A_P \Phi_Q + \frac{5}{6} A_M A_N A_P \Phi_Q \end{aligned} \tag{242}$$

In the heavy quark limit it is best to redefine $\Phi_M = \phi_M e^{-im_H x_0}$ for particles. The anti-particle case follows through $m_Q \to -m_H$ with pertinent sign changes. As a result, the preceding field equations remain unchanged for ϕ_M with the substitution $D_0\phi_M \to (D_0 \mp im_H)\phi_M$ understood for particles $(-)$ or anti-particles $(+)$ respectively.

6.4.2 Double limit

In the double limit of $\lambda \to \infty$ followed by $m_H \to \infty$, the leading contributions are of order λm_H^0 from the light effective action in (353), and of order

$\lambda^0 m_H$ from the heavy-light interaction term S_1 in (298). This double limit is justified if we note that in leading order, the mass of the heavy meson follows from the straight pending string shown in Fig 29, with a value [165]

$$\frac{m_H}{\lambda M_{KK}} = \frac{2}{9\pi}(M_{KK}u_H)^{\frac{2}{3}} \tag{243}$$

where u_H is the holographic height of the heavy brane. The double limit requires the ratio in (243) to be parametrically small.

With the above in mind, we have

$$\frac{S_{1,m}}{aN_c} = 4im_H\phi_m^\dagger D_0\phi_m - 2im_H(\phi_0^\dagger D_M\phi_M - \text{c.c.}) \tag{244}$$

and from the Chern-Simons term in (298) we have

$$\frac{m_H N_c}{16\pi^2}\epsilon_{MNPQ}\phi_M^\dagger F_{NP}\phi_Q = \frac{m_H N_c}{8\pi^2}\phi_M^\dagger F_{MN}\phi_N \tag{245}$$

The constraint equation (301) simplifies considerably to order m_Q,

$$D_M\phi_M = 0 \tag{246}$$

implying that ϕ_M is covariantly transverse in leading order in the double limit.

6.4.3 Vector to spinor zero-mode

The instanton solution A_M in (294) carries a field strength

$$F_{MN} = \frac{2\,\bar{\sigma}_{MN}\rho^2}{(x^2+\rho^2)^2} \tag{247}$$

We now observe that the heavy field equation (300) in combination with the constraint equation (246) are equivalent to the vector zero-mode equation in the fundamental representation. To show that, we recall that the field

strength (296) is self-dual, and S_0 in (298) can be written in the compact form

$$\begin{aligned} S_0 = & \quad -f^\dagger_{MN} f_{MN} + 2\phi^\dagger_M F_{MN} \phi_N \\ = & \quad -f^\dagger_{MN} f_{MN} + 2\epsilon_{MNPQ} \phi^\dagger_M D_M D_Q \phi_N \\ = & \quad -f^\dagger_{MN} f_{MN} + f^\dagger_{MN} \star f_{MN} \\ = & \quad -\frac{1}{2}(f_{MN} - \star f_{MN})^\dagger (f_{MN} - \star f_{MN}) \end{aligned} \tag{248}$$

after using the Hodge dual $\star$ notation, and defining

$$f_{MN} = \partial_{[M} \phi_{N]} + A_{[M} \phi_{N]} \tag{249}$$

Therefore, the second order field equation (300) can be replaced by the anti-self-dual condition (first order) and the transversality condition (246) (first order),

$$\begin{aligned} f_{MN} - \star f_{MN} &= 0 \\ D_M \phi_M &= 0 \end{aligned} \tag{250}$$

which are equivalent to

$$\sigma_M D_M \psi = D\psi = 0 \qquad with \qquad \psi = \bar{\sigma}_M \phi_M \tag{251}$$

The spinor zero-mode ψ is unique, and its explicit matrix form reads

$$\psi^a_{\alpha\beta} = \epsilon_{\alpha a} \chi_\beta \frac{\rho}{(x^2 + \rho^2)^{\frac{3}{2}}} \tag{252}$$

which gives the vector zero-mode in the form

$$\phi^a_M = \chi_\beta (\sigma_M)_{\beta\alpha} \epsilon_{\alpha a} \frac{\rho}{(x^2 + \rho^2)^{\frac{3}{2}}} \tag{253}$$

or in equivalent column form

$$\phi_M = \bar{\sigma}_M \chi \frac{\rho}{(x^2+\rho^2)^{\frac{3}{2}}} \equiv \bar{\sigma}_M f(x) \chi \tag{254}$$

Here χ_α is a constant two-component spinor. It can be checked explicitly that (254) is a solution to the first order equations (306). The interplay between (308) and (253) is remarkable as it shows that in holography a heavy vector meson binds to an instanton in bulk in the form of a vector zero mode that is equally described as a spinor. This duality illustrates the transmutation from a spin 1 to a spin $\frac{1}{2}$ in the instanton field.

6.5 Quantization

Part of the classical moduli of the bound instanton-zero-mode breaks rotational and translational symmetry, which will be quantized by slowly rotating or translating the bound state. In addition, it was noted in [162] that while the deformation of the instanton size and holographic location are not collective per say as they incur potentials, they are still soft in comparison to the more massive quantum excitations in bulk and should be quantized as well. The ensuing quantum states are vibrational and identified with the breathingh modes (size vibration) and odd parity states (holographic vibration).

6.5.1 Collectivization

The leading λN_c contribution is purely instantonic and its quantization is standard and can be found in [163]. For completeness we have summarized it in the Appendix. The quantization of the subleading $\lambda^0 m_H$ contribution involves the zero-mode and is new, so we will describe iin more details. For that, we let the zero-mode slowly translates, rotates and deforms through

$$\begin{aligned} \Phi \to \quad & V(a_I(t))\Phi(X_0(t), Z(t), \rho(t), \chi(t)) \\ \Phi_0 \to \quad & 0 + \delta\phi_0 \end{aligned} \tag{255}$$

Here X_0 is the center in the 123 directions and Z is the center in the z directon. a_I is the SU(2) gauge rotation moduli. We denote the moduli by $X_\alpha \equiv (X, Z, \rho)$ with

$$
\begin{aligned}
-iV^\dagger\partial_0 V = \quad & \Phi = -\partial_t X_N A_N + \chi^a \Phi_a \\
\chi^a = \quad & -i\mathrm{Tr}\left(\tau^a\, a_I^{-1}\partial_t\, a_I\right)
\end{aligned}
\tag{256}
$$

a_I is the SU(2) rotation which carries the isospin and angular momentum quantum numbers. The constraint equation (301) for ϕ_0 has to be satisfied, which fixes $\delta\phi_0$ at sub-leading order

$$
\begin{aligned}
&-D_M^2\delta\phi_0 + D_M\bar\sigma_M(\partial_t X_i\partial_{X_i} f\chi + \partial_t\chi) \\
&+i(\partial_t X_\alpha\partial_\alpha\Phi_M - D_M\Phi)\bar\sigma_M\chi + \delta S_{cs} = 0
\end{aligned}
\tag{257}
$$

The solution to (257) can be inserted back into the action for a general quantization of the ensuing moduli.

6.5.2 Leading heavy mass terms

There are three contributions to order $\lambda^0 m_H$, namely

$$
16im_H\chi^\dagger\partial_t\chi f^2 + 16im_H\chi^\dagger\chi A_0 f^2 - m_H f^2\chi^\dagger\sigma_\mu\Phi\bar\sigma_\mu\chi
\tag{258}
$$

with the rescaled U(1) field A_0, and the Chern-Simons term

$$
\frac{im_H N_c}{8\pi^2}\phi_M^\dagger F_{MN}\phi_N = \frac{i3m_H N_c}{\pi^2}\frac{f^2\rho^2}{(x^2+1)^2}\chi^\dagger\chi
\tag{259}
$$

with the field strength given in (296). Explicit calculations show that the third contribution in (258) vanishes owing to the identity $\sigma_\mu\tau_a\bar\sigma_\mu = 0$.

The coupling $\chi^\dagger\chi A_0$ term in (258) induces a Coulomb-like back-reaction. To see this, we set $\psi = iA_0$ and collect all the U(1) Coulomb-like couplings in the rescaled effective action to order $\lambda^0 m_H$

$$
\begin{aligned}
\frac{S_C(A_0)}{aN_c} = \quad & \int\left(\frac{1}{2}(\nabla\psi)^2 + \psi(\rho_0[A] - 16m_H f^2\chi^\dagger\chi)\right) \\
\rho_0[A] = \quad & \frac{1}{64\pi^2 a}\epsilon_{MNPQ}F_{MN}F_{PQ}
\end{aligned}
\tag{260}
$$

The static action contribution stemming from the coupling to the U(1) charges ρ_0 and $\chi^\dagger\chi$ is

$$\frac{S_C}{aN_c} \to \frac{S_C[\rho_0]}{aN_c} + 16m_H\chi^\dagger\chi\int f^2(-iA_0^{cl}) - \frac{(16m_H\chi^\dagger\chi)^2}{24\pi^2} \tag{261}$$

The last contribution is the Coulomb-like self-interaction induced by the instanton on the heavy meson through the U(1) Coulomb-like field in bulk. It is repulsive and tantamount of fermion number repulsion in holography.

6.5.3 Moduli effective action

Putting all the above contributions together, we obtain the effective action density on the moduli in leading order in the heavy meson mass

$$\begin{aligned}\mathcal{L} = \mathcal{L}_0[a_I, X_\alpha] + 16aN_cm_H\Bigg(i\chi^\dagger\partial_0\chi^\dagger\int d^4x\, f^2 \\ -\chi^\dagger\chi\int d^4x\, f^2\left(iA_0^{cl} - \frac{3}{16a\pi^2}\frac{\rho^2}{(x^2+\rho^2)^2}\right)\Bigg) \\ -aN_c\frac{(16m_H\chi^\dagger\chi)^2}{24\pi^2\rho^2}\end{aligned} \tag{262}$$

with $\mathcal{L}_0$ referring to the effective action density on the moduli stemming from the contribution of the light degrees of freedom in the instanton background. It is identical to the one derived in [162] and to which we refer the reader for further details. In (262) We have made explicit the new contribution due to the bound heavy meson through χ. To this order there is no explicit coupling of the light collective degrees of freedom a_I, to the heavy spinor degree of freedom χ, a general reflection on heavy quark symmetry in leading order. However, there is a coupling to the instanton size ρ through the holographic direction which does not upset this symmetry. After using the normalization $\int d^4x\, f^2 = 1$, inserting the explicit form of A_0^{cl} from (294), and rescaling $\chi \to \chi/2\sqrt{aN_cm_H}$, we finally have

$$\mathcal{L} = \mathcal{L}_0[a_I, X_\alpha] + \chi^\dagger i\partial_t\chi + \frac{3}{32\pi^2a\rho^2}\chi^\dagger\chi - \frac{(\chi^\dagger\chi)^2}{24\pi^2a\rho^2N_c} \tag{263}$$

Remarkably, the bound vector zero-mode to the instanton transmutes to a massive spinor with a repulsive Coulomb-like self- interaction. The mass is *negative* which implies that the heavy meson lowers its energy in the presence of the instanton to order λ^0. We note that the preceding arguments carry verbatum to an anti-heavy meson in the presence of an instanton, leading (318) with a *positive* mass term. This meson raises its energy in the presence of the instanton to order λ^0. These effects originate from the Chern-Simons action in holography. They are the analogue of the effects due to the Wess-Zumino-Witten term in the standard Skyrme model [166, 167]. While they are leading in $1/N_c$ in the latter causing the anti-heavy meson to unbind in general, they are subleading in $1/\lambda$ in the former where to leading order the bound state is always a BPS zero mode irrespective of heavy-meson or anti-heavy-meson.

6.5.4 Heavy-light spectra

The quantization of (318) follows the same arguments as those presented in [162] for $\mathcal{L}_0[a_I, X_\alpha]$ and to which we refer for further details in general, and the Appendix for the notations in particular. Let H_0 be the Hamiltonian associated to $\mathcal{L}_0[a_I, X_\alpha]$, then the Hamiltonian for (318) follows readily in the form

$$H = H_0[\pi_I, \pi_X, a_I, X_\alpha] - \frac{3}{32\pi^2 a\rho^2}\chi^\dagger\chi + \frac{(\chi^\dagger\chi)^2}{24\pi^2 a\rho^2 N_c} \tag{264}$$

with the new quantization rule for the spinor

$$\chi_i\chi_j^\dagger \pm \chi_j^\dagger\chi_i = \delta_{ij} \tag{265}$$

The statistics of χ needs to be carefully determined. For that, we note the symmetry transformation

$$\chi \to U\chi \qquad and \qquad \phi_M \to U\Lambda_{MN}\phi_N \tag{266}$$

since $U^{-1}\bar{\sigma}_M U = \Lambda_{MN}\bar{\sigma}_N$. So a rotation of the spinor χ is equivalent to a spatial rotation of the heavy vector meson field ϕ_M which carries spin 1.

Since χ is in the spin $\frac{1}{2}$ representation it should be quantized as a fermion. So only the plus sign is to be retained in (320). Also, χ carries opposite parity to ϕ_M, i.e. positive. With this in mind, the spin $\mathbf{J}$ and isospin $\mathbf{I}$ are then related by

$$\vec{\mathbf{J}} = -\vec{\mathbf{I}} + \vec{\mathbf{S}}_\chi \equiv -\vec{\mathbf{I}} + \chi^\dagger \frac{\vec{\tau}}{2} \chi \tag{267}$$

We note that in the absence of the heavy-light meson $\mathbf{J} + \mathbf{I} = 0$ as expected from the spin-flavor hedgehog character of the bulk instanton (see also the Appendix).

The spectrum of (319) follows from the one discussed in details in [162] with the only modification of Q entering in H_0 as given in the Appendix

$$Q \equiv \frac{N_c}{40a\pi^2} \to \frac{N_c}{40a\pi^2}\left(1 - \frac{15}{4N_c}\chi^\dagger\chi + \frac{5(\chi^\dagger\chi)^2}{3N_c^2}\right) \tag{268}$$

The quantum states with a single bound state $N_Q = \chi^\dagger\chi = 1$ and IJ^π assignments are labeled by

$$|N_Q, JM, lm, n_z, n_\rho\rangle \;\; with \;\; IJ^\pi = \frac{l}{2}\left(\frac{l}{2} \pm \frac{1}{2}\right)^\pi \tag{269}$$

with $n_z = 0, 1, 2, ..$ counting the number of quanta associated to the collective motion in the holographic direction, and $n_\rho = 0, 1, 2, ..$ counting the number of quanta associated to the radial breathing of the instanton core, a sort of Roper-like excitations. Following [162], we identify the parity of the heavy baryon bound state as $(-1)^{n_z}$. Using (323) and the results in [162] as briefly summarized in the Appendix, the mass spectrum for the bound heavy-light states is

$$\begin{aligned} M_{NQ} &= +M_0 + N_Q m_H \\ &+ \left(\frac{(l+1)^2}{6} + \frac{2}{15}N_c^2\left(1 - \frac{15N_Q}{4N_c} + \frac{5N_Q^2}{3N_c^2}\right)\right)^{\frac{1}{2}} M_{KK} \\ &+ \frac{2(n_\rho + n_z) + 2}{\sqrt{6}} M_{KK} \end{aligned} \tag{270}$$

with M_{KK} the Kaluza-Klein mass and $M_0/M_{KK} = 8\pi^2\kappa$ the bulk instanton mass. The Kaluza-Klein scale is usually set by the light meson spectrum and is fit to reproduce the rho mass with $M_{KK} \sim m_\rho/\sqrt{0.61} \sim 1$ GeV [157]. Whenever possible, we will try to eliminate the uncertainties on the value of M_{KK} through model independent relations for fixed N_Q.

We note that the net effect of the heavy-meson is among other thinghs, an increase in the iso-rotational inertia by expanding (325) in $1/N_c$. The negative N_Q/N_c contribution in (325) reflects on the fact that a heavy meson with a heavy quark mass is attracted to the instanton to order λ^0. As we noted earlier, a heavy meson with a heavy anti-quark will be repelled to order λ^0 hence a similar but positive contribution. The positive N_Q^2/N_c^2 contribution is the repulsive Coulomb-like self-interaction. Note that it is of the same order as the rotational contribution which justifies keeping it in our analysis.

(325) is to be contrasted with the mass spectrum for baryons with no heavy quarks or $N_Q = 0$, where the nucleon state is idendified as $N_Q = 0, l = 1, n_z = n_\rho = 0$ and the Delta state as $N_Q = 0, l = 3, n_z = n_\rho = 0$ [162]. The radial excitation with $n_\rho = 1$ can be identified with the radial Roper excitation of the nucleon and Delta, while the holographic excitation with $n_z = 1$ can be interpreted as the odd parity excitation of the nucleon and Delta.

6.5.5 Single-heavy baryons

Since the bound zero-mode transmuted to spin $\frac{1}{2}$, the lowest heavy baryons with one heavy quark are characterized by $N_Q = 1, l = even, N_c = 3$ and $n_z, n_\rho = 0, 1$, with the mass spectrum

$$M_{X_Q} = +M_0 + m_H \tag{271}$$

$$+\left(\frac{(l+1)^2}{6} - \frac{7}{90}\right)^{\frac{1}{2}} M_{KK}$$

$$+\frac{2(n_\rho + n_z) + 2}{\sqrt{6}} M_{KK} \tag{272}$$

6.5.6 Heavy baryons

Consider the states with $n_z = n_\rho = 0$. We identify the state with $l = 0$ with the heavy-light iso-singlet Λ_Q with the assignments $IJ^\pi = 0\frac{1}{2}^+$. We identify the state with $l = 2$ with the heavy-light iso-triplet Σ_Q with the assignment $1\frac{1}{2}^+$, and $\Sigma_Q^\star$ with the assignment $1\frac{3}{2}^+$. By subtracting the nucleon mass from (327) we have

$$\begin{aligned} M_{\Lambda_Q} - M_N - m_H &= -1.06\, M_{KK} \\ M_{\Sigma_Q} - M_N - m_H &= -0.17\, M_{KK} \\ M_{\Sigma_Q^*} - M_N - m_H &= -0.17\, M_{KK} \end{aligned} \tag{273}$$

Hence the holographic and model independent relations

$$\begin{aligned} M_{\Lambda_{Q'}} &= M_{\Lambda_Q} + (m_{H'} - m_H) \\ M_{\Sigma_{Q'}} &= 0.84\, m_N + m_{H'} + 0.16\, (M_{\Lambda_Q} - m_H) \end{aligned} \tag{274}$$

with $Q, Q' = c, b$. Using the heavy meson masses $m_D \approx 1870$ Mev, $m_B = 5279$ MeV and $m_{\Lambda_c} = 2286$ Mev we find that $M_{\Lambda_b} = 5655$ MeV in good agreement with the measured value of 5620 MeV. Also we find $M_{\Sigma c} = 2725$ Mev and $M_{\Sigma b} = 6134$ Mev, which are to be compared to the empirical values of $M_{\Sigma c} = 2453$ Mev and $M_{\Sigma b} = 5810$ Mev respectively.

6.5.7 Excited heavy baryons

Now, consider the low-lying breathing modes R with $n_\rho = 1$ for the even assignments $0\frac{1}{2}^+, 1\frac{1}{2}^+, 1\frac{3}{2}^+$, and the odd parity excited states O with $n_z = 1$ for the odd assigments $0\frac{1}{2}^-, 1\frac{1}{2}^-, 1\frac{3}{2}^-$. (327) shows that the R-excitations are degenerate with the O-excitations. We obtain $(E = O, R)$

$$\begin{aligned} M_{\Lambda_{EQ'}} &= +0.23\, M_{\Lambda_Q} + 0.77\, m_N - 0.23\, m_H + m_{H'} \\ M_{\Sigma_{EQ'}} &= -0.59\, M_{\Lambda_Q} + 1.59\, m_N + 0.59\, m_H + m_{H'} \end{aligned} \tag{275}$$

We found $M_{\Lambda_{Oc}} = 2686$ MeV which is to be compared to the mass 2595 MeV for the reported charm $0\frac{1}{2}^-$ state, and $M_{\Lambda_{Ob}} = 6095$ MeV which is close

to the mass 5912 MeV for the reported bottom $0\frac{1}{2}^-$ state. (275) predicts a mass of $M_{\Sigma_{Oc}} = 3126$ MeV for a possible charm $1\frac{1}{2}^-$ state, and a mass of $M_{\Sigma_{Ob}} = 6535$ MeV for a possible bottom $1\frac{1}{2}^-$ state.

6.6 Double-heavy baryons

For heavy baryons containing also anti-heavy quarks we note that a rerun of the preceding arguments using instead the reduction $\Phi_M = \phi_M e^{+im_H x_0}$, amounts to binding an anti-heavy-light meson to the bulk instanton in the form of a zero-mode also in the fundamental representation of spin. Most of the results are unchanged except for pertinent minus signs. For instance, when binding one heavy-light and one anti-heavy-light meson, (318) now reads

$$\begin{aligned}\mathcal{L} = \quad & +\mathcal{L}_0[a_I, X_\alpha] \\ & +\chi_Q^\dagger i\partial_t \chi_Q + \frac{3}{32\pi^2 a\rho^2}\chi_Q^\dagger \chi_Q \\ & -\chi_{\bar{Q}}^\dagger i\partial_t \chi_{\bar{Q}} - \frac{3}{32\pi^2 a\rho^2}\chi_{\bar{Q}}^\dagger \chi_{\bar{Q}} \\ & +\frac{(\chi_Q^\dagger \chi_Q - \chi_{\bar{Q}}^\dagger \chi_{\bar{Q}})^2}{24\pi^2 a\rho^2 N_c}\end{aligned} \tag{276}$$

As we indicated earlier the mass contributions are opposite for a heavy-light and anti-heavy-light meson. The general mass spectrum for baryons with N_Q heavy-quarks and $N_{\bar{Q}}$ anti-heavy quarks is

$$\begin{aligned}& M_{\bar{Q}Q} = +M_0 + (N_Q + N_{\bar{Q}})m_H \\ & + \left(\frac{(l+1)^2}{6} \right. \\ & \left. + \frac{2}{15}N_c^2 \left(1 - \frac{15(N_Q - N_{\bar{Q}})}{4N_c} + \frac{5(N_Q - N_{\bar{Q}})^2}{3N_c^2} \right) \right)^{\frac{1}{2}} M_{KK} \\ & + \frac{2(n_\rho + n_z) + 2}{\sqrt{6}} M_{KK}\end{aligned} \tag{277}$$

6.6.1 Pentaquarks

For $N_Q = N_{\bar{Q}} = 1$ we identify the lowest state with $l = 1, n_z = n_\rho = 0$ with pentaquark baryonic states with the IJ^π assignments $\frac{1}{2}\frac{1}{2}^-$ and $\frac{1}{2}\frac{3}{2}^-$, and masses given by

$$M_{\bar{Q}Q} - M_N - 2\,m_H = 0 \tag{278}$$

Amusingly the spectrum is BPS as both the attraction and repulsion balances, and the two Coulomb-like self repulsions balance against the Coulomb-like pair attraction. Thus we predict a mass of $M_{\bar{c}c} = 4678$ MeV for the $\frac{1}{2}\frac{3}{2}^-$ which is close to the reported $P_c^+(4380)$ and $P_c^+(4450)$. We also predict a mass of $M_{\bar{b}c} = 8087$ MeV and $M_{\bar{b}b} = 11496$ MeV for the yet to be oberved pentaquarks. Perhaps a better estimate for the latters is to trade M_N in (333) for the observed light charmed pentaquark mass $M_{\bar{c}c} = 4678$ MeV using instead

$$M_{\bar{Q}Q} = M_{\bar{Q}'Q'} + 2\,(m_H - m_{H'}) \tag{279}$$

Using (279) we predict $M_{\bar{b}c} = 7789$ MeV and $M_{\bar{b}b} = 11198$ MeV, which are slightly lighter than the previous estimates. The present holographic construction based on the bulk instanton as a hedgehog in flavor-spin space does not support the $\frac{1}{2}\frac{5}{2}^+$ assignment suggested for the observed $P_c^+(4450)$ through the bound zero-mode for the case $N_f = 2$.

6.6.2 Excited pentaquarks

For $N_Q = N_{\bar{Q}} = 1$ we now identify the lowest state with $l = 1, n_z = 1, n_\rho = 0$ with the odd parity pentaquarks O with assignments $\frac{1}{2}\frac{1}{2}^+$ and $\frac{1}{2}\frac{3}{2}^+$, and the $l = 1, n_z = 0, n_\rho = 1$ with the breathing or Roper R pentaquarks with the same assignments as the ground state. The mass relations for these states are $(E = O, R)$

$$M_{E\bar{Q}Q} - M_N - 2\,m_H = 0.82\,M_{KK} \tag{280}$$

which can be traded for model independent relations

$$M_{E\bar{Q}Q} = 1.51\, m_N + 2m_H + 0.51\, (m_{H'} - M_{\lambda_{Q'}}) \tag{281}$$

by eliminating M_{KK} using the first relation in (329). Using (281) we predict $M_{E\bar{c}c} = 4944$ MeV, $M_{E\bar{b}c} = 8353$ MeV, $M_{E\bar{b}b} = 11762$ MeV as the new low lying excitations of heavy pentaquarks with the preceding assignments.

6.6.3 Delta-like pentaquarks

For $N_Q = N_{\bar{Q}} = 1$, the present construction allows also for Delta-type pentaquarks which we identify with $l = 3, n_z = n_\rho = 0$. Altogether, we have one $\frac{3}{2}\frac{1}{2}^-$, two $\frac{3}{2}\frac{3}{2}^-$, and one $\frac{3}{2}\frac{5}{2}^-$ states, all degenerate to leading order, with heavy flavor dependent masses

$$M_{\Delta\bar{Q}Q} - M_N - 2\, m_Q = 0.71\, M_{KK} \tag{282}$$

Again we can trade M_{KK} using the first relation in (329) to obtain the model independent relation

$$M_{\Delta\bar{Q}Q} = 1.57\, m_N + 2\, m_H + 0.57\, (m_{H'} - M_{\Lambda_{Q'}}) \tag{283}$$

In particular, we predict $M_{\Delta\bar{c}c} = 4976$ MeV, $M_{\Delta\bar{c}b} = 8385$ MeV, and $M_{\Delta\bar{b}b} = 11794$ MeV, which are yet to be observed.

6.7 Conclusions

We have presented a top-down holographic approach to the single- and double-heavy baryons in the variant of $D4$-$D8$ we proposed recently [165] (first reference). To order λm_Q^0, the heavy baryons emerge from the zero mode of a reduced (massless) vector meson that transmutes both its spin and negative parity, to a spin $\frac{1}{2}$ with positive parity in the bulk flavor instanton. Heavy mesons and anti-mesons bind on equal footing to the core instanton in holography in leading order in λ even in the presence of the Chern-Simons contribution. This is not the case in non-holographic models where the anti-heavy meson binding is usually depressed by the sign flip in the Wess-Zumino-Witten contribution [166]. Unlike in the Skyrme model,

the bulk flavor instanton offers a model independent description of the light baryon core. The binding of the heavy meson over its Compton wavelength is essentially geometrical in the double limit of large λ followed by large m_Q.

We have shown that the bound state moduli yields a rich spectrum after quantization, that involves coupled rotational, translational and vibrational modes. The model-independent mass relations for the low-lying single-heavy baryon spectrum yield masses that are in overall agreement with the reported masses for the corresponding charm and bottom baryons. The spectrum also contains some newly excited states yet to be observed. When extended to double-heavy baryon spectra, the holographic contruction yields a pair of degenerate heavy iso-doublets with $IJ^\pi = \frac{1}{2}\frac{1}{2}^-, \frac{1}{2}\frac{3}{2}^-$ assignments. The model gives naturally a charmed pentaquark . It also predicts a number of new pentaquarks with both hidden charm and bottom, and five new Delta-like pentaquarks with hidden charm. The hedgehog flavor instanton when collectively quantized, excludes the $IJ^\pi = \frac{1}{2}\frac{5}{2}^+$ assignment for $N_f = 2$.

The shortcomings of the heavy-light holographic approach stem from the triple limits of large N_c and strong $'$t Hooft coupling $\lambda = g^2 N_c$, and now large m_H as well. The corrections are clear in principle but laborious in practice. Our simple construct can be improved through a more realistic extension such as improved holographic QCD [171]. Also a simpler, bottom-up formulation following the present general reasoning is also worth formulating for the transparency of the arguments.

Finally, it would be interesting to extend the current analysis for the heavy baryons to the more realistic case of $N_f = 3$ with a realistic mass for the light strange quark as well. Also, the strong decay widths of the heavy baryons and their exotics should be estimated. They follow from $1/N_c$ type corrections using the self-generated Yukawa-type potentials in bulk, much like those studied in the context of the Skyrme model [24]. We expect large widths to develop through S-wave decays, and smaller widths to follow from P-wave decays because of a smaller phase space. Also the hyperfine splitting in the heavy spectra is expected to arise through subleading couplings between the emerging spin degrees of freedom and the collective rotations and vibrations. The pertinent electromagnetic and weak form factors of the holographically bound heavy baryons can also be obtained following standard arguments [162, 163]. Some of these issues will be addressed next.

7 Heavy and Strange Holographic Baryons

This section is an edited version of my previous publication :
Heavy and Strange Holographic Baryons
Yizhuang Liu, Ismail Zahed (SUNY, Stony Brook)May 3, 2017. 12 pp
Phys.Rev. D96 (2017) no.5, 056027

7.1 Introduction

Fowllow the treatment of $N_f = 2$ heavy-light system in previous section, in this section we will move to $N_f = 3$. In subsection 2 and 3 we briefly recall the geometrical set up for the derivation of the heavy-light effective action for three flavors in terms of the bulk DBI and CS actions. We detail the heavy-meson interactions to the flavor instanton, and the ensuing heavy meson bound state to the instanton in bulk in the double limit of large coupling and heavy meson mass. In subsection 4 and 5, we use the collective quantization approach to derive the pertinent spectra for holographic heavy baryons and their exotics with strangeness. Our conclusions are in subsection 6. In the Appendix we briefly review the collective quantization of the light baryons for $N_f = 2, 3$.

7.2 Holographic effective action

7.2.1 The setup and the DBI action

Here the setup are essentially the same as for the $N_f = 2$ case so we omit most details. We have N_c D_4 branes and $N_f = 3$ U shape light probe $D_8\bar{D}_8$ flavor brane pairs connecting smoothly in the infrared region. The heavy-light messons are massive vectorial fields near the probe brane and the effective action on the probe light-branes consists of the non-Abelian DBI and CS action. After integrating over the S^4, the leading contribution in $1/\lambda$ to the DBI action is

$$S_{\rm DBI} \approx -\kappa \int d^4x dz \, {\rm Tr}\, (f(z)\mathbf{F}_{\mu\nu}\mathbf{F}^{\mu\nu} + g(z)\mathbf{F}_{\mu z}\mathbf{F}^{\nu z}) \tag{284}$$

Our conventions are $(-1, 1, 1, 1)$ with $A^\dagger_M = -A_M$. The warping factors are

$$f(z) = \frac{R^3}{4U_z}\,, \qquad g(z) = \frac{9}{8}\frac{U_z^3}{U_{KK}} \tag{285}$$

with $U_z^3 = U_{KK}^3 + U_{KK} z^2$, and $\kappa \equiv a\lambda N_c$ and $a = 1/(216\pi^3)$ [157]. The effective fields in the field strengths are (M, N run over (μ, z))

$$\mathbf{F}_{MN} = \begin{pmatrix} F_{MN} - \Phi_{[M}\Phi^\dagger_{N]} & \partial_{[M}\Phi_{N]} + A_{[M}\Phi_{N]} \\ -\partial_{[M}\Phi^\dagger_{N]} - \Phi^\dagger_{[M}A_{N]} & -\Phi^\dagger_{[M}\Phi_{N]} \end{pmatrix} \tag{286}$$

The matrix valued 1-form gauge field is

$$\mathbf{A} = \begin{pmatrix} A & \Phi \\ -\Phi^\dagger & 0 \end{pmatrix} \tag{287}$$

For N_f coincidental branes, the Φ multiplet is massless. However, their brane world-volume supports an adjoint and traceless scalar Ψ in addition to the adjoint gauge field A_M, which we have omitted from the DBI action for notational simplicity. The scalar admits a quartic potential with finite extrema and a vev v for the diagonal of Ψ [161], leading to a Higgs-like mass for the Φ multiplet

$$\frac{1}{2}m_H^2 \mathrm{Tr}\left(\Phi^\dagger_M \Phi_M\right) \sim \frac{1}{2}v^2 \mathrm{Tr}\left(\Phi^\dagger_M \Phi_M\right) \tag{288}$$

The vev is related to the separation between the light and heavy branes [161], which is about the length of the HL string. Below, m_H will be taken as the heavy meson mass for the heavy-light $(0^-, 1^-)$, i.e. (D, D^*) for charm and (B, B^*) for bottom. The introduction of a finite non-zero strange quark mass will be discussed also below.

7.2.2 Chern-Simons action

For $N_f > 2$, the naive Chern-Simons 5-form

$$S_{CS} = \frac{iN_c}{24\pi^2}\int_{M_5} \mathrm{Tr}\left(AF^2 - \frac{1}{2}A^3F + \frac{1}{10}A^5\right) \tag{289}$$

fails to reproduce the correct transformation law under the combined gauge and chiral transformations [181]. In particular, when addressing the $N_f = 3$ baryon spectra, (289) fails to reproduce the important hypercharge constraint [181]

$$J_8 = \frac{N_c}{2\sqrt{3}} \tag{290}$$

This issue was recently revisited in [182] where boundary contributions were added to (289) to address these shortcomings. Specifically, the new Chern-Simons (nCS) contribution is [182]

$$\begin{aligned} &S_{nCS} = S_{CS} \\ &+ \int_{N_5} \frac{1}{10} \operatorname{Tr}\left(h^{-1}dh\right)^5 + \int_{\partial M_5} \alpha_4\left(dhh^{-1}, A\right) \end{aligned} \tag{291}$$

Here N_5 is a 5-dimensional manidold whose boundaries are $\partial N_5 = \partial M_5 = M_{4+\infty} - M_{4-\infty}$, with the asymptotic flavor gauge field

$$A|_{z\to\pm\infty} = \hat{A}^{\pm h^\pm} = h^\pm(d + \hat{A}^\pm)h^{\pm -1} \tag{292}$$

The gauged 4-form α_4 is given in [182]. $\hat{A}^\pm$ refer to the external gauge fields, and $h|_{\partial M_5} = (h^+, h^-)$. A is assumed to be well defined throughout M_5 and produces no-boundary contributions. In other words, in this gauge all topological information is moved to the holographic boundaries at $z = \pm\infty$. We can actually work in the $A_z = 0$ gauge, and for the instanton profile (as discussed below) we have

$$(h^-, h^+) \equiv \left(1, Pe^{-\int_{-\infty}^{\infty} A_z dz}\right) \tag{293}$$

Note that in our case $A \to \mathbf{A}$ as defined in (358). As a result, the contributions from (289) are similar to those in the $N_f = 2$ case discussed in [165]. The contributions from the new terms in (291) will be detailed in the quantization approach below.

7.3 Heavy-Light Baryons

7.3.1 Bulk instanton

In the original Sakai and Sugimoto model [157] light baryons are identified with small size flavor instantons in bulk [162]. This construction carries to our current set up as we have recently shown for the $N_f = 2$ case in [165]. For the present $N_f = 3$ case shown in Fig. 29, a small size instanton translates to a flat space 4-dimensional instanton in the $[1-4]$ directions. Specifically, the SU(3) flavor instanton A_M and its time components are [181]

$$\begin{aligned} A_M = & \quad \text{diag}\left(-\bar{\sigma}_{MN}\frac{x_N}{x^2+\rho^2}, 0\right) \\ A_0 = & \quad \frac{-1}{8\pi^2 a x^2}\sqrt{\frac{2}{3}}\left(1-\frac{\rho^2}{(x^2+\rho^2)^2}\right)\text{diag}(1,1,0) \\ & +\frac{1}{16\pi^2 a x^2}\left(1-\frac{\rho^2}{(x^2+\rho^2)^2}\right)\text{diag}\left(\frac{1}{3},\frac{1}{3},-\frac{2}{3}\right) \end{aligned} \tag{294}$$

where the rescaling

$$\begin{aligned} & x_0 \to x_0, x_M \to x_M/\sqrt{\lambda}, \sqrt{\lambda}\rho \to \rho \\ & (A_0, \Phi_0) \to (A_0, \Phi_0), \\ & (A_M, \Phi_M) \to \sqrt{\lambda}(A_M, \Phi_M) \end{aligned} \tag{295}$$

was used. From here on M, N runs only over $1, 2, 3, z$ unless specified otherwise. The instanton solution A_M in (294) carries a field strength

$$F_{MN} = \text{diag}\left(2\frac{\bar{\sigma}_{MN}\rho^2}{(x^2+\rho^2)^2}, 0\right) \tag{296}$$

7.3.2 Heavy-light effective action

To order λ^0 the rescaled contributions describing the interactions between the light gauge fields A_M and the heavy fields Φ_M to quadratic order split to several contributions

$$\mathcal{L} = aN_c\lambda\mathcal{L}_0 + aN_c\mathcal{L}_1 + \mathcal{L}_{CS} \tag{297}$$

with each contribution given by

$$\begin{aligned}
\mathcal{L}_0 = \quad & -(D_M\Phi_N^\dagger - D_N\Phi_M^\dagger)(D_M\Phi_N - D_N\Phi_M) \\
& +2\Phi_M^\dagger F_{MN}\Phi_N \\
\mathcal{L}_1 = \quad & +2(D_0\Phi_M^\dagger - D_M\Phi_0^\dagger)(D_0\Phi_M - D_M\Phi_0) \\
& -2\Phi_0^\dagger F^{0M}\Phi_M - 2\Phi_M^\dagger F^{M0}\Phi_0 \\
& -2m_H^2\Phi_M^\dagger\Phi_M + \tilde{S}_1 \\
\mathcal{L}_{CS} = \quad & -\frac{iN_c}{24\pi^2}(d\Phi^\dagger A d\Phi + d\Phi^\dagger dA\Phi + \Phi^\dagger dAd\Phi) \\
& -\frac{iN_c}{16\pi^2}(d\Phi^\dagger A^2\Phi + \Phi^\dagger A^2 d\Phi + \Phi^\dagger(AdA + dAA)\Phi) \\
& -\frac{5iN_c}{48\pi^2}\Phi^\dagger A^3\Phi + S_C(\Phi^4, A)
\end{aligned} \tag{298}$$

and

$$\begin{aligned}
\tilde{\mathcal{L}}_1 = \quad & +\frac{1}{3}z^2(D_i\Phi_j - D_j\Phi_i)^\dagger(D_i\Phi_j - D_j\Phi_i) \\
& -2z^2(D_i\Phi_z - D_z\Phi_i)^\dagger(D_i\Phi_z - D_z\Phi_i) \\
& -\frac{2}{3}z^2\Phi_i^\dagger F_{ij}\Phi_j + 2z^2(\Phi_z^\dagger F_{zi}\Phi_i + \text{c.c.})
\end{aligned} \tag{299}$$

The additional boundary contributions in (291) do not generate any new heavy meson contribution besides those generated by the standard Chern-Simons contributions quoted in (298).

7.3.3 Φ equation of motion

We now consider the bound state solution of the heavy meson field Φ_M in the (rescaled) instanton background 294). We note that the field equation for Φ_M is independent of Φ_0 and reads

$$D_M D_M\Phi_N + 2F_{NM}\Phi_M - D_N D_M\Phi_M = 0 \tag{300}$$

while the (contraint) field equation for Φ_0 depends on Φ_M through the Chern-Simons term

$$
\begin{aligned}
&D_M(D_0\Phi_M - D_M\Phi_0) \\
&-F^{0M}\Phi_M - \frac{\epsilon_{MNPQ}}{64\pi^2 a}K_{MNPQ} = 0
\end{aligned}
\tag{301}
$$

with K_{MNPQ} defined as

$$
\begin{aligned}
K_{MNPQ} = \quad &+\partial_M A_N \partial_P \Phi_Q + A_M A_N \partial_P \Phi_Q \\
&+\partial_M A_N A_P \Phi_Q + \frac{5}{6} A_M A_N A_P \Phi_Q
\end{aligned}
\tag{302}
$$

7.3.4 Heavy meson limit

In the heavy meson mass limit it is best to redefine $\Phi_M = \phi_M e^{-im_H x_0}$ for particles. The anti-particle case follows through $m_H \to -m_H$ with pertinent sign changes. In the double limit of $\lambda \to \infty$ followed by $m_H \to \infty$, the leading contributions are of order λm_H^0 from the ligh effective action, and of order $\lambda^0 m_H$ from the heavy-light interaction term $\mathcal{L}_1$ in (298)

$$
\frac{\mathcal{L}_{1,m}}{aN_c} = 4im_H \phi_m^\dagger D_0 \phi_m - 2im_H(\phi_0^\dagger D_M \phi_M - \text{c.c.})
\tag{303}
$$

and the standard Chern-Simons term in (298)

$$
\frac{m_H N_c}{16\pi^2}\epsilon_{MNPQ}\phi_M^\dagger F_{NP}\phi_Q = \frac{m_H N_c}{8\pi^2}\phi_M^\dagger F_{MN}\phi_N
\tag{304}
$$

The constraint equation (301) simplifies considerably to order m_H, that is $D_M\phi_M = 0$ and implying that ϕ_M is transverse in leading order in the double limit.

7.3.5 Zero-Mode

We now observe that the heavy field equation (300) in combination with the constraint equation (301) are equivalent to the vector zero-mode equation in the fundamental representation. For that, we recall that the field strength (296) is self-dual, and $\mathcal{L}_0$ in (298) can be written in the compact form

$$\mathcal{L}_0 = -\frac{1}{2}\left|f_{MN} - \star f_{MN}\right|^2 \tag{305}$$

using the Hodge $\star$ product, with $f_{MN} = \partial_{[M}\phi_{N]} + A_{[M}\phi_{N]}$. Therefore, the second order field equation (300) can be replaced by the anti-self-dual condition (first order) and the transversality condition (first order),

$$f_{MN} - \star f_{MN} = 0 \qquad and \qquad D_M\phi_M = 0 \tag{306}$$

which are equivalent to

$$\sigma_M D_M \psi = D\psi = 0 \qquad with \qquad \psi = \bar{\sigma}_M \phi_M \tag{307}$$

The spinor zero-mode ψ is unique, and its explicit matrix form reads

$$\psi^a_{\alpha\beta} = \epsilon_{\alpha a}\chi_\beta \frac{\rho}{(x^2+\rho^2)^{\frac{3}{2}}} \qquad with \qquad a = 1, 2 \tag{308}$$

with explicitly $\phi_M = (\bar{\sigma}_M f(x)\chi, 0)$. Here χ_α is a constant two-component spinor. We have to understand that only the first two component of the spin-zero modes are non-zero. It can be checked explicitly that ϕ_M is a solution to the first order equations (306). In the presence of the instanton, the spin-1 vector field binds and transmutes to a spin $\frac{1}{2}$ spinor.

7.4 Quantization

The classical bound instanton-zero-mode breaks iso-rotational, rotational and translational symmetries. To quantize it, we promote the solution to a slowly moving and rotating solution. The leading contribution for large λ is purely instantonic and its quantization is standard and can be found in [163], so we will assume it here. The quantization of the subleading $\lambda^0 m_H$ contribution involves the zero-mode and for $N_f = 2$ was recently addressed in [180]. Here, we will address the new elements of the quantization for $N_f = 3$.

The collective quantization method proceeds by first slowly rotating and translating the instanton configuration in bulk using

$$\Phi \to V(a_I(t))\Phi(X_0(t), Z(t), \rho(t), \chi(t)) \tag{309}$$

with $\Phi_0 = 0$. Here X_0 is the center in the 123 directions and Z is the center in the z directon. a_I is the SU(3) gauge rotation moduli. The moduli is composed of the collective coordinates $X_\alpha \equiv (X, Z, \rho)$ and by the collective SU(3) rotation a_I. The time-dependent configuration is then introduced in the heavy-light effective action described earlier and expanded in leading order in the time-derivatives as we now detail.

7.4.1 The new Chern-Simons contributions

The additional Chern-Simons contributions in (291) picks up from the collectively quantized instanton by defining

$$\begin{aligned} h^- &= \text{diag}\left(a_I(t)^{-1}, 1\right) \\ h^+ &= h_0\, \text{diag}\left(a_I(t)^{-1}, 1\right) \end{aligned} \tag{310}$$

We now note that the field $\mathbf{A}$ composed of the instanton solution A plus the zero-mode solution $\mathbf{\Phi}$, carries the same topological number as the field with the instanton solution A but $\mathbf{\Phi} = 0$. Therefore, h_0 in (310) can be represented by only the latter. With this in mind, we insert (310) in the new contributions in (291) to obtain

$$S_{nCS} = S_{CS} - \frac{iN_c}{48\pi^2}\int_{M^4} dt\, \text{Tr}\left((a_I{}^{-1}\partial_t a_I)(h_0^{-1}dh_0)^3\right) \tag{311}$$

The heavy-light contributions from S_{CS} are those in (298), while the new second contribution is identical to the one obtained in the light sector [182]

$$\frac{N_c}{2\sqrt{3}}a^8 \tag{312}$$

When combined to terms emerging from the heavy sector it will give rise to the correct hypercharge constraint as we will show next.

7.5 Heavy contributions in leading order

There are four contributions to order $\lambda^0 m_H$ from the heavy meson sector, namely

$$\begin{aligned}\frac{\mathcal{L}}{aN_c} = \quad & +16im_H\chi^\dagger\partial_t\chi f^2 - 16m_H\chi^\dagger\chi f^2\frac{2\sqrt{6}+1}{6}A_0 \\ & -m_H f^2\chi^\dagger\sigma_\mu\Phi\bar{\sigma}_\mu\chi + m_H\chi^\dagger\chi f^2\frac{3}{a\pi^2}\frac{\rho^2}{(x^2+\rho^2)^2}\end{aligned} \tag{313}$$

The second contribution is from the A_0 coupling, and the third contribution simplifies for the zero-mode

$$\chi^\dagger\sigma_\mu\Phi\bar{\sigma}_\mu\chi = a^8\frac{8\chi^\dagger\chi}{\sqrt{3}} \tag{314}$$

The last contribution originates from the heavy terms in naive CS term, and also simplifies using the instanton field strength and the zero-mode

$$\frac{im_H N_c}{8\pi^2}\phi_M^\dagger F_{MN}\phi_N = \frac{i3m_H N_c}{\pi^2}\frac{f^2\rho^2}{(x^2+1)^2}\chi^\dagger\chi \tag{315}$$

In addition to the terms retained in (313) the $\chi^\dagger\chi$ coupling to the U(1) flavor gauge field A_0 induces a Coulomb-like correction of the form $(\chi^\dagger\chi)^2$ as we have shown in [180]. With this in mind and after using the rescaling $\chi \to \chi/\sqrt{4aN_c m_H}$ in (313) we obtain

$$\begin{aligned}\mathcal{L} = \quad & +\mathcal{L}_0[a_I, X_\alpha] \\ & +i\chi^\dagger\partial_t\chi + \frac{\eta\,\chi^\dagger\chi}{32\pi^2 a\rho^2} - \frac{\mu\,(\chi^\dagger\chi)^2}{24\pi^2 aN_c\rho^2} \\ & +a^8\frac{N_c}{2\sqrt{3}}\left(1-\frac{\chi^\dagger\chi}{N_c}\right)\end{aligned} \tag{316}$$

where the parameters η, μ are given by

$$\eta \equiv 2x+1 \equiv \frac{2\sqrt{6}+1}{3}+1 \approx 2.966 \;\; and \;\; \mu = \frac{13}{12} \tag{317}$$

Here $\mathcal{L}_0[a_I, X_\alpha]$ refers to the effective action density on the moduli stemming from the contribution of the light degrees of freedom in the instanton background without the a^8 term [162] .

The term linear in a^8 in (316) couples to the hypercharge $J_8 = \frac{N_c}{2\sqrt{3}}(1 - \frac{\chi^\dagger\chi}{N_c})$. So (316) can be seen as an action density of light and heavy degrees of freedom supplemented by a hypercharge constraint, namely

$$\begin{aligned} \mathcal{L} &\to \mathcal{L}_0[a_I, X_\alpha] + \chi^\dagger i\partial_t \chi + \frac{\eta\,\chi^\dagger\chi}{32\pi^2 a\rho^2} - \frac{\mu\,(\chi^\dagger\chi)^2}{24\pi^2 a N_c \rho^2} \\ J^8 &= \frac{N_c}{2\sqrt{3}}\left(1 - \frac{\chi^\dagger\chi}{N_c}\right) \end{aligned} \tag{318}$$

From (317) we note that $\eta \approx 3$ and $\mu \approx 1$ which are remarkably close to the same parameters derived in [180] for the $N_f = 2$ case. These terms are inertial and not sensitive to the value of N_f.

7.5.1 Heavy-light spectra

The quantization of (318) follows the same arguments as those presented in [162, 181] for $\mathcal{L}_0[a_I, X_\alpha]$ as we briefly recall in the Appendix. Let H_0 be the Hamiltonian associated to $\mathcal{L}_0[a_I, X_\alpha]$, then the full heavy-light Hamiltonian for (318) is

$$H = H_0[\pi_I, \pi_X, a_I, X_\alpha] - \frac{\eta\,\chi^\dagger\chi}{32\pi^2 a\rho^2} + \frac{\mu\,(\chi^\dagger\chi)^2}{24\pi^2 a N_c \rho^2} \tag{319}$$

with the new quantization rule for the spinor and the hypercharge constraint

$$\begin{aligned} &\chi_i\chi_j^\dagger + \chi_j^\dagger\chi_i = \delta_{ij} \\ &J^8 = \frac{N_c}{2\sqrt{3}}\left(1 - \frac{\chi^\dagger\chi}{N_c}\right) \end{aligned} \tag{320}$$

We recall that the statistics and parity of χ were fixed in [180]. Specifically, we note the symmetry transformation

$$\chi \to U\chi \qquad and \qquad \phi_M \to U\Lambda_{MN}\phi_N \tag{321}$$

since $U^{-1}\bar{\sigma}_M U = \Lambda_{MN}\bar{\sigma}_N$. So a rotation of the spinor χ is equivalent to a spatial rotation of the heavy vector meson field ϕ_M. Since χ is in the spin $\frac{1}{2}$ representation it should be quantized as a fermion. Its parity is opposite to that of ϕ_M, hence positive. With this in mind, the total spin $\mathbf{J}$ is given by

$$\vec{\mathbf{J}} = -\vec{\mathbf{I}}_{SU(2)} + \vec{\mathbf{S}}_\chi \equiv -\vec{\mathbf{I}}_{SU(2)} + \chi^\dagger \frac{\vec{\tau}}{2}\chi \tag{322}$$

Here for a general SU(3) representation, $\vec{\mathbf{I}}_{SU(2)}$ means the induced representation for the first three generators, $J_{1,2,3}$ as noted in the Appendix.

The spectrum of (319) follows from the one discussed in [162, 181] and recalled in the Appendix, with two key modifications

$$Q \equiv \frac{N_c}{40a\pi^2} \to \frac{N_c}{40a\pi^2}\left(1 - \frac{5\eta}{4N_c}\chi^\dagger\chi + \frac{5\mu(\chi^\dagger\chi)^2}{3N_c^2}\right) \tag{323}$$

and the change of the hypercharge as obtained in (320). The quantum states with a single bound state $N_Q = \chi^\dagger\chi = 1$ and the general (p,q) representation for SU(3) and spin j are labeled by

$$|N_Q, p, q, j, n_z, n_\rho\rangle \;\; with \;\; IJ^\pi = \frac{l}{2}\left(\frac{l}{2} \pm \frac{1}{2}\right)^\pi \tag{324}$$

with $n_z = 0, 1, 2, ..$ counting the number of quanta associated to the collective motion in the holographic direction, and $n_\rho = 0, 1, 2, ..$ counting the number of quanta associated to the radial breathing of the instanton core, a sort of Roper-like excitations. Following [162], we identify the parity of the heavy baryon bound state as $(-1)^{n_z}$. Using (323), the mass spectrum for the bound heavy-light states is

$$\begin{aligned} M_{NQ} &= M_0 + N_Q\, m_H + \\ &\sqrt{\frac{49}{24} + \frac{\mathbf{K}}{3}} + \sqrt{\frac{2}{3}}(n_z + n_\rho + 1)M_{KK} \end{aligned} \tag{325}$$

with

$$\begin{aligned}\mathbf{K} = \quad & +\frac{2N_c^2}{5}\left(1-\frac{5\eta N_Q}{4N_c}+\frac{5\mu N_Q^2}{3N_c^2}\right)-\frac{N_c^2}{3}\left(1-\frac{N_Q}{N_c}\right)^2 \\ & +\frac{4}{3}(p^2+q^2+pq+3(p+q))-2j(j+1) \end{aligned} \tag{326}$$

with M_{KK} the Kaluza-Klein mass and $M_0/M_{KK} = 8\pi^2\kappa$ the bulk instanton mass. The Kaluza-Klein scale is usually set by the light meson spectrum and is fit to reproduce the rho mass with $M_{KK} \sim m_\rho/\sqrt{0.61} \sim 1$ GeV [157].

(325) is to be contrasted with the mass spectrum for baryons with no heavy quarks or $N_Q = 0$, where the nucleon state is idendified as $N_Q = 0, l = 1, n_z = n_\rho = 0$ and the Delta state as $N_Q = 0, l = 3, n_z = n_\rho = 0$ [162]. The radial excitation with $n_\rho = 1$ can be identified with the radial Roper excitation of the nucleon and Delta, while the holographic excitation with $n_z = 1$ can be interpreted as the odd parity excitation of the nucleon and Delta.

7.5.2 Single-heavy baryons

Since the bound zero-mode transmutes to a spin $\frac{1}{2}$, the lowest heavy baryons with one heavy quark are characterized by $n_z, n_\rho = 0, 1, N_Q = 1$, and $(p, q, j) = (0, 1, 0)$ for $\bar{\mathbf{3}}$ and $(p, q, j) = (2, 0, 1)$ for $\mathbf{6}$. The $\bar{\mathbf{3}}$-plet states have spin and parity $\frac{1}{2}^+$. We identify them with $\Lambda_Q, \Xi_Q(\bar{\mathbf{3}})$. The $\mathbf{6}$-plet states have $J = \frac{1}{2}, \frac{3}{2}$. We identify them with $\Sigma_Q, \Xi_Q(\mathbf{6}), \Omega_Q$ and $\Sigma_Q^\star, \Xi_Q(\mathbf{6})^\star, \Omega_Q^\star$, respectively. In the absence of symmetry breaking, the mass spectra are degenerate

$$\begin{aligned} M_{\bar{\mathbf{3}}} = \quad & +M_0 + m_H + 1.75 M_{KK} \\ & +\frac{2(n_\rho+n_z)+2}{\sqrt{6}} M_{KK} \end{aligned} \tag{327}$$

$$\begin{aligned} M_{\mathbf{6}} = \quad & +M_0 + m_H + 2.103 M_{KK} \\ & +\frac{2(n_\rho+n_z)+2}{\sqrt{6}} M_{KK} \end{aligned} \tag{328}$$

or equivalently

$$M_{\bar{\mathbf{3}}} - M_{p=q=1,N_Q=0,j=1/2} - m_H = -0.570\, M_{KK}$$
$$M_{\mathbf{6}} - M_{p=q=1,N_Q=0,j=1/2} - m_H = -0.236\, M_{KK} \tag{329}$$

with the mass splitting $M_{\mathbf{6}} - M_{\bar{\mathbf{3}}} = 0.334\, M_{KK}$.

7.5.3 Double-heavy baryons: QQ

While the binding of a pair of heavy mesons with QQ or $Q\bar{Q}$ content is always BPS-like to leading order in $1/\lambda$, the Chern-Simons contribution is twice more attractive with the QQ content than with the $Q\bar{Q}$ content (see below), although the Coulomb induced contribution penalizes the former and not the latter. With this in mind, heavy baryons with two heavy quarks follow the same construct with $N_Q = 2$ or $\chi^\dagger\chi \to 2$ in (319-320) and $J^8 = 1/2\sqrt{3}$. As a result, the lowest heavy baryons with two bound heavy mesons are now characterized by $n_z, n_\rho = 0, 1$ and $(p, q, j) = (1, 0, 0)$ for the flavor **3**-plet with assignment $\frac{1}{2}^+$, which we identify as Ξ_{QQ} with u, d light content, and Ω_{QQ} with s content. To this order, their degenerate masses are given by

$$M_{\mathbf{3}} - M_{p=q=1,N_Q=0,j=1/2} - 2m_H = -0.844\, M_{KK} \tag{330}$$

7.5.4 Double-heavy baryons: $Q\bar{Q}$

For heavy baryons containing also anti-heavy quarks we note that a rerun of the preceding arguments using instead the reduction $\Phi_M = \phi_M e^{+im_H x_0}$, amounts to binding an anti-heavy-light meson to the bulk instanton also in the form of a zero-mode in the fundamental representation of spin, much like the heavy-light meson binding. Most of the results are unchanged except for pertinent minus signs. For instance, when binding one heavy-light and one anti-heavy-light (318) now reads

$$\begin{aligned}\mathcal{L} = \quad & \mathcal{L}_0[a_I, X_\alpha] \\ & +\chi_Q^\dagger i\partial_t \chi_Q + \frac{\eta}{32\pi^2 a\rho^2}\chi_Q^\dagger \chi_Q \\ & -\chi_{\bar{Q}}^\dagger i\partial_t \chi_{\bar{Q}} - \frac{\eta}{32\pi^2 a\rho^2}\chi_{\bar{Q}}^\dagger \chi_{\bar{Q}} \\ & -\frac{\mu(\chi_Q^\dagger \chi_Q - \chi_{\bar{Q}}^\dagger \chi_{\bar{Q}})^2}{24\pi^2 a N_c \rho^2}\end{aligned} \tag{331}$$

with the hypercharge constraint

$$J_8 = \frac{N_c}{2\sqrt{3}}\left(1 - \frac{\chi_Q^\dagger \chi_Q}{N_c} + \frac{\chi_{\bar{Q}}^\dagger \chi_{\bar{Q}}}{N_c}\right) \tag{332}$$

The mass spectrum for baryons with N_Q heavy-quarks and $N_{\bar{Q}}$ anti-heavy quarks is the same as in (325) with the substitution $N_Q \to N_Q - N_{\bar{Q}}$ to the present order of the analysis or $\lambda^0 m_H$. For $N_Q = N_{\bar{Q}} = 1$ the hypercharge constraint is simply $J_8 = \sqrt{3}/2$. Therefore the lowest states carry $(p, q, j) = (1, 1, 1/2)$ and are identified with the baryonic states in the **8**-plet representation with the J^π assignments $\frac{1}{2}^-$ and $\frac{3}{2}^-$, and $(p, q, j) = (3, 0, 3/2)$ in the **10**-plet representation with J^π assignments (one) $\frac{5}{2}^-$, (two) $\frac{3}{2}^-$ and (one) $\frac{1}{2}^-$. Their masses are given by

$$\begin{aligned}M_{\bar{Q}Q}^{\mathbf{8}} &= M_N + 2m_H + \frac{2(n_z + n_\rho)}{\sqrt{6}} M_{KK} \\ M_{\bar{Q}Q}^{\mathbf{10}} &= M_N + 2m_H + 0.386 M_{KK} + \frac{2(n_z + n_\rho)}{\sqrt{6}} M_{KK}\end{aligned} \tag{333}$$

with the mass splitting $M_{\bar{Q}Q}^{\mathbf{10}} - M_{\bar{Q}Q}^{\mathbf{8}} = 0.386\, M_{KK}$.

7.6 Strange quark mass correction

To compare the previous results for single-heavy and double-heavy baryons to some of the reported physical spectra, we need to address the role of a

finite strange quark mass. In so far, the light flavor branes $D\bar{8}$-$D8$ only connect at U_{KK} because of the bulk gravity induced by $D4$, thereby spontaneously breaking chiral symmetry. To break explicitly chiral symmetry, say by introducing a finite strange quark mass, an additional bulk $D6$ brane can be introduced to connect $D\bar{8}$ to $D8$ [183, 184]. For the $N_f = 3$ case with $m_u = m_d = 0$ and finite m_s, the worldsheet instanton in $D6$ interpolating $D\bar{8}$ to $D8$, induces an explicit light mass breaking term for the light baryons, which takes the following form on the moduli [184]

$$H_{SB} = \tau\rho^3(1 - D_{88}(a_I)) \tag{334}$$

with $\tau \approx |m_s \langle \bar{s}s \rangle|$. Aside from the dependence on the moduli parameter through ρ^3, the explicit symmetry breaking term (334) is standard. An estimate of τ follows from holography, but here we will use τ as a free parameter to be adjusted below through the baryonic spectrum. (334) will be treated in perturbation theory by averaging ρ^3 using the radial baryonic wavefunctions $\phi_{n_\rho,\mathbf{K}}$ discussed in the Appendix. For $n_\rho = n_z = 0$, the averaged result is

$$\left\langle \rho^3 \right\rangle_{n_\rho=0,\mathbf{K}} = \frac{1}{f_\pi^3}\left(\frac{\sqrt{6}}{4\pi^3}\right)^{\frac{3}{2}} \frac{\Gamma\left(1+\sqrt{\frac{49}{4}+2\mathbf{K}}+\frac{3}{2}\right)}{\Gamma\left(1+\sqrt{\frac{49}{4}+2\mathbf{K}}\right)} \tag{335}$$

The emergence of the pion decay constant $f_\pi = 93$ MeV follows from the holographic ρ-wavefunction as discussed in the Appendix. For the $\bar{\mathbf{3}}$-plet and $\mathbf{6}$-plet representations, we have specifically

$$\begin{aligned} \left\langle \rho^3 \right\rangle_{\bar{3}} &= \frac{1}{f_\pi^3}\left(\frac{\sqrt{6}}{4\pi^3}\right)^{\frac{3}{2}} \times 13.65 \\ \left\langle \rho^3 \right\rangle_{6} &= \frac{1}{f_\pi^3}\left(\frac{\sqrt{6}}{4\pi^3}\right)^{\frac{3}{2}} \times 16.70 \end{aligned} \tag{336}$$

The corresponding mass shifts induced by the explicit symmetry breaking term (334) on the heavy-light baryonic spectra is then

$$\Delta M_i = b_i(1-a_i)\frac{\tau}{f_\pi^3}\left(\frac{\sqrt{6}}{4\pi^3}\right)^{\frac{3}{2}} \equiv b_i(1-a_i)m_0 \tag{337}$$

with the representation dependent parameters

$$
\begin{aligned}
b_i &= \frac{\Gamma(1+\sqrt{\frac{49}{4}+2\mathbf{K}_i}+\frac{3}{2})}{\Gamma(1+\sqrt{\frac{49}{4}+2\mathbf{K}_i})} \\
a_i &= \langle pq, j|D_{88}|pq, j\rangle
\end{aligned}
\tag{338}
$$

For the specific representations of relevance to our analysis we have

$$
\begin{aligned}
a_N &= \frac{3}{10}, \qquad & b_N &= 18.97 \\
a_\Lambda &= \frac{1}{4}, \qquad & a_{\Xi^3} &= -\frac{1}{8} \\
a_\Sigma &= \frac{1}{10}, \qquad & a_{\Xi^6} &= -\frac{1}{20}, \qquad & a_\Omega &= -\frac{1}{5}
\end{aligned}
\tag{339}
$$

7.6.1 Single-heavy baryon spectrum

Combining all the previous results for the heavy-light masses, including the correction induced by the strange quark mass symmetry breaking term (334) yield the following mass spectrum for the single-heavy baryons

$$
\begin{aligned}
m_{\Lambda_Q} &= m_N + m_H - 0.57 M_{KK} - 3.04 m_0 \\
m_{\Xi(\bar{3})_Q} &= m_N + m_H - 0.57 M_{KK} + 2.08 m_0 \\
m_{\Sigma_Q} &= m_N + m_H - 0.236 M_{KK} + 1.75 m_0 \\
m_{\Xi(6)_Q} &= m_N + m_H - 0.236 M_{KK} + 4.25 m_0 \\
m_{\Omega_Q} &= m_N + m_H - 0.236 M_{KK} + 6.76 m_0
\end{aligned}
\tag{340}
$$

In the original Sakai and Sugimoto analysis, the Kaluza-Klein parameter is fixed by the light rho mass as indicated earlier with $M_{KK} \approx 1$ GeV. Although we will use this value for all the heavy-light baryon masses to follow, we note that this value of M_{KK} was noted to be large in [162, 181]. The nucleon mass $m_N = 938$ MeV is set to its empirical value. The symmetry breaking parameter m_0 will be fitted to reproduce the mass splitting between the nucleon in the octet and the $\Omega^- = sss$ in the decuplet as it is the baryon with the largest strangeness. Specifically, we set

$$m_{\Omega^-} - m_N = 0.386\, M_{KK} + 15.32\, m_0 = 732\,\mathrm{MeV} \tag{341}$$

which fixes $m_0 = 22.6$ MeV.

So for $n_z = n_\rho = 0$, the lowest heavy-light mass spectra corrected in first order by the light strange quark symmetry breaking, with their J^π assignments are

$$\begin{aligned}
&\Lambda_Q(\frac{1}{2})^+, M = m_N + m_H - 0.57 M_{KK} - 3.04 m_0 \\
&\Xi_Q^{\bar{3}}(\frac{1}{2})^+, M = m_N + m_H - 0.57 M_{KK} + 2.08 m_0 \\
&\Sigma_Q(\frac{1}{2})^+, M = m_N + m_H - 0.236 M_{KK} + 1.75 m_0 \\
&\Xi_Q^{6}(\frac{1}{2})^+, M = m_N + m_H - 0.236 M_{KK} + 4.25 m_0 \\
&\Omega_Q(\frac{1}{2})^+, M = m_N + m_H - 0.236 M_{KK} + 6.76 m_0 \\
&\Sigma_Q^\star(\frac{3}{2})^+, M = m_N + m_H - 0.236 M_{KK} + 1.75 m_0 \\
&\Xi_Q^{6\star}(\frac{3}{2})^+, M = m_N + m_H - 0.236 M_{KK} + 4.25 m_0 \\
&\Omega_Q^\star(\frac{3}{2})^+, M = m_N + m_H - 0.236 M_{KK} + 6.76 m_0
\end{aligned} \tag{342}$$

The lowest excited states of these heavy-light baryons carry finite n_ρ, n_z. For instance, for $n_\rho = 1$, $n_z = 0$ we have the even-parity or Roper-like excitation corresponding to $\Omega_{EQ}(\frac{1}{2})^+$, and for $n_\rho = 0$ and $n_z = 1$ we have the odd-parity excitation corresponding to $\Omega_Q(\frac{1}{2})^-$. Their masses are

$$\begin{aligned}
\Omega_Q(\frac{1}{2})^-, M &= m_N + m_H + 0.580 M_{KK} + 6.76 m_0 \\
\Omega_{EQ}(\frac{1}{2})^+, M &= m_N + m_H + 0.580 M_{KK} + 10.74 m_0
\end{aligned} \tag{343}$$

The masses of the single-heavy light baryons with charm follow by setting the charm heavy meson mass m_H to its empirical value $m_H = m_D = 1870$ MeV,

and similarly for the bottom heavy meson mass $m_H = m_B = 5279$ MeV. The specifics mass values are quoted below in [MeV] with the measured masses from [185] indicated in bold numbers.

7.6.2 Charm baryon masses [MeV]

$$\begin{aligned}
\Lambda_c(\frac{1}{2})^+, M &= 2117\,[\mathbf{2286}] \\
\Xi_c^{\bar{3}}(\frac{1}{2})^+, M &= 2320\,[\mathbf{2468}] \\
\Sigma_c(\frac{1}{2})^+, \Sigma_c^\star(\frac{3}{2})^+, M &= 2641\,[\mathbf{2453}, \mathbf{2518}] \\
\Xi_c^6(\frac{1}{2})^+, \Xi_c^{6\star}(\frac{3}{2})^+, M &= 2740\,[\mathbf{2576}, \mathbf{2646}] \\
\Omega_c(\frac{1}{2})^+, \Omega_c^\star(\frac{3}{2})^+, M &= 2840\,[\mathbf{2695}, \mathbf{2766}] \\
\Omega_c(\frac{1}{2})^-, \Omega_c^\star(\frac{3}{2})^-, M &= 3656\,[\mathbf{3050}, \mathbf{3066}] \\
\Omega_{Ec}(\frac{1}{2})^+, \Omega_{Ec}^\star(\frac{3}{2})^+, M &= 3813\,[\mathbf{3090}, \mathbf{3119}]
\end{aligned} \tag{344}$$

7.6.3 Bottom baryon masses [MeV]

$$\begin{aligned}
\Lambda_b(\frac{1}{2})^+, M &= 5580\,[\mathbf{5619}] \\
\Xi_b^{\bar{3}}(\frac{1}{2})^+, M &= 5696\,[\mathbf{5799}] \\
\Sigma_b(\frac{1}{2})^+, \Sigma_b^\star(\frac{3}{2})^+, M &= 6022\,[\mathbf{5813}, \mathbf{5834}] \\
\Xi_b^6(\frac{1}{2})^+, \Xi_b^{6\star}(\frac{3}{2})^+, M &= 6079\,[***, \mathbf{5955}] \\
\Omega_b(\frac{1}{2})^+, \Omega_b^\star(\frac{3}{2})^+, M &= 6153\,[\mathbf{6048}, ***] \\
\Omega_b(\frac{1}{2})^-, \Omega_b^\star(\frac{3}{2})^-, M &= 6951 \\
\Omega_{Eb}(\frac{1}{2})^+, \Omega_{Eb}^\star(\frac{3}{2})^+, M &= 7041
\end{aligned} \tag{345}$$

7.7 Double-heavy baryon spectrum

The double-heavy baryons with hidden charm or bottom are currently referred to as pentaquarks. Their masses in the **8**-plet of the flavor representation (333) corrected by the strange quark mass are

$$\begin{aligned} N_{\bar{Q}Q}^{(\frac{1}{2},\frac{3}{2})^-}, M &= m_N + 2m_H \\ \Lambda_{\bar{Q}Q}^{(\frac{1}{2},\frac{3}{2})^-}, M &= m_N + 2m_H + 3.80m_0 \\ \Sigma_{\bar{Q}Q}^{(\frac{1}{2},\frac{3}{2})^-}, M &= m_N + 2m_H + 7.59m_0 \\ \Xi_{\bar{Q}Q}^{(\frac{1}{2},\frac{3}{2})^-}, M &= m_N + 2m_H + 9.48m_0 \end{aligned} \tag{346}$$

The penta-quark masses in the **10**-plet representation corrected by the strange quark mass are

$$\begin{aligned} \Delta_{\bar{Q}Q}^{(\frac{1}{2},\frac{3}{2},\frac{5}{2})^-}, M &= m_N + 2m_H + 0.386M_{KK} + 6.74m_0 \\ \Sigma_{\bar{Q}Q}^{\star(\frac{1}{2},\frac{3}{2},\frac{5}{2})^-}, M &= m_N + 2m_H + 0.386M_{KK} + 9.60m_0 \\ \Xi_{\bar{Q}Q}^{\star(\frac{1}{2},\frac{3}{2},\frac{5}{2})^-}, M &= m_N + 2m_H + 0.386M_{KK} + 12.46m_0 \\ \Omega_{\bar{Q}Q}^{(\frac{1}{2},\frac{3}{2},\frac{5}{2})^-}, M &= m_N + 2m_H + 0.386M_{KK} + 15.32m_0 \end{aligned} \tag{347}$$

The double heavy baryons consisting of two heavy bound mesons with explicit charm or bottom will be referred to by Ξ_{QQ} and Ω_{QQ} in the flavor **3**-plet representation as we noted earlier. Their strangeness corrected masses are

$$\begin{aligned} \Xi_{QQ}^{(\frac{1}{2})^+}, M &= m_N + 2m_H - 0.844M_{KK} - 2.67\, m_0 \\ \Omega_{QQ}^{(\frac{1}{2})^+}, M &= m_N + 2m_H - 0.844M_{KK} - 0.54\, m_0 \end{aligned} \tag{348}$$

It is clear, that the holographic construct also describes their excited Roper-like with even parity as well as their odd parity partners, which can be retrieved from our formula.

7.7.1 Charm penta-quark masses [MeV]

$$
\begin{aligned}
N_{\bar{c}c}(\frac{1}{2},\frac{3}{2})^{-},\, M &= 4680\,[\mathbf{4380},\mathbf{4450}] \\
\Lambda_{\bar{c}c}(\frac{1}{2},\frac{3}{2})^{-},\, M &= 4766 \\
\Sigma_{\bar{c}c}(\frac{1}{2},\frac{3}{2})^{-},\, M &= 4852 \\
\Xi_{\bar{c}c}(\frac{1}{2},\frac{3}{2})^{-},\, M &= 4894 \\
\Delta_{\bar{c}c}(\frac{1}{2},\frac{3}{2},\frac{5}{2})^{-},\, M &= 5218 \\
\Sigma^{\star}_{\bar{c}c}(\frac{1}{2},\frac{3}{2},\frac{5}{2})^{-},\, M &= 5283 \\
\Xi^{\star}_{\bar{c}c}(\frac{1}{2},\frac{3}{2},\frac{5}{2})^{-},\, M &= 5348 \\
\Omega_{\bar{c}c}(\frac{1}{2},\frac{3}{2},\frac{5}{2})^{-},\, M &= 5412
\end{aligned}
\tag{349}
$$

7.7.2 Mixed penta-quark masses [MeV]

$$
\begin{aligned}
N_{\bar{b}c}(\frac{1}{2},\frac{3}{2})^{-},\, M &= 8089 \\
\Lambda_{\bar{b}c}(\frac{1}{2},\frac{3}{2})^{-},\, M &= 8175 \\
\Sigma_{\bar{b}c}(\frac{1}{2},\frac{3}{2})^{-},\, M &= 8261 \\
\Xi_{\bar{b}c}(\frac{1}{2},\frac{3}{2})^{-},\, M &= 8303 \\
\Delta_{\bar{b}c}(\frac{1}{2},\frac{3}{2},\frac{5}{2})^{-},\, M &= 8627 \\
\Sigma^{\star}_{\bar{b}c}(\frac{1}{2},\frac{3}{2},\frac{5}{2})^{-},\, M &= 8692 \\
\Xi^{\star}_{\bar{b}c}(\frac{1}{2},\frac{3}{2},\frac{5}{2})^{-},\, M &= 8757 \\
\Omega_{\bar{b}c}(\frac{1}{2},\frac{3}{2},\frac{5}{2})^{-},\, M &= 8821
\end{aligned}
\tag{350}
$$

7.7.3 Bottom penta-quark masses [MeV]

$$
\begin{aligned}
N_{\bar{b}b}(\frac{1}{2},\frac{3}{2})^{-},\, M &= 11498 \\
\Lambda_{\bar{b}b}(\frac{1}{2},\frac{3}{2})^{-},\, M &= 11583 \\
\Sigma_{\bar{b}b}(\frac{1}{2},\frac{3}{2})^{-},\, M &= 11670 \\
\Xi_{\bar{b}b}(\frac{1}{2},\frac{3}{2})^{-},\, M &= 11712 \\
\Delta_{\bar{b}b}(\frac{1}{2},\frac{3}{2},\frac{5}{2})^{-},\, M &= 12036 \\
\Sigma^{\star}_{\bar{b}b}(\frac{1}{2},\frac{3}{2},\frac{5}{2})^{-},\, M &= 12101 \\
\Xi^{\star}_{\bar{b}b}(\frac{1}{2},\frac{3}{2},\frac{5}{2})^{-},\, M &= 12166 \\
\Omega_{\bar{b}b}(\frac{1}{2},\frac{3}{2},\frac{5}{2})^{-},\, M &= 12230
\end{aligned}
\tag{351}
$$

7.7.4 Charm and bottom 3-plet masses [MeV]

$$
\begin{aligned}
\Xi_{cc}(\frac{1}{2})^{+},\, M &= 3776\,[\mathbf{3519}] \\
\Omega_{cc}(\frac{1}{2})^{+},\, M &= 3848 \\
\Xi_{cb}(\frac{1}{2})^{+},\, M &= 7184 \\
\Omega_{cb}(\frac{1}{2})^{+},\, M &= 7257 \\
\Xi_{bb}(\frac{1}{2})^{+},\, M &= 10584 \\
\Omega_{bb}(\frac{1}{2})^{+},\, M &= 10657
\end{aligned}
\tag{352}
$$

7.8 Conclusions

We have presented a top-down holographic approach to the single- and double-heavy baryons in the variant of $D4$-$D8$ we proposed recently [165] (first reference). To order λm_H^0, the heavy baryons emerge from the zero

mode after binding a heavy meson in the multiplet $(0^-, 1^-)$ to the instanton. Remarkably, in the bulk instanton field the spin 1 and odd parity heavy meson transmutes equally to a spin $\frac{1}{2}$ and even parity massless fermion and anti-fermion. At subleading order, the Chern-Simons term is attractive for the bound meson with a heavy quark content and repulsive for the bound meson with heavy anti-quark content.

One of the key differences between the $N_f = 2$ and $N_f = 3$ case is the role played by the amended form of the Chern-Simons term which results in a good hypercharge quantization rule [181, 182]. We have shown that the rule gets modified by the presence of the bound zero mode states, leading to a rich heavy-light spectra for single-heavy and double-heavy baryons with hidden charm and bottom. In particular, the formers follow from the $\bar{\mathbf{3}}$ and $\mathbf{6}$ flavor representations, while the latters from the $\mathbf{8}$ and $\mathbf{10}$ representations for the lowest states. The holographic set up allows for a simple description of the low-lying odd-parity and Roper-like excitations of the heavy baryons. Our results for $N_f = 3$ with massive strangeness confirm and extend our previous findings for massless $N_f = 2$.

To compare our results with currently known heavy-light charm and meson spectra, it is necessary to account for the light strange quark mass. In holography this is induced by a worldsheet instanton that connects $D8$ and $D\bar{8}$ [183]. By accounting for this correction in leading order perturbation theory, we have found reasonable agreement for the lowest single-heavy baryons with a single adjustable parameter, namely the overall strength of the symmetry breaking term. The holographic model describes 2 neutral $\Omega_c^0, \Omega_c^{*0}$ states with $\frac{1}{2}^+, \frac{3}{2}^+$ assignments as the odd parity partners of the lowest $\Omega_c^0, \Omega_c^{*0}$ states, and 2 Roper-like neutral states with $\frac{1}{2}^+, \frac{3}{2}^+$ assignments as the even parity partners also of the lowest $\Omega_c^0, \Omega_c^{*0}$ states. The $\frac{1}{2}^- \frac{3}{2}^-$ are predicted to be lighter than the excited $\frac{1}{2}^+ \frac{3}{2}^+$ states, however both pairs are found to be heavier than the 5 neutral Ω_c^0 states reported recently by the LHCb collaboration.

The holographic set up for the heavy baryons is remarkable by the limited number of parameters it carries. Once the initial parameter κ is traded for the pion decay constant f_π, only the symmetry breaking parameter m_0 was left to be fixed in either the light or heavy sector. We choose the latter to fix it. Clearly, the model can and should be made more realitic through the use of improved holographic QCD [171].

The shortcomings of the heavy-light holographic approach stem from the

triple limits of large N_c, strong $'$t Hooft coupling $\lambda = g^2 N_c$, and heavy meson mass. The corrections in $1/m_H$ are straighforward but laborious and should be studied as they shed important light on the hyperfine type splittings. Also, it should be useful to explore the sensitivity of our results by relaxing the value of M_{KK} as fixed in the light meson sector and addressing the strangeness mass correction beyond leading order perturbation theory. The one-meson radiative decays of the heavy baryons and their exotics can be addressed in this model for further comparison with the experimentally reported partial widths.

Part IV: Random matrix models for QCD

8 Polaykov line model in 1+2,3 dimensions

This section is an edited version of my publication:
Hydrodynamics of the Polyakov line in SU(Nc) Yangills
Yizhuang Liu (Stony Brook U.), Piotr Warcho(Jagiellonian U.), Ismail Zahed (SUNY, Stony Brook). May 8, 2015. 4 pp. Phys.Lett.B753 (2016) 65-68

1. Polyakov line in $1+2$ dimensions. The matrix model partition function for the eigenvalues of the Polyakov line for SU(N_c) in 1+2 dimensions was discussed in [87]. If we denote by diag$(e^{i\theta_1},...,e^{i\theta_{N_c}})$ with $\sum_i \theta_i = 0$ the gauge invariant eigenvalues of the Polyakov line, then [87]

$$Z[\alpha,\beta] = \int \prod_{i=1}^{N_c} d\theta_i \prod_{i<j}^{N_c} |z_{ij}|^{\beta(T)} e^{-\alpha(T)\sum_{i<j} V(|z_{ij}|)} \tag{353}$$

with $z_{ij} = z_i - z_j$ and $z_i = e^{i\theta_i}$. The perturbative potential $V(z_{ij})$ is center symmetric and quadratic in leading order or $V(|z_{ij}|) \approx |z_{ij}|^2$, with $\alpha(T) = T^2\, V_2/2\pi$ and V_2 the spatial 2-volume [87]. The mass expansion of the one-loop determinant gives $\beta(T) = m_D^2\, V_2/\pi$ [87]. The Debye mass is self-consistently defined as $m_D^2 = N_c g^2 T(\ln(T/m_D) + C)/2\pi$ [94] to tame all infra-red divergences, with $C \approx 1.3$ from lattice simulations [95, 96].

(353) can be regarded as the normalization of the squared and real many-body wave-function $\mathbf{\Psi}_0[z_i]$ which is the zero-mode solution to the Shrodinger equation $H_0\Psi_0 = 0$ with the self-adjoint squared Hamiltonian

$$H_0 \equiv \sum_{i=1}^{N_c} (-\partial_i + \mathbf{a}_i)\,(\partial_i + \mathbf{a}_i) \tag{354}$$

with $\partial_i \equiv \partial/\partial\theta_i$ and the pure gauge potential $\mathbf{a}_i \equiv \partial_i S$. Here $S[z] = -\ln\Psi_0[z]$ is half the energy in the defining partition function in (353). In (354) the mass parameter is 1/2.

2. Hydrodynamics. We can use the collective coordinate method in [91] to re-write (354) in terms of the density of eigenvalues as a collective variable $\rho(\theta) = \sum_{i=1}^{N_c} \delta(\theta - \theta_i)$. For that, we re-define $H_0 \to H$ through a similarity transformation to re-absorb the diverging 2-body part induced by the Vandermond contribution $\Delta = \prod_{i<j} |z_{ij}|^{\beta(T)}$, i.e. $\Psi = \Psi_0/\sqrt{\Delta}$ and $\sqrt{\Delta}\, H = H_0\sqrt{\Delta}$. Now H is of the general form discussed in [91] and is amenable after some algebra to

$$H = \int d\theta \left(\partial_\theta \pi \rho\, \partial_\theta \pi + \rho \mathbf{u}[\rho]\right) \tag{355}$$

with the potential-like contribution

$$\mathbf{u}[\rho] = \left(A(\theta) - \frac{\pi\beta(T)\rho_H}{2} + \frac{1}{2}\partial_\theta \ln\rho\right)^2 \equiv \mathbf{A}^2 \tag{356}$$

Here

$$A(\theta) = \frac{1}{2}\alpha(T) \int d\theta' \rho(\theta')\, \partial_\theta V\left(2\sin\left(\frac{\theta - \theta'}{2}\right)\right) \tag{357}$$

and ρ_H is the periodic Hilbert transform of ρ

$$[\rho]_H \equiv \rho_H(\theta) = \frac{1}{2}\frac{\mathrm{P}}{\pi} \int \rho(\theta')\, \mathrm{cotan}\left(\frac{\theta - \theta'}{2}\right) \tag{358}$$

As conjugate pairs, $\pi(\theta)$ and $\rho(\theta)$ satisfy the equal-time commutation rule $[\pi(\theta), \rho(\theta')] = -i\left(\delta(\theta - \theta') - 1/2\pi\right)$. We identify the collective fluid velocity with $v = \partial_\theta \pi$ and re-write (355) in the more familiar hydrodynamical form

$$H \approx \int d\theta \rho(\theta) \left(v^2 + \mathbf{u}[\rho]\right) \approx \int d\theta \rho(\theta) \left|v + i\mathbf{A}\right|^2 \tag{359}$$

modulo ultra-local terms. The Heisenberg equation for ρ yields the current conservation law $\partial_t \rho = -2\partial_\theta(\rho v)$, and the Heisenberg equation for v gives the Euler equation

$$\partial_t v = i[H,v] = \\ -\partial_\theta \left(v^2 + \mathbf{A}^2 - \partial_\theta \mathbf{A} - \mathbf{A}\partial_\theta \ln\rho + \pi\beta[\mathbf{A}\rho]_H - 2\alpha[\mathbf{A}\rho]_S \right) \tag{360}$$

with the sine-transform $[\mathbf{A}\rho]_S = \int \sin(\theta-\theta')\mathbf{A}(\theta')\rho(\theta')$. Note that all the relations hold for large but finite N_c.

3. Hydro-static solution. The static hydrodynamical density follows from the minimum of (358) with $v(\theta)=0$,

$$\beta(T)\pi\rho_H(\theta) - \partial_\theta \ln\rho(\theta) = 2A(\theta) \tag{361}$$

To solve (361), we insert the leading quadratic contribution $A(\theta) \approx 2\alpha(T)\sin^2(\theta/2)$ in (361)

$$\rho\rho_H - a\partial_\theta\rho = bc_1\rho\sin(\theta) \tag{362}$$

with $a \equiv 1/\pi\beta(T)$, $b \equiv 2\alpha(T)/\beta(T)$ and c_1 the first moment of the density or $\pi c_1 \equiv \int_0^{2\pi} \rho(\theta)\cos\theta d\theta$. Let $\rho_0 = N_c/2\pi$ be the uniform eigenvalue density and $\rho_1 = \rho - \rho_0$ its deviation. Consider the Cauchy transform

$$G(z) = \frac{1}{\pi i}\int_{\mathcal{C}} \frac{\rho_1(\eta)}{\eta - z} d\eta \tag{363}$$

with $\eta = e^{i\theta}$. The contour $\mathcal{C}$ is counter-clockwise along the unit circle. $G(z)$ is a holomorphic function in the complex z-plane. Let G^+ and G^- be its realization inside and outside $\mathcal{C}$ respectively, so that

$$G^{\pm}(z \to e^{i\theta}) = \pm\rho_1(\theta) + i\rho_H(\theta) \tag{364}$$

We now carry the Hilbert transform on both sides of (362). Setting $G(z) = G^+(z)$ and using $2[\rho_1\rho_H]_H = \rho_H^2 - \rho_1^2$, we have for (362)

$$\frac{1}{2}G^2 + (\rho_0 - \frac{1}{2}bc_1(z - z^{-1}))G + az\partial_z G = bc_1\rho_0 z + \frac{1}{2}bc_1^2 \tag{365}$$

on the boundary $\mathcal{C}$, thus within the circle. Here, we should require $G(z = 0) = 0$ to ensure that ρ_1 integrates to zero.

$a \approx 1/V_2$ is subleading and will be dropped. Thus (365) is algebraic in $G(z)$. Since $\rho(\theta) = \rho_0 + \mathrm{Re}\, G^+(z = e^{i\theta})$, careful considerations of the singularity structures of the quadratic solutions to (365) yield (Θ is a step function)

$$\rho(\theta) = \sqrt{bc_1}(\cos\theta + 1)^{\frac{1}{2}}(\cos\theta - \cos\theta_0)^{\frac{1}{2}}\,\Theta(|\theta_0| - |\theta|) \tag{366}$$

The analytic properties of $G(z)$ fix $c_1/\rho_0 = 1 + (1 - 1/b)^{\frac{1}{2}}$ and θ_0 at $\cos\theta_0 = 1 - 2\rho_0/bc_1$. For $b < 1$ the non-uniform solution with $\rho_1 \neq 0$ is absent. For $b \gg 1$, $c_1 \to 2\rho_0$ and

$$\rho(\theta) \to \frac{N_c}{2\pi}\sqrt{8b - 4b^2\theta^2} \tag{367}$$

Therefore (366) interpolates between a uniform density distribution ρ_0 (confined phase) and a Wigner semi-circle (deconfined phase) with a transition at $b = 1$ or $T_c = m_D$. In $1 + 2$ dimensions the fundamental string tension is given to a good accuracy by $\sqrt{\sigma_1}/g^2N_c = ((1 - 1/N_c^2)/8\pi)^{\frac{1}{2}}$ [99]. Thus the ratio in $1 + 2$ dimensions

$$\frac{T_c}{\sqrt{\sigma_1}} = \frac{C}{2\pi}\left(\frac{8\pi}{1 - 1/N_c^2}\right)^{\frac{1}{2}} \to \sqrt{\frac{2}{\pi}}\,C \tag{368}$$

with $C \approx 1.3$ [95, 96]. In Fig. 30 we show the behavior of (368) (upper curve) versus N_c, in comparison to the numerical fit $T_c/\sqrt{\sigma_1} = 0.9026 + 0.880/N_c^2$ to the lattice results (lower curve) in [100]. Amusingly, (368) at large N_c is consistent with $\sqrt{3/\pi}$ in the string model [97].

4. Dyson Coulomb gas. We note that (361) coincides with the saddle point equation to (353) by re-writing it using Dyson charged particle analogy on S^1 with the energy $2S[z] = \sum_{i<j} G(z_{ij})$ and the pair interaction

$$G(z_{ij}) = -\ln|z_{ij}|^{\beta(T)} + \alpha(T)V(|z_{ij}|) \equiv \mathbf{G}(\theta_i - \theta_j) \tag{369}$$

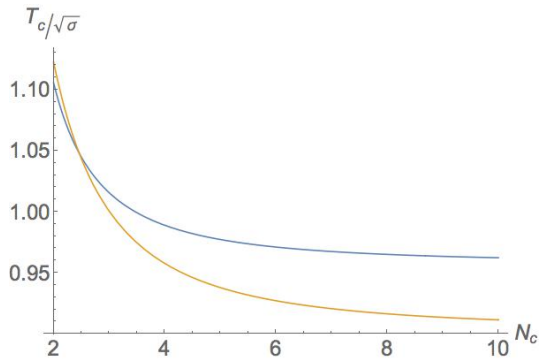

Figure 30: $T_c/\sqrt{\sigma_1}$ versus N_c in (368) (upper curve) compared to the numerical fit to the lattice results (lower curve) from [100].

At large N_c the ensemble described by (353) is sufficiently dense to allow the change in the measure. Following Dyson [120] we obtain

$$Z[\alpha,\beta] \to \int D\rho\, e^{-\Gamma[\alpha,\beta;\rho]} \tag{370}$$

with the effective action

$$\begin{aligned}\Gamma[\alpha,\beta;\rho] = \quad & \frac{1}{2}\int \rho(\theta)\mathbf{G}(\theta-\theta')\rho(\theta') \\ & -\left(\frac{\beta(T)}{2}-1\right)\int d\theta\rho(\theta)\ln\left(\frac{\rho(\theta)}{\rho_0}\right)\end{aligned} \tag{371}$$

The β contribution is the self Coulomb subtraction and is consistent with the subtraction in the Hilbert transform. The saddle point equation $\delta\Gamma/\delta\rho = 0$ following from (370-371) is in agreement with the hydro-static equation (361),

$$\frac{d}{d\theta}\frac{\delta\Gamma[\alpha,\beta;\rho]}{\delta\rho(\theta)} = 2\mathbf{A} = 0 \tag{372}$$

5. Hydrodynamical instanton. The fixed time zero energy solution to (359) is an instanton with imaginary velocity $v = -i\mathbf{A}$. We have checked

that this is a solution to (360) for all times. The current $j \equiv \rho v = -i\rho\mathbf{A}$ is conserved.Thus $\partial_\tau \rho - 2\partial_\theta(\rho\mathbf{A}) = 0$ or

$$\partial_\tau \rho + \beta(T)\partial_\theta(\pi\rho\rho_H) = \partial_\theta^2\rho + 2\partial_\theta(\rho A(\theta)) \tag{373}$$

for Euclidean times $\tau = it$. For $A = 0$ and $\beta(T) = 2$, (373) agrees with the viscid Burger′s equation describing large Wilson loops in $1+1$ dimensions [176]. Following [120] we identify τ with the stochastic (Langevin) time. (373) describes the stochastic relaxation of the eigenvalue density of the Polyakov line (out of equilibrium) to its asymptotic (in equilibrium) hydro-static solution.

6. Sound waves. The hydrodynamical action follows from standard procedure.The momentum $\pi(\theta) = (1/\partial_\theta)v$ is canonically conjugate to the density ρ, and the Lagrange density is $\mathbf{L} = \pi\partial_t\rho - H$. Thus the action $\mathbf{S} = \int dtd\theta\, \rho(\theta)\,(v^2 - \mathbf{u}[\rho])$, which is linearized by

$$\rho \approx \rho_0(\theta) + 2\partial_\theta\varphi \qquad \text{and} \qquad \rho v \approx -\partial_t\varphi \tag{374}$$

Inserting (374) into $\mathbf{S}$ yields

$$\mathbf{S}_2 = \int dt \frac{d\theta}{\rho_0(\theta)}\, \left((\partial_t\varphi)^2 - \rho_0^2(\theta)W^2[\varphi]\right) \tag{375}$$

with the potential

$$W[\varphi] = 2\alpha(T)[\partial_\theta\varphi]_S - \pi\beta(T)[\partial_\theta\varphi]_H + \partial_\theta\left(\frac{\partial_\theta\varphi}{\rho_0(\theta)}\right) \tag{376}$$

For constant ρ_0 and large N_c, (375) simplifies to

$$\mathbf{S}_2 \approx m_D^2 V_2 \int dtd\theta\, \left((\partial_t\varphi)^2 - (\partial_\theta\varphi)^2\right) \tag{377}$$

after the rescaling $v_s t \to t$ with $v_s = \pi\rho_0\beta(T)$. (377) describes sound waves in the large N_c space of holonomies.

7. Z(N_c) bubble. In a de-confined phase of infinite volume, the Yang-Mills ground state settles in one of the degenerate Z(N_c) vacua. In a finite volume, bubbles of different vacua may form [102]. Consider a de-confined bubble of volume $\mathbb{V}_2$ immersed in a confined volume $\overline{\mathbb{V}}_2$. In $\mathbb{V}_2$ all the eigenvalues are localized initially within a small $\Delta\theta$ around the origin with $\rho(\tau = 0, \theta) = N_c/\Delta\theta \equiv \rho_B$, and zero otherwise.

Using this piece-wise wave as an initial condition we solve (373) with $A = 0$ for simplicity. For large times τ, the result is

$$\rho(\tau, \theta) \approx \rho_0 - \left(\frac{2}{\pi}\rho_B \sin\left(\frac{\Delta\theta}{2}\right)\right) \cos\theta \, e^{-v_s\tau} \tag{378}$$

which shows the relaxation of the piece-wise wave over a time $\tau \approx 1/v_s$ set by the speed of sound. Using (378) in $\mathbf{S}$ yields the Euclidean action estimate for small $\Delta\theta$

$$\mathbf{S}_E(\mathbb{V}_2) \approx \mathbb{V}_2 \left(\pi m_D \rho_B \sin\left(\frac{\Delta\theta}{2}\right)\right)^2 \to \mathbb{V}_2 \left(\frac{\pi}{2} N_c m_D\right)^2 \tag{379}$$

The bubble formation probability or fugacity is $e^{-\mathbf{S}_E(\mathbb{V}_2)}$.

8. Polyakov line in $1+3$ dimensions. To extend our analysis to $1+3$ dimensions, we approximate the Yang-Mills thermal state by a dense plasma of dyons and anti-dyons [83, 111]. This semi-classical description reproduces a number of key features of the Yang-Mills phase both in the confined (center-symmetric) and de-confined (center-broken) phase. There are two key differences with the $1+2$ dimensional partition function in (1). First the many-body energy $2S[z] = -2\ln\Psi_0[z]$ in (1) is now shifted

$$2S[z] \to 2S[z] - \gamma(T) \prod_i^{N_c} (\theta_{i+1} - \theta_i)^{\frac{1}{N_c}} \tag{380}$$

with $\gamma(T) = 4\pi N_c f V_3$ and $f = 4\pi\Lambda^4/Tg^4$ the dyon fugacity [83]. Second and more importantly $\beta(T) = 2$ and is not extensive with the spatial 3-volume V_3. Finally, $\alpha(T) = T^3 V_3/3$. Since $(\theta_{i+1} - \theta_i) \approx 1/2\pi\rho(\theta_i)$, then in the continuum the additional string of factors in (380) is

$$\prod_i^{N_c} (\theta_{i+1} - \theta_i)^{\frac{1}{N_c}} \to e^{\frac{1}{N_c}\int d\theta \rho(\theta) \ln(1/2\pi\rho(\theta))} \tag{381}$$

With this in mind, a re-run of the preceding arguments yields the Hamiltonian in (355-356) with the shifted potential

$$A \to A + \frac{\gamma(T)}{4\pi N_c^2} e^{-\gamma_0[\rho]} \partial_\theta \ln\rho(\theta) \tag{382}$$

and $N_c \ln\gamma_0[\rho] = \int d\theta \rho(\theta) \ln(\rho(\theta)/N_c)$. The hydro-static equation (361) now reads

$$\beta\pi\rho_H(\theta) - 2A(\theta) = \left(1 + \frac{\gamma(T)}{4\pi N_c^2} e^{-\gamma_0[\rho]}\right) \partial_\theta \ln\rho(\theta) \tag{383}$$

The $\beta = 2$ contribution is now sub-leading and can be dropped. The corresponding solution to (383) is a localized density for $\pi c_1 = \int_0^{2\pi} d\theta \rho(\theta) \cos\theta \neq 0$, and a uniform density $\rho_0 = N_c/2\pi$ for $c_1 = 0$. Specifically

$$\frac{\rho(\theta)}{\rho_0} = \frac{e^{\frac{8\pi\alpha\gamma_0}{\gamma'} c' \cos\theta}}{I_0(\frac{8\pi\alpha\gamma_0}{\gamma'} c')} \tag{384}$$

with $c' = c_1/N_c$ and $\gamma' = \gamma/N_c^3$. The two parameters $\eta = 8\pi\alpha(T)/\gamma'$ and $x = c'\,\eta\gamma_0$ are fixed by the transcendental equations

$$\frac{I_1(x)}{I_0(x)} = \frac{\pi x}{\eta\gamma_0} \qquad \text{and} \qquad \frac{I_1(x)}{I_0^2(x)} e^{x\frac{I_1(x)}{I_0(x)}} = \frac{2\pi^2 x}{\eta} \tag{385}$$

A solution exists only for $\gamma' < 2\alpha(T)/\pi$. Else the density is uniform. Thus the transition temperature from center symmetric (confining) to center-broken (deconfining) occurs for $\alpha(T_c)/\gamma(T_c) = \pi/2N_c^3$ or $T_c^4 = \frac{3}{8\pi}\frac{\Lambda^4}{\lambda^2}$ with $\lambda = g^2 N_c/8\pi^2$. For the dyon model, the fundamental string tension is given by $\sigma_1 = (N_c/\pi)\sin(\pi/N_c)\,\Lambda^2/\lambda$ [83]. Thus the model independent ratio in $1+3$ dimensions

$$\frac{T_c}{\sqrt{\sigma_1}} = \left(\frac{3\pi}{8N_c^2 \sin^2(\pi/N_c)}\right)^{\frac{1}{4}} \to \left(\frac{3}{8\pi}\right)^{\frac{1}{4}} \tag{386}$$

(386) compares favorably to the lattice results [101] even for small N_c as shown in Fig. 31. At large N_c, (386) is consistent with the value of $\sqrt{3/2\pi}$ in the string model [97].

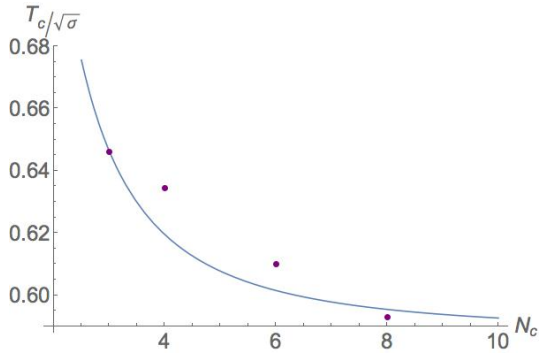

Figure 31: $T_c/\sqrt{\sigma_1}$ versus N_c in (386). The dots are the lattice results from [101].

9. Conclusions. The hydrodynamical description of the Polyakov line captures aspects of the center dynamics in Yang-Mills theory in terms of the gauge invariant density of eigenvalues. The hydro-static equations yield solutions that interpolate between a center symmetric (confining) and a center-broken (de-confining) phase. The transition temperatures normalized to the string tension compare well to the lattice results over a broad range of N_c, and asymptote the string model results at $N_c = \infty$. The hydrodynamical set-up supports a hydrodynamical instanton that describes the stochastic relaxation of the eigenvalues of the Polyakov line viewed as a fluid. The fluid supports sound waves that can be used to estimate the probability of formation of $\mathrm{Z(N}_c\mathrm{)}$ bubbles. The relaxation of a fluid of holonomies across the critical temperature may prove useful for understanding the onset of equilibration in a Yang-Mills plasma.

9 Chiral matrix evolution at finite chemical potential.

This section is an edited version of my publication :
Chiral Random Matrix Model at Finite Chemical Potential: Characteristic Determinant and Edge Universality
Yizhuang Liu (Stony Brook U.), Maciej A. Nowak (Jagiellonian U. (main)), Ismail Zahed (SUNY, Stony Brook). Feb 2, 2016. 29 pp. Nucl.Phys.B909 (2016) 14-42

9.1 Introduction

The organization of this section is as follows: In subsection II, we review the matrix model description of the partition function for N_f flavors at finite μ and its phase quenched approximation. In subsection III we show that a pertinent characteristic determinant is the phased quenched matrix-model partition function for $N_f = 4$. We follow the recent work analysis in [116] and identify a mathematical time with a continuous deformation of the harmonic trap. We explicit the evolution equation for the characteristic determinant and show that it is parabolic asymptotically. In subsection IV we use the WKB method to solve the evolution equation for the boundary of the eigenvalue droplet in leading order. In subsection V we derive an exact solution for the evolution of the characteristic determinant using the method of characteristics. In subsection VI we develop a semi-classical expansion of the exact solution to explicit the universal character of the edges of the droplet of complex Dirac eigenvalues. At the chiral point, the characteristic determinant in the microscopic limit follows from a universal Bessel kernel. Our conclusions are in subsection VII. In Appendix I we detail an alternative scaling law for the characteristic determinant on the real edge of the complex spectrum. In Appendix II, we briefly quote the results for the characteristic determinant following from a 2-matrix model and confirm its microscopic universality at the chiral point.

9.2 Chiral Matrix Model

The low lying eigenmodes of the QCD Dirac operator capture some aspects of the spontaneous breaking of chiral symmetry both in vacuum and in matter.

Remarkably, their fluctuations follow by approximating the entries in the Dirac operator by purely random matrix elements which are chiral (paired spectrum) and fixed by time-reversal symmetry (Dyson ensembles). At finite μ the Dirac spectrum on the lattice is complex [122, 123]. The matrix models at finite μ [110, 112] capture this aspect of the lattice spectra and the nature of the chiral phase transition [103, 114, 115].

In this section, we will briefly review the salient features of the standard or 1-matrix model and explicit the relationship between the chiral Dirac ensemble and a deformed Wishart ensemble both at finite μ. For that, consider the 1-matrix model at finite chemical potential for N_f fundamental quarks in the complex representation or $\beta = 2$ [110, 111]

$$\begin{aligned} \mathbf{Z}_{N_f}[\tau, \mathbf{z} = -im_f, \mu] &= \left\langle \det\left(\mathbf{z} - \mathbf{D}\right)^{N_f} \right\rangle \\ &\equiv \int d\mathbf{T}\, d\mathbf{T}^\dagger\, \mathbf{P}(\tau, \mathbf{T})\, \det \begin{pmatrix} \mathbf{z} & \mathbf{T} - i\mu \\ \mathbf{T}^\dagger - i\mu & \mathbf{z} \end{pmatrix}^{N_f} \end{aligned} \tag{387}$$

for equal quark masses m_f in the complex representation. Here

$$\mathbf{P}(\tau, \mathbf{T}) = e^{-\frac{N}{\tau}\mathrm{Tr}(\mathbf{T}^\dagger \mathbf{T})} \tag{388}$$

and $\mathbf{T}$ is $(N + \nu) \times N$ valued complex matrix. ν accounts for the difference between the number of zero modes and anti-zero modes. The chiral Dirac matrix $\mathbf{D}$ in (387) has ν unpaired zero modes and N paired eigenvalues $\pm iz_j$ in the massless limit. The paired eigenvalues delocalize and are represented by (387). The unpaired zero-modes decouple. Throughout we will set $\nu = 0$ and $\mathbf{T}$ is a square complex matrix. In the vacuum, the Banks-Casher formula [105] fixes the dimensionful parameter to a constant $\tau \to 1/a$ with $\sqrt{a} = |q^\dagger q|_0/\mathbf{n}$ in terms of the massless quark condensate and the density of zero modes $\mathbf{n} = N/V_4$.

In Fig. 32 we display the distribution of eigenvalues following from the 1-matrix model with $\mathbf{T}$ sampled from a Gaussian ensemble of 200×200 matrices with $\nu = 0$ and $\mu = 0.9$. The eigenvalue distribution forms a connected droplet in the z-plane for $\mu < \mu_c = \sqrt{\tau}$, and splits into two droplets symmetric about the real-axis for $\mu > \mu_c = \sqrt{\tau}$, restoring chiral symmetry [110, 111]. In the spontaneously broken phase, all droplets are connected and symmetric about the real-axis. Some of these feature are shared by the lattice droplets of Dirac eigenvalues [122, 123].

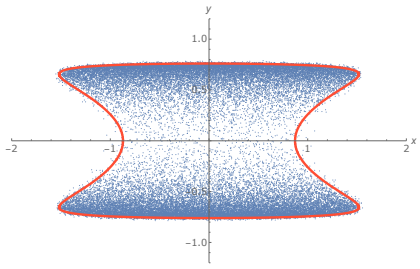

Figure 32: Eigenvalue distribution for the chiral Dirac matrices $\mathbf{D}$ for $\mu/\mu_c = 0.9$ and $\tau = 1$.

The complex nature of the eigenvalues entering in the determinant in (387) yields to the so-called sign problem when evaluating the complex partition function. In lattice numerical analyses, the phase quenched partition function whereby the phase of the determinant is dropped is usually used. In the 1-matrix model this amounts to using

$$\mathbb{Z}_{N_f}[\tau, \mathbf{z} = -im_f, \mu] = \left\langle \det |\mathbf{z} - \mathbf{D}|^{N_f} \right\rangle \tag{389}$$

where the averaging is carried using (388). In leading order in large N, the distribution of eigenvalues and its boundaries are the same for both the unquenched and quenched partition functions since the phase factor is subleading in $1/N$. If we set $z = \mathbf{z}^2 + \mu^2$, (389) can be re-written as

$$\mathbb{Z}_{N_f}[\tau, z, \mu] = \left\langle |\det (z - \mathbf{W})|^{\frac{N_f}{2}} \right\rangle \tag{390}$$

with the deformed Wishart matrix

$$\mathbf{W} = \mathbf{T}^\dagger \mathbf{T} - i\mu(\mathbf{T}^\dagger + \mathbf{T}) \tag{391}$$

The eigenvalue distribution for the deformed Wishart matrices (391) is shown in Fig. 33 for 20×20 matrices sampled from a similar Gaussian ensemble with $\mu/\mu_c = 0.9$. The droplet spreads and stretches vertically for increasing μ but does not break. The density of eigenvalues within the droplets in Figs. 32, 33

breaks spontaneously conformal symmetry [110, 111]. This breaking is best captured through the following regulated partition function

$$Z_{N_f}[\tau, z, w, \mu] \equiv \left\langle \left(\det \left(|z - \mathbf{W}|^2 + \overline{w} w \right) \right)^{\frac{N_f}{4}} \right\rangle \tag{392}$$

which gives the partition function in the double limit

$$\mathbb{Z}_{N_f}[\tau, z, \mu] = \lim_{w \to 0} \lim_{N \to \infty} Z_{N_f}[\tau, z, w, \mu] \tag{393}$$

The measure in (387-392) acts as a harmonic trap for the complex eigenvalues that are deformed and split by the chemical potential. Following [116] we will identify τ with a mathematical and continuous time deformation of the harmonic trap. (388) satisfies the formal matrix diffusion equation

$$N \partial_\tau \mathbf{P} = \frac{\partial^2 \mathbf{P}}{\partial \mathbf{T}^\dagger \partial \mathbf{T}} \qquad \text{with} \qquad \mathbf{P}(0, \mathbf{T}) \approx \delta(\mathbf{T}) \tag{394}$$

(394) shows that the diffusive equation is purely kinetic with no potential or pressure like contribution. This is to be contrasted with the many-body hydrodynamics expansion of the Dirac eigenvalues where both kinetic and pressure terms are identified in the Eulerian flow in [117].

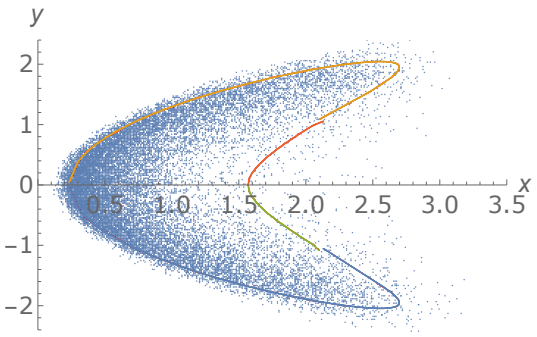

Figure 33: Eigenvalue distribution for the deformed Wishart $\mathbf{W}$ matrices for $\mu/\mu_c = 0.9$ and $\tau = 1$.

9.3 Diffusion

In this subsection we will define a pertinent characteristic determinant that will be used to analyze the nature and evolution of the complex eigenvalues of the deformed Wishart ensemble. We will show that the evolution of the characteristic determinant obeys a non-local equation that is diffusion-like asymptotically.

Indeed, a simple understanding of the accumulation and diffusion of the eigenvalues of the Dirac operator in the complex plane follows by identifying the phase quenched and regulated partition function (392) for $N_f = 4$ with the characteristic determinant

$$\mathbf{\Psi}(\tau, z, w) \equiv Z_{N_f=4}[\tau, z, w, \mu] \tag{395}$$

(395) defines a $2N$-degree polynomial which asymptotes $|z|^{2N}$ [114]. The zeros of the characteristic determinant are the complex eigenvalues of the deformed Wishart matrix $\mathbf{W}$ in (391). They are related to the eigenvalues of the Dirac operator $\mathbf{D}$ in the complex 2-plane by recalling the mapping $z = \mathbf{z}^2 + \mu^2$. The macroscopic density of complex and deformed Wishart eigenvalues is

$$\rho_W(\tau, z) = \lim_{w\to 0} \lim_{N\to\infty} \frac{1}{N\pi} \partial^2_{z\bar{z}} \ln \mathbf{\Psi}(\tau, z, w) \tag{396}$$

with $\ln\mathbf{\Psi}/N$ acting as a Coulomb-like potential at large N. The corresponding eigenvalue density for the chiral Dirac operator as a function of τ, follows from (396) through

$$\rho_D(\tau, \mathbf{z}) = 2|\mathbf{z}|\, \rho_W(\tau, \mathbf{z}^2 + \mu^2) \tag{397}$$

The eigenvalues condense in a droplet, with $\mathbf{\Psi} \approx 0$ inside and $\mathbf{\Psi}/|z|^{2N} \approx 1$ (order parameter), as the corresponding pressure $\ln\mathbf{\Psi}$ changes sign across the droplet boundary (phase change) [111, 114].

Unwinding the determinant in $\mathbf{\Psi}$ through a Grassmannian quark q and conjugate quark Q, yields

$$
\begin{aligned}
&\mathbf{\Psi}(\tau,z,w) \equiv \left\langle e^{\mathbf{F}+\mathbf{G}} \right\rangle \\
&\equiv \int d\mathbf{T} d\mathbf{T}^\dagger dq\, dq^\dagger\, dQ\, dQ^\dagger\ \mathbf{P}(\tau,\mathbf{T}) \\
&\times\ e^{q^\dagger(z-\mathbf{W})q+Q^\dagger(\bar{z}-\mathbf{W}^\dagger)Q-\bar{w}q^\dagger Q+wQ^\dagger q}
\end{aligned}
\tag{398}
$$

where we have defined

$$
\begin{aligned}
&\mathbf{F} = q^\dagger(z-\mathbf{W})q + Q^\dagger(\bar{z}-\mathbf{W}^\dagger)Q \\
&\mathbf{G} = -\bar{w}q^\dagger Q + wQ^\dagger q
\end{aligned}
\tag{399}
$$

Note that the complex eigenvalues $z, \bar{z}$ act as complex masses for the pair of quark bilinears $q^\dagger q$, $Q^\dagger Q$, while $w, \bar{w}$ act as complex mixing masses for the pair of mixed quark bilinears $Q^\dagger q$ and $q^\dagger Q$. The formers preserve holomorphy, while the latters do not [114]. (398) obeys the evolution equation

$$
\begin{aligned}
&N\partial_\tau \mathbf{\Psi}(\tau,z,w,\mu) = \\
&\big\langle \big(-N(q^\dagger q + Q^\dagger Q) \\
&-q^\dagger q q^\dagger \mathbf{W} q - Q^\dagger Q Q^\dagger \mathbf{W}^\dagger Q - q^\dagger Q Q^\dagger \mathbf{W} q - Q^\dagger q q^\dagger \mathbf{W}^\dagger Q \\
&+2i\mu\, Q^\dagger q q^\dagger \mathbf{T} Q - 2i\mu\, q^\dagger Q Q^\dagger \mathbf{T} q \\
&-2\mu^2\, q^\dagger Q Q^\dagger q + \mu^2\,(q^\dagger q + Q^\dagger Q)\big)\ e^{\mathbf{F}+\mathbf{G}} \big\rangle
\end{aligned}
\tag{400}
$$

where we have used (394) . With the help of the identity

$$
\begin{aligned}
&\left\langle \left(+2i\mu\, Q^\dagger q q^\dagger \mathbf{T} Q - 2i\mu\, q^\dagger Q Q^\dagger \mathbf{T} q \right)\ e^{\mathbf{F}+\mathbf{G}} \right\rangle \\
&= -4\mu^2\tau^2 \frac{\partial_w \partial_{\bar{w}} (\partial_w \partial_{\bar{w}} + \partial_z \partial_{\bar{z}})}{(1-\tau\partial_z)(1-\tau\partial_{\bar{z}}) + \tau^2 \partial_w \partial_{\bar{w}}} \left\langle e^{\mathbf{F}+\mathbf{G}} \right\rangle
\end{aligned}
\tag{401}
$$

most of the terms on the right-hand-side of (400) can be turned either to ordinary z-derivatives of $e^{\mathbf{F}}$ or some Grassmannian derivative of $e^{\mathbf{F}}$ or $e^{\mathbf{G}}$. The final result is a closed but non-local evolution of the characteristic determinant (398), i.e.

$$
\begin{aligned}
N\partial_\tau \mathbf{\Psi} = \quad & \Bigg(-2(\partial_z + \partial_{\bar{z}}) \\
& -(z\partial_z^2 + \bar{z}\partial_{\bar{z}}^2 - (z+\bar{z})\partial_{\bar{w}w}^2) \\
& -(\partial_z + \partial_{\bar{z}})(w\partial_w + \bar{w}\partial_{\bar{w}}) \\
& +2\mu^2\partial_{\bar{w}w}^2 + \mu^2(\partial_z^2 + \partial_{\bar{z}}^2) \\
& - \left(\frac{2\mu\tau}{N}\right)^2 \frac{\partial_w\partial_{\bar{w}}(\partial_w\partial_{\bar{w}} + \partial_z\partial_{\bar{z}})}{\left|1 - \frac{\tau}{N}\partial_z\right|^2 + \left|\frac{\tau}{N}\partial_w\right|^2} \Bigg) \mathbf{\Psi}
\end{aligned}
\tag{402}
$$

which is diffusive-like or parabolic at asymptotic times, subject to the initial condition

$$
\mathbf{\Psi}(\tau = 0, z, w) = (|z_0|^2 + |w_0|^2)^N \tag{403}
$$

(402-403) is the first main result of this section.

The stochastic evolution of $\mathbf{\Psi}$ involves the evolution in both the normal $z, \bar{z}$ and mixed $w, \bar{w}$ masses to allow for the spontaneous breaking of chiral symmetry as well as the spontaneous breaking of holomorphy, respectively. The spontaneous breaking of chiral symmetry is signaled by the accumulation of Dirac eigenvalues around zero or $\mathbf{z} = 0$ ($z = \mu^2$), i.e. a non-vanishing $\langle q^\dagger q \rangle$. The spontaneous breaking of holomorphy is signaled by the spreading of Dirac eigenvalues in the complex plane, i.e. a non-vanishing $\langle |q^\dagger Q|^2 \rangle$ [110, 111, 114].

9.4 WKB approximation

In this section we will provide a WKB analysis of the non-local and diffusion-like equation for the characteristic determinant derived in the previous section. We will use it to derive a polynomial and parametric equation for the time-dependent envelope of the complex eigenvalues for the deformed Wishart ensemble, and by mapping for the standard but diffusing Dirac ensemble at finite μ.

(402) is a non-local Schroedinger-like evolution equation in Euclidean time. Some insights to this evolution can be obtained using the WKB method in the large $N(= 1/\hbar)$ limit. For that we identify

$$\mathbf{\Psi} \approx e^{N\mathbb{S}} \tag{404}$$

in (402) and define the conjugate momenta $p_\xi = \partial_\xi \mathbb{S}$ with $\xi = z, \bar{z}, r = \sqrt{w\bar{w}}$. Note that in leading N, the eigenvalue density for the deformed Wishart class in (391) is given by

$$\rho_W(\tau, z) = \lim_{w\to 0} \frac{1}{\pi} \partial_{\bar{z}} p_z \tag{405}$$

which is non-holomorphic inside the droplet.

9.4.1 Hamilton-Jacobi Equations

Using the rescaling $N\tau \to \tau$, the effective semi-classical action $\mathbb{S}$ obeys

$$\partial_\tau \mathbb{S} + \mathbb{H}(\tau, \xi, p_\xi) = 0 \tag{406}$$

with the τ-dependent and non-local effective Hamiltonian

$$\begin{aligned} \mathbb{H} = \quad & +z p_z^2 + \bar{z} p_{\bar{z}}^2 - (z+\bar{z}) p_r^2/4 \\ & + r(p_z + p_{\bar{z}}) p_r - \mu^2 (p_z^2 + p_{\bar{z}}^2) - \frac{\mu^2 p_r^2}{2} \\ & + \mu^2 \tau^2 \frac{p_r^2 (\frac{p_r^2}{4} + p_z p_{\bar{z}})}{(1-\tau p_z)(1-\tau p_{\bar{z}}) + \tau^2 \frac{p_r^2}{4}} \end{aligned} \tag{407}$$

The initial condition is $\mathbb{S}(0) = \ln(|z_0|^2 + r_0^2)$.

The semi-classical equations are the standard Hamilton-Jacobi equations,

$$\begin{aligned} \frac{dp_z}{d\tau} &= -\frac{\partial \mathbb{H}}{\partial z} = -p_z^2 + p_r^2/4 \\ \frac{dp_{\bar{z}}}{d\tau} &= -\frac{\partial \mathbb{H}}{\partial \bar{z}} = -p_{\bar{z}}^2 + p_r^2/4 \\ \frac{dp_r}{d\tau} &= -\frac{\partial \mathbb{H}}{\partial r} = -p_r(p_z + p_{\bar{z}}) \end{aligned} \tag{408}$$

which are readily integrated

$$
\begin{aligned}
p_x(\tau) &= \frac{x_0+\tau}{(x_0+\tau)^2+y_0^2+r_0^2} \\
p_y(\tau) &= \frac{-y_0}{(x_0+\tau)^2+y_0^2+r_0^2} \\
p_r(\tau) &= \frac{2r_0}{(x_0+\tau)^2+y_0^2+r_0^2}
\end{aligned}
\tag{409}
$$

and

$$
\begin{aligned}
\frac{dz}{d\tau} &= \frac{\partial \mathbb{H}}{\partial p_z} \\
\frac{dr}{d\tau} &= \frac{\partial \mathbb{H}}{\partial p_r}
\end{aligned}
\tag{410}
$$

which are in general involved.

9.4.2 Expanding droplet boundary

The initialization of the characteristic determinant through (404) at the droplet edge or $r_0 = 0$, allows for a simplification of (410) at the edge. Indeed, (410) for $z(\tau)$ at the edge, yields

$$
\frac{z(\tau)-\mu^2}{z_0-\mu^2} = \left(1+\frac{\tau}{z_0}\right)^2 \tag{411}
$$

while (410) for small $r(\tau)$ gives

$$
\begin{aligned}
\frac{dr}{d\tau} &= f_1(\tau) r + r_0 f_2(\tau) \\
f_1(\tau) &= \frac{1}{z_0+\tau} + \frac{1}{\bar{z}_0+\tau} \\
f_2(\tau) &= -\frac{4\mu^2\left(1-\frac{\tau^2}{|z_0|^2}\right) + \left((z_0-\mu^2)(1+\frac{\tau}{z_0}) + \text{c.c.}\right)}{(x_0+\tau)^2+y_0^2}
\end{aligned}
\tag{412}
$$

The formal solution of (412) is

$$r(\tau) = r_0 \left(1 + \int_0^\tau d\tau' f_2(\tau') e^{-\int_0^{\tau'} d\tau'' f_1(\tau'')}\right) e^{\int_0^\tau d\tau' f_1(\tau')} \tag{413}$$

The boundary of the eigenvalue droplet is set by the condition

$$1 + \int_0^\tau f_2(\tau') e^{-\int_0^{\tau'} f_1(\tau'') d\tau''} d\tau' = 0 \tag{414}$$

Inserting

$$e^{-\int_0^{\tau'} f_1(\tau'') d\tau''} = \frac{|z_0|^2}{(x_0+\tau')^2 + y_0^2} \tag{415}$$

in (414) and using

$$\begin{aligned} \int_0^\tau d\tau' \frac{x_0^2 + y_0^2 - \tau'^2}{|(x_0+\tau')^2 + y_0^2|^2} &= \frac{\tau}{(x_0+\tau)^2 + y_0^2} \\ \int_0^\tau d\tau' \frac{(x_0 + iy_0 + \tau')^2}{|(x_0+\tau')^2 + y_0^2|^2} &= \frac{\tau}{\bar{z}_0(\bar{z}_0+\tau)} \end{aligned} \tag{416}$$

yield the polynomial condition for $z_0 = x_0 + iy_0$

$$\frac{4\mu^2\tau}{(x_0+\tau)^2 + y_0^2} + \frac{z_0 - \mu^2}{z_0} \frac{\tau}{\bar{z}_0 + \tau} + \frac{\bar{z}_0 - \mu^2}{\bar{z}_0} \frac{\tau}{z_0 + \tau} = 1 \tag{417}$$

A simple check of the result (417) follows for $\mu = 0$, for which we have

$$z_0 + \bar{z}_0 + 2\tau = \frac{1}{\tau}(z_0 + \tau)(\bar{z}_0 + \tau) \tag{418}$$

The general solution is $z_0 = \tau e^{i\theta}$. Inserting this solution in (411), we have

$$z(\tau) = \tau(2 + e^{-i\theta} + e^{i\theta}) = 4\cos^2(\theta/2) \tag{419}$$

which is the support of the τ-expanding Wishart line segment on the real-axis, i.e. $[0, 4\tau]$. For general μ, (417) yields the expanding 4 branches ($\mathbf{s}, \mathbf{s}' = \pm$)

$$y_0^{\mathbf{ss}'}(x_0) = \tag{420}$$
$$\mathbf{s}\tau\left(-\frac{x_0^2}{\tau^2} + \left(\frac{1}{2} + \frac{\mu^2}{\tau}\right)\left(1 + \mathbf{s}'\left(1 - \frac{8\mu^2 x_0}{(\tau + 2\mu^2)^2}\right)^{\frac{1}{2}}\right)\right)^{\frac{1}{2}}$$

which once inserted in (417) give a parametric description of the evolving τ-expanding boundary, as the envelope of the eigenvalues of the deformed Wishart eigenvalues as shown in Fig. 33. The envelope for the distributions of Dirac eigenvalues in Fig. 32 follows from the deformed Wishart envelope by using the inverse mapping $\mathbf{z} = \pm\sqrt{z - \mu^2}$. It is in agreement with the original envelope obtained in [110, 111] using different arguments.

9.4.3 Characteristic determinant

In this section, we will provide a formal solution for the stochastically evolving characteristic determinant for the deformed Wishart ensemble, that is exact for finite size N and time τ. For that, we will use the method of characteristics to solve exactly the partial differential equation (402) in Fourier space.

A formal but exact solution to the diffusion-like equation (400) for the characteristic determinant can be obtained by recasting (402) in conjugate or Fourier space. Specifically,

$$\mathbf{\Psi}(\tau, z, w) = \int \frac{d^2k}{(2\pi)^2}\frac{d^2p}{(2\pi)^2} e^{ik\cdot w + ip\cdot z}\ \tilde{\mathbf{\Psi}}(\tau, k, p) \tag{421}$$

Taking the Fourier transform of (402) yields

$$N\partial_\tau \tilde{\mathbf{\Psi}} = \tilde{\mathbb{H}}\,\tilde{\mathbf{\Psi}} \tag{422}$$

with the conjugate Hamiltonian

$$\tilde{\mathbb{H}} = 2p_1 + \frac{\mu^2}{2}(k^2 + p_1^2 - p_2^2)$$
$$-\frac{\mu^2\tau^2}{4N^2}\frac{k^2(p^2+k^2)}{(1-\frac{\tau p_1}{2N})^2 + \frac{\mu^2\tau^2}{N^2}\frac{p_2^2+k^2}{4}}$$
$$+\frac{p_1^2 - p_2^2 - k^2}{2}\partial_{p_1} + p_1 p_2 \partial_{p_2} + p_1 k \partial_k \tag{423}$$

after the shifts $k \to -ik$ and $p \to -ip$. Here k is the conjugate to $\sqrt{w\bar{w}} \equiv r$.

9.4.4 Characteristic lines

The evolution equation (422) is now first order with rational coefficients. It can be solved by the characteristic method exactly. The characteristic lines are

$$\begin{aligned}
\frac{d\tau}{ds} &= N \\
\frac{dp_1}{ds} &= -\frac{p_1^2 - p_2^2 + k^2}{2} \\
\frac{dp_2}{ds} &= -p_1 p_2 \\
\frac{dk}{ds} &= -p_1 k
\end{aligned} \tag{424}$$

They are readily solved

$$\begin{aligned}
p_1(s) &= \frac{p_{10} + \frac{s}{2}(k_0^2 + p_{10}^2 + p_{20}^2)}{(1+\frac{s}{2}p_{10})^2 + \frac{s^2}{4}(k_0^2 + p_{20}^2)} \\
p_2(s) &= \frac{p_{20}}{(1+\frac{s}{2}p_{10})^2 + \frac{s^2}{4}(k_0^2 + p_{20}^2)} \\
k(s) &= \frac{k_0}{(1+\frac{s}{2}p_{10})^2 + \frac{s^2}{4}(k_0^2 + p_{20}^2)}
\end{aligned} \tag{425}$$

and inverted

$$
\begin{aligned}
p_{10} &= \frac{p_1 - \frac{s}{2}(p_1^2 + p_2^2 + k^2)}{(1 - \frac{s}{2}p_1)^2 + \frac{s^2}{4}(p_2^2 + k^2)} \\
p_{20} &= \frac{p_2}{(1 - \frac{s}{2}p_1)^2 + \frac{s^2}{4}(p_2^2 + k^2)} \\
k_0 &= \frac{k}{(1 - \frac{s}{2}p_1)^2 + \frac{s^2}{4}(p_2^2 + k^2)}
\end{aligned} \tag{426}
$$

We note the identity ($p_0^2 = p_{10}^2 + p_{20}^2$)

$$
\frac{p^2 + k^2}{(1 - \frac{sp_1}{2})^2 + s^2\frac{p_2^2 + k^2}{4}} = p_0^2 + k_0^2 \tag{427}
$$

9.4.5 Exact determinant

We are now set to evaluate the exact τ-evolution of $\mathbf{\Psi}$. Inserting (424-427) into (423) yield

$$
\frac{d\ln\tilde{\mathbf{\Psi}}}{ds} = 2p_1 - \mu^2\left(-\frac{k^2 + p_1^2 - p_2^2}{2} + (p_0^2 + k_0^2)\frac{s^2k^2}{4}\right) \tag{428}
$$

Using (425) into (428) and undoing the derivative, we have

$$
\begin{aligned}
\tilde{\mathbf{\Psi}}(\tau, k, p) = \quad & e^{-\mu^2\frac{s\left(-sp_{10}\left(p_0^2 + k_0^2\right) - 2\left(p_{10}^2 - p_{20}^2 - k_0^2\right)\right)}{s^2\left(k_0^2 + p_0^2\right) + 4p_{10}s + 4}} \\
& \times \frac{\tilde{\mathbf{\Psi}}_0(k_0, p_0)}{\left((1 + \frac{sp_{10}}{2})^2 + s^2\frac{p_{20}^2 + k_0^2}{4}\right)^{-2}}
\end{aligned} \tag{429}
$$

We now re-write (k_0, p_0) in terms of (k, p) and then undo the shifts through $(k \to ik, p \to ip)$. The results are

$$
\begin{aligned}
\tilde{\mathbf{\Psi}}(\tau, k, p) &= \mathbb{K}(\tau, k, p)\tilde{\mathbf{\Psi}}_0(k_0(k, p), p_0(k, p)) \\
\mathbb{K}(\tau, k, p) &= \frac{((2 - p_1 s)^2 + s^2(p_2^2 + k^2))^{-2}}{16} e^{-\mu^2\mathbf{S}(k,p,\tau)} \\
\mathbf{S}(\tau, k, p) &= \frac{s\left(sp_1\left(p^2 + k^2\right) - 2\left(p_1^2 - p_2^2 - k^2\right)\right)}{s^2\left(k^2 + p^2\right) - 4p_1 s + 4}
\end{aligned} \tag{430}
$$

In terms of the initial variables, the formal solution for $\mathbb{K}$ is

$$\mathbb{K}(\tau, k_0, p_0) = \frac{e^{-\mu^2 \frac{s\left(-sp_{10}\left(p_0^2+k_0^2\right)-2\left(p_{10}^2-p_{20}^2-k_0^2\right)\right)}{s^2\left(k_0^2+p_0^2\right)+4p_{10}s+4}}}{\left((1+\frac{sp_{10}}{2})^2+s^2\frac{p_{20}^2+k_0^2}{4}\right)^{-2}} \tag{431}$$

The initial condition in Fourier space is

$$\tilde{\mathbf{\Psi}}_0(k,p) = (\nabla_p^2+\nabla_k^2)^N \delta^2(k)\delta^2(p) \tag{432}$$

Thus

$$\begin{aligned}&\mathbf{\Psi}(\tau,z,w) = \\ &\left((\nabla_{p_0}^2+\nabla_{k_0}^2)^N e^{p(p_0,k_0)\cdot z + k(k_0,p_0)\cdot w}\mathbb{J}\mathbb{K}(\tau,k_0,p_0)\right)_{p_0=k_0=0}\end{aligned} \tag{433}$$

Here, $\mathbb{J} \equiv \mathbb{J}(k,p;k_0,p_0)$ is the Jacobian for the variable transformation $(k_0,p_0) \to (k,p)$ evaluated at (k_0,p_0), i.e.

$$\mathbb{J} \equiv \left(\left(1+\frac{\tau p_{10}}{2}\right)^2+\frac{\tau^2}{4}(p_{20}^2+k_0^2)\right)^{-3} \equiv \frac{1}{F_0^3} \tag{434}$$

Although (433) is exact for finite N, taking the large N limit and assessing its corrections is in general more subtle.

9.5 Universality at the Edge

The depletion of the zeros away from the droplet is captured by the way $\mathbf{\Psi}$ departs from zero away from the sharp boundary. The microscopic and universal changes in the eigenvalue density at the edges are commensurate with the microscopic rate of depletion of the zeros of the characteristic determinant. We now develop a semi-classical expansion in $1/N$ and a pertinent microscopic re-scaling at the edge to show this.

9.5.1 Saddle point approximation

To explicit this universal behavior, it is more appropriate to insert (430) in (421) and carry a semi-classical expansion around the saddle point in terms of the initial coordinates (k_0, p_0). For notational convenience in this section we will re-label the coordinates (k_0, p_0) by (k, p), and the previous coordinates (k, p) by (K, P). This means that $P \equiv P(p, k)$ and $K \equiv K(p, k)$. With this in mind, we have

$$\begin{aligned} &\mathbf{\Psi}(\tau, z, w) = \\ &\int \frac{d^2k}{(2\pi)^2}\frac{d^2p}{(2\pi)^2} d^2z' d^2w' \frac{e^{Nf(\tau,p,k,z,w,z',w')}}{\left((1+\frac{\tau p_1}{2})^2 + \tau^2\frac{p_2^2+k^2}{4}\right)} \end{aligned} \tag{435}$$

with

$$\begin{aligned} &f(\tau, p, k, z, w, z', w') = P(p,k)\cdot z + K(p,k)\cdot w \\ &-p\cdot z' - k\cdot w' - \mu^2 \mathbf{S}(p,k) + \ln(|z'|^2 + |w'|^2) \end{aligned} \tag{436}$$

$$\mathbf{S}(p,k) = \frac{p_1 + \frac{\tau}{2}(p_1^2 + p_2^2 - k^2)}{(1+\frac{\tau p_1}{2})^2 + \tau^2\frac{p_2^2+k^2}{4}} - p_1 \tag{437}$$

The saddle point corresponds to $\partial_{z',w',p,k} f = 0$, which are respectively

$$\begin{aligned} &\frac{\partial P}{\partial p} z + \frac{\partial K}{\partial p} w + \mu^2 \frac{\partial S}{\partial p} = z' \\ &\frac{\partial P}{\partial k} z + \frac{\partial K}{\partial k} w + \mu^2 \frac{\partial S}{\partial k} = w' \\ &p_i = \frac{2z_i'}{|z'|^2 + |w'|^2} \\ &k = \frac{2r'}{|z'|^2 + |r'|^2} \end{aligned} \tag{438}$$

Near the boundary the first saddle point equation in (438) reduces to

$$(z - \mu^2)\frac{z_0^2}{(\tau + z_0)^2} + \mu^2 = z_0 \tag{439}$$

in agreement with (411). The second saddle point equation in (438) becomes

$$\lim_{r'\to 0}\left(\frac{r'}{k}\right)\frac{2(z_0+\tau)(\bar{z}_0+\tau)}{|z_0|^2} = \\ \tau\left(4\mu^2+\frac{z_0-\mu^2}{z_0}(z_0+\tau)+\frac{\bar{z}_0-\mu^2}{z_0}(\bar{z}_0+\tau)\right) \tag{440}$$

which reduces to (417) after using the last two saddle point equations in (438). In principle, the inversion of the above saddle point equations will determine (z,w) as a function of (z',w'). In practice, this inversion is involved. Fortunately, at the boundary there are simplifications since $(w=0,w'=0)$, and since (417) and (438) relate the saddle point initial positions to the current positions.

9.5.2 Microscopic correction

The correction to the saddle point in momenta will be sought in holomorphic coordinates, i.e

$$p_1 - ip_2 = p \\ x_1p_2 + x_2p_2 = \frac{1}{2}(pz+\bar{p}\bar{z}) \tag{441}$$

and by expanding around the boundary using the following microscopic rescalings

$$z = z(z_0)+\frac{\delta z}{\sqrt{N}} \\ z' = z_0+\frac{\delta z'}{\sqrt{N}} \\ w' = \frac{\delta r'}{N^{\frac{1}{4}}} \\ p = p_0(z_0)+\frac{\eta}{\sqrt{N}} \\ k = \frac{\omega}{N^{\frac{1}{4}}} \tag{442}$$

The re-scaling in $\delta z', \delta z/\sqrt{N}$ at the boundary is natural, since the droplet area scales as $\mathcal{A} \approx N$ to keep the density of eigenvalues finite, while its length grows as $\sqrt{\mathcal{A}} \approx \sqrt{N}$. Inserting (441-442) in (421) and expanding to order N^0 at large N, we obtain

$$\begin{aligned}
&N(f-f_0) - \ln\left(\left(1+\frac{\tau p_1}{2}\right)^2 + \tau^2\frac{p_2^2+k^2}{4}\right) \approx \\
&\mathbf{Q}(\eta,\omega,\delta z,\delta z',\delta r') + \sqrt{N}\left(\frac{\delta z}{z_0+\tau} + \frac{\delta\bar{z}}{\bar{z}_0+\tau}\right) \\
&+\sqrt{N}\left(\frac{(\delta r')^2}{|z_0|^2} + \frac{\omega^2|z_0|^2}{4} - \omega\cdot\delta r'\right) \\
&-\frac{1}{2}\left(\frac{(\delta z')^2}{z_0^2} + \frac{(\bar{\delta} z')^2}{\bar{z}_0^2}\right) - (\delta r')^2\left(\frac{\delta z'}{z_0} + \frac{\delta\bar{z}'}{\bar{z}_0}\right) - \frac{(\delta r')^4}{2|z_0|^4}
\end{aligned} \tag{443}$$

with f_0 the value of f in (435) at the saddle point and

$$\begin{aligned}
&\mathbf{Q}(\eta,\omega,\delta z,\delta z',\delta r') = \\
&-\frac{\tau z_0^3(z-\mu^2)}{4(z_0+\tau)^3}\eta^2 - \frac{\tau\bar{z}_0^3(\bar{z}-\mu^2)}{4(\bar{z}_0+\tau)^3}\bar{\eta}^2 \\
&+\left(\frac{z_0^2}{2(z_0+\tau)^2}\delta z - \frac{\delta z'}{2}\right)\eta + \left(\frac{\bar{z}_0^2}{2(\bar{z}_0+\tau)^2}\delta\bar{z} - \frac{\delta\bar{z}'}{2}\right)\bar{\eta} \\
&+\frac{\tau|z_0|^2\omega^2}{4|(z_0+\tau)|^2}\left(\frac{z_0\delta z}{z_0+\tau} + \frac{\bar{z}_0\delta\bar{z}}{\bar{z}_0+\tau}\right) - \frac{\tau^2\omega^4|z_0|^4}{16|(z_0+\tau)|^2} \\
&-\frac{\tau\omega^2|z_0|^2(\eta(\bar{z}_0+\tau)(z_0) + \bar{\eta}(z_0+\tau)\bar{z}_0}{8|(z_0+\tau)|^2} \\
&-\frac{\tau^2\omega^2|z_0|^2}{8|z_0+\tau|^2}(\eta(z_0-\mu^2) + \bar{\eta}(\bar{z}_0-\mu^2))
\end{aligned} \tag{444}$$

Here $z = z(\tau)$ is defined in (411). Under the shift

$$\omega = \frac{2\delta r'}{|z_0|^2} + \alpha \tag{445}$$

the α-integration is subleading and decouples. With this in mind, we can re-structure and simplify $\mathbf{Q}$ in (444) as

$$\mathbf{Q}(\eta,\omega,\delta z,\delta z',\delta r') = \\ Q(\eta)+\bar{Q}(\bar{\eta})+(\bar{\eta},\eta)\cdot(\bar{J},J)+Q_3(\delta r',\delta z)+Q_4(\delta r') \tag{446}$$

with

$$\begin{aligned} Q(\eta) &= -\frac{\tau z_0(z_0-\mu^2)}{4(z_0+\tau)}\eta^2 \\ J &= \frac{1}{2}\frac{z_0^2}{(z_0+\tau)^2}\delta z-\frac{1}{2}\delta z'-\frac{\tau(\delta r')^2((1+\frac{\tau}{\bar{z}_0})+\tau\frac{z_0-\mu^2}{|z_0|^2})}{2|(z_0+\tau)|^2} \\ Q_3 &= \frac{\tau(\delta r')^2}{|z_0|^2|(z_0+\tau)|^2}\left(\frac{z_0\delta z}{z_0+\tau}+\frac{\bar{z}_0\delta\bar{z}}{\bar{z}_0+\tau}\right) \\ Q_4 &= -\frac{\tau^2(\delta r')^4}{|z_0|^4|z_0+\tau|^2} \end{aligned} \tag{447}$$

The partial integration in (435) of the quadratic contribution over (η,ω) gives

$$\begin{aligned} &\mathbf{Q}(\delta z,\delta z',\delta r') = \\ &+\frac{J^2}{\frac{\tau z_0(z_0-\mu^2)}{(z_0+\tau)}}+\frac{\bar{J}^2}{\frac{\tau\bar{z}_0(\bar{z}_0-\mu^2)}{(\bar{z}_0+\tau)}}-\frac{\tau^2(\delta r')^4}{|z_0|^4|z_0+\tau|^2} \\ &+\frac{\tau(\delta r')^2}{|z_0|^2|(z_0+\tau)|^2}\left(\frac{z_0\delta z}{z_0+\tau}+\frac{\bar{z}_0\delta\bar{z}}{\bar{z}_0+\tau}\right) \end{aligned} \tag{448}$$

9.5.3 Microscopic egde profile

The integration around $\delta z'$ is Gaussian and is readily performed, leaving the last and non-Gaussian integral in $\delta r'$ undone. The result for the characteristic determinant close to the boundary and in the microscopic limit is

$$\begin{aligned} &\Psi(\tau,z(z_0)+\delta z/\sqrt{N},0)\approx e^{Nf_0+\sqrt{N}(\frac{\delta z+\delta\bar{z}}{z_0+\tau})} \\ &\times\int_0^\infty x dx\, e^{-A(z_0)x^4+B(z_0,\delta z)x^2+C(z_0,\delta z)} \end{aligned} \tag{449}$$

with

$$
\begin{aligned}
A(z_0) &= \frac{1}{2|z_0|^4} + \frac{\tau^2}{|z_0|^4|z_0+\tau|^2} + \\
&\left(\left(\frac{1}{|z_0|^2 z_0} - \frac{\mathbb{A}}{\mathbb{B}} \right)^2 \left(\frac{1}{\mathbb{B}} - \frac{2}{z_0^2} \right)^{-1} - \frac{\mathbb{A}^2}{\mathbb{B}} + \text{c.c.} \right) \\
B(z_0, \delta z) &= \delta z \left(\frac{\tau z_0}{|z_0|^2|z_0+\tau|^2(z_0+\tau)} \right. \\
&\left. -2\mathbb{C} \left(\frac{1}{z_0|z_0|^2} - \frac{2\mathbb{A}}{z_0^2} \right) \left(1 - \frac{2\mathbb{B}}{z_0^2} \right)^{-1} \right) + \text{c.c} \\
C(z_0, \delta z) &= \frac{z_0^2 \delta z^2}{4\tau(z_0-\mu^2)(z_0+\tau)^2} \\
&\times \left(\frac{z_0}{z_0+\tau} - \frac{1}{\frac{z_0+\tau}{z_0} - \frac{2\tau(z_0-\mu^2)}{z_0^2}} \right) + \text{c.c.}
\end{aligned} \tag{450}
$$

and

$$
\begin{aligned}
\mathbb{A} &= \frac{\tau((1+\frac{\tau}{\bar{z}_0}) + \tau\frac{z_0-\mu^2}{|z_0|^2})}{2|z_0+\tau|^2} \\
\mathbb{B} &= \frac{\tau z_0(z_0-\mu^2)}{(z_0+\tau)} \\
\mathbb{C} &= \frac{z_0^2}{2(z_0+\tau)^2}
\end{aligned} \tag{451}
$$

The depletion of the eigenvalues of the deformed Wishart matrices at the boundary as defined by (411) and (417), follows the product of a Gaussian times an incomplete Error Function (Erfc)

$$\Psi(\tau, z(z_0) + \delta z/\sqrt{N}, 0) \approx e^{Nf_0 + \sqrt{N}(\frac{\delta z + \delta \bar{z}}{z_0 + \tau})}$$
$$\times e^{\frac{B^2(z_0,\delta z)}{4A(z_0,\delta z)} + C(z_0,\delta z)} \int_{\frac{-B(z_0,\delta z)}{2A(z_0)}}^{\infty} dy e^{-A(z_0)y^2}$$
$$\equiv e^{Nf_0 + \sqrt{N}(\frac{\delta z + \delta \bar{z}}{z_0 + \tau})}$$
$$\times e^{\frac{B^2(z_0,\delta z)}{4A(z_0)} + C(z_0,\delta z)} \operatorname{Erfc}\left(\frac{-B(z_0,\delta z)}{2\sqrt{A(z_0)}}\right) \tag{452}$$

Recall that z_0 refers to the boundary value as a solution to (411) and is valid throughout the edge of the deformed Wishart droplet shown in Fig. 33. We note that for $A > 0$

$$\lim_{B \to -\infty} \left(e^{\frac{B^2}{4A}} \operatorname{Erfc}\left(-\frac{B}{2\sqrt{A}}\right)\right) = 0 \tag{453}$$

(452) is the second main result of this section.

9.5.4 Special edge points

The depletion at the edge of the Wishart spectrum (452) translates to a depletion at the edge of the Dirac spectrum. We now make it explicit for the 4 cardinal points where the Dirac droplet crosses the eigenvalue spectrum along the real and imaginary axes, e.g. see Fig. 32. Specifically, the edge of the Dirac droplet on the real axis corresponds to $\mathbf{y}(\tau) = 0$. It maps onto the Wishart boundary point $z_0 = x_0 + i0$ with x_0 in (452) the real solution to

$$x_0^4 - 2\tau\left(\frac{\tau}{2} + \mu^2\right) x_0^2 + 2\mu^2\tau^2\, x_0 = 0 \tag{454}$$

In general, the two real solutions to (454) are $x_0 = \tau$ and $x_1/\tau = \frac{1}{2}(-1 - \sqrt{1 + 8\mu^2/\tau})$. They correspond to the outer and inner edge of the Wishart distribution in Fig. 33.

The real solution $x_0 = 1$ yields $x(\tau) = \mu^2 + 4(\tau - \mu^2)$ using (411), which is the outer edge along the real axis in Fig. 33. It maps onto the two outer edges along the real z axis of the Dirac spectrum in Fig. 32 or $\mathbf{z} = \pm 2\sqrt{\tau - \mu^2}$ using

the Wishart to Dirac map $z = \mu^2 + \mathbf{z}^2$. The corresponding edge parameters in (450) are

$$\begin{aligned} A(x_0) &= \frac{(\mu^2-\tau)^2}{16\mu^2\tau^5} \\ B(x_0) &= \frac{\mu^2-\tau}{16\mu^2\tau^3}(\delta z + \delta\bar{z}) \\ C(x_0) &= -\frac{1}{32\mu^2\tau}(\delta z^2 + \delta\bar{z}^2) \end{aligned} \tag{455}$$

and the scaling law (452) on the Wishart envelope is ($\delta z = \delta x + i\delta y$)

$$\begin{aligned} &\Psi(\tau, z(x_0) + \delta z/\sqrt{N}, 0) \approx \\ &e^{Nf_0}\, e^{\frac{\sqrt{N}\delta x}{\tau}}\, e^{\frac{\delta y^2}{16\mu^2\tau^2}}\, \text{Erfc}\left(\frac{\delta x}{4\mu\sqrt{\tau}}\right) \end{aligned} \tag{456}$$

Finally, the real solution $x_1/\tau = \frac{1}{2}(-1-\sqrt{1+8\mu^2/\tau})$ corresponds to the inner edge of the Wishart distribution in Fig. 33 with $z(\tau) < \mu^2$. It maps onto the two outer edges along the imaginary axis of the Dirac spectrum shown in Fig. 32. The corresponding edge parameters in (450) are too lengthy to report here.

9.5.5 Application to $\mu = \frac{\sqrt{\tau}}{2}$

To be more specific consider the special case of $\mu/\sqrt{\tau} = 1/2$, for which the two real solutions are $z_0 = x_0 = \tau$ and $z_0 = x_0 = -(\sqrt{3}+1)\tau/2$. The first solution corresponds to the outer edge along the real axis of the Wishart spectrum and maps onto the outer edge of the Dirac spectrum also along the real axis. It gives

$$\begin{aligned} A(z_0 = \tau) &= \frac{0.14}{\tau^4} \\ B(z_0 = \tau) &= -\frac{0.19}{\tau^3}(\delta z + \delta\bar{z}) \\ C(z_0 = \tau) &= -\frac{1}{8\tau^2}(\delta z^2 + \delta\bar{z}^2) \end{aligned} \tag{457}$$

The scaling law at the edge of the Wishart spectrum along the real axis is

$$\Psi \approx e^{Nf_0}\, e^{\sqrt{N}\frac{\delta x}{\tau}}\, e^{\frac{\delta y^2}{4\tau^2}}\, \mathrm{Erfc}\left(\frac{0.5\,\delta x}{\tau}\right) \tag{458}$$

The second solution corresponds to the inner edge along the real axis of the Wishart spectrum ($z < \mu^2$) and maps onto the outer edge of the Dirac spectrum along the imaginary axis. It gives

$$\begin{aligned} A(z_0 = -(\sqrt{3}+1)\tau/2) &= \frac{3}{\tau^4} \\ B(z_0 = -(\sqrt{3}+1)\tau/2) &= \frac{11.19}{\tau^3}(\delta z + \delta \bar{z}) \\ C(z_0 = -(\sqrt{3}+1)\tau/2) &= -\frac{6.96}{\tau^2}(\delta z^2 + \delta \bar{z}^2) \end{aligned} \tag{459}$$

with $A > 0$ in this case. Inserting the parameters in (452) we have

$$\Psi \approx e^{Nf_0}\, e^{\sqrt{N}\frac{\delta x}{\tau}}\, e^{27.83\frac{\delta x^2}{\tau^2}+13.92\frac{\delta y^2}{\tau^2}}\, \mathrm{Erfc}\left(-\frac{6.46\,\delta x}{\tau}\right) \tag{460}$$

9.5.6 Translation to Dirac

The general result (452) holds around the envelope or boundary of the deformed Wishart ensemble (391) as illustrated in Fig. 33. Its translation to the envelope of the Dirac ensemble as illustrated in Fig. 32, follows from the mapping between the complex eigenvalues or $z = \mu^2 + \mathbf{z}^2$. An infinitesimal displacement δz on the Wishart boundary or $z = z_0 + \delta z/\sqrt{N}$, translates to the infinitesimal displacement $\delta \mathbf{z}$ on the Dirac boundary

$$\begin{aligned} \mathbf{z} = \quad & \mathbf{z}_0 + \frac{\delta \mathbf{z}}{\sqrt{N}} \\ = \quad & \pm\left(z_0 - \mu^2 + \frac{\delta z}{\sqrt{N}}\right)^{\frac{1}{2}} \\ \approx \quad & \pm\left(\mathbf{z}_0 + \frac{\delta z}{2(z_0-\mu^2)^{\frac{1}{2}}\sqrt{N}}\right) \end{aligned} \tag{461}$$

Therefore, (452) maps onto the Dirac boundary through the substitution

$$\delta z \to \pm 2\sqrt{z_0 - \mu^2}\,\delta \mathbf{z} \tag{462}$$

In this spirit, the translation of the Wishart result (456) to Dirac follows using the substitution (462), with $z_0 = \tau$ in this case. The scaling law at the real edge of the Dirac spectrum is sensitive to the chiral condensate, which follows from the large N saddle point of the full or unquenched partition function (387),

$$\begin{aligned} \langle \bar{q} q \rangle = & \quad \lim_{m_f \to\, 0} \lim_{N \to\, \infty} \left(-\frac{1}{N N_f} \frac{\partial \ln \mathbf{Z}_{N_F}}{\partial i m_f} \right) \\ = & \quad -2\,\tau\, \left(\tau - \mu^2\right)^{\frac{1}{2}} \end{aligned} \tag{463}$$

which is seen to vanish for $\mu = \mu_c = \sqrt{\tau}$ in the massless case (second order transition). This is remarkable, as it allows for a determination of the physical chiral condensate (463) from the microscopic scaling law at the edge of the quenched Dirac spectrum. Indeed, if we set $\Sigma \equiv |\langle \bar{q} q \rangle|$ at finite μ, the Wishart edge scaling law (456) translates to the Dirac edge scaling law

$$\begin{aligned} & \Psi_D(\tau, \mathbf{z}_0 + \delta \mathbf{z}/\sqrt{N}, 0) \approx \\ & e^{N f_0}\, e^{\sqrt{N}\Sigma \frac{\delta \mathbf{x}}{\tau^2}}\, e^{\Sigma^2 \frac{\delta \mathbf{y}^2}{16 \mu^2 \tau^3}}\, \mathrm{Erfc}\left(\frac{\Sigma}{4\mu\tau} \frac{\delta \mathbf{x}}{\sqrt{\tau}} \right) \end{aligned} \tag{464}$$

While the exponent in the second factor in (464) grows initially with $\delta \mathbf{x}$, it is countered by the rapid fall off of the complementary error function along the real axis. (464) is vanishingly small for positively large $\delta \mathbf{x}$.

In [125] it was shown that for a class of normal matrices, the spectral density is related to the characteristic determinant for $w \to 0$, with a proportionality factor related to some pertinent weight factor. This result suggests that in our case which is non-normal, the first two factors in (464) may be part of an underlying weight factor as they follow from a standard $1/N$ saddle point approximation, i.e. order N and order N^0. The last factor in (464) does not. It emerges from the specific $1/\sqrt{N}$ level spacing law in (442). We identify it with the edge scaling law for the Dirac spectral density

$$\rho_D(\tau, \mathbf{x}_0 + \delta\mathbf{x}/\sqrt{N}, 0) \approx \frac{1}{2\pi\tau}\,\mathrm{Erfc}\left(\frac{\Sigma}{4\mu\tau}\frac{\delta\mathbf{x}}{\sqrt{\tau}}\right) \tag{465}$$

In the microscopic limit, the Dirac eigenvalue density along the real-axis follows the universal profile of a complementary error function that is sensitive to the physical chiral condensate Σ at finite μ. (465) suggests a complementary scaling law for extracting Σ from the Dirac spectrum.

9.5.7 Check at the edge point $x_0 = \tau$

As a way to check on the general result (452) we will re-analyze (435) by trading $(P, K) \leftrightarrow (p, k)$. Using the complex coordinates (441), this amounts to re-writing (435) as

$$\Psi(\tau, z, w) = \int \frac{d^2p d^2k d^2z' d^2w'}{(2\pi)^4}\,\mathbb{J}\,e^{Nf} \tag{466}$$

with

$$\begin{aligned} f = &\frac{1}{2}pz + \frac{1}{2}\bar{p}\bar{z} + k\cdot r \\ &-P(p,k)z' - \bar{P}(p,k)\bar{z}' - K(p,k)\cdot r' + \frac{\mu^2}{2}(S+\bar{S}) \\ &+\ln(|z'|^2 + (r')^2) \end{aligned} \tag{467}$$

and

$$\begin{aligned} P(p,k) &= \frac{p(1-\frac{\tau\bar{p}}{2}) - \frac{\tau k^2}{2}}{(1-\frac{\tau p}{2})(1-\frac{\tau\bar{p}}{2}) + \frac{\tau^2k^2}{4}} \\ K(p,k) &= \frac{k}{(1-\frac{\tau p}{2})(1-\frac{\tau\bar{p}}{2}) + \frac{\tau^2k^2}{4}} \\ S(p,k) &= \frac{p(1-\frac{\tau\bar{p}}{2}) + \frac{\tau k^2}{2}}{(1-\frac{\tau p}{2})(1-\frac{\tau\bar{p}}{2}) + \frac{\tau^2k^2}{4}} - p \end{aligned} \tag{468}$$

Here $1/\mathbb{J} = ((1-\frac{\tau p}{2})(1-\frac{\tau\bar{p}}{2}) + \frac{\tau^2k^2}{4})^2$.

Around $x_0 = \tau$ at the boundary, we will use the following microscopic rescaling

$$z = 4\tau - 3\mu^2 + \frac{\eta}{\sqrt{N}}, p = \tau + \frac{p}{\sqrt{N}}, k = \frac{k}{N^{1/4}}$$
$$z' = \tau + \frac{\delta z'}{\sqrt{N}}, r' = \frac{r'}{N^{1/4}} \tag{469}$$

and keep only terms that survive at large N. The result in leading order is

$$N(f - f_0) \approx \frac{\sqrt{N}}{2}(p\eta + \bar{p}\bar{\eta}) + \mathbb{F} \tag{470}$$

with

$$\begin{aligned}
&\mathbb{F} = -2p\delta z' - 2\bar{p}\delta z' - \tau(\tau - \mu^2)(p^2 + \bar{p}^2) \\
&+2\tau k^2(\delta z' + \delta\bar{z}') + 4\tau^3 k^2(p + \bar{p}) \\
&+2\tau^2 k^2(\tau - \mu^2)(p + \bar{p}) - 4\tau^4 k^4 - 4\tau k(p + \bar{p})r' \\
&-4\sqrt{N}kr' + \sqrt{N}(r'/\tau)^2 + 4\sqrt{N}\tau^2 k^2 \\
&-\frac{(\delta z')^2 + (\delta\bar{z}')^2}{2\tau^2} - \frac{(r')^4}{2\tau^4} - \frac{(r')^2}{\tau^3}(\delta z' + \delta\bar{z}')
\end{aligned} \tag{471}$$

Using the shift $r' = 2k\tau^2 + \frac{\alpha}{N^{1/4}}$, we can convert the r'-integral to an α-integral which is Gaussian and decouples. The $\delta z'$ integral can be undone. The result is

$$\begin{aligned}
&\Psi(\tau, 4\tau - 3\mu^2 + \eta/\sqrt{N}, 0) \approx \\
&e^{Nf_0} e^{\sqrt{N}\frac{(\eta+\bar{\eta})}{2\tau}} \int \frac{d^2p d^2k}{(2\pi)^4} e^{\frac{p\eta+\bar{p}\bar{\eta}}{2} + k\cdot r + \mathbb{G}(k,p)}
\end{aligned} \tag{472}$$

with

$$\mathbb{G}(k, p) = 2\tau\mu^2(p^2 + \bar{p}^2) + 2\tau^2 k^2(\tau - \mu^2)(p + \bar{p}) \tag{473}$$

For $r = 0$, the momentum integral in (472) gives

$$\int_0^\infty kdk \left| e^{-\frac{1}{8\mu^2}(\frac{\eta}{2}+2\tau^2k^2(\tau-\mu^2))^2} \right|^2$$
$$= \frac{1}{64\pi^2\mu^2(\tau-\mu^2)} e^{\frac{\delta y^2}{16\tau\mu^2}} \text{ Erfc}\left(\frac{x}{4\sqrt{\tau}|\mu|}\right) \tag{474}$$

Thus the scaling law for the characteristic determinant at the edge point $x_0 = \tau$ and fixed but un-scaled μ, is

$$\Psi(\tau, 4\tau - 3\mu^2 + \delta z/\sqrt{N}, 0) \approx$$
$$\frac{\tau^2 e^{Nf_0}\, e^{\sqrt{N}\frac{\delta x}{\tau}}}{64\pi^2\mu^2(\tau-\mu^2)}\, e^{\frac{\delta y^2}{16\tau\mu^2}} \text{ Erfc}\left(\frac{\delta x}{4\sqrt{\tau}\mu}\right) \tag{475}$$

for the Wishart ensemble and in agreement with (456). The translation to the real edge of the Dirac ensemble follows from the substitution (462). The microscopic scaling law of the characteristic determinant near the real edge of the complex Dirac spectrum (boundary of the zero mode zone) allows for a reading of the quenched chiral condensate (463) by fitting to the universal scaling function (475) or its most general form (**??**) in Appendix I. This the third main result of this section.

9.5.8 Airy universality at $\mu = 0$

For $\mu \to 0$ the result (475) is singular. This feature is valid throughout the envelope of the Wishart and Dirac spectra. The large N limit and the $\mu = 0$ do not commute. Indeed, for $\mu = 0$ the spectra are now real, and the new microscopic scaling laws

$$z = 4\tau + \frac{\eta}{N^{\frac{2}{3}}}, \qquad w = \frac{\omega}{N^{\frac{3}{2}}} \tag{476}$$

should replace (469), with the new and re-scaled ansatz

$$\Psi(\tau, 4\tau + \eta/N^{\frac{2}{3}}, \omega/N^{\frac{3}{2}}) \approx$$
$$\tau^{2N} e^{N^{\frac{1}{3}}\frac{(\eta+\bar{\eta})}{2\tau}}\, \psi(\tau, \eta, \bar{\eta}, \omega) \tag{477}$$

To order N^2 and $N^{\frac{5}{3}}$, the equation (402) is satisfied identically, irrespective of ψ. At order $N^{\frac{4}{3}}$, the new equation fixes ψ

$$-4\tau(\partial_\eta^2+\partial_{\bar\eta}^2)\psi+\frac{1}{4\tau^2}(\eta+\bar\eta)\psi+8\tau\partial_{\bar\omega\omega}^2\psi=0 \tag{478}$$

The general solution to (478) is

$$\int d\lambda\,\kappa(\lambda)\,I_0\left(\sqrt{\frac{\lambda}{8\tau^2}}|\,\omega|\right)\left|\mathrm{Ai}\left(2^{\frac{2}{3}}\left(\frac{\eta}{4\tau}-\lambda\right)\right)\right|^2 \tag{479}$$

with $\kappa(\lambda)$ a general positive weight. The microscopic determinant at the right edge of the Wishart ensemble involves an Airy kernel. As expected, the mapping through $z=\mathbf{z}^2$ at $\mu=0$ yields an Airy kernel for both edges of the real Dirac spectrum.

9.6 Chiral Universality

The mapping $z=\mathbf{z}^2+\mu^2$ between the deformed Wishart (z) and Dirac ($\mathbf{z}$) eigenvalues, shows that the zero virtuality point in the Dirac spectrum at finite μ at $\mathbf{z}=0$, maps onto the $z=\mu^2$ point in the deformed Wishart spectrum. For $\mu/\mu_c<1$, this point lies within the Dirac and Wishart droplets, and moves out of both droplets for $\mu/\mu_c>1$. We now analyze the nature of the accumulation of eigenvalues around this point using the characteristic determinant.

9.6.1 Pinch at zero virtuality

To analyze the saddle point equations (438) in the vicinity of $z\approx\mu^2$ for arbitrary μ^2 and w, we will specialize to the case $\mu^2=1/4$ and $\tau=1$ for simplicity. Throughout this section $\tau=1$. With this in mind, the second equation in (438) reads

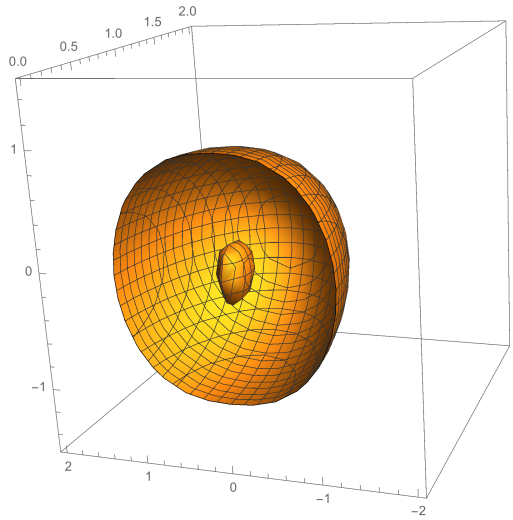

Figure 34: Saddle point surface $r_0(x_0, y_0)$ viewed along $0 < x_0 < 2$ for $\mu^2 = \frac{1}{4}$ and $\tau = 1$. The lateral axis is y_0, the height is r_0 and the depth is x_0.

$$\begin{aligned}(2x_0 - 2x_0^2 - 10x_0^3 - 2x_0^4 + 8x_0^5 + 4x_0^6 - 6y_0^2 - 10x_0y_0^2 \\ -4x_0^2y_0^2 + 16x_0^3y_0^2 + 12x_0^4y_0^2 - 2y_0^4 + 8x_0y_0^4 + 12x_0^2y_0^4 \\ 4y_0^6 - 2r_0^2 - 10x_0r_0^2 - 4x_0^2r_0^2 + 16x_0^3r_0^2 + 12x_0^4r_0^2 \\ -4y_0^2r_0^2 + 16x_0y_9^2r_0^2 + 24x_0^2y_0^2r_0^2 + 12y_0^4r_0^2 - 2r_0^4 \\ +8x_0r_0^4 + 12x_0^2r_0^4 + 12y_0^2r_0^4 + 4r_0^6)/D = 0\end{aligned} \tag{480}$$

with the denominator

$$D \propto x_0(r_0^2 + (x_0 + 1)^2)(3x_0^2 + x_0^3 + r_0^2 + 3xr^2) \tag{481}$$

The positivity of r_0^2 defines a 3-dimensional surface $r_0(x, 0, y_0)$. In Fig. 35 (front surface) we show a cut of the surface through the plane $x_0 = 0$ for $x_0 < 0$, while in Fig. 34 (back surface) we show a cut of the same surface for $x_0 > 0$. As shown, the front surface is composed of an inner and outer surfaces. In both figures, the side is y_0, the height is r_0 and the depth is x_0.

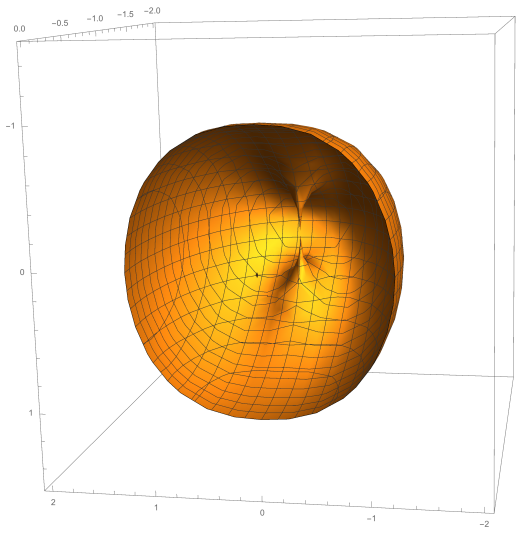

Figure 35: Saddle point surface $r_0(x_0, y_0)$ viewed along $-2 < x_0 < 0$ for $\mu^2 = \frac{1}{4}$ and $\tau = 1$. The lateral axis is y_0, the height is r_0 and the depth is x_0. The pinch at $r_0(x_0, y_0) \equiv 0(-1, 0)$ is the chiral point in the deformed Wishart spectrum.

The inner surface excludes a region in parameter space (r_0, x_0, y_0) where no mixed condensate develops. Indeed, for $D \neq 0$ and in the plane $r_0 = 0$ the surface defines a curve

$$\begin{aligned} &(1 + 2x_0 + x_0^2 + y_0^2) \\ &(x_0 - 3x_0^2 + 2x_0^4 - 3y_0^2 + 4x_0^2 y_0^2 + 2y_0^4) = 0 \end{aligned} \tag{482}$$

The second contribution in (482) is the boundary curve (417). It contains two connected pieces also, the inner part is just the intersection between the small island and the (x,y) plane. The first contribution in (482) vanishes at the point $x_0 = -1, y_0 = r_0 = 0$ which is where the back surface is pinching the plane $r_0 = 0$ in Fig. 35. This zero is not spurious as can be seen through the plane (x_0, r_0) plane, where (480) simplifies to

$$\begin{aligned} &(-1 + x_0^2 + r_0^2) \\ &(-x_0 + x_0^2 + 4x_0^3 + 2x_0^4 + r_0^2 + 4x_0 r_0^2 + 4x_0^2 r_0^2 + 2r_0^4) = 0 \end{aligned} \tag{483}$$

There is a continuous limit to $x_0 = -1$ from the parameter space for a mixed condensate for arbitrary small r_0. The factor $(r_0^2 + x_0^2 - 1)$ cannot be cancelled by the denominator D which is non-vanishing at this point. Thus, the intersection of the condensation region with the real axis shows $x_0 = -1$ as an accumulation point. Now, within the real axis and the branch of the surface determined by $r_0^2 = 1 - x_0^2$, which is the "outer layer" of the condensation region, the first equation for (438) can be solved at once

$$x = \frac{1}{4}(7 + 6x_0) \qquad\qquad y = 0 \tag{484}$$

The point $x_0 = -1, y_0 = 0, r_0 = 0$ correspond to the chiral point $z = \mu^2 = \frac{1}{4}$. But, at this point, the saddle point momentum and the free energy f in (436) diverge. The chiral point $z = \mu^2$ is a singular point on the surface $r_0 = r_0(x_0, y_0)$ defined by (480), as the outer surface develops two sharp holes that connects through a pinch. The standard $1/N$ expansion breaks down.

9.6.2 Chiral microscopic universality

To analyze the chiral point more accurately we need an alternative to the the standard $1/N$ expansion, that resumes a class of corrections around the chiral point. For that it is useful to go back to (466-468) and use the following microscopic rescaling at the chiral point

$$\begin{aligned} &z - \mu^2 \to \frac{z}{N^2}, \mu^2 \to \frac{\mu^2}{N} \\ &w \to \frac{w}{N^2}, p \to Np, k \to Nk \end{aligned} \tag{485}$$

In leading order (466) simplifies

$$\begin{aligned} &\Psi(\tau, \mu^2/N + z/N^2, 0) \approx \\ &\int \frac{d^2pkdkd^2z'd^2w'}{(2\pi)^3} \frac{e^F}{(p^2 + k^2)^2} \end{aligned} \tag{486}$$

with

$$F \approx +\frac{N(\bar{z}'+z')}{\tau} + N\ln(|z'|^2+(r')^2)$$
$$+\frac{pz+\bar{p}\bar{z}}{2} + kr + 2\frac{\bar{p}z'+p\bar{z}'}{\tau^2(\bar{p}p+k^2)} - \frac{4\mu^2\bar{p}p}{\tau(k^2+\bar{p}p)} \tag{487}$$

We use the saddle point solution in z', r' to undo this double integration, i.e. $z' = -1+\alpha$ and $r' = 0+\beta$. The resulting Gaussian integrations in α, β decouple. Thus

$$\Psi(\tau, \mu^2/N + z/N^2, 0)$$
$$\approx \int \frac{d^2p\, kdk}{(2\pi)^2} \frac{e^{\frac{pz+\bar{p}\bar{z}}{2} - 2\frac{\bar{p}+p}{\tau(\bar{p}p+k^2)} - \frac{4\mu^2\bar{p}p}{(k^2+\bar{p}p)\tau}}}{(p^2+k^2)^2} \tag{488}$$

The k-integration in (488) can be done by expanding part of the exponent,

$$\begin{aligned}
&\Psi(\tau, \mu^2/N + z/N^2, 0) \\
&\approx \int \frac{dpd\bar{p}}{(2\pi)^2} \sum_{n=0}^{\infty} \int kdk \frac{(-2(p+\bar{p}) - 4\mu^2\bar{p}p)^n}{\tau^n(k^2+\bar{p}p)^{n+2}n!} e^{\frac{\bar{p}\bar{z}+pz}{2}} \\
&= \int \frac{dpd\bar{p}}{(2\pi)^2} \sum_{n=0}^{\infty} \frac{1}{\bar{p}p} \frac{(-2(p+\bar{p}) - 4\mu^2\bar{p}p)^n}{\tau^n(n+1)!(\bar{p}p)^n} e^{\frac{\bar{p}\bar{z}+pz}{2}} \\
&= \int_0^1 dt \int \frac{dpd\bar{p}}{(2\pi)^2} \frac{1}{\bar{p}p} e^{-t\frac{2(\bar{p}+p+4\mu^2\bar{p}p)}{\bar{p}p\tau}} e^{\frac{\bar{p}\bar{z}+pz}{2}} \\
&= \int_0^1 dt e^{-\frac{4\mu^2 t}{\tau}} \int \frac{dp}{2\pi p} e^{pz/2 - 2t/p\tau} \int \frac{d\bar{p}}{2\pi\bar{p}} e^{\bar{p}\bar{z}/2 - 2t/\bar{p}\tau}
\end{aligned} \tag{489}$$

We note that

$$\xi(z) = \int \frac{dp}{2\pi p} e^{pz/2 - 2t/p\tau} \tag{490}$$

satisfies

$$\left(z\partial_z^2 + \partial_z + \frac{t}{\tau} \right) \xi(z) = 0 \tag{491}$$

$\xi(z) = J_0(2\sqrt{tz/\tau})$ is the unique solution regular at the origin. So as long as we can set the p-integration contour in (489) so that Ψ is regular at $z = 0$, we have $\xi(z) = J_0(2\sqrt{tz/\tau})$. Thus the microscopic form of the characteristic determinant at the chiral point is

$$\begin{aligned} &\Psi(\tau, \mu^2/N + z/N^2, 0) \approx \\ &\approx \tau^{2N} \int_0^1 dt\, e^{-\frac{4\mu^2 t}{\tau}} \left| J_0\left(2\sqrt{\frac{tz}{\tau}} \right) \right|^2 \end{aligned} \tag{492}$$

Here μ^2 is short for the fixed combination $N\mu^2$ at large N, as defined through the re-scaling in (485). This is the fourth main result of this section.

In contrast to (475) the scaling law for the characteristic determinant at the chiral point (492) does not record the quenched chiral condensate at finite μ. We note the similarity of (492) with the microscopic law at the chiral point for the phase phase quenched density of eigenvalues in [124].

For completeness, we note that (402) simplifies at the chiral point for large N, but fixed $N\mu^2$ and $N^2 z$, i.e. $\mu^2 \to \mu^2/N$, $z \to \mu^2/N + z/N^2$ and $w \to w/N^2$. In the microscopic limit, the resulting differential equation is

$$\begin{aligned} &\Bigg(2\left(\partial_z + \partial_{\bar{z}}\right) + \left(z\partial_z^2 + \bar{z}\partial_{\bar{z}}^2\right) \\ &-(z+\bar{z})\partial_{\bar{w}w}^2 + (\partial_z + \partial_{\bar{z}})(w\partial_w + \bar{w}\partial_{\bar{w}}) + \\ &\frac{4\mu^2}{\tau} \frac{\left(\partial_z + \partial_{\bar{z}}\right)\partial_{\bar{w}w}^2}{(\partial_z\partial_{\bar{z}} + \partial_{\bar{w}w}^2)} \Bigg) \mathbf{\Psi} \approx \mathbf{0} \end{aligned} \tag{493}$$

The solution to (493) as $w \to 0$ is (492).

9.7 Conclusions

The QCD Dirac spectrum at finite chemical potential contains subtle information on the chiral dynamics of light quarks in matter. Using a random

matrix model, we have shown that the characteristic determinant of phase quenched QCD with $N_f = 4$ massless quarks is related to the characteristic determinant of a class of deformed Wishart matrices through a conformal mapping in the space of eigenvalues.

We have constructed a stochastic evolution for the deformed Wishart matrices by allowing the Gaussian weights in random matrices to diffuse. The mathematical diffusion time is identified with the stochastic time. We have derived an exact solution to the stochastic diffusion equation for any finite N and derived the explicit time-evolving boundary condition of the envelope of the deformed Wishart eigenvalues through a semi-classical expansion.

Contrary to the lore of random matrix approaches to QCD [126], which focus on the spectral density distributions of the Dirac operator, we studied here the characteristic determinant. Following a recent observation in [116], that the spectral evolution of non-Hermitean and non-normal ensembles involves a hidden complex variable w [114], we have embedded the Dirac operator into this general algebraic structure. The explicit dependence on w is key to closing and obtaining the main evolution equations (402-**??**). While the complex variable z reflects on the standard quark condensate, the complex variable w reflects on the "spurious" quark condensate [110, 111, 114], whose formation is an artifact of quenching or ignoring the phase of the fermionic determinant. This evolution equation is exact for any finite N. This fact allows to trace the co-evolution of both type of condensates, and to perform all kinds of rescalings in the vicinity of the physically pertinent points.

In general, the complex eigenvalues form a droplet in the complex eigenvalue plane that breaks conformal symmetry. The deformed Wishart droplet deforms but never breaks. Its boundary is sharp at large N, and smoothens out in $1/N$ through a universal edge function in leading order. At the chiral point, the characteristic determinant follows universally from a pertinent Bessel kernel.

The edge universality and the chiral universality derived in this work can be numerically checked. In particular, the microscopic scaling law at the edge of the spectrum scales with the chiral condensate at finite μ, allowing for its possible extraction directly from current and quenched lattice data. In practice and in the absence of an apparent edge in real QCD spectra, this can be achieved by rescaling the numerical eigenvalues within a sliding window along the real axis, and checking for the edge scaling law for the Dirac spectrum using for instance (464-465), or along the w-axis using (**??**-**??**). When extended to finite temperature, this practical analysis will allow

for a determination of the QCD phase diagram solely from the quenched lattice simulations, without having to solve the QCD sign problem, a major achievement in this field.

Finally and on general grounds, most of our results for the deformed Wishart ensemble may be of relevance to a wider audience of practitioners using non-hermitean random matrix methods in the fields of wireless communication, biological and neural information, and finance [119]

References

[1] T. Schafer and E. V. Shuryak, Rev. Mod. Phys. **70**, 323 (1998) [hep-ph/9610451]; D. Diakonov, Prog. Part. Nucl. Phys. **51**, 173 (2003) [hep-ph/0212026]; M. A. Nowak, M. Rho and I. Zahed, Singapore, Singapore: World Scientific (1996) 528 p

[2] N. I. Kochelev, Phys. Lett. B **426**, 149 (1998) [hep-ph/9610551]; D. Ostrovsky and E. Shuryak, Phys. Rev. D **71**, 014037 (2005) [hep-ph/0409253]; Y. Qian and I. Zahed, Phys. Rev. D **86**, 014033 (2012) [Erratum-ibid. D **86**, 059902 (2012)] [arXiv:1112.4552 [hep-ph]]; Y. Qian and I. Zahed, Phys. Rev. D **90**, no. 11, 114012 (2014) [arXiv:1404.6270 [hep-ph]].

[3] Kraan-Van-Baal NPB 533 1998 T. C. Kraan and P. van Baal, Nucl. Phys. B **533**, 627 (1998) [hep-th/9805168]; T. C. Kraan and P. van Baal, Phys. Lett. B **435**, 389 (1998) [hep-th/9806034]; K. M. Lee and C. h. Lu, Phys. Rev. D **58**, 025011 (1998) [hep-th/9802108].

[4] D. Diakonov and V. Petrov, Phys. Rev. D **76**, 056001 (2007) [arXiv:0704.3181 [hep-th]]; D. Diakonov and V. Petrov, Phys. Rev. D **76**, 056001 (2007) [arXiv:0704.3181 [hep-th]]. D. Diakonov and V. Petrov, AIP Conf. Proc. **1343**, 69 (2011) [arXiv:1011.5636 [hep-th]]; D. Diakonov, arXiv:1012.2296 [hep-ph].

[5] D. Diakonov, N. Gromov, V. Petrov and S. Slizovskiy, Phys. Rev. D **70**, 036003 (2004) [hep-th/0404042].

[6] A. R. Zhitnitsky, hep-ph/0601057; S. Jaimungal and A. R. Zhitnitsky, hep-ph/9905540; A. Parnachev and A. R. Zhitnitsky, Phys. Rev. D **78** (2008) 125002 [arXiv:0806.1736 [hep-ph]]; A. R. Zhitnitsky, Nucl. Phys. A **921** (2014) 1 [arXiv:1308.0020 [hep-ph]].

[7] V. A. Fateev, I. V. Frolov and A. S. Shvarts, Nucl. Phys. B **154**, 1 (1979); B. Berg and M. Luscher, Commun. Math. Phys. **69**, 57 (1979).

[8] B. Martemyanov, S. Molodtsov, Y. Simonov and A. Veselov, JETP Lett. **62**, 695 (1995) [Pisma Zh. Eksp. Teor. Fiz. **62**, 679 (1995)]; B. V. Martemyanov, S. V. Molodtsov, Y. A. Simonov and A. I. Veselov, Phys. Atom. Nucl. **60**, 490 (1997) [Yad. Fiz. **60**, 565 (1997)]; Y. A. Simonov, In

Varenna 1995, Selected topics in nonperturbative QCD 339-364 [hep-ph/9509403]; A. Gonzalez-Arroyo and Y. A. Simonov, Nucl. Phys. B **460**, 429 (1996) [hep-th/9506032].

[9] G. 't Hooft, Nucl. Phys. B **138**, 1 (1978).

[10] S. Mandelstam, Phys. Rev. D **19**, 2391 (1979).

[11] N. Seiberg and E. Witten, Nucl. Phys. B **426**, 19 (1994) [Erratum-ibid. B **430**, 485 (1994)] [hep-th/9407087].

[12] A. M. Polyakov, Phys. Lett. B **59**, 82 (1975); A. M. Polyakov, Nucl. Phys. B **120**, 429 (1977).

[13] M. Unsal and L. G. Yaffe, Phys. Rev. D **78**, 065035 (2008) [arXiv:0803.0344 [hep-th]]; M. Unsal, Phys. Rev. D **80**, 065001 (2009) [arXiv:0709.3269 [hep-th]].

[14] T. H. Hansson, H. B. Nielsen and I. Zahed, Nucl. Phys. B **451**, 162 (1995) [hep-ph/9405324].

[15] E. Poppitz, T. Schfer and M. Unsal, JHEP **1210**, 115 (2012) [arXiv:1205.0290 [hep-th]]; E. Poppitz and M. Unsal, JHEP **1107** (2011) 082 [arXiv:1105.3969 [hep-th]].

[16] D. J. Gross, R. D. Pisarski and L. G. Yaffe, Rev. Mod. Phys. **53**, 43 (1981). N. Weiss, Phys. Rev. D **25**, 2667 (1982);

[17] E. Shuryak and T. Sulejmanpasic, Phys. Lett. B **726** (2013) 257 [arXiv:1305.0796 [hep-ph]].

[18] E. Shuryak and T. Sulejmanpasic, Phys. Rev. D **86**, 036001 (2012) [arXiv:1201.5624 [hep-ph]];

[19] P. Faccioli and E. Shuryak, Phys. Rev. D **87**, no. 7, 074009 (2013) [arXiv:1301.2523 [hep-ph]].

[20] F. Bruckmann, S. Dinter, E. M. Ilgenfritz, M. Muller-Preussker and M. Wagner, Phys. Rev. D **79**, 116007 (2009) [arXiv:0903.3075 [hep-ph]]; F. Bruckmann, S. Dinter, E. M. Ilgenfritz, B. Maier, M. Muller-Preussker and M. Wagner, Phys. Rev. D **85**, 034502 (2012) [arXiv:1111.3158 [hep-ph]].

[21] R.N. Larsen and E. Shuryak, arXiv:1408.6563 [hep-ph].

[22] B. A. Gelman, E. V. Shuryak and I. Zahed, Phys. Rev. C **74**, 044909 (2006) [nucl-th/0605046]; S. Cho and I. Zahed, Phys. Rev. C **79**, 044911 (2009) [arXiv:0812.1736 [nucl-th]]; S. Cho and I. Zahed, Phys. Rev. C **80** (2009) 014906 [arXiv:0812.1741 [nucl-th]].

[23] S. Cho and I. Zahed, Phys. Rev. C **82**, 054907 (2010) [arXiv:0910.2666 [nucl-th]]; S. Cho and I. Zahed, Phys. Rev. C **82**, 044905 (2010) [arXiv:0909.4725 [nucl-th]]; V. S. Filinov, Y. B. Ivanov, V. E. Fortov, M. Bonitz and P. R. Levashov, Phys. Rev. C **87**, no. 3, 035207 (2013) [arXiv:1210.2664 [nucl-th]]; V. S. Filinov, Y. B. Ivanov, M. Bonitz, V. E. Fortov and P. R. Levashov, Phys. Lett. A **376**, 1096 (2012) [arXiv:1203.2191 [hep-ph]]; V. S. Filinov, Y. B. Ivanov, M. Bonitz, P. R. Levashov and V. E. Fortov, Phys. Atom. Nucl. **74**, 1364 (2011) [arXiv:1006.3390 [nucl-th]].

[24] C. Adami, T. Hatsuda and I. Zahed, Phys. Rev. D **43**, 921 (1991).

[25] M. Fisher and Y. Levin, Phys. Rev. Lett. **71**, 3826 (1993) and references therein.

[26] V. G. Bornyakov and V. K. Mitrjushkin, Phys. Rev. D **84**, 094503 (2011) [arXiv:1011.4790 [hep-lat]].

[27] O. Kaczmarek, F. Karsch, F. Zantow and P. Petreczky, Phys. Rev. D **70**, 074505 (2004) [Erratum-ibid. D **72**, 059903 (2005)] [hep-lat/0406036].

[28] B. Lucini, M. Teper and U. Wenger, JHEP **0502**, 033 (2005) [hep-lat/0502003].

[29] T. J. Hollowood, hep-th/9110010.

[30] Y. Liu and I. Zahed, arXiv:1710.02895 [hep-ph].

[31] J. Greensite and R. Hllwieser, arXiv:1411.5091 [hep-lat].

[32] J. Greensite, B. Lucini and A. Patella, Phys. Rev. D **83**, 125019 (2011) [arXiv:1101.5344 [hep-th]].

[33] G. 't Hooft, Nucl. Phys. B **138**, 1 (1978).

[34] L. Del Debbio, A. Di Giacomo and B. Lucini, Nucl. Phys. B **594**, 287 (2001) [hep-lat/0006028]; L. Del Debbio, A. Di Giacomo and B. Lucini, Phys. Lett. B **500**, 326 (2001) [hep-lat/0011048].

[35] R. N. Larsen, private communication.

[36] R .N. Larsen and E. Shuryak, Interacting Ensemble of Instanton-dyons and Confinement in SU(2) Gauge Theory, in preparation.

[37] C. Korthals-Altes, A. Kovner and M. A. Stephanov, Phys. Lett. B **469**, 205 (1999) [hep-ph/9909516].

[38] H. Reinhardt, Phys. Lett. B **557**, 317 (2003) [hep-th/0212264].

[39] S. Sharma, V. Dick, F. Karsch, E. Laermann and S. Mukherjee, arXiv:1311.3943 [hep-lat].

[40] E. V. Shuryak, Phys. Lett. B **196**, 373 (1987). T. Schaefer, E. V. Shuryak and J. J. M. Verbaarschot, Phys. Rev. D **51** (1995) 1267 [hep-ph/9406210].

[41] M. Rho, S. J. Sin and I. Zahed, Phys. Lett. B **689**, 23 (2010) [arXiv:0910.3774 [hep-th]]; V. Kaplunovsky and J. Sonnenschein, JHEP **1404** (2014) 022 [arXiv:1304.7540 [hep-th]]; S. Bolognesi and P. Sutcliffe, J. Phys. A **47**, 135401 (2014) [arXiv:1311.2685 [hep-th]].

[42] Y. Liu, E. Shuryak and I. Zahed, Light quarks in the screened Dyon-Anti-Dyon Coulomb Liquid Model II, arXiv:1503.09148.

[43] Y. Liu, E. Shuryak and I. Zahed, Phys. Rev. D **92**, no. 8, 085006 (2015); Y. Liu, E. Shuryak and I. Zahed, Phys. Rev. D **92**, no. 8, 085007 (2015); Y. Liu, E. Shuryak and I. Zahed, Phys. Rev. D **94**, no. 10, 105011 (2016) [arXiv:1606.07009 [hep-ph]]; Y. Liu, E. Shuryak and I. Zahed, Phys. Rev. D **94**, no. 10, 105012 (2016) [arXiv:1605.07584 [hep-ph]].

[44] M. Unsal and L. G. Yaffe, Phys. Rev. D **78**, 065035 (2008) [arXiv:0803.0344 [hep-th]]; M. Unsal, Phys. Rev. D **80**, 065001 (2009) [arXiv:0709.3269 [hep-th]]; E. Poppitz, T. Schafer and M. Unsal, JHEP **1210**, 115 (2012) [arXiv:1205.0290 [hep-th]]; E. Poppitz and M. Unsal, JHEP **1107** (2011) 082 [arXiv:1105.3969 [hep-th]]; E. Poppitz, T. Schafer and M. Unsal, JHEP **1303**, 087 (2013) [arXiv:1212.1238].

[45] E. Poppitz and T. Sulejmanpasic, JHEP **1309** (2013) 128 [arXiv:1307.1317 [hep-th]].

[46] R. Larsen and E. Shuryak, Nucl. Phys. A **950**, 110 (2016) [arXiv:1408.6563 [hep-ph]].

[47] H. Frisch and J.L. Lebowitz ,The Equilibrium Theory of Classical Fluids, New York: Benjamin (1964).

[48] M. D'Elia and F. Negro, Phys. Rev. Lett. **109**, 072001 (2012) [arXiv:1205.0538 [hep-lat]].

[49] M. Rho, S. J. Sin and I. Zahed, Phys. Lett. B **689**, 23 (2010) [arXiv:0910.3774 [hep-th]]; I. Zahed, arXiv:1010.5980 [hep-ph]; P. Sutcliffe, Mod. Phys. Lett. B **29**, no. 16, 1540051 (2015); V. Kaplunovsky, D. Melnikov and J. Sonnenschein, Mod. Phys. Lett. B **29**, no. 16, 1540052 (2015) [arXiv:1501.04655 [hep-th]].

[50] A. Vilenkin, Phys. Rev. D **20**, 1807 (1979); A. Vilenkin, Phys. Rev. D **22**, 3080 (1980).

[51] S. Ebihara, K. Fukushima and T. Oka, Phys. Rev. B **93**, no. 15, 155107 (2016) [arXiv:1509.03673 [cond-mat.str-el]].

[52] D. E. Kharzeev, K. Landsteiner, A. Schmitt and H. U. Yee, Lect. Notes Phys. **871**, 1 (2013); [arXiv:1211.6245 [hep-ph]].

[53] Y. Liu and I. Zahed, arXiv:1509.00812 [hep-ph].

[54] K. Hattori and Y. Yin, Phys. Rev. Lett. **117**, no. 15, 152002 (2016) [arXiv:1607.01513 [hep-th]].

[55] Y. Jiang and J. Liao, Phys. Rev. Lett. **117**, no. 19, 192302 (2016) [arXiv:1606.03808 [hep-ph]].

[56] S. Ebihara, K. Fukushima and K. Mameda, Phys. Lett. B **764**, 94 (2017) [arXiv:1608.00336 [hep-ph]]; H. L. Chen, K. Fukushima, X. G. Huang and K. Mameda, Phys. Rev. D **93**, no. 10, 104052 (2016) [arXiv:1512.08974 [hep-ph]].

[57] A. Ayala, P. Mercado and C. Villavicencio, Phys. Rev. C **95**, no. 1, 014904 (2017) [arXiv:1609.02595 [hep-ph]].

[58] X. G. Huang, K. Nishimura and N. Yamamoto, arXiv:1711.02190 [hep-ph].

[59] G. E. Volovik, The Universe in a Helium Droplet (Oxford University Press, Oxford, 2003).

[60] M. N. Chernodub and S. Gongyo, JHEP **1701** (2017) 136 [arXiv:1611.02598 [hep-th]]; M. N. Chernodub and S. Gongyo, Phys. Rev. D **95**, no. 9, 096006 (2017) [arXiv:1702.08266 [hep-th]]; M. N. Chernodub and S. Gongyo, arXiv:1706.08448 [hep-th].

[61] R. Loganayagam, arXiv:1106.0277 [hep-th].

[62] V. P. Gusynin, V. A. Miransky and I. A. Shovkovy, Phys. Rev. D **52**, 4718 (1995) [hep-th/9407168].

[63] G. W. Semenoff and L. C. R. Wijewardhana, Phys. Rev. Lett. **63**, 2633 (1989).

[64] R. A. Janik, M. A. Nowak, G. Papp and I. Zahed, Phys. Rev. Lett. **81**, 264 (1998); [hep-ph/9803289]. M. A. Nowak, M. Sadzikowski and I. Zahed, Acta Phys. Polon. B **47**, 2173 (2016) [arXiv:1304.6020 [hep-ph]].

[65] I. A. Shushpanov and A. V. Smilga, Phys. Lett. B **402**, 351 (1997) [hep-ph/9703201].

[66] G. S. Bali, F. Bruckmann, G. Endrodi, Z. Fodor, S. D. Katz and A. Schafer, Phys. Rev. D **86** (2012) 071502 [arXiv:1206.4205 [hep-lat]].

[67] I. Zahed, Hydrodynamics of the Polyakov loop and Dirac spectra, 2015-11-04, SCGP video portal.

[68] F. Becattini, F. Piccinini and J. Rizzo, Phys. Rev. C **77**, 024906 (2008) [arXiv:0711.1253 [nucl-th]].

[69] Y. Jiang, Z. W. Lin and J. Liao, Phys. Rev. C **94**, no. 4, 044910 (2016) Erratum: [Phys. Rev. C **95**, no. 4, 049904 (2017)] [arXiv:1602.06580 [hep-ph]]; W. T. Deng and X. G. Huang, Phys. Rev. C **93**, no. 6, 064907 (2016) [arXiv:1603.06117 [nucl-th]].

[70] L. Adamczyk *et al.* [STAR Collaboration], Nature **548**, 62 (2017) [arXiv:1701.06657 [nucl-ex]].

[71] H. L. Chen, K. Fukushima, X. G. Huang and K. Mameda, Phys. Rev. D **96**, no. 5, 054032 (2017) [arXiv:1707.09130 [hep-ph]].

[72] Y. Liu and I. Zahed, arXiv:1711.08354 [hep-ph].

[73] D. E. Kharzeev, J. Liao, S. A. Voloshin and G. Wang, Prog. Part. Nucl. Phys. **88**, 1 (2016) [arXiv:1511.04050 [hep-ph]].

[74] V. Begun, Phys. Rev. C **94**, no. 5, 054904 (2016) [arXiv:1603.02254 [nucl-th]].

[75] A. Vilenkin, Phys. Rev. D **20**, 1807 (1979); A. Vilenkin, Phys. Rev. D **22**, 3080 (1980).

[76] S. Ebihara, K. Fukushima and T. Oka, Phys. Rev. B **93**, no. 15, 155107 (2016) [arXiv:1509.03673 [cond-mat.str-el]].

[77] D. E. Kharzeev, K. Landsteiner, A. Schmitt and H. U. Yee, Lect. Notes Phys. **871**, 1 (2013); [arXiv:1211.6245 [hep-ph]].

[78] J. Adam *et al.* [ALICE Collaboration], Phys. Rev. C **93** (2016) no.5, 054908 [arXiv:1512.08902 [nucl-ex]].

[79] A. Yamamoto and Y. Hirono, Phys. Rev. Lett. **111**, 081601 (2013) [arXiv:1303.6292 [hep-lat]].

[80] G. Boyd, J. Engels, F. Karsch, E. Laermann, C. Legeland, M. Lutgemeier and B. Petersson, Nucl. Phys. B **469**, 419 (1996) [hep-lat/9602007];

[81] P. Bialas, L. Daniel, A. Morel and B. Petersson, Nucl. Phys. B **836**, 91 (2010) [arXiv:0912.0206 [hep-lat]].

[82] B. Lucini and M. Panero, Phys. Rept. **526**, 93 (2013) [arXiv:1210.4997 [hep-th]]. M. C. Ogilvie, J. Phys. A **45**, 483001 (2012) [arXiv:1211.2843 [hep-th]].

[83] D. Diakonov and V. Petrov, Phys. Rev. D **76**, 056001 (2007) [arXiv:0704.3181 [hep-th]].

[84] Y. Liu, E. Shuryak and I. Zahed, arXiv:1503.03058 [hep-ph].

[85] V.L. Berezinskii, Sov. Phys. JETP **32**, 493 (1971); J. M. Kosterlitz and D. J. Thouless, J. Phys. C **6**, 1181 (1973).

[86] S. Chakravarty and C. H. Hsu, arXiv:1503.01126 [cond-mat.str-el].

[87] P. Bicudo, R. D. Pisarski and E. Seel, Phys. Rev. D **89**, no. 8, 085020 (2014) [arXiv:1402.5137 [hep-ph]]; P. Bicudo, R. D. Pisarski and E. Seel, Phys. Rev. D **88**, no. 3, 034007 (2013) [arXiv:1306.2943 [hep-ph]].

[88] K. Dusling, C. Ratti and I. Zahed, Phys. Rev. D **79**, 034027 (2009) [arXiv:0807.2879 [hep-ph]].

[89] D. J. Gross and E. Witten, Phys. Rev. D **21**, 446 (1980).

[90] F. J. Dyson, J. Math. Phys. **3**, 140 (1962); **3**, 157 (1962); **3**, 1191 (1962).

[91] A. Jevicki and B. Sakita, Nucl. Phys. B **165**, 511 (1980); A. Jevicki, Nucl. Phys. B **376**, 75 (1992).

[92] A. P. Polychronakos, Phys. Rev. Lett. **74**, 5153 (1995) [hep-th/9411054].

[93] E. Bettelheim, A. G. Abanov and P. Wiegmann, Phys. Rev. Lett. **97**, 246401 (2006) [cond-mat/0606778].

[94] E. D'Hoker, Nucl. Phys. B **201**, 401 (1982).

[95] P. Bialas, A. Morel, B. Petersson and K. Petrov, Nucl. Phys. Proc. Suppl. **106**, 882 (2002) [hep-lat/0110219].

[96] This value follows from an overall fit to both the 3D and the reduced 2D lattice data in [95].

[97] R. D. Pisarski and O. Alvarez, Phys. Rev. D **26**, 3735 (1982).

[98] J. P. Blaizot and M. A. Nowak, Phys. Rev. Lett. **101**, 102001 (2008) [arXiv:0801.1859 [hep-th]]; H. Neuberger, Phys. Lett. B **666**, 106 (2008) [arXiv:0806.0149 [hep-th]].

[99] D. Karabali, C. j. Kim and V. P. Nair, Phys. Lett. B **434**, 103 (1998) [hep-th/9804132]; V. P. Nair, [hep-th/0309061].

[100] J. Liddle and M. Teper, arXiv:0803.2128 [hep-lat].

[101] B. Lucini, M. Teper and U. Wenger, JHEP **0401**, 061 (2004) [hep-lat/0307017]; B. Lucini, M. Teper and U. Wenger, JHEP **0502** (2005) 033 [hep-lat/0502003].

[102] K. Kajantie and L. Karkkainen, Phys. Lett. B **214** (1988) 595; T. Bhattacharya, A. Gocksch, C. Korthals Altes and R. D. Pisarski, Nucl. Phys. B **383**, 497 (1992) [hep-ph/9205231].

[103] M. A. Nowak, M. Rho and I. Zahed, Singapore, Singapore: World Scientific (1996) 528 p

[104] C. Bernard, C. E. DeTar, L. Levkova, S. Gottlieb, U. M. Heller, J. E. Hetrick, J. Osborn and D. B. Renner *et al.*, PoS LAT **2007**, 090 (2007) [arXiv:0710.1118 [hep-lat]].

[105] T. Banks and A. Casher, Nucl. Phys. B **169**, 103 (1980).

[106] R. A. Janik, M. A. Nowak, G. Papp and I. Zahed, Phys. Rev. Lett. **81**, 264 (1998) [hep-ph/9803289]; R. A. Janik, M. A. Nowak, G. Papp and I. Zahed, Prog. Theor. Phys. Suppl. **131**, 471 (1998); R. A. Janik, M. A. Nowak, G. Papp and I. Zahed, in the Proceedings, 34th Rencontres de Moriond. ed. J. Tran Thanh Van, Hanoi: The Gioi (2001). hep-ph/9905274.

[107] E. V. Shuryak and J. J. M. Verbaarschot, Nucl. Phys. A **560**, 306 (1993) [hep-th/9212088]; J. J. M. Verbaarschot and I. Zahed, Phys. Rev. Lett. **70**, 3852 (1993) [hep-th/9303012].

[108] M. A. Nowak, J. J. M. Verbaarschot and I. Zahed, Phys. Lett. B **217**, 157 (1989).

[109] A. Gocksch, Phys. Rev. Lett. **61**, 2054 (1988); I. Barbour, N. E. Behilil, E. Dagotto, F. Karsch, A. Moreo, M. Stone and H. W. Wyld, Nucl. Phys. B **275**, 296 (1986); I. M. Barbour, S. E. Morrison, E. G. Klepfish, J. B. Kogut and M. P. Lombardo, Nucl. Phys. Proc. Suppl. **60A**, 220 (1998) [hep-lat/9705042].

[110] M. A. Stephanov, Phys. Rev. Lett. **76**, 4472 (1996) [hep-lat/9604003].

[111] R. A. Janik, M. A. Nowak, G. Papp and I. Zahed, Phys. Rev. Lett. **77**, 4876 (1996) [hep-ph/9606329].

[112] J. C. Osborn, Phys. Rev. Lett. **93**, 222001 (2004) [hep-th/0403131].

[113] G. Akemann, J. Phys. A **36**, 3363 (2003) [hep-th/0204246]; G. Akemann, Acta Phys. Polon. B **38**, 3981 (2007) [arXiv:0710.2905 [hep-th]].

[114] R. A. Janik, M. A. Nowak, G. Papp and I. Zahed, Phys. Lett. B **440**, 123 (1998) [hep-ph/9806479]. R. A. Janik, M. A. Nowak, G. Papp and I. Zahed, In *Zakopane 1997, New developments in quantum field theory* 297-314 [hep-ph/9708418]. R. A. Janik, M. A. Nowak, G. Papp and I. Zahed, Acta Phys. Polon. B **28**, 2949 (1997) [hep-th/9710103]. R. A. Janik, M. A. Nowak, G. Papp, J. Wambach and I. Zahed, Phys. Rev. E **55**, 4100 (1997) [hep-ph/9609491]; R. A. Janik, M. A. Nowak, G. Papp and I. Zahed, Nucl. Phys. B **501**, 603 (1997) [cond-mat/9612240].

[115] A. M. Halasz, J. C. Osborn and J. J. M. Verbaarschot, Phys. Rev. D **56**, 7059 (1997) [hep-lat/9704007]. J. J. M. Verbaarschot, Nucl. Phys. A **642**, 305 (1998) [hep-ph/9807296]. F. Basile and G. Akemann, JHEP **0712**, 043 (2007) [arXiv:0710.0376 [hep-th]]; K. Splittorff and J. J. M. Verbaarschot, Phys. Rev. D **75**, 116003 (2007) [hep-lat/0702011 [HEP-LAT]]; J. Han and M. A. Stephanov, Phys. Rev. D **78**, 054507 (2008) [arXiv:0805.1939 [hep-lat]]; H. Fujii and T. Sano, Phys. Rev. D **83**, 014005 (2011) [arXiv:1009.5977 [hep-ph]]; G. Akemann, T. Kanazawa, M. J. Phillips and T. Wettig, JHEP **1103**, 066 (2011) [arXiv:1012.4461 [hep-lat]]; A. Mollgaard and K. Splittorff, Phys. Rev. D **91**, no. 3, 036007 (2015) [arXiv:1412.2729 [hep-lat]].

[116] J. P. Blaizot, M. A. Nowak and P. Warchoł, Phys. Rev. E **89**, no. 4, 042130 (2014); J. P. Blaizot, M. A. Nowak and P. Warchoł, Phys. Lett. B **724**, 170 (2013) [arXiv:1303.2357 [hep-ph]]; J. P. Blaizot, M. A. Nowak and P. Warchoł, Phys. Rev. E **89**, no. 4, 042130 (2014); Z. Burda, J. Grela, M. A. Nowak, W. Tarnowski and P. Warchoł, Phys. Rev. Lett. **113** (2014) 104102; Z. Burda, J. Grela, M. A. Nowak, W. Tarnowski and P. Warchoł, Nucl. Phys. B **897**, 421 (2015); J. P. Blaizot, J. Grela, M. A. Nowak and P. Warchoł, Acta Phys. Polon. B **46**, no. 9, 1785 (2015); J. Grela, J. Phys. A: Math. Theor. **49** (2015) 015201;

J. P. Blaizot, J. Grela, M. A. Nowak, W. Tarnowski and P. Warchoł, arXiv:1512.06599 [math-ph].

[117] Y. Liu, P. Warchoł and I. Zahed, arXiv:1505.02107 [hep-ph]; Y. Liu, P. Warchoł and I. Zahed, arXiv:1506.08787 [hep-ph]; P. J. Forrester and J. Grela, J. Phys. A: Math. Theor. **49** (2016) 085203, arXiv:1507.07274 [math-ph].

[118] J. Gasser and H. Leutwyler, Phys. Lett. B **188**, 477 (1987); J. Gasser and H. Leutwyler, Phys. Lett. B **184**, 83 (1987).

[119] K. Rajan and L.F. Abbot, Phys. Rev. Lett. **97** (2006) 188104; Ch. Biely and S. Thurner, Quant. Finance **8** (2008) 705; F. Krzakala et al., Proc. Natl. Acad. Sci. USA **110** (2-13) 20935; R. Couillet and M. Debbah, " Random Matrix Methods for Wireless Communications", Cambridge University Press (2011); H. Rouault and S. Druckmann, arXiv:1509.01983 [q-bio.NC].

[120] F. J. Dyson, J. Math. Phys. **3**, 140 (1962); **3**, 157 (1962); **3**, 1191 (1962).

[121] Y. Liu, P. Warchol and I. Zahed, arXiv:1507.05599 [hep-ph].

[122] I. Barbour, N. E. Behilil, E. Dagotto, F. Karsch, A. Moreo, M. Stone and H. W. Wyld, Nucl. Phys. B **275**, 296 (1986);

[123] H. Markum, R. Pullirsch and T. Wettig, Phys. Rev. Lett. **83**, 484 (1999) [hep-lat/9906020].

[124] J. J. M. Verbaarschot, in the Proceedings, NATO Advanced Study Institute, Les Houches, ed. E. Brezin et al, Dordrecht, Springer (2006). hep-th/0502029; J. C. Osborn, K. Splittorff and J. J. M. Verbaarschot, Phys. Rev. D **78** (2008) 065029.

[125] G. Akemann and G. Vernizzi, Nucl. Phys. B **660**, 532 (2003); [hep-th/0212051].

[126] For a review, see J.J.M. Verbaarschot, in "Oxford Handbook of Random Matrix Theory", edited by G. Akemann, J. Baik and Ph. Di Francesco, OUP Oxford, 2015.

[127] E. V. Shuryak, Nucl. Phys. B **198**, 83 (1982); N. Isgur and M. B. Wise, Phys. Rev. Lett. **66** (1991) 1130; A. V. Manohar and M. B. Wise, "Heavy quark physics," Camb. Monogr. Part. Phys. Nucl. Phys. Cosmol. **10**, 1 (2000).

[128] M. A. Nowak, M. Rho and I. Zahed, Phys. Rev. D **48**, 4370 (1993) [hep-ph/9209272]; M. A. Nowak, M. Rho and I. Zahed, Acta Phys. Polon. B **35**, 2377 (2004) [hep-ph/0307102].

[129] W. A. Bardeen and C. T. Hill, Phys. Rev. D **49** (1994) 409 [hep-ph/9304265]; W. A. Bardeen, E. J. Eichten and C. T. Hill, Phys. Rev. D **68**, 054024 (2003) [hep-ph/0305049].

[130] B. Aubert *et al.* [BaBar Collaboration], Phys. Rev. Lett. **90**, 242001 (2003) [hep-ex/0304021].

[131] D. Besson *et al.* [CLEO Collaboration], Phys. Rev. D **68**, 032002 (2003) Erratum: [Phys. Rev. D **75**, 119908 (2007)] [hep-ex/0305100].

[132] I. Adachi [Belle Collaboration], arXiv:1105.4583 [hep-ex]; A. Bondar *et al.* [Belle Collaboration], Phys. Rev. Lett. **108**, 122001 (2012) [arXiv:1110.2251 [hep-ex]].

[133] M. Ablikim *et al.* [BESIII Collaboration], Phys. Rev. Lett. **110**, 252001 (2013) [arXiv:1303.5949 [hep-ex]].

[134] V. M. Abazov *et al.* [D0 Collaboration], [arXiv:1602.07588 [hep-ex]].

[135] R. Aaij *et al.* [LHCb Collaboration], arXiv:1606.07895 [hep-ex]; R. Aaij *et al.* [LHCb Collaboration], arXiv:1606.07898 [hep-ex].

[136] R. Aaij *et al.* [LHCb Collaboration], Phys. Rev. Lett. **115** (2015) 072001 [arXiv:1507.03414 [hep-ex]]; R. Aaij *et al.* [LHCb Collaboration], Phys. Rev. Lett. **117** (2016) no.8, 082002 [arXiv:1604.05708 [hep-ex]]; R. Aaij *et al.* [LHCb Collaboration], Phys. Rev. Lett. **117** (2016) no.8, 082003 Addendum: [Phys. Rev. Lett. **117** (2016) no.10, 109902] [arXiv:1606.06999 [hep-ex]].

[137] R. Aaij *et al.* [LHCb Collaboration], arXiv:1703.04639 [hep-ex].

[138] M. B. Voloshin and L. B. Okun, JETP Lett. **23**, 333 (1976) [Pisma Zh. Eksp. Teor. Fiz. **23**, 369 (1976)];

[139] N. A. Tornqvist, Phys. Rev. Lett. **67**, 556 (1991); N. A. Tornqvist, Z. Phys. C **61**, 525 (1994) [hep-ph/9310247]; N. A. Tornqvist, Phys. Lett. B **590**, 209 (2004) [hep-ph/0402237].

[140] M. Karliner and H. J. Lipkin, arXiv:0802.0649 [hep-ph]; M. Karliner and J. L. Rosner, Phys. Rev. Lett. **115** (2015) no.12, 122001 [arXiv:1506.06386 [hep-ph]]; M. Karliner, Acta Phys. Polon. B **47**, 117 (2016).

[141] C. E. Thomas and F. E. Close, Phys. Rev. D **78**, 034007 (2008) [arXiv:0805.3653 [hep-ph]]; F. Close, C. Downum and C. E. Thomas, Phys. Rev. D **81**, 074033 (2010) [arXiv:1001.2553 [hep-ph]].

[142] S. Ohkoda, Y. Yamaguchi, S. Yasui, K. Sudoh and A. Hosaka, Phys. Rev. D **86**, 034019 (2012) [arXiv:1202.0760 [hep-ph]]; S. Ohkoda, Y. Yamaguchi, S. Yasui, K. Sudoh and A. Hosaka, arXiv:1209.0144 [hep-ph].

[143] M. T. AlFiky, F. Gabbiani and A. A. Petrov, Phys. Lett. B **640**, 238 (2006) [hep-ph/0506141]; I. W. Lee, A. Faessler, T. Gutsche and V. E. Lyubovitskij, Phys. Rev. D **80**, 094005 (2009) [arXiv:0910.1009 [hep-ph]]; M. Suzuki, Phys. Rev. D **72**, 114013 (2005) [hep-ph/0508258]; J. R. Zhang, M. Zhong and M. Q. Huang, Phys. Lett. B **704**, 312 (2011) [arXiv:1105.5472 [hep-ph]]; D. V. Bugg, Europhys. Lett. **96**, 11002 (2011) [arXiv:1105.5492 [hep-ph]]; J. Nieves and M. P. Valderrama, Phys. Rev. D **84**, 056015 (2011) [arXiv:1106.0600 [hep-ph]]; M. Cleven, F. K. Guo, C. Hanhart and U. G. Meissner, Eur. Phys. J. A **47**, 120 (2011) [arXiv:1107.0254 [hep-ph]]; T. Mehen and J. W. Powell, Phys. Rev. D **84**, 114013 (2011) [arXiv:1109.3479 [hep-ph]]; F. K. Guo, C. Hidalgo-Duque, J. Nieves and M. P. Valderrama, Phys. Rev. D **88**, 054007 (2013) [arXiv:1303.6608 [hep-ph]]; Q. Wang, C. Hanhart and Q. Zhao, Phys. Rev. Lett. **111**, no. 13, 132003 (2013) [arXiv:1303.6355 [hep-ph]]; F. K. Guo, C. Hanhart, Q. Wang and Q. Zhao, Phys. Rev. D **91** (2015) no.5, 051504 [arXiv:1411.5584 [hep-ph]]; X. W. Kang, Z. H. Guo and J. A. Oller, Phys. Rev. D **94** (2016) no.1, 014012 [arXiv:1603.05546 [hep-ph]]; X. W. Kang and J. A. Oller, arXiv:1612.08420 [hep-ph].

[144] E. S. Swanson, Phys. Rept. **429**, 243 (2006) [hep-ph/0601110]; Z. F. Sun, J. He, X. Liu, Z. G. Luo and S. L. Zhu, Phys. Rev. D **84**, 054002 (2011) [arXiv:1106.2968 [hep-ph]];

[145] Y. Liu and I. Zahed, Phys. Lett. B **762**, 362 (2016) [arXiv:1608.06535 [hep-ph]]; Y. Liu and I. Zahed, Int. J. Mod. Phys. E **26**, 1740017 (2017) [arXiv:1610.06543 [hep-ph]]; Y. Liu and I. Zahed, arXiv:1611.04400 [hep-ph].

[146] M. Albaladejo, F. K. Guo, C. Hidalgo-Duque and J. Nieves, Phys. Lett. B **755**, 337 (2016) doi:10.1016/j.physletb.2016.02.025 [arXiv:1512.03638 [hep-ph]].

[147] A. V. Manohar and M. B. Wise, Nucl. Phys. B **399**, 17 (1993) [hep-ph/9212236]; N. Brambilla *et al.*, Eur. Phys. J. C **71**, 1534 (2011) [arXiv:1010.5827 [hep-ph]]; M. B. Voloshin, Prog. Part. Nucl. Phys. **61**, 455 (2008) [arXiv:0711.4556 [hep-ph]]; J. M. Richard, arXiv:1606.08593 [hep-ph].

[148] D. O. Riska and N. N. Scoccola, Phys. Lett. B **299**, 338 (1993).

[149] M. A. Nowak, I. Zahed and M. Rho, Phys. Lett. B **303**, 130 (1993).

[150] S. Chernyshev, M. A. Nowak and I. Zahed, Phys. Rev. D **53**, 5176 (1996) [hep-ph/9510326].

[151] M. Nielsen, F. S. Navarra and S. H. Lee, Phys. Rept. **497**, 41 (2010) [arXiv:0911.1958 [hep-ph]].

[152] M. Karliner and J. L. Rosner, Phys. Rev. Lett. **115**, no. 12, 122001 (2015) [arXiv:1506.06386 [hep-ph]]; M. Karliner, EPJ Web Conf. **130**, 01003 (2016).

[153] R. Chen, X. Liu, X. Q. Li and S. L. Zhu, Phys. Rev. Lett. **115**, no. 13, 132002 (2015) [arXiv:1507.03704 [hep-ph]]; H. X. Chen, W. Chen, X. Liu, T. G. Steele and S. L. Zhu, Phys. Rev. Lett. **115**, no. 17, 172001 (2015) [arXiv:1507.03717 [hep-ph]]; L. Roca, J. Nieves and E. Oset, Phys. Rev. D **92**, no. 9, 094003 (2015) [arXiv:1507.04249 [hep-ph]]; T. J. Burns, Eur. Phys. J. A **51**, no. 11, 152 (2015) [arXiv:1509.02460 [hep-ph]]. H. Huang, C. Deng, J. Ping and F. Wang, Eur. Phys. J. C **76**, no. 11, 624 (2016) [arXiv:1510.04648 [hep-ph]]; L. Roca and E. Oset, Eur. Phys. J. C **76**, no. 11, 591 (2016) [arXiv:1602.06791 [hep-ph]]; Q. F. L and Y. B. Dong, Phys. Rev. D **93**, no. 7, 074020 (2016) [arXiv:1603.00559 [hep-ph]]; Y. Shimizu, D. Suenaga and M. Harada, Phys. Rev. D **93**, no.

11, 114003 (2016) [arXiv:1603.02376 [hep-ph]]; C. W. Shen, F. K. Guo, J. J. Xie and B. S. Zou, Nucl. Phys. A **954**, 393 (2016) [arXiv:1603.04672 [hep-ph]]; M. I. Eides, V. Y. Petrov and M. V. Polyakov, Phys. Rev. D **93**, no. 5, 054039 (2016) [arXiv:1512.00426 [hep-ph]]; I. A. Perevalova, M. V. Polyakov and P. Schweitzer, Phys. Rev. D **94**, no. 5, 054024 (2016) [arXiv:1607.07008 [hep-ph]]; V. Kopeliovich and I. Potashnikova, Phys. Rev. D **93**, no. 7, 074012 (2016); Y. Yamaguchi and E. Santopinto, arXiv:1606.08330 [hep-ph]; S. Takeuchi and M. Takizawa, Phys. Lett. B **764**, 254 (2017) [arXiv:1608.05475 [hep-ph]].

[154] N. N. Scoccola, D. O. Riska and M. Rho, Phys. Rev. D **92**, no. 5, 051501 (2015) [arXiv:1508.01172 [hep-ph]].

[155] G. Rossi and G. Veneziano, JHEP **1606**, 041 (2016) [arXiv:1603.05830 [hep-th]].

[156] J. Sonnenschein and D. Weissman, arXiv:1606.02732 [hep-ph].

[157] T. Sakai and S. Sugimoto, Prog. Theor. Phys. **113**, 843 (2005) [hep-th/0412141]; T. Sakai and S. Sugimoto, Prog. Theor. Phys. **114**, 1083 (2005) [hep-th/0507073].

[158] T. Fujiwara, T. Kugo, H. Terao, S. Uehara and K. Yamawaki, Prog. Theor. Phys. **73**, 926 (1985).

[159] A. Paredes and P. Talavera, Nucl. Phys. B **713**, 438 (2005) [hep-th/0412260]; J. Erdmenger, N. Evans and J. Grosse, JHEP **0701**, 098 (2007); [hep-th/0605241]. J. Erdmenger, K. Ghoroku and I. Kirsch, JHEP **0709** (2007) 111 [arXiv:0706.3978 [hep-th]]; C. P. Herzog, S. A. Stricker and A. Vuorinen, JHEP **0805**, 070 (2008) [arXiv:0802.2956 [hep-th]]; Y. Bai and H. C. Cheng, JHEP **1308**, 074 (2013) [arXiv:1306.2944 [hep-ph]]; K. Hashimoto, N. Ogawa and Y. Yamaguchi, JHEP **1506**, 040 (2015) [arXiv:1412.5590 [hep-th]]. J. Sonnenschein and D. Weissman, arXiv:1606.02732 [hep-ph].

[160] G. F. de Teramond, S. J. Brodsky, A. Deur, H. G. Dosch and R. S. Sufian, arXiv:1611.03763 [hep-ph]; H. G. Dosch, G. F. de Teramond and S. J. Brodsky, Phys. Rev. D **92** (2015) no.7, 074010 [arXiv:1504.05112 [hep-ph]]; H. G. Dosch, G. F. de Teramond and S. J. Brodsky, Phys. Rev. D **95** (2017) no. 3, 034016 [arXiv:1612.02370 [hep-ph]].

[161] R. C. Myers, JHEP **9912**, 022 (1999) [hep-th/9910053].

[162] H. Hata, T. Sakai, S. Sugimoto and S. Yamato, Prog. Theor. Phys. **117** (2007) 1157 [hep-th/0701280 [HEP-TH]].

[163] K. Hashimoto, T. Sakai and S. Sugimoto, Prog. Theor. Phys. **120** (2008) 1093 [arXiv:0806.3122 [hep-th]]; K. Y. Kim and I. Zahed, JHEP **0809**, 007 (2008) [arXiv:0807.0033 [hep-th]].

[164] I. Zahed and G. E. Brown, Phys. Rept. **142**, 1 (1986); Multifaceted Skyrmion, Eds. M. Rho and I. Zahed, World Scientific, 2016.

[165] Y. Liu and I. Zahed, Phys. Rev. D **95**, no. 5, 056022 (2017) [arXiv:1611.03757 [hep-ph]]. Y. Liu and I. Zahed, arXiv:1611.04400 [hep-ph].

[166] N. N. Scoccola, Nucl. Phys. A **532**, 409C (1991); M. Rho, D. O. Riska and N. N. Scoccola, Z. Phys. A **341**, 343 (1992); D. P. Min, Y. s. Oh, B. Y. Park and M. Rho, hep-ph/9209275. Y. s. Oh, B. Y. Park and D. P. Min, Phys. Rev. D **49**, 4649 (1994) [hep-ph/9402205]; Y. s. Oh, B. Y. Park and D. P. Min, Phys. Rev. D **50**, 3350 (1994) [hep-ph/9407214]; D. P. Min, Y. s. Oh, B. Y. Park and M. Rho, Int. J. Mod. Phys. E **4**, 47 (1995) [hep-ph/9412302]; Y. s. Oh and B. Y. Park, Phys. Rev. D **51**, 5016 (1995) [hep-ph/9501356]; J. Schechter, A. Subbaraman, S. Vaidya and H. Weigel, Nucl. Phys. A **590**, 655 (1995) Erratum: [Nucl. Phys. A **598**, 583 (1996)] [hep-ph/9503307]; Y. s. Oh and B. Y. Park, Z. Phys. A **359**, 83 (1997) [hep-ph/9703219]; C. L. Schat and N. N. Scoccola, Phys. Rev. D **61**, 034008 (2000) [hep-ph/9907271]; N. N. Scoccola, arXiv:0905.2722 [hep-ph]; J. P. Blanckenberg and H. Weigel, Phys. Lett. B **750**, 230 (2015) [arXiv:1505.06655 [hep-ph]].

[167] N. Itzhaki, I. R. Klebanov, P. Ouyang and L. Rastelli, Nucl. Phys. B **684**, 264 (2004) [hep-ph/0309305].

[168] J. M. Maldacena, Int. J. Theor. Phys. **38**, 1113 (1999) [Adv. Theor. Math. Phys. **2**, 231 (1998)] [hep-th/9711200]; S. S. Gubser, I. R. Klebanov and A. M. Polyakov, Phys. Lett. B **428**, 105 (1998) [hep-th/9802109]; E. Witten, Adv. Theor. Math. Phys. **2**, 505 (1998) [hep-th/9803131]; I. R. Klebanov and E. Witten, Nucl. Phys. B **556**, 89 (1999) [hep-th/9905104].

[169] J. Erlich, E. Katz, D. T. Son and M. A. Stephanov, Phys. Rev. Lett. **95**, 261602 (2005) [hep-ph/0501128]; L. Da Rold and A. Pomarol, Nucl. Phys. B **721**, 79 (2005) [hep-ph/0501218].

[170] S. Hong, S. Yoon and M. J. Strassler, JHEP **0604**, 003 (2006) [hep-th/0409118]; J. Erlich, G. D. Kribs and I. Low, Phys. Rev. D **73**, 096001 (2006) doi:10.1103/PhysRevD.73.096001 [hep-th/0602110]; H. R. Grigoryan and A. V. Radyushkin, Phys. Rev. D **76**, 095007 (2007) [arXiv:0706.1543 [hep-ph]]; H. R. Grigoryan and A. V. Radyushkin, Phys. Lett. B **650**, 421 (2007) [hep-ph/0703069]; S. S. Afonin and I. V. Pusenkov, EPJ Web Conf. **125**, 04004 (2016) [arXiv:1606.06091 [hep-ph]]; N. R. F. Braga, M. A. Martin Contreras and S. Diles, Europhys. Lett. **115**, no. 3, 31002 (2016) [arXiv:1511.06373 [hep-th]]; A. Gorsky, S. B. Gudnason and A. Krikun, Phys. Rev. D **91**, no. 12, 126008 (2015) [arXiv:1503.04820 [hep-th]].

[171] U. Gursoy and E. Kiritsis, JHEP **0802**, 032 (2008) [arXiv:0707.1324 [hep-th]]; U. Gursoy, E. Kiritsis and F. Nitti, JHEP **0802**, 019 (2008) [arXiv:0707.1349 [hep-th]].

[172] M. Karliner and J. L. Rosner, arXiv:1703.07774 [hep-ph]; G. Yang and J. Ping, arXiv:1703.08845 [hep-ph]; K. L. Wang, L. Y. Xiao, X. H. Zhong and Q. Zhao, arXiv:1703.09130 [hep-ph]; W. Wang and R. L. Zhu, arXiv:1704.00179 [hep-ph]; H. Y. Cheng and C. W. Chiang, arXiv:1704.00396 [hep-ph]; H. Huang, J. Ping and F. Wang, arXiv:1704.01421 [hep-ph]; B. Chen and X. Liu, arXiv:1704.02583 [hep-ph]; T. M. Aliev, S. Bilmis and M. Savci, arXiv:1704.03439 [hep-ph]; H. C. Kim, M. V. Polyakov and M. Praszalowicz, arXiv:1704.04082 [hep-ph].

[173] M. Padmanath and N. Mathur, arXiv:1704.00259 [hep-ph].

[174] D. Ebert, R. N. Faustov and V. O. Galkin, Phys. Rev. D **84**, 014025 (2011) [arXiv:1105.0583 [hep-ph]]; D. Ebert, R. N. Faustov and V. O. Galkin, Phys. Lett. B **659**, 612 (2008) [arXiv:0705.2957 [hep-ph]]; W. Roberts and M. Pervin, Int. J. Mod. Phys. A **23**, 2817 (2008) [arXiv:0711.2492 [nucl-th]].

[175] E. V. Shuryak, Nucl. Phys. B **198**, 83 (1982); N. Isgur and M. B. Wise, Phys. Rev. Lett. **66** (1991) 1130; A. V. Manohar and M. B. Wise, "Heavy

quark physics," Camb. Monogr. Part. Phys. Nucl. Phys. Cosmol. **10**, 1 (2000).

[176] M. A. Nowak, M. Rho and I. Zahed, Phys. Rev. D **48**, 4370 (1993) [hep-ph/9209272]; M. A. Nowak, M. Rho and I. Zahed, Acta Phys. Polon. B **35**, 2377 (2004) [hep-ph/0307102].

[177] W. A. Bardeen and C. T. Hill, Phys. Rev. D **49** (1994) 409 [hep-ph/9304265]; W. A. Bardeen, E. J. Eichten and C. T. Hill, Phys. Rev. D **68**, 054024 (2003) [hep-ph/0305049].

[178] B. Aubert *et al.* [BaBar Collaboration], Phys. Rev. Lett. **90**, 242001 (2003) [hep-ex/0304021].

[179] D. Besson *et al.* [CLEO Collaboration], Phys. Rev. D **68**, 032002 (2003) Erratum: [Phys. Rev. D **75**, 119908 (2007)] [hep-ex/0305100].

[180] Y. Liu and I. Zahed, arXiv:1704.03412 [hep-ph].

[181] H. Hata and M. Murata, Prog. Theor. Phys. **119**, 461 (2008) [arXiv:0710.2579 [hep-th]];

[182] P. H. C. Lau and S. Sugimoto, arXiv:1612.09503 [hep-th].

[183] O. Aharony and D. Kutasov, Phys. Rev. D **78**, 026005 (2008) [arXiv:0803.3547 [hep-th]]; K. Hashimoto, T. Hirayama, F. L. Lin and H. U. Yee, JHEP **0807**, 089 (2008) [arXiv:0803.4192 [hep-th]].

[184] K. Hashimoto, N. Iizuka, T. Ishii and D. Kadoh, Phys. Lett. B **691**, 65 (2010) [arXiv:0910.1179 [hep-th]].

[185] C. Patrignani et al. (Particle Data Group), Chin. Phys. **C40** 100001 (2016).